Oxidative Medicine and Cellular Longevity

Mechanisms, Biomarkers, and Therapeutics involved in Inflammatory Disorders and Tissue Repair 2021

Lead Guest Editor: Reggiani Vilela Gonçalves
Guest Editors: Mariaurea Matias Sarandy, Débora Esposito, and Maria do Carmo Gouveia Peluzio

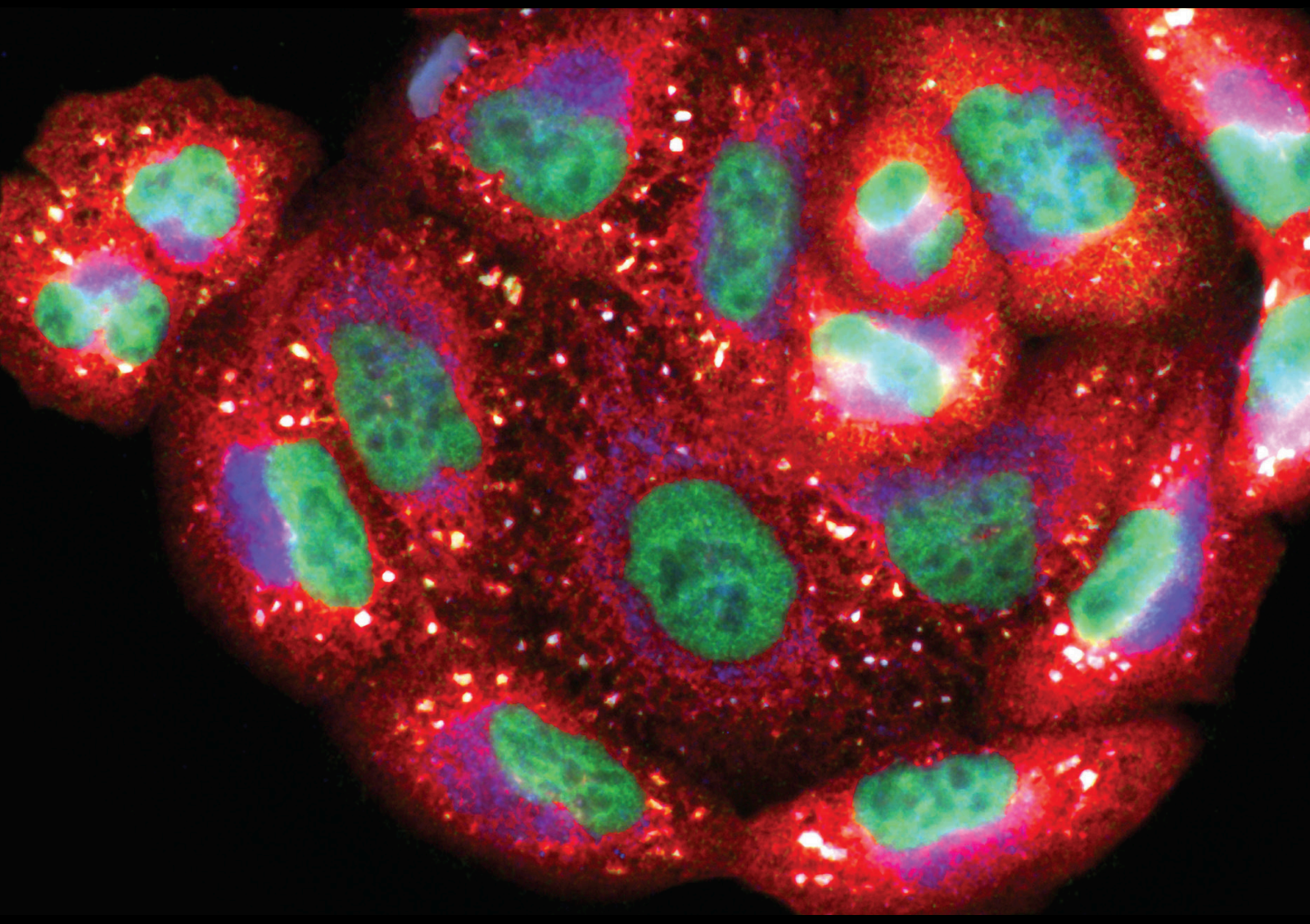

Mechanisms, Biomarkers, and Therapeutics involved in Inflammatory Disorders and Tissue Repair 2021

Oxidative Medicine and Cellular Longevity

Mechanisms, Biomarkers, and Therapeutics involved in Inflammatory Disorders and Tissue Repair 2021

Lead Guest Editor: Reggiani Vilela Gonçalves
Guest Editors: Mariaurea Matias Sarandy, Débora Esposito, and Maria do Carmo Gouveia Peluzio

Contents

Melatonin Ameliorates Corticosterone-Mediated Oxidative Stress-Induced Colitis in Sleep-Deprived Mice Involving Gut Microbiota

Ting Gao, Zixu Wang, Jing Cao, Yulan Dong, and Yaoxing Chen

Research Article (24 pages), Article ID 9981480, Volume 2021 (2021)

Hindawi
Oxidative Medicine and Cellular Longevity
Volume 2022, Article ID 9806128, 2 pages
https://doi.org/10.1155/2022/9806128

Editorial

Mechanisms, Biomarkers, and Therapeutics Involved in Inflammatory Disorders and Tissue Repair 2021

Reggiani Vilela Gonçalves,[1,2] **Mariáurea Matias Sarandy**,[1,2] **Débora Esposito**,[3] **and Maria do Carmo Gouveia Peluzio**[4]

[1]*Animal Biology Department, Federal University of Viçosa, Viçosa, 36570-000 Minas Gerais, Brazil*
[2]*Animal Biology and Cellular and Structural Biology Graduate Program, Federal University of Viçosa, Viçosa, 36570-000 Minas Gerais, Brazil*
[3]*Department of Animal Science, Regenerative Medicine, North Carolina State University, 28081 NC, USA*
[4]*Department of Nutrition and Health, Federal University of Viçosa, Viçosa, 36570-000 Minas Gerais, Brazil*

Correspondence should be addressed to Reggiani Vilela Gonçalves; reggysvilela@yahoo.com.br

Received 21 January 2022; Accepted 21 January 2022; Published 20 March 2022

The inflammation during wound healing process is characterized by activation of cellular, vascular, and biochemical mechanisms that occur to perform a fast tissue repair and avoid complications [1, 2]. The first cells to migrate to the injured area are neutrophils, which recruit macrophages by chemotaxis. These cells promote the release of cytokines, growth factors, and reactive oxygen species (ROS) and nitrogen (RNS) responsible for a good evolution of the wound healing process [3]. The excess of ROS and RNS generated during inflammation can lead to cell damage, such as membrane disorganization and protein oxidation, altering cell functions [4, 5]. Furthermore, the excess of proinflammatory mediators promotes an increase in the content of hydrogen peroxide (H_2O_2) and nitric oxide, which accelerates the peroxidation of cell components [6, 7]. The balance between ROS production and antioxidant defenses is important for the resolution of inflammatory diseases as well as for efficient tissue repair [4, 5, 6]. Therefore, a controlled inflammation process is necessary to avoid persistent tissue damage through the continuous action of free radicals, ROS, and RNS [7].

Cytokines, growth factors, oxidative markers, and other molecular markers are considered biomarkers that allow understanding the progression of inflammatory disorders and tissue repair processes. Currently, different therapeutic interventions and their mechanism of action (cellular and extracellular) have been investigated to better understand this complex process [8]. In this context, several interventions have been investigated for the treatment of inflammatory diseases, and in this edition, we observed the high potential of these compounds for the treatment of inflammatory diseases (e.g., melatonin; Hibiscus sabdariffa; atorvastatin; olaparib, curcumin, and plant extracts in general) exhibiting antioxidant and anti-inflammatory actions. In many cases, these properties are based on the interruption of cellular redox metabolism, suppressing oxidative stress, a pharmacological effect that opens new spaces for the reuse of drugs, and the development of new strategies for the treatment of inflammatory disorders and tissue repair. Furthermore, the anti-inflammatory action of different interventions has been attributed to modulation of the STAT-3, AP-1, NFkB, and Nrf2 pathways.

This special issue brings together a set of thirteen studies in an interdisciplinary platform that addresses the inflammatory subcellular, cellular, and molecular bases associated with redox metabolism. This special issue also highlights the ongoing effort to understand the redox systems associated with inflammatory disorders and tissue repair at all levels and to understand how the action of different treatments can lead to reduced gene expression of inflammatory proteins and increased levels of antioxidant enzymes. Thus, this issue contains seven articles that describe different mechanisms involved in this complex process, under different pathological conditions, which are briefly mentioned in the following.

Some studies have shown that external agents such as food, lack of sleep, and physical activity reflect an imbalance between oxidant and antioxidant mechanisms in favor of oxidants, in addition to inhibiting anti-inflammatory pathways, thus causing tissue damage. These prooxidant mechanisms are related to genetic and epigenetic regulation and can regulate the expression of molecules that can activate the signal transduction pathways responsible for inflammation and cause oxidative damage to proteins, lipids, and DNA. Thus, antioxidant systems seem to play a crucial role in maintaining tissue morphological and functional integrity. Phenolic compounds present in herbal medicines, in addition to oncological drugs, drugs of the statin class, and hormones, have shown efficacy in inflammatory disorders and intestinal preneoplastic lesions, testicular, oral mucositis, and muscle inflammatory damage by suppressing oxidative stress, attenuating cellular responses, activating intracellular pathways, and reducing cell death.

Ideally, inflammatory modulators should be able to reduce proinflammatory cytokines and increase anti-inflammatory cytokines and antioxidant defenses. Furthermore, it is important to emphasize that chronic inflammation associated with high oxidative stress can cause organelle damage, leading to a lot of diseases that compromise the good function of the cells. In this context, we can highlight that Hibiscus sabdariffa reduces intestinal preneoplastic lesions in a murine model, attenuating inflammation cellular responses in the initial phase of these lesions. On the other hand, curcumin associated with physical activity reduces muscle damage as well as proinflammatory markers. In contrast, the increase in oxidative stress promoted by plant extracts used with sex inhibitors was reported in a systematic review of this special issue. Furthermore, high levels of inflammatory cytokines were found in patients with exotropia, associating this condition with the inflammatory process. The hormone melatonin reduced colitis and restored the intestinal microbiota by reducing oxidative stress and the inflammatory response.

We hope that the readers of this special issue will find these findings interesting and useful to advance the understanding of such a complex and multifaceted theme, suggesting update for this interesting topic.

Conflicts of Interest

The authors declare that there is no conflict of interest regarding the publication of this special issue.

Acknowledgments

The editorial teams are very grateful to the different groups who submitted their scientific findings to this special issue and to the reviewers who kindly provided their time and experience to improve the quality of each study.

Reggiani Vilela Gonçalves
Mariáurea Matias Sarandy
Débora Esposito
Maria do Carmo Gouveia Peluzio

References

[1] M. Cano Sanchez, S. Lancel, E. Boulanger, and R. Neviere, "Targeting oxidative stress and mitochondrial dysfunction in the treatment of impaired wound Healing: A Systematic Review," *Antioxidants*, vol. 7, no. 8, p. 98, 2018.

[2] L. A. Abdulkhaleq, M. A. Assi, R. Abdullah, M. Zamri-Saad, Y. H. Taufiq-Yap, and M. N. M. Hezmee, "The crucial roles of inflammatory mediators in inflammation: a review," *Phytochemistry Reviews*, vol. 11, no. 5, pp. 627–635, 2018.

[3] A. Weidinger and A. V. Kozlov, "Biological activities of reactive oxygen and nitrogen species: oxidative stress versus signal transduction," *Biomolecules*, vol. 5, no. 2, pp. 472–484, 2015.

[4] D. André-Lévigne, A. Modarressi, M. S. Pepper, and B. Pittet-Cuénod, "Reactive oxygen species and NOX enzymes are emerging as key players in cutaneous wound repair," *International Journal of Molecular Sciences*, vol. 18, p. 2149, 2017.

[5] D. Pitocco, F. Zaccardi, E. Di Stasio, F. Romitelli, S. A. Santini, C. Zuppi et al., "Oxidative stress, nitric oxide, and diabetes," *The Review of Diabetic Studies*, vol. 7, pp. 15–25, 2010.

[6] M. Mittal, M. R. Siddiqui, K. Tran, S. P. Reddy, and A. B. Malik, "Reactive oxygen species in inflammation and tissue injury," *Antioxidants & Redox Signaling*, vol. 20, pp. 1126–1167, 2014.

[7] I. Marrocco, F. Altieri, and I. Peluso, "Measurement and clinical significance of biomarkers of oxidative stress in humans," *Oxidative Medicine and Cellular Longevity*, vol. 2017, Article ID 6501046, 32 pages, 2017.

[8] B. C. F. Nogueira, A. K. Campos, R. S. Alves et al., "What is the impact of depletion of immunoregulatory genes on wound healing? A systematic review of preclinical evidence," *Oxidative Medicine and Cellular Longevity*, vol. 2020, Article ID 8862953, 19 pages, 2020.

Hindawi
Oxidative Medicine and Cellular Longevity
Volume 2022, Article ID 9004014, 21 pages
https://doi.org/10.1155/2022/9004014

Research Article

Beta-caryophyllene as an antioxidant, anti-inflammatory and re-epithelialization activities in a rat skin wound excision model

Lucas Fernando Sérgio Gushiken,[1] **Fernando Pereira Beserra**,[1] **Maria Fernanda Hussni**,[2] **Murilo Tireli Gonzaga**,[1] **Victor Pena Ribeiro**,[3] **Patrícia Fernanda de Souza**,[3] **Jacqueline Costa Lima Campos**,[3] **Taís Nader Chrysostomo Massaro**,[3] **Carlos Alberto Hussni**,[2] **Regina Kiomi Takahira**,[2] **Priscyla Daniely Marcato**,[3] **Jairo Kenupp Bastos**,[3] **and Cláudia Helena Pellizzon**[1]

[1]*São Paulo State University-UNESP, Institute of Biosciences of Botucatu-IBB, São Paulo, Brazil*
[2]*São Paulo State University-UNESP, School of Veterinary Medicine and Zootechnics-FMVZ, São Paulo, Brazil*
[3]*University of São Paulo-USP, School of Pharmaceutical Science of Ribeirão Preto-FCFRP, São Paulo, Brazil*

Correspondence should be addressed to Lucas Fernando Sérgio Gushiken; lucas.gushiken@unesp.br

Received 3 June 2021; Accepted 13 January 2022; Published 3 February 2022

Academic Editor: Reggiani Vilela Gonçalves

The skin is a critical organ for the maintenance of the integrity and protection of the organism. When a wound occurs, a sequence of healing mechanisms is triggered to reconstruct the wounded area. β-caryophyllene is a sesquiterpene in *Copaifera langsdorffii* oleoresin with antioxidant and anti-inflammatory potential. On the basis of previous studies with *C. langsdorffii*, β-caryophyllene was selected to evaluate its wound healing potential and pharmacological mechanisms. The excision wound model was used with male *Wistar* rats and macroscopic, histological, immunohistochemical and biochemical analyses were performed with skin samples, comparing the β-caryophyllene-treated group with reference drugs. The results showed macroscopic retraction of the wounds treated with β-caryophyllene. Biochemical assays revealed the antioxidant and anti-inflammatory mechanisms of the β-caryophyllene-treated group with increasing levels of IL-10 and GPx and decreasing levels of pro-inflammatory molecules, including TNF-α, IFN-γ, IL-1β and IL-6. After β-caryophyllene treatment, immunohistochemical assays showed enhanced re-epithelialization, through the increase in laminin-γ2 and desmoglein-3 immunolabeling. β-caryophyllene also act in the remodeling mechanism, increasing the collagen content in the Masson's trichrome staining. These findings indicated the wound-healing potential of β-caryophyllene topical formulation in rat skin wounds, mediated by antioxidant, anti-inflammatory and re-epithelialization mechanisms.

1. Introduction

Skin wounds are major health problems that affect millions of people every year, causing physical and psychological deficiencies when not treated correctly [1]. The comorbidities associated with unhealed wounds increase every year, and the costs of healing treatments have reached billions of dollars worldwide [2]. The wound-healing process involves overlapping and interdependent mechanisms (inflammation, epithelialization, angiogenesis, wound retraction and matrix remodeling) to reconstruct the skin [3]. When there is an imbalance among these mechanisms, the healing process enters a pathologic state, resulting in errors of healing, such as hypertrophic scars and unhealed wounds [4]. To prevent pathologic mechanisms of wound healing, there are several treatments on the market used to promote cutaneous healing by acting as antimicrobial or anti-inflammatory agents, improving tissue debridement, epithelialization and/or remodeling mechanisms. However, the existing treatments may not be efficient in treating cutaneous wounds depending on the type, extension and location of the injury [5]. Therefore, studies have focused on

discovering alternative drugs that accelerate skin wound healing without scarring [6].

β-caryophyllene (trans-(1,9)-8-methylene-4,11,11-trimethylbicycloundec-4-ene) is a natural bicyclical sesquiterpene found in several plants and essential oils, including *C. langsdorffii* (Leguminosae) oil [7]. β-caryophyllene is a volatile compound that is poorly soluble in water and has high pharmaceutical potential due to its analgesic, antioxidant, antimicrobial and anti-inflammatory activities [8–10]. Previous studies on *C. langsdorffii* have suggested the healing potential of *C. langsdorffii* oil resin in a 10% formulation [11]. Therefore, our group tested a 1% β-caryophyllene emulgel formulation to analyze the wound-healing potential and the mechanisms of action of this new formulation in a rat excision wound model.

2. Materials and Methods

2.1. Chemicals and reagents. The reference drugs neomycin sulfate (5 mg/g) + bacitracin zinc (250 IU/g), dexpanthenol 5% and collagenase 1.2 IU were purchased from pharmaceutical industries. SOD, CAT, MPO, GSH, GPx and silica gel 60H chromatoplates were obtained from Sigma-Aldrich Chemicals (Saint Louis, USA). ELISA kits of TNF-α, IFN-γ, IL-1β, IL-6 and IL-10 were bought from R&D Systems (Minneapolis, USA). Biochemical colorimetric kits for quantification of AST, ALT, γ-GT, urea and creatinine were purchased from Interteck-Katal (Belo Horizonte, Brazil). The primary antibodies Lamγ2 was purchased from Santa Cruz Biotechnology (Dallas, USA). Dsg3, Ki-67, α-SMA antibodies and immunohistochemistry reveal kits were purchased from Abcam (Cambridge, USA). Sepineo P600, propylene glycol and methyldibromo glutaronitrile/phenoxyethanol were obtained from Spectrum Chemical Manufacturing Corporation (New Brunswick, USA). Labrafac lipophile WL 1349 was purchased from Gattefossé (Lyon, France).

2.2. Extraction and isolation of β-caryophyllene. The extraction and isolation of β-caryophyllene have been previously reported by Ribeiro et al. [12] [12]. Briefly, *C. langsdorffii* oleoresin was collected in the northern and southeastern regions of Brazil, and the plant voucher was identified by Silvana Tavares Rodrigues at the Herbarium from EMBRAPA Amazônia Oriental (SPFR 10120). One hundred milliliters of a volatile fraction of oleoresin was added to 500 mL of water and subjected to hydrodistillation for 12 hours using a Clevenger-type apparatus. Then, the volatile fraction was subjected to a spinning band distillation process to obtain fractions rich in β-caryophyllene. β-caryophyllene was purified from these fractions by classical column chromatography packed with Sigma-Aldrich 60H silica gel impregnated with $AgNO_3$ with a gradient of hexane-ethyl acetate used as the mobile phase.

2.3. Formulation of emulgel and 1% β-caryophyllene emulsion. The emulgel was synthesized homogenizing Sepineo P600 (3% w/w), propylene glycol (5% w/w), Labrafac lipophile WL1349 (10% w/w), methyldibromo glutaronitrile/phenoxyethanol (0.1% w/w) and water at room temperature (±25°C) with a Polytron PT 10-35 GT (Kinematica, Switzerland) at 600 rpm. The 1% β-caryophyllene emulsion was synthesized homogenizing the β-caryophyllene (1% w/w) with the emulgel at room temperature (±25°C). The rheological behavior of the emulgel was analyzed in a Rheometer R/S plus (Brookfield) equipped with a C50-1 spindle and RHEO Software 2000 version 2.8. The sample behavior was monitored at a constant temperature (25°C) using a water bath/circulator.

2.4. Animals. In total, 105 male 7-week-old *Wistar* rats weighing 250 ± 20 g (Central Animal House, UNESP, Botucatu) were used in the experiments. The animals were housed individually for one week before the experiments and subjected to a temperature of 23 ± 2°C and a 12-hour dark-light cycle, and the animals had free access to food and water until the experimental procedure were initiated. This study was approved by the Ethics Committee on Animal Use at São Paulo State University under protocol 976/2017.

2.5. Experimental protocol of excision wound. The rats were anesthetized with intraperitoneal ketamine (100 mg/kg) and xylazine (10 mg/kg) [13]. The hair of their back was shaved and a full-thickness skin wound excision was made in the dorsum (in the subscapular area) using a 3 cm diameter punch. The wound placed in this area could not be reached by the animals, which prevented self-licking [14]. Each rat was topically treated twice per day for three different experimental periods: 3, 7 or 14 days (n = 35 animals/period). After each period, the animals were euthanized, and samples of the skin wounds and blood were collected for analyses. The animals were allocated into the following seven groups (n = 5/group):

(i) FST: wounded animal without treatment

(ii) NeBa: wounded animal treated with neomycin 5 mg/g + bacitracin zinc 250 IU/g

(iii) Dex: wounded animals treated with dexpanthenol 5%

(iv) Col: wounded animals treated with collagenase 1.2 IU

(v) Emulgel: wounded animals treated with emulgel (vehicle)

(vi) Car: wounded animals treated with 1% β-caryophyllene emulgel

(vii) Control: animals without lesion and treatment – physiologic pattern

2.6. Wound contraction analysis. To measure the contraction of the wounded area, each wound was photographed using a digital camera with a scale bar on days 0, 3, 7 and 14 after the excision wound was induced (day 0). A morphometric analysis was performed through measurement of wounded areas using specific software, and the percentage of wound

contraction of each rat was calculated using the following formula [11, 15]:

$$\text{Wound concentration (\%)} = \{(\text{initial wound area} - \text{analyzed area})/\text{initial wound area}\} * 100 \quad (1)$$

2.7. Hepatic and renal toxicity. Immediately after the euthanasia of each animal, blood was collected and centrifuged for 15 minutes at 6000 rpm and 4°C. The supernatant was collected and used to determine liver and kidney toxicity using AST, ALT and γ-GT (IU/L) parameters as well as the concentrations of urea and creatinine (mg/dL).

2.8. Inflammatory mediators and antioxidant enzymes. Samples of wounded skin of each animal were collected to quantify the IFN-γ, IL-1β, IL-6, IL-10 and TNF-α inflammatory cytokines and the antioxidant enzymes, including SOD, CAT, GPx and GSH. Halves of each wound were cut using a scalpel, including the border and center of the lesions. The skin samples were instantly homogenized (1 : 5 m/v) in phosphate buffer (pH 7.4) and centrifuged for 15 minutes at 10000 rpm and 4°C. The supernatant of each sample was collected, and the cytokines were quantified by ELISA as described by the supplier. The results were expressed in pg/mg of protein. The following molecules involved in oxidative stress pathways were quantified through biochemical assays according to protocols: SOD (IU/mg of protein) [16], CAT (IU/mg of protein) [17], GPx (nmol NADPH/min/mg of protein) [18] and GSH (nmol/mg of protein) [19].

2.9. Histological parameters. The other halves of wounded skin samples from each rat were fixed with 10% buffered formaldehyde, embedded in paraffin, sectioned (5 μm) and stained with HE and Masson's trichrome stain. Each section was submitted to morphometric analysis via light microscopy. With HE staining, the epidermis thickness (μm), number of total cells in the epidermis and dermis (μm^2) and the quantity of blood vessels in the dermis (number of blood vessels) were analyzed. With Masson's trichrome staining, the collagen content of the dermis (μm^2) was analyzed. The border and center regions of the wounds were analyzed with five different photomicrographs of each region in the sections. AvSoft BioView Spectra software was used to perform the analysis.

2.10. Immunohistochemistry. Skin samples from each rat were processed routinely (fixation with 10% buffered formaldehyde, embedded in paraffin and sectioned; 5 μm thickness). Immunohistochemistry was then performed with primary antibodies against laminin-γ2 (1 : 200 μL), desmoglein-3 (1 : 200 μL), Ki-67 (1 : 100 μL) and α-SMA (1 : 400 μL) according to the protocols of a specific HRP/DAB detection kit. The areas (μm^2) and positive cells (count of positive cells) for each antibody were quantified in the border and center of wounds with five different photomicrographs for each region of the sections. AvSoft BioView Spectra software was used to perform the analysis.

2.11. Statistical analysis. The data are expressed as the means ± standard deviation. Two-way ANOVA with Bonferroni post-test was used in the analysis of wound contraction. The inflammatory mediator, oxidative stress and toxicity data were submitted to one-way ANOVA with Tukey's post-hoc test. Histological parameters and immunohistochemical data were analyzed according to the Kruskal-Wallis test with Dunn's post-test. GraphPad Prism 5.01 software (GraphPad Software Inc., San Diego, USA) was used to perform the analyses with a significance of 5%.

3. Results

3.1. Emulgel and 1% β-caryophyllene emulsion stability test. The rheological behavior of emulgel and 1% β-caryophyllene emulsion showed a non-Newtonian characteristic, with pseudoplastic behavior ($n < 1$). This result demonstrates that, with the increase of the shear rate, the viscosity reduces (data not shown).

3.2. Wound contraction analysis. The contraction of the wounds was analyzed on days 3, 7 and 14 (Figure 1). The data showed macroscopic contraction of wounds and a decrease in local edema in the groups treated with NeBa and Car for three days compared to the FST and Emulgel groups. After seven and fourteen days of treatment, the Col and Car formulations showed the best results in terms of macroscopic contraction compared to the FST and emulgel formulations. Furthermore, in both periods of treatment, the rats treated with Car showed decreased fibrinous exudate compared to the other groups.

3.3. Hepatic and renal toxicity. To analyze the hepatic and renal toxicity of the formulation containing β-caryophyllene, the liver enzymes (AST, ALT and γ-GT) and kidney proteins (creatinine and urea) were evaluated in the blood of the rats after 14 days of treatment (the longest period of treatment). No significant differences among the values of all the treatment measurements and the normal parameters were found during the three experimental periods of treatment (Table 1).

3.4. Quantification of inflammatory mediators. The concentrations of the IFN-γ, IL-1β, IL-6, IL-10 and TNF-α cytokines as evaluated by ELISA are shown in Figure 2. The level of IFN-γ was reduced in the Car group compared to the FST group after three days. In the two other treatment periods, the NeBa, Dex and Col commercial formulations, as well as the tested Car drug, decreased the levels of IFN-γ compared to the FST and Emulgel. After three days, a reduction in the IL-1β level in NeBa and Dex treated groups compared to FST group was observed. Within seven days, decreased levels of IL-1β were observed in the NeBa, Dex, Col and Car groups compared to the FST and Emulgel groups. In the last period of treatment, the Car group showed decreased IL-1β concentrations compared to all wounded groups. The IL-6 levels were decreased in the

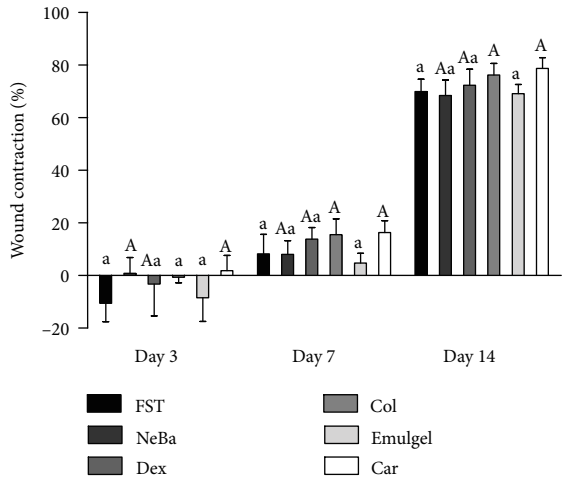

Figure 1: Wound contraction (%) in FST, NeBa, Dex, Col, Emulgel and Car treatments during 3, 7 and 14 days. Equal letters represents no statistical difference. Capital letters indicate statistical difference compared to groups with small letters, according to two-way ANOVA followed by Bonferroni test, with $p \leq 0.05$ ($n = 5$).

Table 1: Systemic toxicity analysis data for liver (AST, ALT, γ-GT) and renal (creatinine, urea) parameters in the serum of rats treated for 14 days.

Groups	AST (IU/L)	ALT (IU/L)	γ-GT (IU/L)	Creatinine (mg/dL)	Urea (mg/dL)
FST	143 ± 28	62 ± 12	1.2 ± 0.4	0.30 ± 0.03	44 ± 2.1
NeBa	138 ± 17	65 ± 7.7	1.1 ± 0.3	0.31 ± 0.04	44 ± 6.2
Dex	150 ± 28	80 ± 17	0.9 ± 0.3	0.27 ± 0.03	43 ± 5.6
Col	153 ± 29	63 ± 12	1.0 ± 0.2	0.30 ± 0.05	45 ± 4.6
Emulgel	146 ± 6.1	65 ± 8.5	1.1 ± 0.2	0.26 ± 0.04	44 ± 4.7
Car	124 ± 14	60 ± 9.5	1.1 ± 0.2	0.31 ± 0.03	42 ± 7.6
Control	147 ±25	65 ± 9.1	1.0 ± 0.2	0.30 ± 0.02	44 ± 4.9

One-way ANOVA followed by Tukey test, with $p \leq 0.05$ ($n = 5$). FST: wounded animal without treatment; NeBa: wounded animal treated with neomycin 5 mg/g + sulfate bacitracin zinc 250 IU/g; Dex: wounded animals treated with dexpanthenol 5%; Col: wounded animals treated with collagenase 1.2 IU; Emulgel: wounded animals treated with emulgel (vehicle); Car: wounded animals treated with β-caryophyllene emulsion; Control: animals without lesion and treatment – physiologic pattern.

NeBa, Dex and Car groups after three and seven days of treatment compared to the FST and Emulgel groups. The levels of IL-10 were not different among the treatments on days three and seven. In the last period of treatment, an increase in IL-10 was observed in the NeBa, Dex, Col and Car treatment groups compared to the FST and Emulgel treatment groups. The TNF-α levels were reduced in the NeBa, Dex and Car groups compared to the FST and Emulgel groups on day fourteen, and there were no significant differences in the two other periods (Figure 2).

3.5. Oxidative stress analysis. The CAT activity, GPx activity, SOD activity and GSH concentration are shown in Figure 3. The activity of CAT was decreased in the Col and Car groups compared to the FST and Emulgel groups on day fourteen, with the same level of Control, demonstrating the normality of the enzyme in the groups. During the first two periods of treatment, there was no significant difference in the CAT activity. The GPx activity was increased in the NeBa, Col and Car treatment groups compared to the other groups during the seven-day treatment period with no differences on days three and fourteen. The GSH concentration and SOD activity was not different among the wounded groups in any period (Figure 3).

3.6. Histological parameters. There was no difference in the quantification of cells from the epidermis, border of center of the dermis among the wounded groups in any period of treatment (Figures 4–6 and Supplementary materials 1). The morphometric analysis showed a reduction in the epidermis thickness of the animals treated with the NeBa, Dex, Col and Car formulations compared to that of the animals in the FST and Emulgel groups after seven and fourteen days. Moreover, the results of the Car group on day fourteen were similar to those of the Control group, resulting in normal epidermis thickness in the Car treatment (Figures 4 and 7). The quantification of blood vessels in the border and center of the wounds did not reveal a significant difference during any period of treatment (Figures 5 and 6, Supplementary materials 2). The quantification of total collagen in the border of the wounds showed no difference on days three, seven and fourteen. In the central area of wounds, there was an increase in collagen amount in the Car group compared to the FST and Emulgel on day three, with

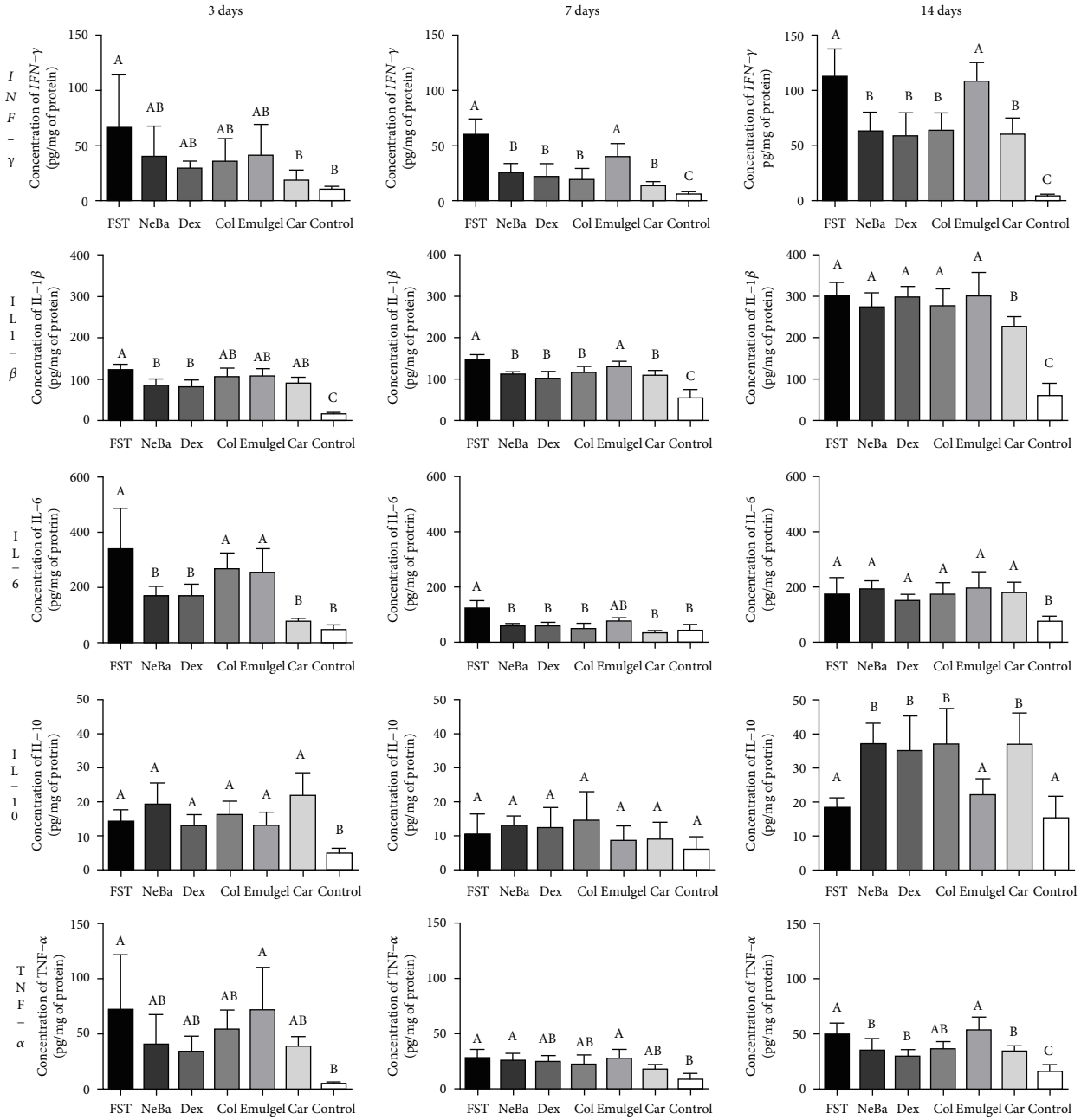

Figure 2: Concentrations of IFN-γ, IL-1β, IL-6, IL-10 and TNF-α (pg/mg protein) in cutaneous wounds at 3, 7 and 14 days. Equal letters show no statistical difference and different letters indicate statistical difference compared to the other groups, according to one-way ANOVA followed by Tukey test, with $p \leq 0.05$ ($n = 5$).

a similar concentration compared to Control. After seven and fourteen days, no differences were observed (Figures 8–10).

3.7. Immunohistochemistry. There was an increase in α-SMA-immunolabeled fibroblasts in the NeBa, Dex, Col and Car samples compared to FST and emulgel samples after three and seven days of treatment with no differences on day fourteen. However, the commercial treatments and Car formulation showed results similar to the control, indicating normalization of α-SMA in these groups (Figures 11 and 12). Immunolabeling for Dsg3 showed a reduction in the labeled area of the NeBa and Car groups compared to the FST group after three days. There was a decrease in Dsg3 immunolabeling in the Col and Car groups compared to the FST and Emulgel groups after seven days. There was no significant difference in the last period of treatment (Figures 11 and 13). There was an increase in Lamγ2 immunolabeling in the Col and Car groups compared to the FST and Emulgel groups on day three and an increased area in the Car group compared to the FST and Emulgel groups on day fourteen (Figures 11 and 14). There were no significant differences among the wounded groups in the number of Ki-67-immunolabeled cells in the epidermis, border region of central region of the dermis after three, seven

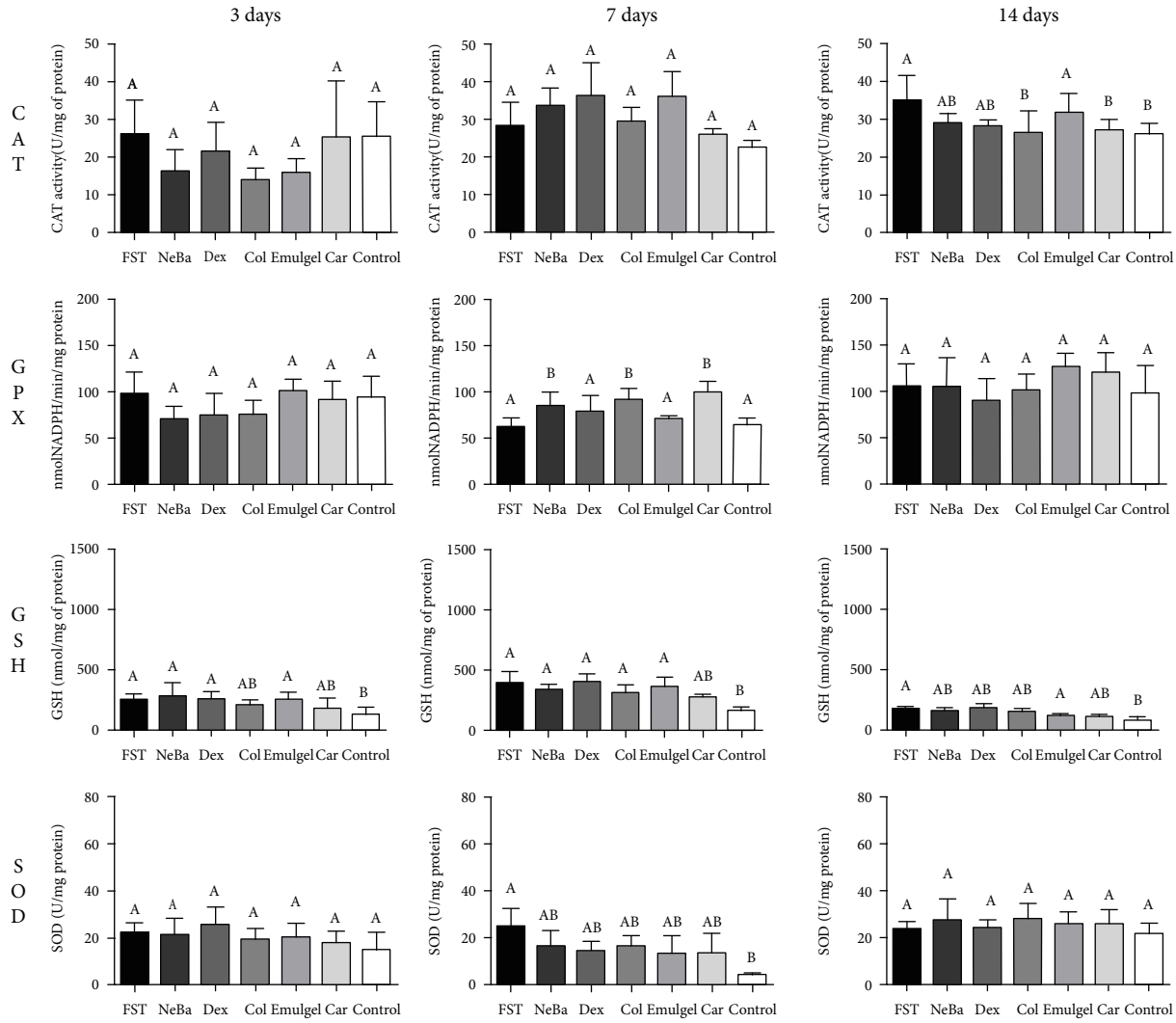

Figure 3: Concentrations of CAT, GPx, GSH and SOD in skin wounds at 3, 7 and 14 days. Equal letters show no statistical difference and different letters indicate statistical difference compared to the other groups, according to one-way ANOVA followed by Tukey test, with $p \leq 0.05$ ($n = 5$).

and fourteen days (Figures 15–17 and Supplementary materials 3).

4. Discussion

β-Caryophyllene is a sesquiterpene in many consumable plants and essential oils with related antioxidant, anti-inflammatory and antimicrobial potentials [8–10]. Previous studies using *C. langsdorffii* oil resin as a treatment for skin excision wounds have shown that the best effective concentration of the oil resin was 10%, and the phytochemical profile of the oil resin has been determined [11, 20]. Therefore, we calculated the concentration of the sesquiterpene based on these studies to synthesize the emulgel formulation for this study, resulting in a concentration of 1%. The present study confirmed the wound-healing activity of an emulgel formulation containing 1% β-caryophyllene in a rat excision model, demonstrating the antioxidant and anti-inflammatory activities as well as the improvement in remodeling and re-epithelialization mechanisms mediated by the sesquiterpene.

There are some topical drugs on the market with different mechanisms of action to treat wounds aiming to reduce the time of cutaneous healing and treat errors in tissue repair. Topical formulations containing neomycin and bacitracin zinc sulfate are used in the initial phase of skin wounds to prevent injury from infection, one of the major factors of delayed wound healing [5]. Dexpanthenol (5%) is also used in skin injuries with previous studies reporting the proliferative potential of keratinocytes and fibroblasts with this treatment [21]. Another common drug used to treat cutaneous wounds is collagenase, a protease of *Clostridium histolyticum,* which has been show to play a role in the debridement of provisional extracellular matrix and to have a remodeling mechanism that makes it useful to treat wounds in the clinic [22, 23]. Therefore, these three drugs were used in our study as positive controls to compare the new treatment containing β-caryophyllene.

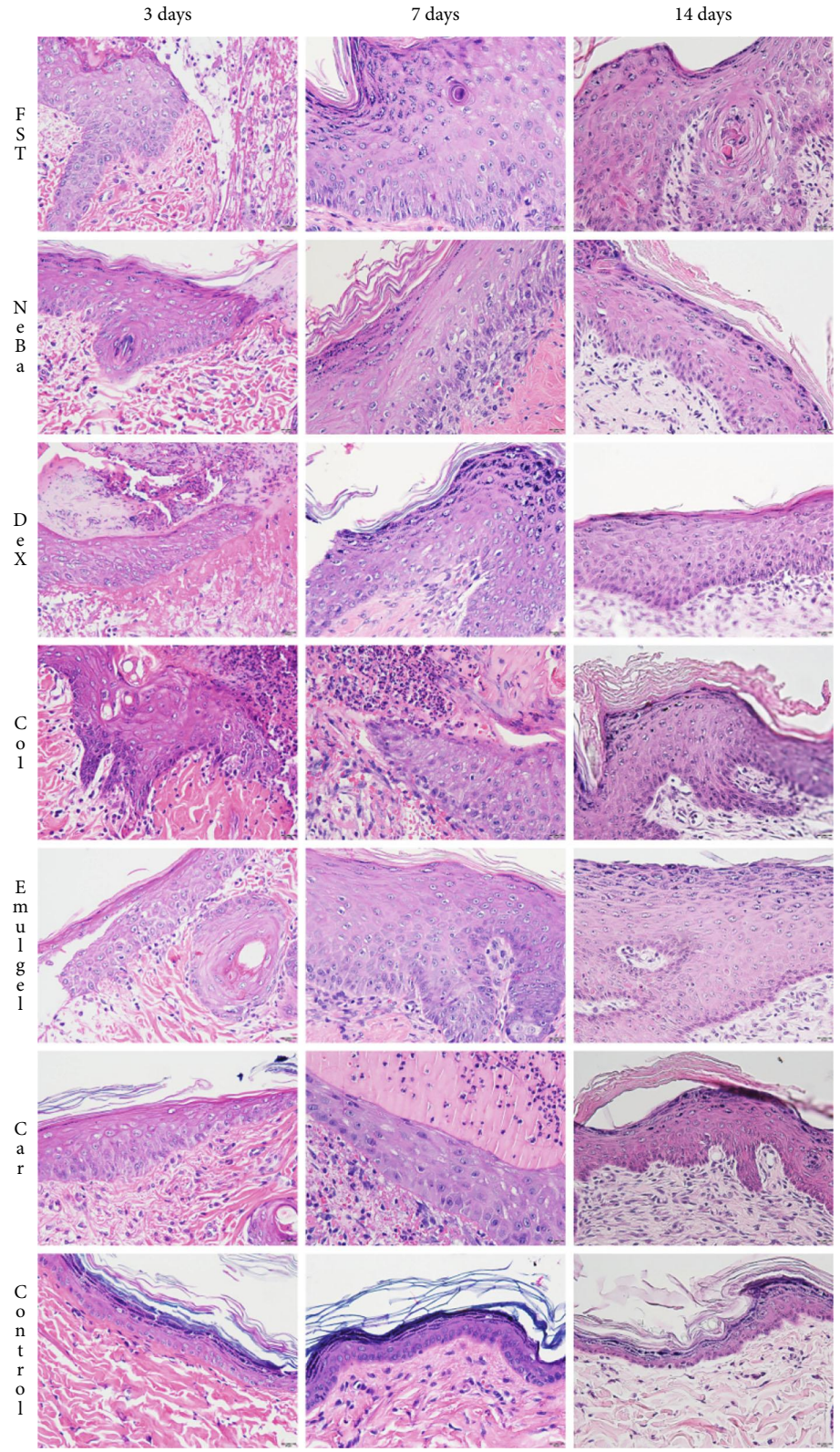

Figure 4: HE photomicrographs of the epidermis in FST, NeBa, Dex, Col, Emulgel, Car and Control groups during 3, 7 and 14 days.

AST, ALT and γ-GT are enzymes that catalyze reactions in some peptides and are highly expressed in hepatocytes. When drugs cause a toxic effect in the liver, there is an increase in these enzymes in blood flow, and they are used in the evaluation of hepatic toxicity [24]. Creatinine and urea are proteins physiologically synthesized by the body and are filtered by the kidneys for elimination from the organisms. The increase in plasma levels of these proteins

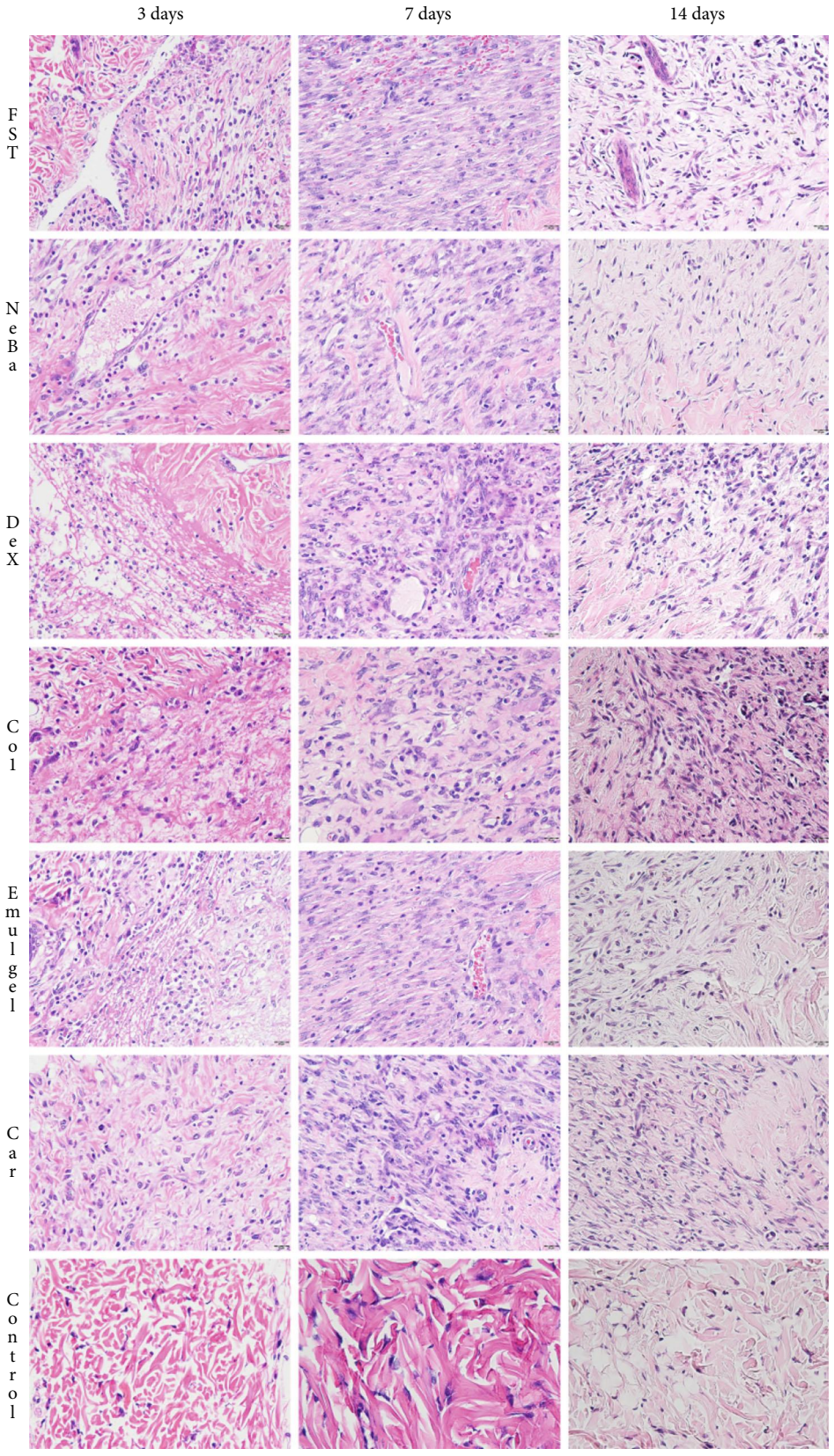

Figure 5: HE photomicrographs of the border of the wounds in the dermis of FST, NeBa, Dex, Col, Emulgel, Car and Control groups during 3, 7 and 14 days.

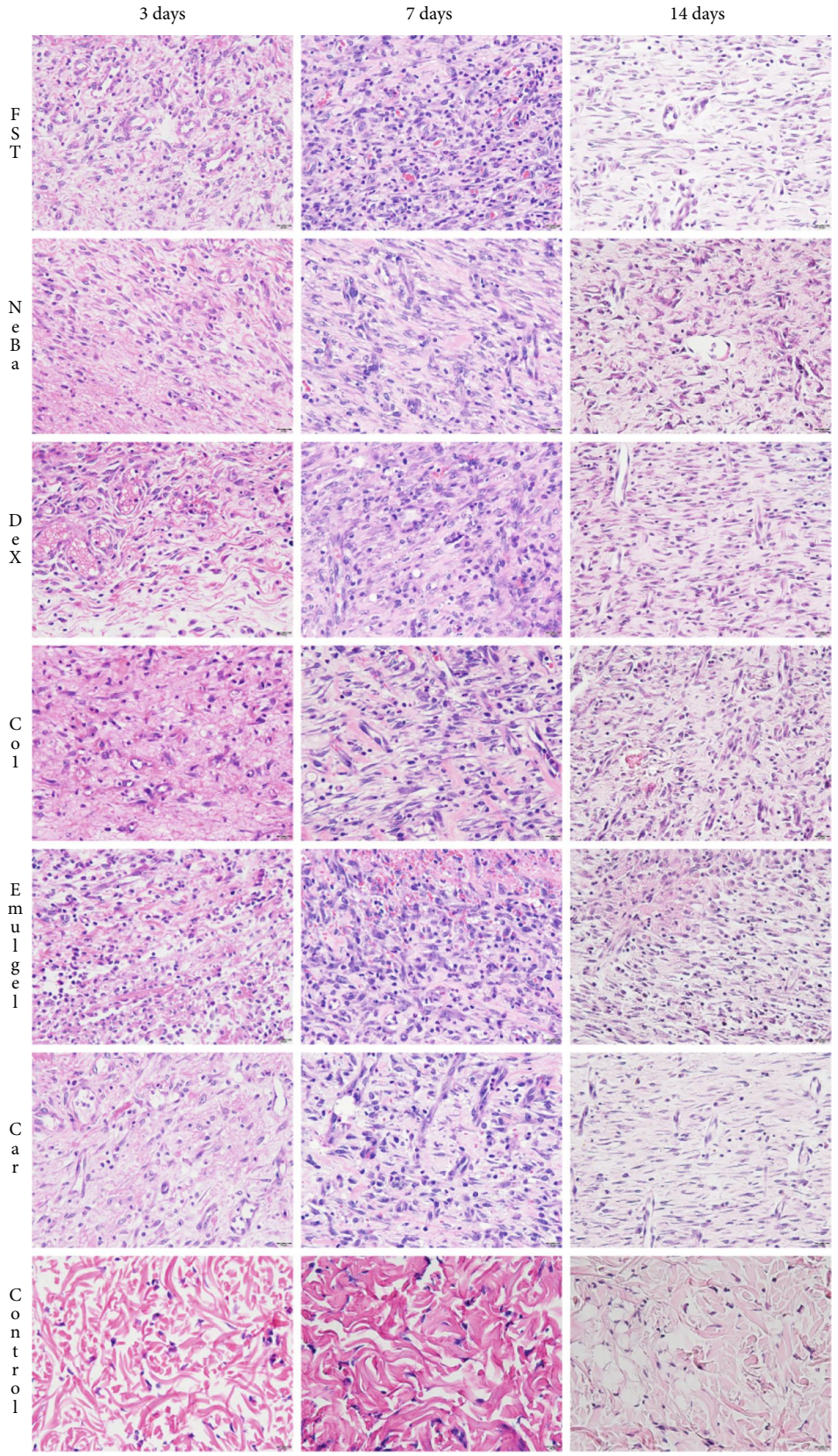

Figure 6: HE photomicrographs of the center of wounds in the dermis of FST, NeBa, Dex, Col, Emulgel, Car and Control groups during 3, 7 and 14 days.

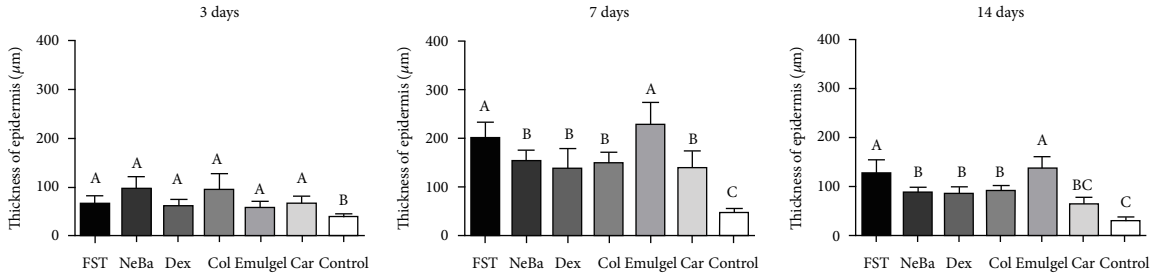

FIGURE 7: Thickness of epidermis (μm) of FST, NeBa, Dex, Col, Emulgel, Car and Control groups during 3, 7 and 14 days. Equal letters show no statistical difference and different letters indicate statistical difference compared to the other groups, according to the Kruskal-Wallis test, followed by the Dunn post-test, with $p \leq 0.05$ (n =5).

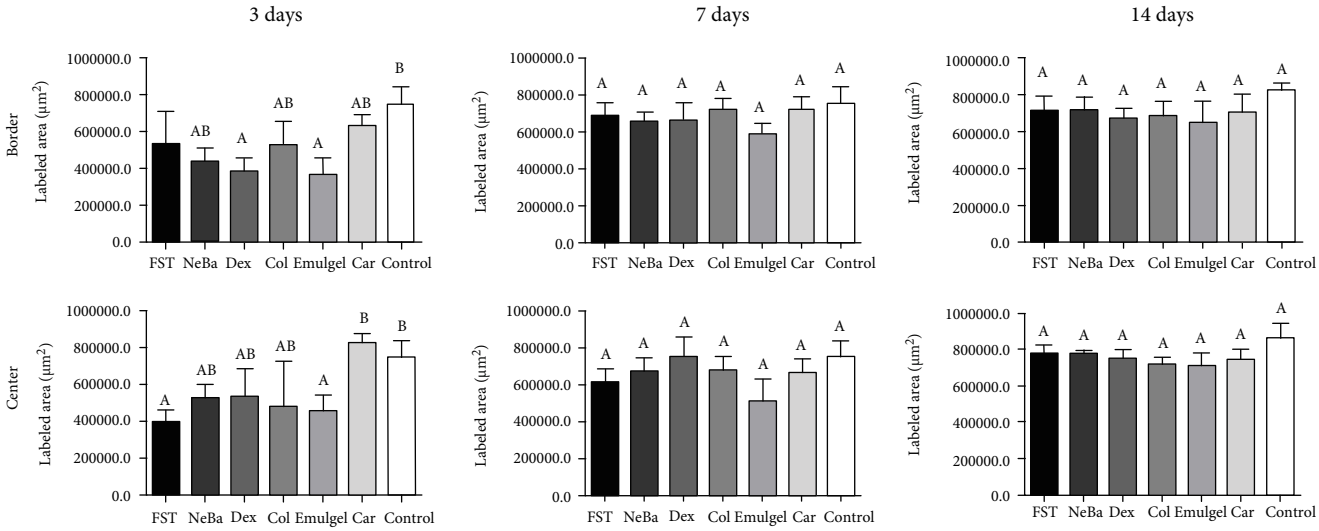

FIGURE 8: Quantification of collagen (μm^2) at the border and center of wounds of FST, NeBa, Dex, Col, Emulgel, Car and Control groups during 3, 7 and 14 days. Equal letters show no statistical difference and different letters indicate statistical difference compared to the other groups, according to the Kruskal-Wallis test, followed by the Dunn post-test, with $p \leq 0.05$ (n =5).

represents the instability of renal filtration due to a toxic effect [25]. The plasma levels of hepatic and renal proteins of β-caryophyllene and positive controls were similar to those measured for physiological quantification (Control), demonstrating that the local treatment containing the sesquiterpene did not have systemic toxicity.

Cutaneous injury results in the synthesis and release of mediators of the hemostatic cascade and the death of cells in the wounded area with the local release of reactive oxygen species (ROS) [26]. Although the released free radicals and ROS have important roles in the antimicrobial pathway, exacerbated release of ROS can cause chronic inflammation and impairment in the healing process, resulting in hypertrophic scars or unhealed wounds [27]. To control the concentration of ROS, the cells of the area synthesize antioxidant mediators that are involved in the superoxide and hydrogen peroxide pathways. Superoxide radicals are highly reactive molecules that are processed into hydrogen peroxide, a less reactive molecule, by SOD [16]. However, at high concentrations, hydrogen peroxide is a toxic compound to cells. Thus, hydrogen peroxide is metabolized by CAT and GPx (with consumption of GSH), resulting in water and oxygen molecules [18, 28]. Previous studies have reported the *in vitro* antioxidant potential of β-caryophyllene [8, 29], and our findings showing that GPx increased activity confirmed the antioxidant potential of β-caryophyllene in a rat excision wound model as well as in the NeBa and Col positive controls.

The inflammatory mechanism is essential for the correct healing of skin wounds. The IL-1β, IL-6 and TNF-α proinflammatory cytokines are involved in cell differentiation and proliferation, coordinating the synthesis of granulation tissue, angiogenesis, re-epithelialization and collagen remodeling mechanisms [30]. Furthermore, these cytokines are associated with IFN-γ to enhance the migration to and proliferation of leukocytes at the wound, improving the debridement of necrotic tissue and the phagocytosis of antigens [31]. IL-10 is another interleukin involved in the inflammatory mechanism of skin wounds, acting as an anti-inflammatory mediator inhibiting the synthesis of pro-inflammatory cytokines and playing a role in angiogenesis [32]. However, the imbalance among inflammatory cytokines can lead to a chronic inflammation process, resulting in errors in the subsequent healing mechanisms and the impairment of wound healing [33]. In the present study, the cytokine quantification data showed that the anti-

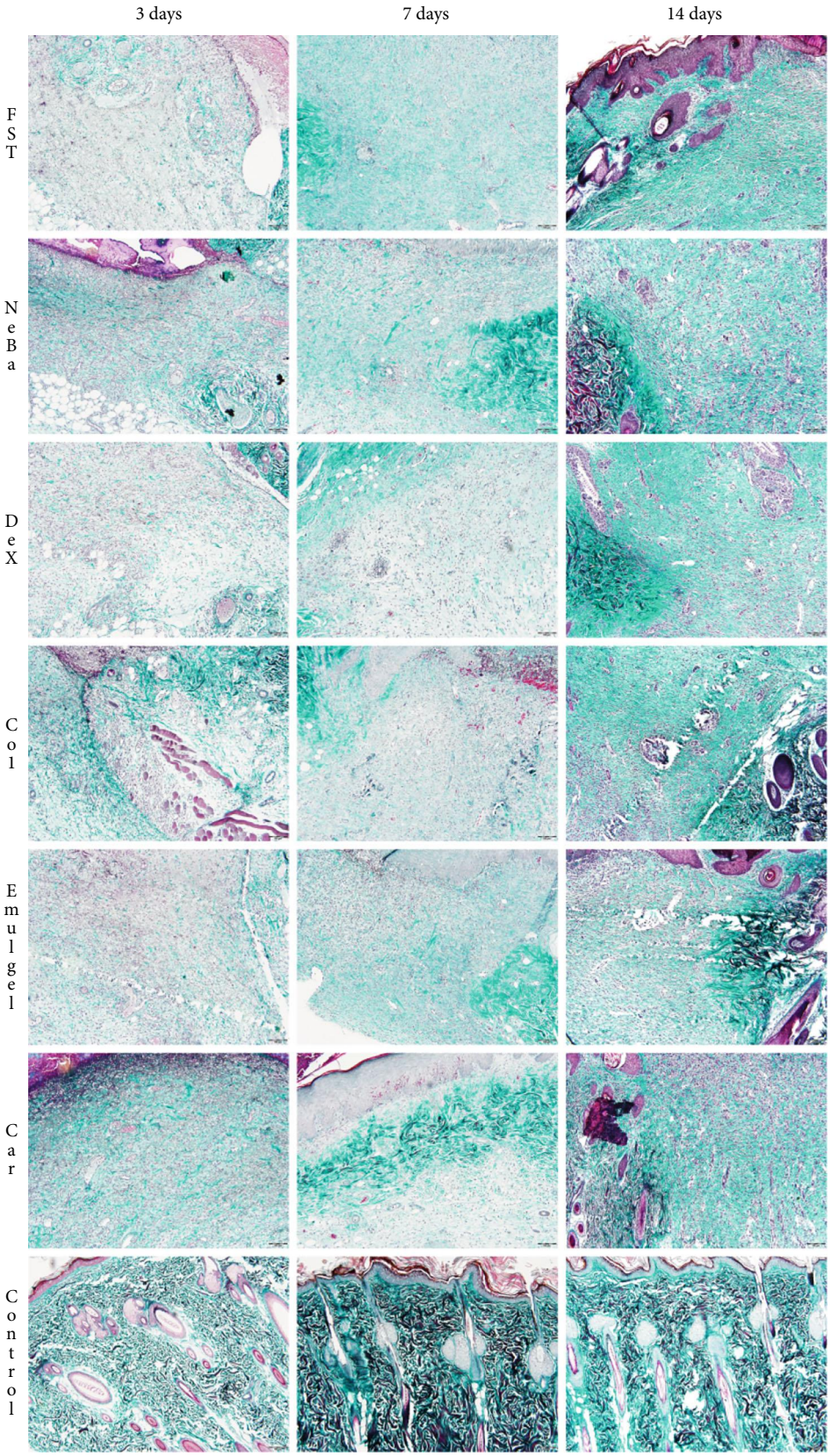

Figure 9: Masson's trichrome photomicrographs of the border of the wounds in the dermis of FST, NeBa, Dex, Col, Emulgel, Car and Control groups during 3, 7 and 14 days.

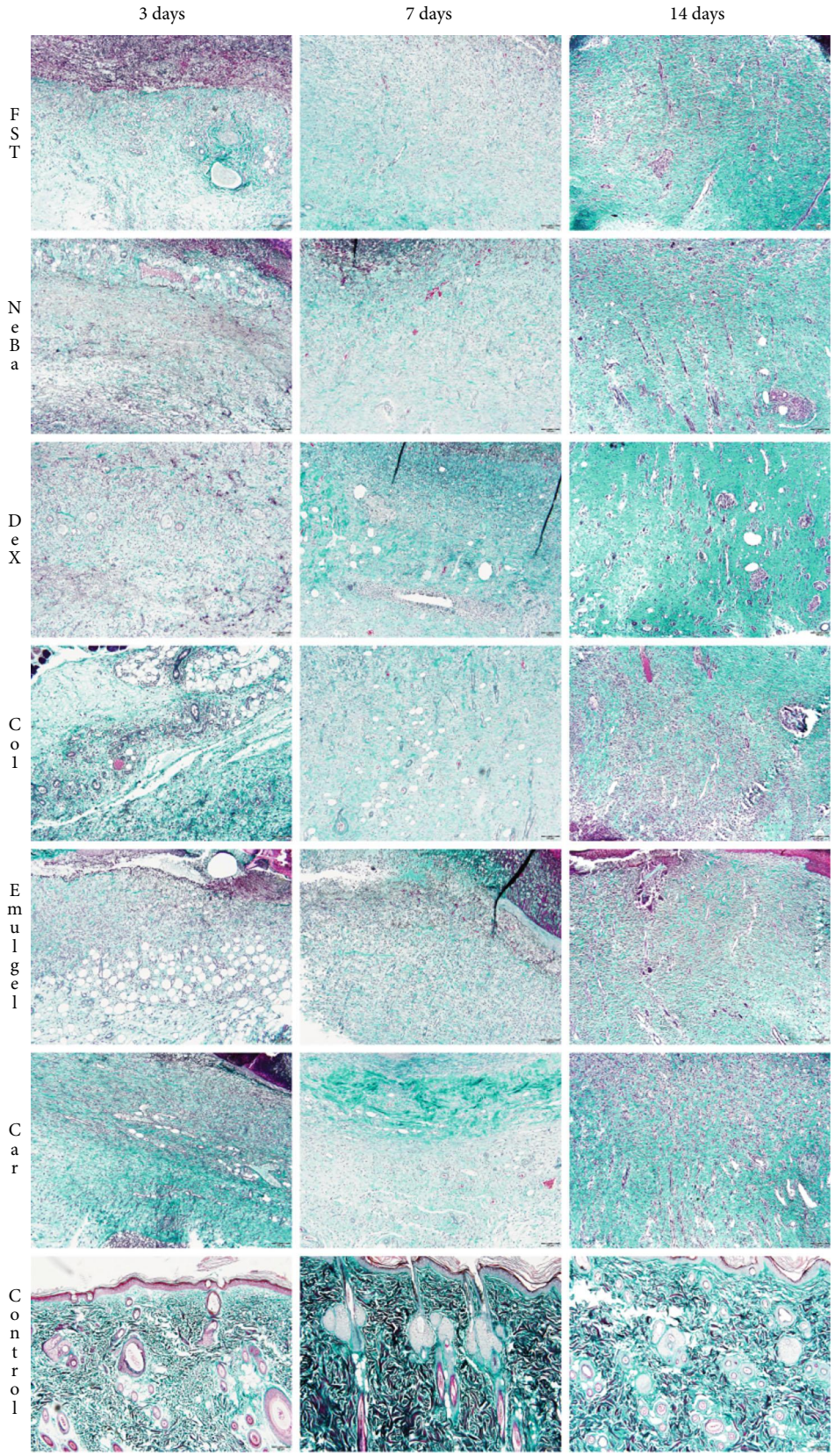

Figure 10: Masson's trichrome photomicrographs of the center of the wounds in the dermis of FST, NeBa, Dex, Col, Emulgel, Car and Control groups during 3, 7 and 14 days.

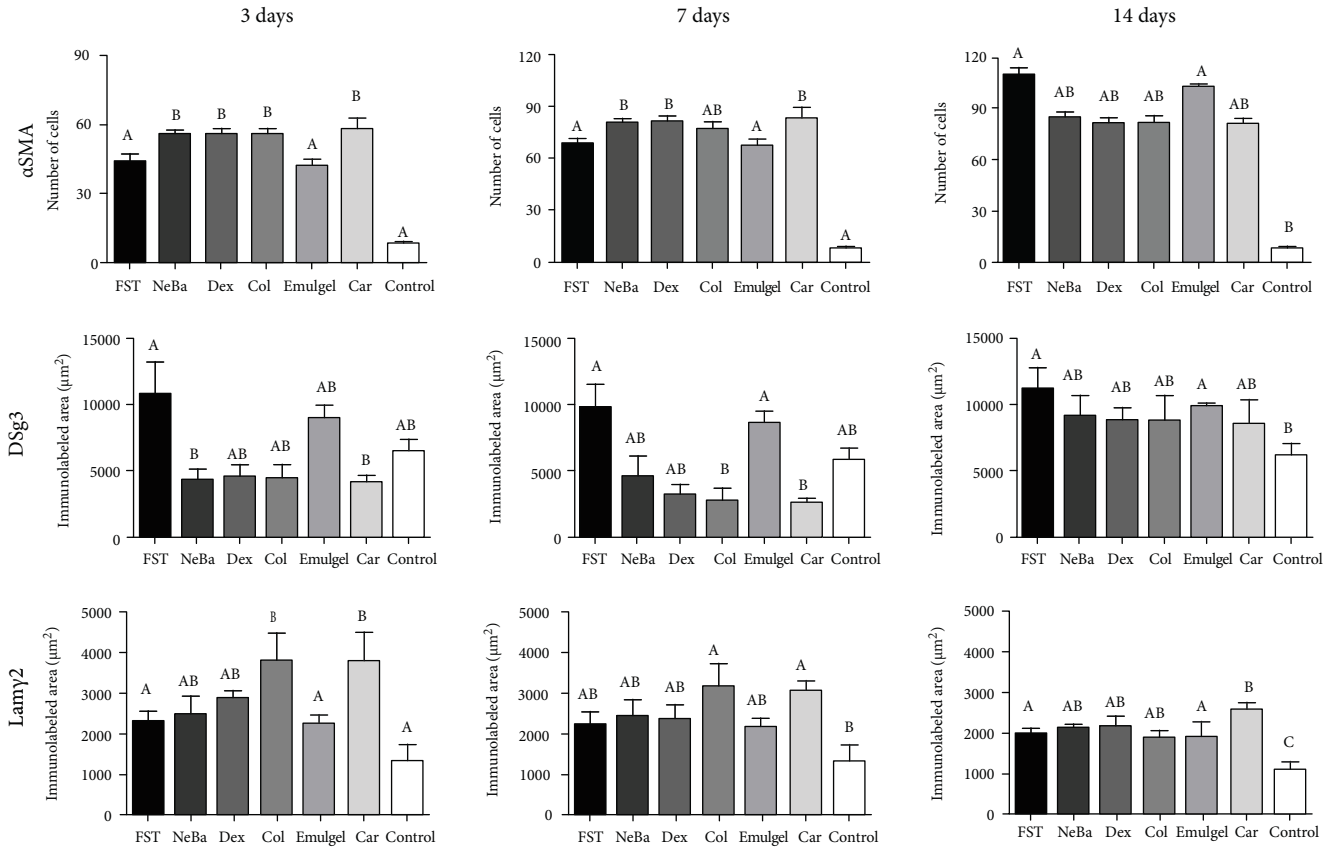

Figure 11: Immunolabeling of α-SMA, Dsg3 and Lamγ2 in wounds of FST, NeBa, Dex, Col, Emulgel, Car and Control groups during 3, 7 and 14 days. Equal letters show no statistical difference and different letters indicate statistical difference compared to the other groups, according to the Kruskal-Wallis test, followed by the Dunn post-test, with $p \leq 0.05$ ($n = 5$).

inflammatory activity of β-caryophyllene in cutaneous wounds was due to the reduction in IFN-γ, IL-1β, IL-6 and TNF-α levels as well as the increase in IL-10 level with anti-inflammatory potential similar to NeBa, Dex and Col.

Another mechanism of wound healing involves the contraction of wounds with the interaction of fibroblasts and extracellular matrix proteins resulting in wound closure [34]. TGF-β1 is a growth factor involved in mechanisms in all phases of wound healing, including the differentiation of fibroblasts. Through TGF-β1 stimulation, fibroblasts located at the border of injuries synthesize α-SMA, an intracellular stress fiber protein, acquiring a contractile phenotype and differentiating into myofibroblasts [35]. The myofibroblasts bind to the collagen I extracellular fibers and initiate the contraction of the stress fibers, reducing the wounded area. [35]. Thus, the role of the β-caryophyllene formulation in wound contraction was validated through macroscopic evaluation, in which a decrease in wounded area was observed in groups treated with β-caryophyllene, neomycin/bacitracin and collagenase. Moreover, the immunohistochemical data of α-SMA suggested that the increase of wound contraction of these groups was mediated by α-SMA as indicated by the increase of immunolabeling of this protein in these treatments.

Re-epithelialization is important in cutaneous wound healing with the proliferation and migration of keratinocytes from the border of injuries. First, proteinases dissolve adhesion molecules among keratinocytes, such as desmoglein-3. These cells proliferate and synthesize the anchoring protein, laminin-γ2, to assist in keratinocyte migration through the extracellular matrix, coordinating the re-epithelialization mechanism [36, 37]. However, the overexpression of proliferating mediators causes the hyperproliferation of keratinocytes at the wounds with an increase of epidermis thickness as a marker of keloid formation [38]. Therefore, the histological results of epidermis thickness and the immunohistochemical data of keratinocyte proliferation (Ki-67), desmoglein-3 and laminin-γ2 demonstrated that β-caryophyllene and collagenase treatments enhanced the re-epithelialization mechanism in which desmoglein-3 and laminin-γ2 involved during the migration of cells. Our findings corroborated the results of Koyama et al. [39], who reported enhanced re-epithelialization of skin wounds after treatment with β-caryophyllene oil in mice [39].

Finally, the provisional extracellular matrix is replaced by permanent tissue to initiate the remodeling mechanism. In this process, type III collagen and other components of the provisional matrix are metabolized by extracellular matrix metalloproteinases. Simultaneously, compounds, such as type I collagen, elastin and proteoglycans, are synthesized and organized as more resistant tissues, and excess myofibroblasts, fibroblasts and endothelial cells proliferate

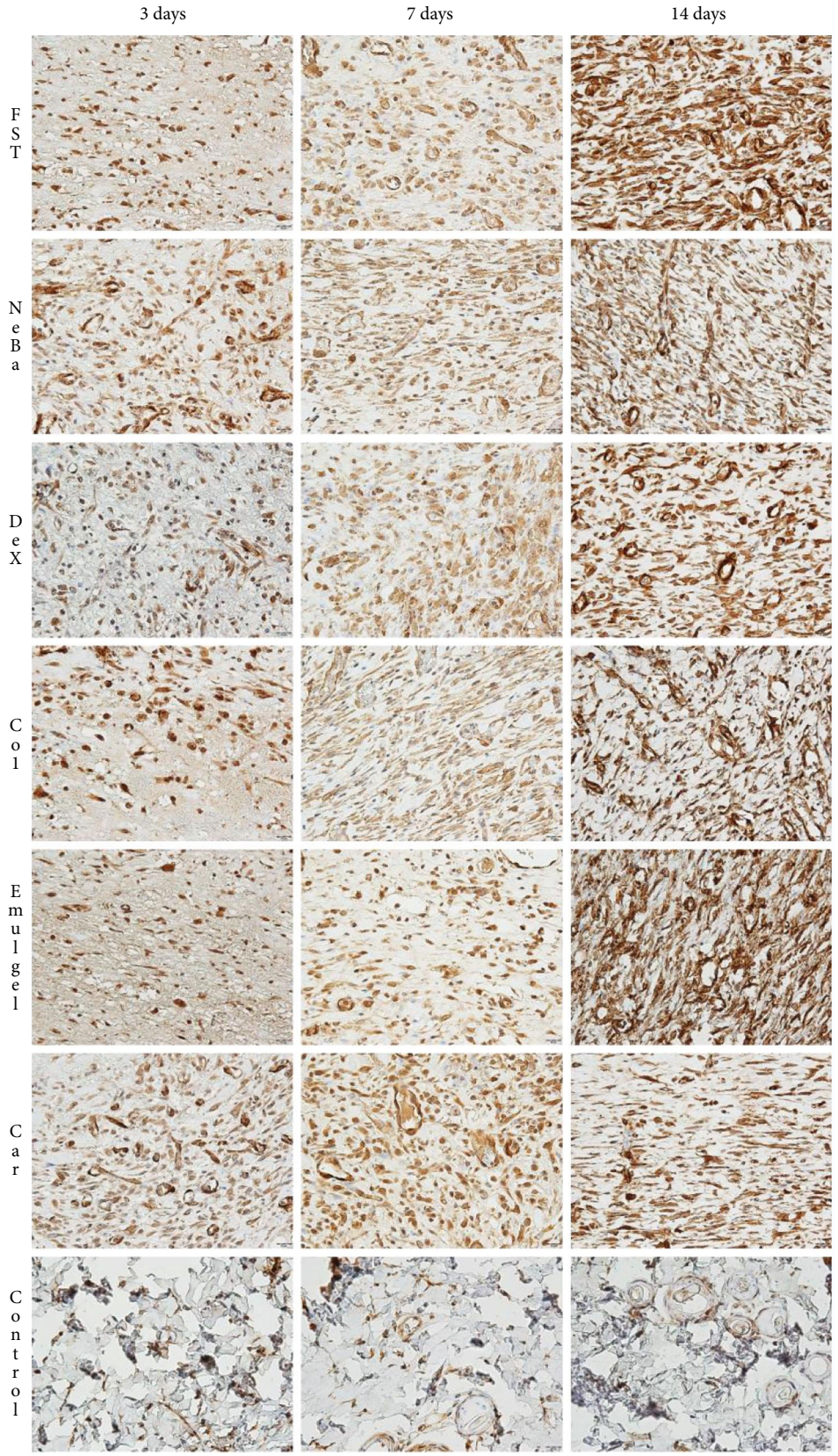

Figure 12: Photomicrographs of the immunolabeling of α-SMA in wounds of FST, NeBa, Dex, Col, Emulgel, Car and Control groups during 3, 7 and 14 days.

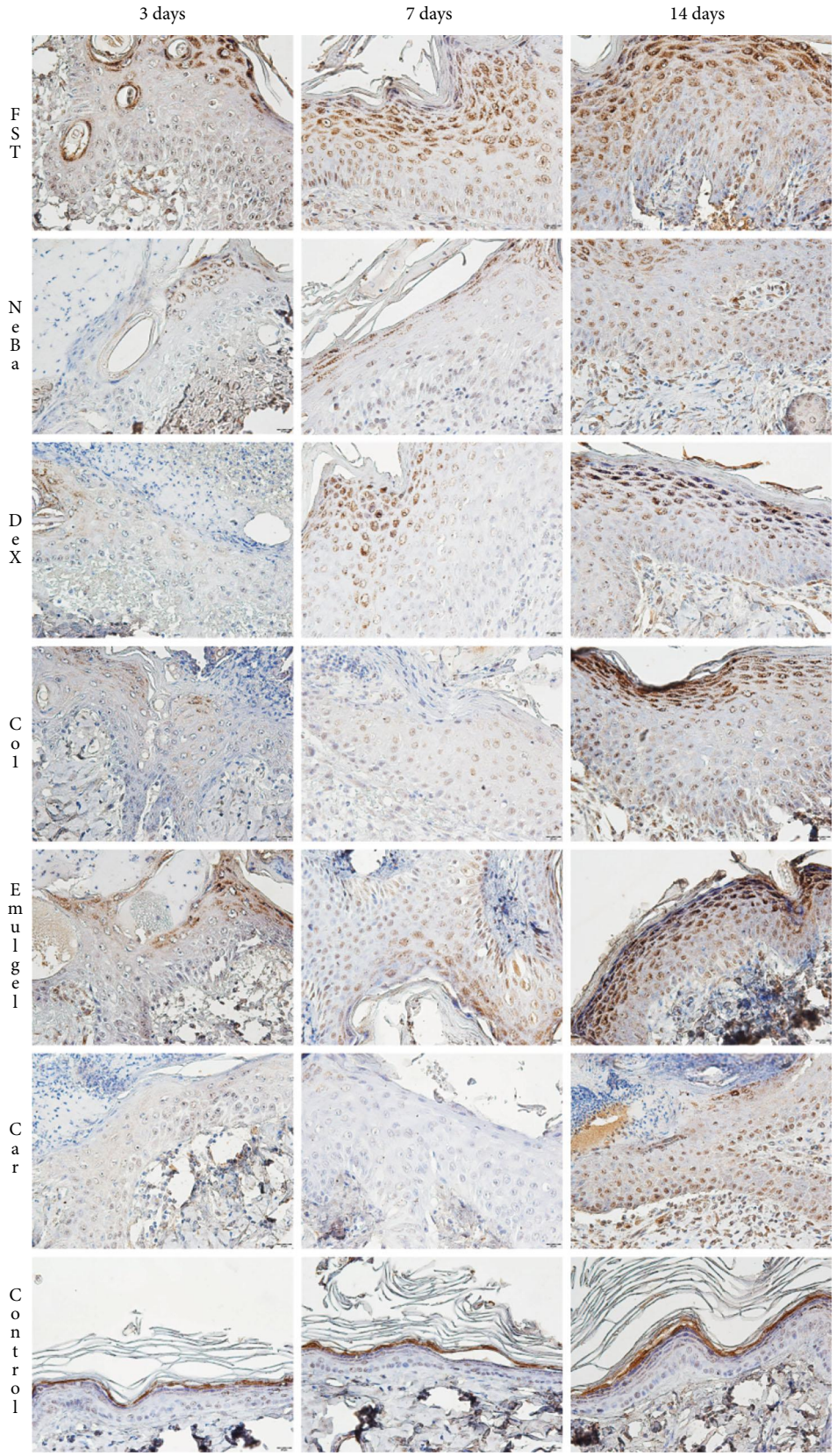

Figure 13: Photomicrographs of the immunolabeling of Dsg3 in wounds of FST, NeBa, Dex, Col, Emulgel, Car and Control groups during 3, 7 and 14 days.

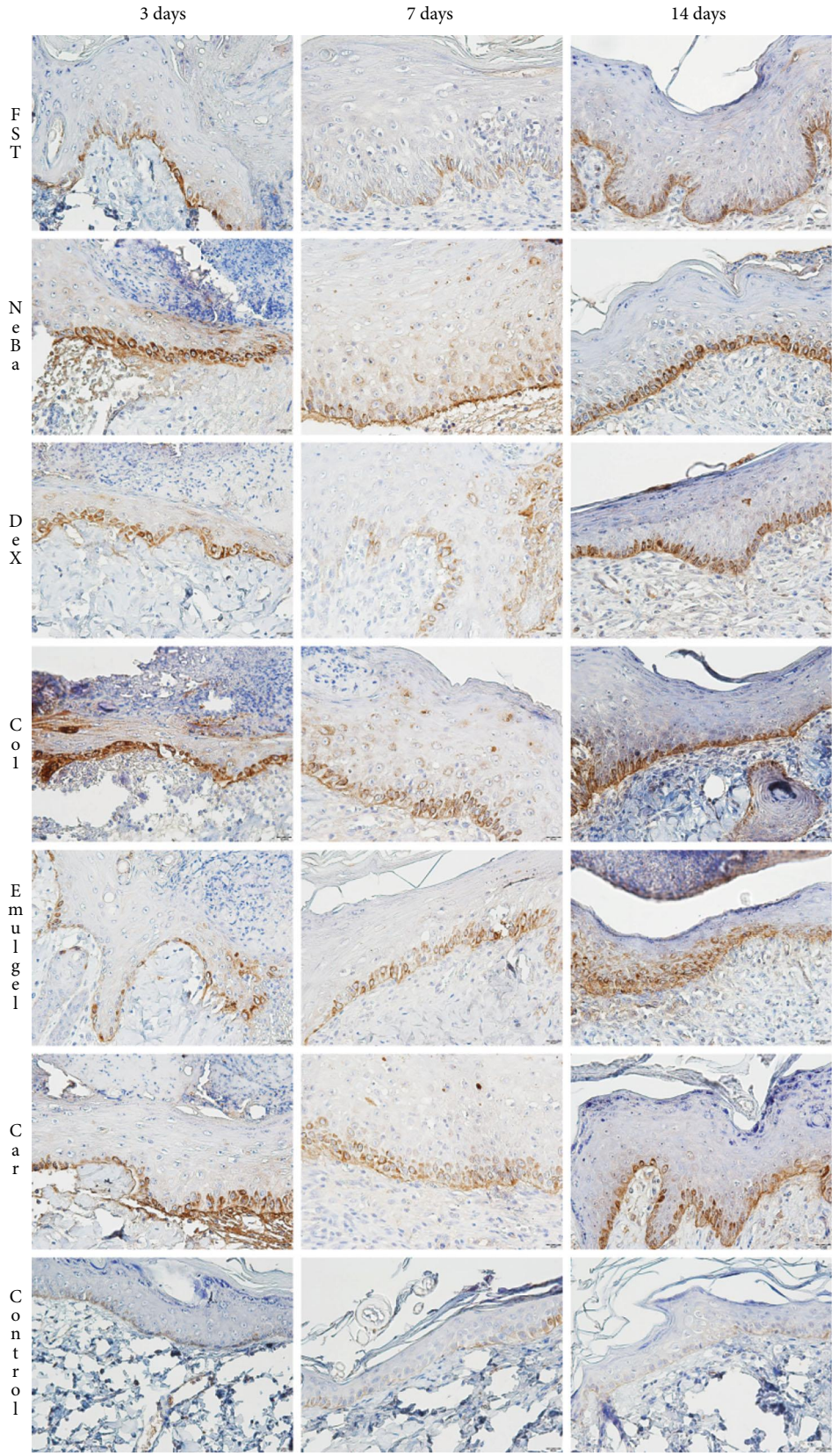

Figure 14: Photomicrographs of the immunolabeling of Lamγ2 in wounds of FST, NeBa, Dex, Col, Emulgel, Car and Control groups during 3, 7 and 14 days.

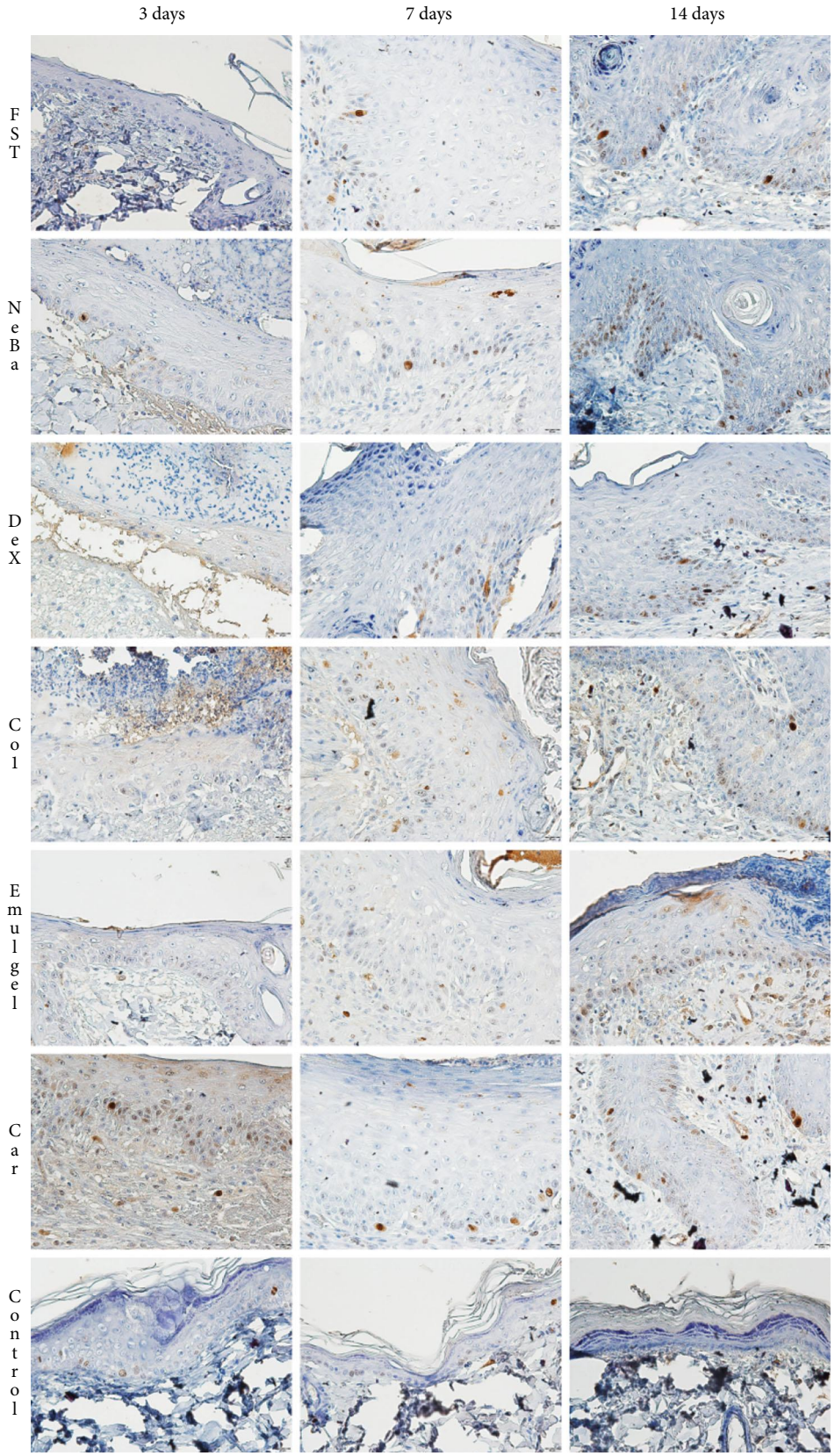

Figure 15: Photomicrographs of the immunolabeling of Ki-67 in the epidermis of FST, NeBa, Dex, Col, Emulgel, Car and Control groups during 3, 7 and 14 days.

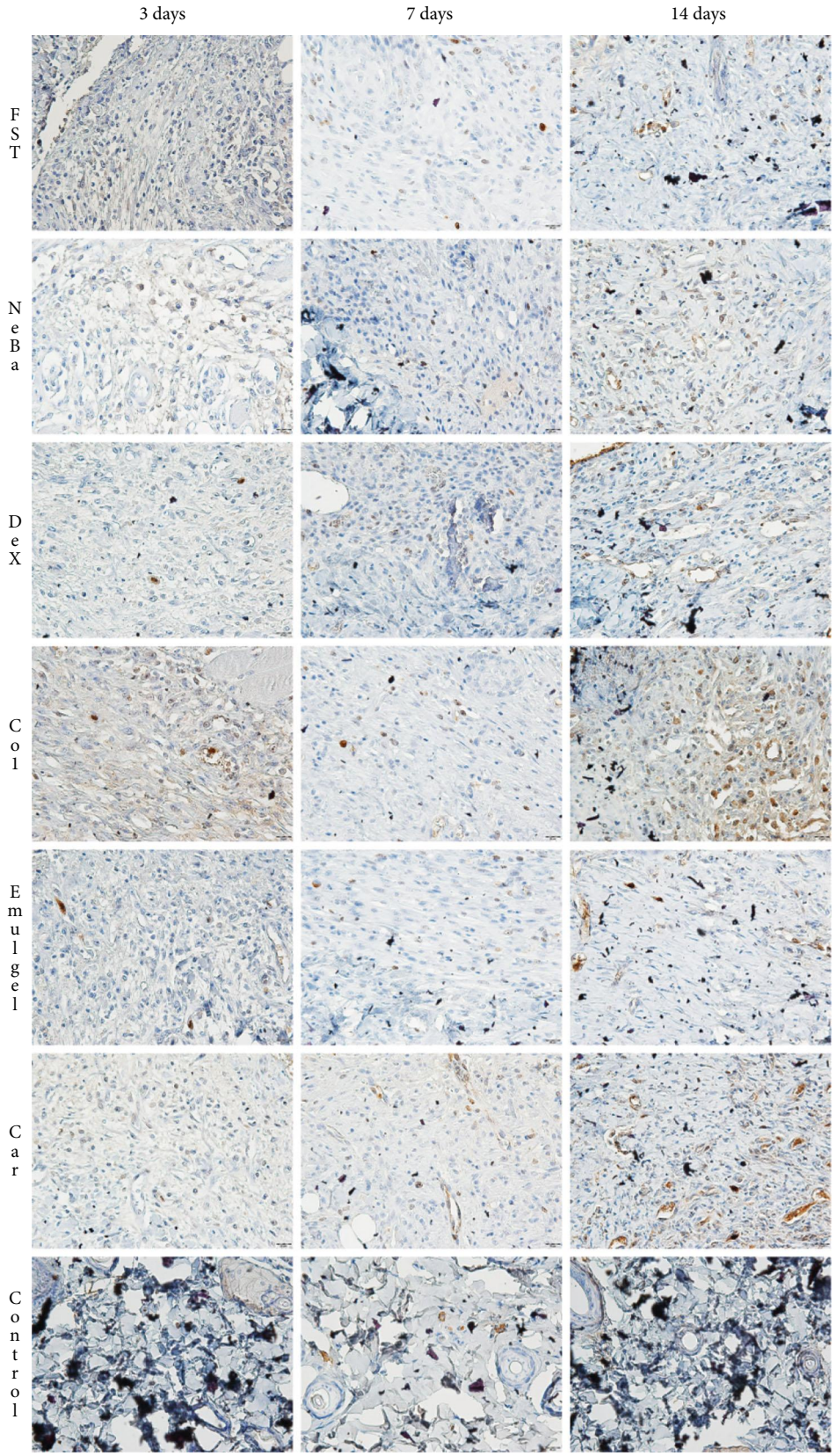

Figure 16: Photomicrographs of the immunolabeling of Ki-67 of the border of the wounds in the dermis of FST, NeBa, Dex, Col, Emulgel, Car and Control groups during 3, 7 and 14 days.

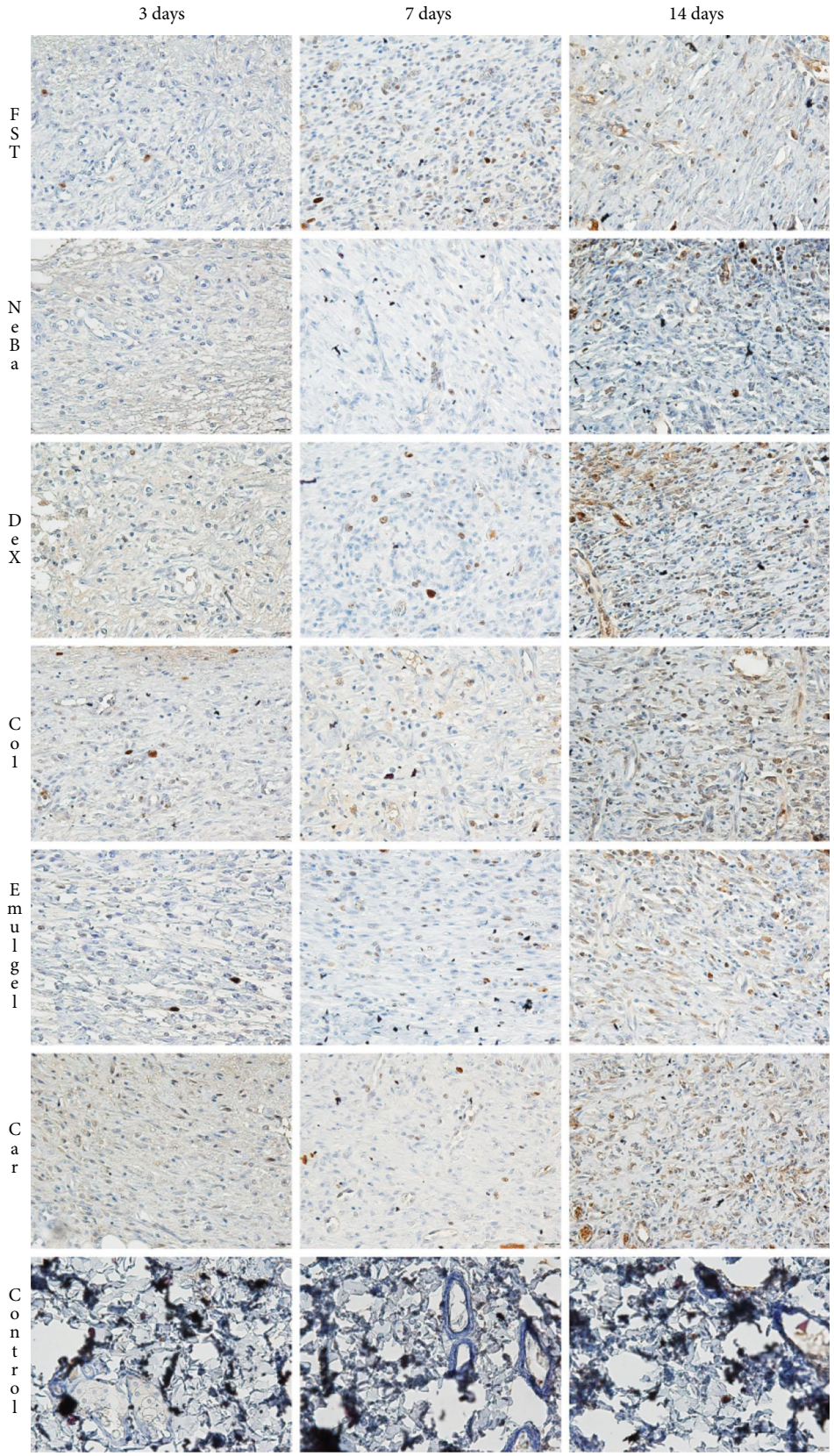

Figure 17: Photomicrographs of the immunolabeling of Ki-67 of the center of the wounds in the dermis of FST, NeBa, Dex, Col, Emulgel, Car and Control groups during 3, 7 and 14 days.

during healing and undergo apoptosis [40]. Our histological evaluation results of Masson's trichrome staining suggested the role of β-caryophyllene in skin repair, increasing collagen synthesis in the central area of wounds during the first period of cutaneous healing with better results in the remodeling mechanism compared to the reference drugs.

5. Conclusions

Considering our results, we conclude that the emulgel formulation containing 1% β-caryophyllene enhances *in vivo* skin wound healing through antioxidant, anti-inflammatory, wound contraction, re-epithelialization and remodeling mechanisms. Our results demonstrated the potential of β-caryophyllene in skin wound therapy compared with three reference drugs, with better results in wound healing compared to reference drugs. Furthermore, the analysis of hepatic and renal parameters confirmed the safety of the tested formulation by showing that there was no systemic toxicity. Therefore, this study provides good evidence that 1% β-caryophyllene has great potential for use in treating full-thickness skin wounds, demonstrating the safety and effectiveness of this drug as a future alternative treatment for wound healing.

Abbreviations

α-SMA:	α-Smooth muscle actin
γ-GT:	γ-Glutamyl transferase
ALT:	Alanine aminotransferase
ANOVA:	Analysis of variance
AST:	Aspartate aminotransferase
CAT:	Catalase
Dsg3:	Desmoglein-3
ELISA:	Enzyme-linked immunosorbent assay
GPx:	Glutathione peroxidase
GSH:	Reduced glutathione
HE:	Hematoxylin and eosin
HRP/DAB:	Horseradish peroxidase/diaminobenzidine
IBB:	Institute of Biosciences of Botucatu
IFN-γ:	Interferon-γ
IL-10:	Interleukin-10
IL-1β:	Interleukin-1β
IL-6:	Interleukin-6
IU:	International units
Lamγ2:	Laminin-γ2
MMP:	Extracellular matrix metaloproteinases
ROS:	Reactive oxygen species
SOD:	Superoxide dismutase
TNF-α:	Tumor necrosis factor-α
UK:	United Kingdom
UNESP:	São Paulo State University
USA:	United States of America.

Data Availability

The informations used to support the findings of this study are included within the article.

Conflicts of Interest

The authors declare no conflict of interest.

Acknowledgments

We would like to thank to São Paulo State University, Institute of Biosciences of Botucatu and São Paulo Research Foundation (FAPESP) for the grant support: 2011/13630-7, 2017/04138-8 and 2017/17600-1.

Supplementary Materials

Supplementary data associated with this article can be found, in the online version of the paper. *(Supplementary Materials)*

References

[1] S. Javanmardi, I. Safari, F. Aghaz, and M. Khazaei, "Wound healing activities of *Gundelia tournefortii* L extract and Milk-cream ointment on second-degree burns of rat skin," *International Journal of Lower Extremity Wounds*, vol. 20, no. 3, pp. 272–281, 2020.

[2] C. K. Sen, "Human wounds and its burden: an updated compendium of estimates," *Advances in Wound Care*, vol. 8, no. 2, pp. 39–48, 2019.

[3] C. Morin, A. Roumegous, G. Carpentier et al., "Modulation of inflammation by Cicaderma ointment accelerates skin wound healing," *Journal of Pharmacology and Experimental Therapeutics*, vol. 343, no. 1, pp. 115–124, 2012.

[4] S.-M. Karppinen, R. Heljasvaara, D. Gullberg, K. Tasanen, and T. Pihlajaniemi, "Toward Understanding Scarless Skin Wound Healing and Pathological Scarring," *F1000Research*, vol. 8, p. 787, 2019.

[5] R. S. Ward and J. R. Saffle, "Topical agents in burn and wound care," *Physical Therapy*, vol. 75, no. 6, pp. 526–538, 1995.

[6] R. C. Rennert, M. Rodrigues, V. W. Wong et al., "Biological therapies for the treatment of cutaneous wounds: phase III and launched therapies," *Expert Opinion on Biological Therapy*, vol. 13, no. 11, pp. 1523–1541, 2013.

[7] H. I. Cho, J.-M. Hong, J.-W. Choi et al., "β-Caryophyllene alleviates d-galactosamine and lipopolysaccharide-induced hepatic injury through suppression of the TLR4 and RAGE signaling pathways," *European Journal of Pharmacology*, vol. 764, pp. 613–621, 2015.

[8] S. S. Dahham, Y. Tabana, M. Iqbal et al., "The anticancer, antioxidant and antimicrobial properties of the Sesquiterpene β-Caryophyllene from the essential oil of Aquilaria Crassna," *Molecules*, vol. 20, no. 7, pp. 11808–11829, 2015.

[9] J. Gertsch, M. Leonti, S. Raduner et al., "Beta-caryophyllene is a dietary cannabinoid," *Proceedings of the National Academy of Sciences of the United States of America*, vol. 105, no. 26, pp. 9099–9104, 2008.

[10] J. I. Jung, E. J. Kim, G. T. Kwon et al., "β-Caryophyllene potently inhibits solid tumor growth and lymph node metastasis of B16F10 melanoma cells in high-fat diet-induced obese C57BL/6N mice," *Carcinogenesis*, vol. 36, no. 9, pp. 1028–1039, 2015.

[11] L. F. S. Gushiken, C. A. Hussni, J. K. Bastos et al., "Skin Wound Healing Potential and Mechanisms of the Hydroalcoholic

Extract of Leaves and Oleoresin of Copaifera langsdorffii Desf. Kuntze in Rats," *Evidence-based Complementary and Alternative Medicine*, vol. 2017, Article ID 6589270, 16 pages, 2017.

[12] V. P. Ribeiro, C. Arruda, J. J. M. da Silva, J. A. Aldana Mejia, N. A. J. C. Furtado, and J. K. Bastos, "Use of spinning band distillation equipment for fractionation of volatile compounds ofCopaiferaoleoresins for developing a validated gas chromatographic method and evaluating antimicrobial activity," *Biomedical Chromatography*, vol. 33, no. 2, pp. 1–12, 2019.

[13] CONCEA, Conselho Nacional de Controle de Experimentação Animal, *Resolução Normativa N°33*, Diário Oficial Da União, 2016, https://www.in.gov.br/materia/-/asset_publisher/Kujrw0TZC2Mb/content/id/22073702/do1-2016-11-21-resolucao-normativa-n-33-de-18-de-novembro-de-2016-22073453.

[14] Y. Lim, M. A. Levy, and T. M. Bray, "Dietary supplementation of *N*-acetylcysteine enhances early inflammatory responses during cutaneous wound healing in protein malnourished mice," *The Journal of Nutritional Biochemistry*, vol. 17, no. 5, pp. 328–336, 2006.

[15] J. H. Zar, *Biostatistical Analysis*, Prentice-Hall, New Jersey, 5th edition, 2009.

[16] C. C. Winterbourn, R. E. Hawkins, M. Brian, and R. W. Carrell, "The estimation of red cell superoxide dismutase activity," *The Journal of Laboratory and Clinical Medicine*, vol. 85, no. 2, pp. 337–341, 1975.

[17] H. Aebi, "[13] Catalase *in vitro*," *Methods in Enzymology*, vol. 105, pp. 121–126, 1984.

[18] T. Yoshikawa, Y. Naito, A. Kishi et al., "Role of active oxygen, lipid peroxidation, and antioxidants in the pathogenesis of gastric mucosal injury induced by indomethacin in rats," *Gut*, vol. 34, no. 6, pp. 732–737, 1993.

[19] P. Faure and J.-L. Lafond, "Measurement of plasma sulfhydryl and carbonyl groups as a possible indicator of protein oxidation," in *Analysis of Free Radicals in Biological Systems*, pp. 237–248, Birkhäuser Basel, Basel, 1995.

[20] J. P. B. Sousa, A. P. S. Brancalion, A. B. Souza et al., "Validation of a gas chromatographic method to quantify sesquiterpenes in copaiba oils," *Journal of Pharmaceutical and Biomedical Analysis*, vol. 54, no. 4, pp. 653–659, 2011.

[21] J. Gorski, E. Proksch, J. M. Baron, D. Schmid, and L. Zhang, "Dexpanthenol in wound healing after medical and cosmetic interventions (Postprocedure wound healing)," *Pharmaceuticals*, vol. 13, no. 7, p. 138, 2020.

[22] J. R. Mekkes, J. E. Zeegelaar, and W. Westerhof, "Quantitative and objective evaluation of wound debriding properties of collagenase and Fibrinolysin/Desoxyribonuclease in a necrotic ulcer animal model," *Archives of Dermatological Research*, vol. 290, no. 3, pp. 152–157, 1998.

[23] A. Tallis, T. A. Motley, R. P. Wunderlich et al., "Clinical and Economic Assessment of Diabetic Foot Ulcer Debridement with Collagenase: Results of a Randomized Controlled Study," *Clinical Therapeutics*, vol. 35, no. 11, pp. 1805–1820, 2013.

[24] E. G. Giannini, R. Testa, and V. Savarino, "Liver enzyme alteration: A guide for clinicians," *CMAJ*, vol. 172, no. 3, pp. 367–379, 2005.

[25] J. Traynor, R. Mactier, C. C. Geddes, and J. G. Fox, "How to measure renal function in clinical practice," *British Medical Journal*, vol. 333, no. 7571, pp. 733–737, 2006.

[26] S. Murthy, M. K. Gautam, S. Goel, V. Purohit, H. Sharma, and R. K. Goel, "Evaluation of In Vivo Wound Healing Activity of Bacopa monniera on Different Wound Model in Rats," *BioMed Research International*, vol. 2013, Article ID 972028, 9 pages, 2013.

[27] M.-J. Kwon, B. H. Kim, Y. S. Lee, and T.-Y. Kim, "Role of superoxide dismutase 3 in skin inflammation," *Journal of Dermatological Science*, vol. 67, no. 2, pp. 81–87, 2012.

[28] S. Soman, A. A. Rauf, M. Indira, and C. Rajamanickam, "Antioxidant and Antiglycative potential of ethyl acetate fraction of Psidium Guajava leaf extract in Streptozotocin-induced diabetic rats," *Plant Foods for Human Nutrition*, vol. 65, no. 4, pp. 386–391, 2010.

[29] M. A. Calleja, J. M. Vieites, T. Montero-Meterdez et al., "The antioxidant effect of β-Caryophyllene protects rat liver from carbon tetrachloride-induced fibrosis by inhibiting hepatic stellate cell activation," *British Journal of Nutrition*, vol. 109, no. 3, pp. 394–401, 2013.

[30] M. B. Serra, W. A. Barroso, N. N. d. Silva et al., "From Inflammation to Current and Alternative Therapies Involved in Wound Healing," *International Journal of Inflammation*, vol. 2017, Article ID 3406215, 17 pages, 2017.

[31] W. Wagner and M. Wehrmann, "Differential cytokine activity and morphology during wound healing in the neonatal and adult rat skin," *Journal of Cellular and Molecular Medicine*, vol. 11, no. 6, pp. 1342–1351, 2007.

[32] Y. Sato, T. Ohshima, and T. Kondo, "Regulatory Role of Endogenous Interleukin-10 in Cutaneous Inflammatory Response of Murine Wound Healing," *Biochemical and Biophysical Research Communications*, vol. 265, no. 1, pp. 194–199, 1999.

[33] R. Zhao, H. Liang, E. Clarke, C. Jackson, and M. Xue, "Inflammation in chronic wounds," *International Journal of Molecular Sciences*, vol. 17, no. 12, p. 2085, 2016.

[34] R. Agha, R. Ogawa, G. Pietramaggiori, and D. P. Orgill, "A Review of the Role of Mechanical Forces in Cutaneous Wound Healing," *The Journal of Surgical Research*, vol. 171, no. 2, pp. 700–708, 2011.

[35] I. A. Darby, B. Laverdet, F. Bonté, and A. Desmoulière, "Fibroblasts and Myofibroblasts in wound healing," *Clinical, Cosmetic and Investigational Dermatology*, vol. 7, pp. 301–311, 2014.

[36] G. Fisher and L. Rittié, "Restoration of the basement membrane after wounding: A Hallmark of young human skin altered with aging," *Journal of Cell Communication and Signaling*, vol. 12, no. 1, pp. 401–411, 2017.

[37] V. Rötzer, E. Hartlieb, J. Winkler et al., "Desmoglein 3-Dependent Signaling Regulates Keratinocyte Migration and Wound Healing," *Journal of Investigative Dermatology*, vol. 136, no. 1, pp. 301–310, 2016.

[38] G. C. Limandjaja, F. B. Niessen, R. J. Scheper, and S. Gibbs, "The keloid disorder: heterogeneity, histopathology, mechanisms and models," *Frontiers in Cell and Developmental Biology*, vol. 8, p. 360, 2020.

[39] S. Koyama, A. Purk, M. Kaur et al., "Beta-caryophyllene enhances wound healing through multiple routes," *PLoS One*, vol. 14, no. 12, article e0216104, 2019.

[40] G. C. Gurtner and M. A. Chapman, "Regenerative Medicine: charting a new course in wound healing," *Advances in Wound Care*, vol. 5, no. 7, pp. 314–328, 2016.

Hindawi
Oxidative Medicine and Cellular Longevity
Volume 2021, Article ID 9264639, 13 pages
https://doi.org/10.1155/2021/9264639

Review Article

Effects of Curcumin Supplementation on Inflammatory Markers, Muscle Damage, and Sports Performance during Acute Physical Exercise in Sedentary Individuals

Kelly Aparecida Dias[1], **Aline Rosignoli da Conceição**[1], **Lívya Alves Oliveira**[1], **Stephanie Michelin Santana Pereira**[1], **Stefany da Silva Paes**[1], **Larissa Farias Monte**[1], **Mariáurea Matias Sarandy**[2], **Rômulo Dias Novaes**[3], **Reggiani Vilela Gonçalves**[2] and **Ceres Mattos Della Lucia**[1]

[1]*Department of Nutrition and Health, Universidade Federal de Viçosa, Viçosa, Minas Gerais, Brazil*
[2]*Department of General Biology, Universidade Federal de Viçosa, Viçosa, Minas Gerais, Brazil*
[3]*Department of Structural Biology, Universidade Federal de Alfenas, Alfenas, Minas Gerais, Brazil*

Correspondence should be addressed to Ceres Mattos Della Lucia; cmdellalucia@ufv.br

Received 8 July 2021; Accepted 23 September 2021; Published 7 October 2021

Academic Editor: Dragan Hrnčić

Exhaustive and acute unusual physical exercise leads to muscle damage. Curcumin has been widely studied due to the variety of its biological activities, attributed to its antioxidant and anti-inflammatory properties. Furthermore, it has shown positive effects on physical exercise practitioners. However, there is no literature consensus on the beneficial effects of curcumin in acute physical activities performed by sedentary individuals. Therefore, we systematically reviewed evidence from clinical trials on the main effects of curcumin supplementation on inflammatory markers, sports performance, and muscle damage during acute physical exercises in these individuals. We searched PubMed/MEDLINE, Scopus, Web of Science, and Embase databases, and only original studies were analyzed according to the PRISMA guidelines. The included studies were limited to supplementation of curcumin during acute exercise. A total of 5 studies were selected. Methodological quality assessments were examined using the SYRCLE's risk-of-bias tool. Most studies have shown positive effects of curcumin supplementation in sedentary individuals undergoing acute physical exercise. Overall, participants supplemented with curcumin showed less muscle damage, reduced inflammation, and better muscle performance. The studies showed heterogeneous data and exhibited methodological limitations; therefore, further research is necessary to ensure curcumin supplementation benefits during acute and high-intensity physical exercises. Additionally, mechanistic and highly controlled studies are required to improve the quality of the evidence and to elucidate other possible mechanisms. This study is registered with Prospero number CRD42021262718.

1. Introduction

Exhaustive physical exercise, especially acute or high intensity with many eccentric contractions, leads to muscle damage and delayed onset muscle soreness (DOMS) [1–3]. The disruption of the sarcolemma can characterize muscle damage, in addition to cytoskeletal damage, distortion of contractile components, and extracellular abnormalities of the myofibril matrix [4]. Furthermore, exercise-induced muscle damage (EIMD) induces an inflammatory response associated with decreased muscle strength, decreased ROM, localized swelling, and an increase in muscle proteins in the blood, such as creatine kinase (CK) [5]. It also raises markers such as C-reactive protein (CRP) and inflammatory interleukins and contributes to the production of reactive oxygen species (ROS) by promoting the activation of transcription factors, such as the nuclear factor nuclear-κB (NF-κB) [6–8].

Impaired muscle function caused by EIMD and DOMS and subsequent inflammatory responses can affect sports performance. In this sense, strategies capable of controlling

or minimizing muscle damage and exacerbated inflammatory responses have been increasingly studied. In this regard, nutritional supplements with antioxidant and anti-inflammatory properties have represented an alternative for such purposes [9, 10]. Among the alternatives, curcumin (1,7-bis (4-hydroxy-3-methoxyphenyl) 1,6-heptadiene-3,5-dione) stands out, being the main polyphenol of *Curcuma longa* L. [11, 12]. The Food and Drug Administration (FDA) of the United States has listed curcumin as "Generally Recognized as Safe" (GRAS), and supplements containing curcumin have been approved for human consumption [13].

A recent review has shown that curcumin has various biological activities, thanks to its antioxidant and anti-inflammatory properties, which could be cardioprotective, immune-regulating, antineoplastic, and hepatoprotective effects, in addition to positive effects on diabetes and the nervous system [14]. Moreover, it has shown positive effects on exercise practitioners and athletes. A clinical trial with individuals of both sexes has shown that, after eccentric exercise, supplementation with curcumin (500 mg) significantly reduced EIMD and CK concentrations, leading to better recovery after exercise [15]. Another study has also shown that curcumin significantly decreased CK levels and muscle pain in men undergoing muscle damage protocol [16]. The study by Sahin et al. [17] showed that curcumin prevented muscle damage and improved performance in animals by regulating the pathways of NF-κB and nuclear factor derived from erythroid 2-like 2 (Nrf2).

From what is known, although curcumin has been extensively studied due to its beneficial potential in physical exercise and sports performance, there is no literature consensus on its effects on acute and/or high-intensity physical exercises. Therefore, from clinical trials, we have summarized the available evidence of the effects of curcumin supplementation on inflammatory markers, sports performance, and muscle damage during acute physical exercises in sedentary individuals.

2. Methods

2.1. Protocol and Registration. This systematic review was guided by the following research question: "What is the impact of curcumin supplementation on sports performance in sedentary individuals? Second, what are the main inflammatory mechanisms involved in this process? Third, what are the main methodological parameters used to assess the effect of curcumin supplementation on sports performance?" This systematic review was developed according to the Preferred Reporting Items for Systematic Reviews and Meta-Analyses (PRISMA) guidelines [18].

2.2. Eligibility Criteria. This study included randomized-controlled clinical trials with sedentary individuals older than 18 years submitted to acute physical exercise. In contrast, studies carried out with children, teenagers, seniors, and physically active individuals were excluded. Concerning the intervention type, we have included studies with any dosage and form of curcumin supplementation. Studies in which curcumin supplementation has occurred in combination with other foods or medication were excluded.

2.3. Search. This systematic review was developed according to the Preferred Reporting Items for Systematic Reviews and Meta-Analysis (PRISMA) guidelines [18], which were used to guide the selection, screening, and eligibility of studies. The participants, intervention comparators, outcomes, and study design (PICOS) criteria adopted in this study are shown in Table 1.

Six authors (ARC, KAD, LFM, LAO, SMSP, and SSP) independently searched for original articles using the following electronic databases: PubMed/MEDLINE (https://www.ncbi.nlm.nih.gov/pubmed), Scopus (https://www.scopus.com/home.uri), Web of Science (https://www.webofknowledge.com), and Embase (https://www.embase.com). The descriptors were structured based on search filters built for three domains: (i) curcumin, (ii) exercise, and (iii) human. The PubMed/MEDLINE platform filters were constructed using a hierarchical distribution of the MeSH terms (Medical Subject Headings) and by the algorithm TIAB (Title and Abstract). These filters were adapted for research in the Scopus platform, Web of Science, and Embase; however, the filter for the original article was provided by the Scopus platform (Table S1). The search strategies were not limited by date and language. The bibliographic search was performed on June 28, 2021.

2.4. Study Selection. The authors (ARC, KAD, LFM, LAO, SMSP, and SSP) selected eligible studies following the analysis of their titles and abstracts. The level of agreement among these reviewers was assessed using kappa (kappa = 0.909). The information was extracted independently and analyzed separately. After reading titles, abstracts, and full-text analysis, we have included all randomized controlled trials that assessed the effects of curcumin consumption in sedentary adults submitted to acute physical exercise. Letters, reviews, observational studies, book chapters, abstracts, unpublished articles, *in vitro* studies, animal experiments, studies with physically active individuals, and studies that associated curcumin supplementation with another food or medicine were excluded. In addition, two reviewers (KAD and LAO) manually searched the reference lists of the studies selected in the previous step independently evaluated to find additional relevant articles. Selections were then compared, and differences were resolved in consultation with another three reviewers (MMS, RVG, and CMDL).

2.5. Data Extraction Process. After selecting the clinical trials, the data of the publications were extracted using standardized information such as an author's name, year of publication, the country where the study was held, sample characteristics (sample size, average age, and anthropometric data), study design, follow-up, intervention characteristics (dose and form of consumption), and primary and secondary outcomes. After the data extraction step, the researchers compared the data to ensure integrity and reliability.

2.6. Risk of Bias. The quality and risk of bias in the studies' methodology were assessed by the criteria described on the SYRCLE's risk-of-bias (RoB) tool (Systematic Review Centre

Table 1: PICOS criteria for study inclusion.

Parameter	Inclusion criteria
Participants	Physically inactive adults
Intervention or exposure	Consumption of curcumin Acute physical exercise
Comparison	Placebo (no curcumin supplementation)
Outcome	Inflammation markers, muscle pain, and damage, sports performance and fatigue, biochemical and oxidative markers
Study design	Randomized clinical trials

for Laboratory animal Experimentation) [19]. The following methodological domains based on RoB were evaluated according to five domains of bias: (1) selection bias (random sequence generation, baseline characteristics, and allocation concealment), (2) performance bias (random housing and blinding of caregivers and/or investigators), (3) detection bias (random outcome assessment, blinding of outcome assessment), (4) attrition bias (incomplete outcome data), (5) reporting bias (selective outcome reporting), and other bias (the ethics committee and statistics).

The studies were categorized independently by the authors in three levels of bias according to the items in the RoB tool and were scored as "low risk of bias," "high risk of bias," or "unclear" (when the experimental information was not sufficient for categorization). We constructed a figure in the Review Manager® 5.4 program from Cochrane Collaboration (RoB 2.0) to demonstrate the risk of bias across all included studies (Copenhagen: The Nordic Cochrane Center 2020).

2.7. Data Analysis. All the clinical trials reviewed in this article were summarized in a standard data extraction model, according to the main characteristics and results of sports performance, muscle damage, and inflammation markers (Table 2). The studies were chronologically ordered by year of publication. Inflammatory and muscle performance markers were considered the primary outcomes. In addition, we analyzed the effect of the tested dose concerning the duration of clinical trials.

3. Results

3.1. Study Selection. The flowchart with the number of selected and excluded articles in each stage was built according to the PRISMA guidelines (Figure 1). After searching PubMed, Scopus, Web of Science, and Embase, we have identified 5331 articles. Posteriorly, 1960 duplicates were removed, resulting in 3371 articles, of which 3356 were excluded after reading the titles. After reading the abstracts and full text, we have excluded ten articles. Nine evaluated the effect of curcumin consumption on physically active or moderately individuals, and one did not evaluate parameters of interest, such as inflammatory markers or pain and damage muscle. We have performed the citation search to identify other relevant studies; however, none met the eligibility criteria. Finally, five articles were included in this study.

3.2. Description of Included Studies. In the five studies included in this review, 98 young adult individuals of both sexes, sedentary and with no comorbidities, were studied. The sample size ranged from 12 to 28 individuals. As for the study sites, three of them were conducted in Japan [2, 3, 20], one in China [21], and one in the United States [22]. All studies were randomized and controlled. The intervention time ranged from 2 days to 4 weeks.

The type of acute exercise performed varied. Regarding the type of acute exercise performed, it was observed that the majority ($n = 3$; 60%) performed eccentric contractions of the elbow flexors, one study (20%) performed a test of six sets of ten leg press repetitions, and one study (20%) performed a three-rep set of drop jump high (DJH) 70%, DJH 100% (defined as the highest jump height), and DJH 130% and an acute bike challenge. In most studies ($n = 4$; 80%), the curcumin was offered as capsules and in one ($n = 20\%$) of them in the form of nanobubble water extract. In all studies (100%), curcumin was ingested alone, and the control group was curcumin-free.

One study (20%) evaluated the effect of consumption of curcumin, divided into two doses, one before exercise and the other 12 hours after exercise, and one study (20%) used curcumin for six days, starting two days before performing acute physical exercise and continuing three days after. Other two studies (40%) also offered curcumin before and after eccentric exercise; in this way, one study evaluated the supplementation of curcumin for seven days before the performance of eccentric exercise of the elbow flexors (PRE group) and for four days after the exercise (POST group); other study evaluated this supplementation in two experimental groups: one group received curcumin for seven days before acute exercise and the other for seven days after exercise. Lastly, one study (20%) evaluated the use of curcumin on performance in acute exercise at two time points, presupplementation and after four weeks (postsupplementation).

The amount of curcumin varied from 180 to 400 mg per day. Two studies (40%) evaluated the effect of 180 mg/day of curcumin supplementation for up to 7 days. One study (20%) offered 230.9 mg/day of curcumin for four weeks. Another study (20%) evaluated the single use of 300 mg/day of curcumin divided into two doses of 150 mg. In addition, one study (20%) evaluated the use of 400 mg/day of curcumin for up to 6 days (Table 3).

3.3. Studies' Main Results

3.3.1. Inflammation. Most studies included in this review ($n = 3$; 60%) evaluated inflammatory markers. Of these, three studies (60%) evaluated the proinflammatory cytokine such as tumor necrosis factor-α (TNF-α), which regulates multiple biological processes and is a mediator of inflammation. One study showed a reduction of TNF-α. Two studies ($n = 40\%$) also evaluated the proinflammatory cytokines

Table 2: Main characteristics of the studies included in the systematic review.

Author, year, country	Sample characteristics	Study design	Intervention characteristics	Follow-up	Exercise test	Main results (curcumin *vs.* control groups) Primary outcome	Secondary outcome
Tanabe et al. (2015) Japan	*n*: 14 young individuals Gender: M: 14 Age: 23.5 ± 2.3 years old Weight: 65.2 ± 11.3 kg	Single-blind crossover randomized controlled trial	G1: 300 mg/day of curcumin (Theracurmin-Theravalues®) G2: 300 mg/day of placebo (starch)	1 day Capsules administered 1 h before (150 mg) and 12 h after exercise (150 mg)	50 maximal eccentric contractions of the elbow flexors separated by 4 weeks	↔ IL-6, TNF-α ↓ CK ↔ muscle pain ↔ ROM ↑ MVC torque	↔ Total work, mean peak torque, upper-arm circumference
McFarlin et al. (2016) USA	*n*: 28 young individuals Gender: M: 10 W: 18 Age: G1: 20 ± 1 years old G2: 19 years old Weight: G1: 62.4 ± 11.4 G2: 65.0 ± 10.3	Double-blind randomized controlled trial	G1: 400 mg/day of curcumin (long-life) G2: 400 mg/day of placebo (rice flour)	6 days 48 h before exercise and for 72 h after	6 series of 10 repetitions of eccentric exercise (leg press) with initial load set at 110% of the estimated 1RM	↓ IL-8 and TNF-α ↔ IL-6 and IL-10 ↓ CK ↔ muscle pain	↔ ADL
Tanabe et al. (2019a) Japan	*n*: 24 healthy adults Gender: M: 24 Age: PRE: 28.8 ± 3.6 years old POST: 29.8 ± 3.4 years old CON: 28 ± 3.2 years old Weight: PRE: 65.2 ± 11 kg POST: 71.2 ± 5.6 kg CON: 65.7 ± 5.9 kg	Single-blind parallel randomized trial	PRE: 180 mg/day of curcumin capsules (Theracurmin-Theravalues®) POST: 180 mg/day of curcumin (Theracurcumin-Theravalues®) CON: 180 mg/day of placebo	PRE: 7 days before exercise POST: 4 days after exercise CON: 4 days after exercise	30 eccentric contractions of the elbow flexors	↔ CK (PRE and POST) ↓ muscle pain on POST ↑ ROM on POST ↔ MVC torque, ROM initially	↔ total work during exercise

Table 2: Continued.

Author, year, country	Sample characteristics	Study design	Intervention characteristics	Follow-up	Exercise test	Main results (curcumin *vs.* control groups) Primary outcome	Secondary outcome
Tanabe et al. (2019b) Japan	*n*: 20 healthy adults Gender: M: 20 Age: Exp 1: 28.5 ± 3.4 years old Exp 2: 29 ± 3.9 years old Weight: Exp 1: 64.9 ± 10.1 kg Exp 2: 70.7 ± 5.8 kg	Double-blind crossover, randomized controlled trial	Exp 1: G1: 180 mg/day of curcumin capsules (Theracurmin-Theravalues®) G2: placebo (starch) Exp 2: G1: 180 mg/day of curcumin capsules (Theracurmin-Theravalues®) G2: placebo (starch)	Exp 1: 7 days before exercise Exp 2: 7 days after exercise	30 eccentric contractions of the elbow flexors	Exp 1: ↓ IL-8 ↔ TNF-α ↔ CK, muscle pain ↔ MVC, ROM Exp 2: ↔ IL-8, TNF-α ↓ CK, muscle pain ↑ MVC torque, ROM	Exp 1: ↔ total work during exercise, d-ROMs, T_2, BAP Exp 2: ↔ total work during exercise, d-ROMs, T_2, BAP
Wang et al. (2019) China	*n*: 12 healthy young individuals Gender: W: 12 Age: 21.2 ± 1.1 years old Weight: G1: 57.1 ± 5.1 kg G2: 56.5 ± 7.6 kg	Double-blind, parallel, randomized, controlled trial	G1: 230.9 mg/day of NCE G2: 15 g/day placebo (maltodextrin)	4 weeks	A single test of 3 repetitions of drop jumps high (DJH) 70%, 100% (defined as the highest jump height), and 130% Acute bicycle challenge for 15 minutes	↔ CK ↓ lactate, NH_3, knee injury index ↑ contact time drop jumps (muscle strength)	↓ ALT, ALP, TG ↑ HDL-c ↔ AST, LDH, albumin, glucose

↑: statistically significant increase; ↔: change without statistical significance; ↓: statistically significant decrease; M: men; W: women; CK: creatine kinase; IL-6: interleukin-6; IL-8: interleukin-8; IL-10: interleukin-10; TNF-α: tumor necrosis factor-alpha; MVC torque: maximum voluntary contraction torque; ROM: range of motion; ALT: alanine aminotransferase; ALP: alkaline phosphatase; AST: aspartate aminotransferase; TG: triglycerides; HDL-c: high-density lipoprotein; LDH: lactate dehydrogenase; ADL: activities of daily living; T2: transverse relaxation time; d-ROMs: derivatives of reactive oxygen metabolites; BAP: biological antioxidant potential; Exp: experiment; PRE: PRE group; POST: POST group; CON: control group; NCE: nanobubble water curcumin extract; RM: repetition maximum.

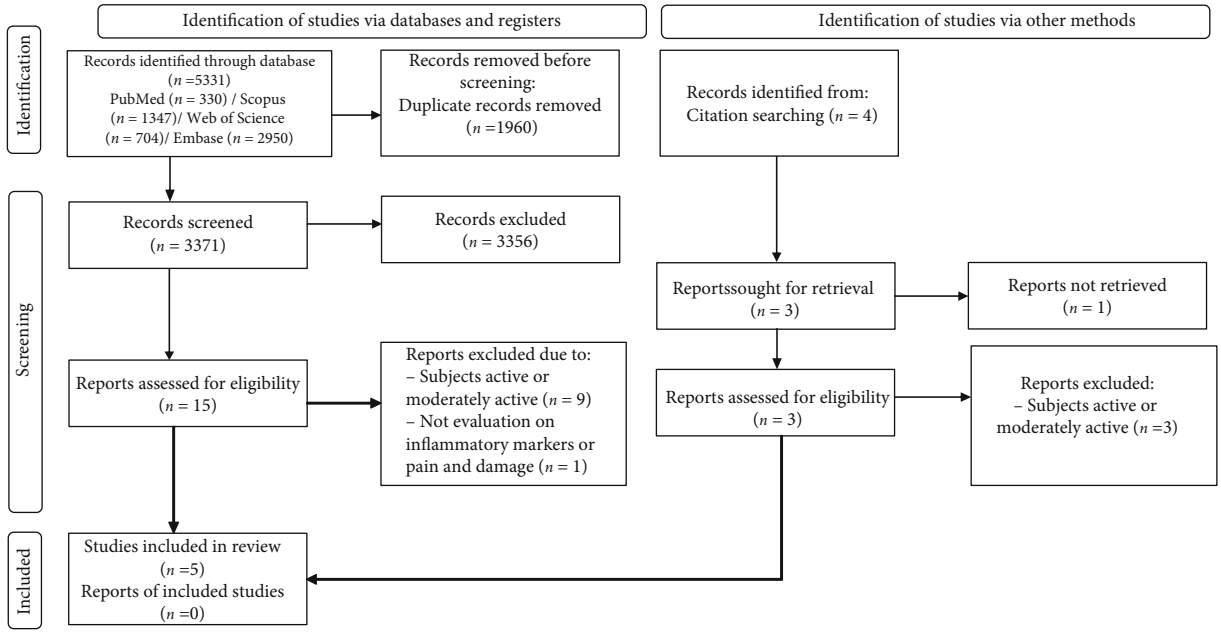

Figure 1: PRISMA diagram. Different phases of the selection of studies for conducting qualitative and quantitative analyses. Flow diagram of the systematic review literature search results. Based on [18].

Table 3: Effects of different concentrations and exposure time of curcumin before and/or after intense physical exercise on different markers.

Evaluated markers	>200 mg of curcumin/day		200–300 mg of curcumin/day		≥300 mg of curcumin/day
	≤7 days		≤7 days	>7 days to 28 days	≤7 days
	BE	AE	BE+AE	AE	BE+AE
Proinflammatory cytokines	$n = 1$	$n = 1$	$n = 1$	—	$n = 1$
Anti-inflammatory cytokines	—	—	—	—	$n = 1$
CK	$n = 2$	$n = 2$	$n = 1$	$n = 1$	$n = 1$
Muscle pain	$n = 2$	$n = 2$	$n = 1$	—	$n = 1$
Muscle performance	$n = 2$	$n = 2$	$n = 1$	$n = 1$	—
Lactate, NH_3	—	—	—	$n = 1$	—
Biochemical (ALT, ALP, TG, HDL, glucose)	—	—	—	$n = 1$	—
Oxidative stress	$n = 1$	$n = 1$	—	—	—

BE: before exercise; AE: after exercise; BE+AE: before and after exercise; n: number of studies.

interleukin-6 (IL-6) and interleukin-8 (IL-8). Decreased expression of these cytokines was observed only for IL-6 and IL-8 in 1 and 2 days after curcumin exposure. These interleukins are related to the acute inflammatory response, stimulating the release of acute-phase proteins, as well as neutrophil chemotaxis [23]. This acute phase, mediated by proinflammatory cytokines, is generally followed by the expression of anti-inflammatory cytokines (Wang et al., 2016). Only one study ($n = 20\%$) evaluated the anti-inflammatory cytokine interleukin-10 (IL-10); however, there was no difference in these cytokines between treated and receiving placebo in 6 days of treatment.

McFarlin et al. found in a study with 28 individuals that supplementation of 400 mg/day of curcumin significantly reduced the levels of IL-8 (-21%; $p = 0.030$) at 1 day (-21%) and 2 days (-18%) and TNF-α (-25%; $p = 0.028$) at 1 day (-25%), 2 days (-23%), and 4 days (-23%) after muscle damage induced by acute leg press exercise. Despite the lack of significance, IL-6 demonstrated a similar response to IL-8 and TNF-α for the curcumin condition [22].

In another study with 20 healthy men, Tanabe et al. found that IL-8 serum concentration 12 h after the resistance exercise was lower ($p = 0.033$) for the supplementation of 180 mg/day of curcumin (experiment 1). However, TNF-α concentration remained similar between groups [3]. Thus, the curcumin supplementation significantly reduced inflammation resulting from acute physical exercise (Table 2).

3.3.2. Muscle Pain and Damage. All studies evaluated creatine kinase (CK) ($n = 5$; 100%) as an essential clinical biomarker for muscle damage. Thus, most studies ($n = 3$; 60%) observed that treatment with curcumin could reduce CK activity, showing the benefits of curcumin supplementation in reducing pain and muscle damage by decreasing CK. Serum CK is an important clinical biomarker for muscle damage, such as muscular dystrophy, severe muscle destruction, and a marker of peripheral fatigue during physical exercises [21, 22]. In addition, most studies ($n = 4$; 80%) evaluated muscle pain; two of these (50%) reported a reduction in muscle pain. Only one study (20%) evaluated skeletal muscle injury and observed a decrease in the index of a knee injury.

Although inconclusive, studies have shown that curcumin was effective for some aspects of muscle damage and pain after the performance of acute physical exercises. Tanabe et al. found in a crossover study with 14 healthy young men that the consumption of a single dose of 150 mg of curcumin 1 hour before and another dose of 150 mg 12 hours after 50 maximum eccentric contractions of the elbow flexors reduced the peak of CK activity, compared to the placebo condition (peak: 7684 ± 8959 IU/L vs. 3398 ± 3562 IU/L; $p < 0.05$).

Similar findings were reported by McFarlin et al. when they found that curcumin resulted in a blunted CK response ($p = 0.035$) at 1 day (-44%), 2 days (-49%), 3 days (-57%), and 4 days (-69%) following performing the acute exercise.

In addition, Tanabe et al. [3] also found a reduction in CK concentrations ($p = 0.020$) 5-7 days after exercise and a reduction in the score for muscle pain for the group supplemented with curcumin (experiment 2) 3–6 days after the exercise when compared to the placebo group. In turn, Tanabe et al. [20] observed that the group supplemented with 180 mg/day of curcumin for 4 days presented reduced muscle pain by palpation on the 3rd day postresistance exercise and reduced muscle pain by the extension of the elbow joint when compared the placebo group.

Finally, Wang et al. found in a study that the supplementation of 230.9 mg/day of the nanobubble water curcumin extract (NCE) before performing a series of drop jumps significantly reduced the knee injury index (15.38%; $p = 0.0467$) (peak vertical ground reaction force (PVGRF)); these results showed that NCE improved skeletal muscle injury [21].

3.3.3. Muscle Performance and Fatigue. Supplementation with curcumin has shown improvement in some markers of muscle performance during acute eccentric exercise. Most studies ($n = 3$; 60%) evaluated a range of motion (ROM) and maximal voluntary contraction (MVC) torque as markers of muscle performance and recovery. Two studies (40%) reported improvement in a range of motion (ROM); also, curcumin supplementation improved MVC torque in two studies (40%), which suggests that supplementation contributed to muscle recovery and performance. To reflect better performance during exercise, fatigue needs to be reduced. Lactate is an oxidizable substrate in skeletal muscle and a precursor to gluconeogenesis in muscles after exercise [24]. In addition, peripheral and central fatigue levels are related to increased ammonia levels during exercise [21]. Only one study (20%) evaluated muscle strength and muscle fatigue markers (lactate and ammonia (NH_3), reporting increased muscle strength through increased contact time in drop jumps and reduction of lactate and NH_3 by supplementation with curcumin.

The supplementation of 180 mg/day of curcumin improved ROM (3–4 days following the exercise) compared to the placebo group, indicating an improvement in sports performance [20]. In addition, the magnitude of decrease in MVC torque for the curcumin condition was significantly smaller immediately after exercise and at 48–96 h after exercise by 13–16% compared to the placebo group [2].

In support of these findings, Tanabe et al. observed that supplementation of 180 mg/day of curcumin (for 7 days—-after acute exercise) showed improvement in MVC torque and ROM compared to the placebo group [3]. Another study [21] has found that the contact time in drop jump high was significantly increased by supplementation with NCE (230.9 mg/day for 4 weeks) ($p = 0.0487$). This increased contact time was due to the increased muscle strength due to the NCE supplementation, corroborating the statement of curcumin's role in improving sports and muscle performance. They also have reported a reduction in lactate (18.67%; $p = 0.0057$) and NH_3 levels (9.02%; $p = 0.0048$) for the group supplemented with curcumin compared to the placebo group, indicating a contribution to reducing fatigue and improving performance.

3.3.4. Biochemical and Oxidative Markers. Only one study (20%) evaluated the effects of curcumin supplementation regarding biochemical markers. Biochemical analyses can provide clinical information about the subject's physiological adaptation. NCE supplementation showed functional activities related to physiological protection and promotion of recovery [21]. Wang et al. found that curcumin consumption significantly decreased hepatic alanine aminotransferase (ALT) (35.66%) and aspartate aminotransferase (ALP) (28.65%) levels compared to the placebo condition. As for lipid-related parameters, triglycerides (TG) were significantly reduced (31.96%) in the treated group compared to the placebo group after four weeks of supplementation. In addition, high-density lipoprotein (HDL) is increased by 1.17 times compared to the placebo group [21].

Regarding oxidative markers, a single study (20%) assessed the levels of serum concentration of derivatives of reactive oxygen metabolites (d-ROMs) and the biological antioxidant potential (BAP). However, there were no significant differences between curcumin and placebo conditions [3].

3.3.5. Risk of Bias. Regarding the selection bias of the participants, the five articles ($n = 5$; 100%) included in this review were randomized; however, they reported insufficient data on the process of sequence generation and allocation secrecy, making evaluation difficult. As for the blinding of participants and personnel, most of the studies ($n = 4$; 80%) were double-blind, thus displaying a low risk for this bias. All studies ($n = 5$; 100%) had a low risk of bias concerning data recording on incomplete outcomes since the

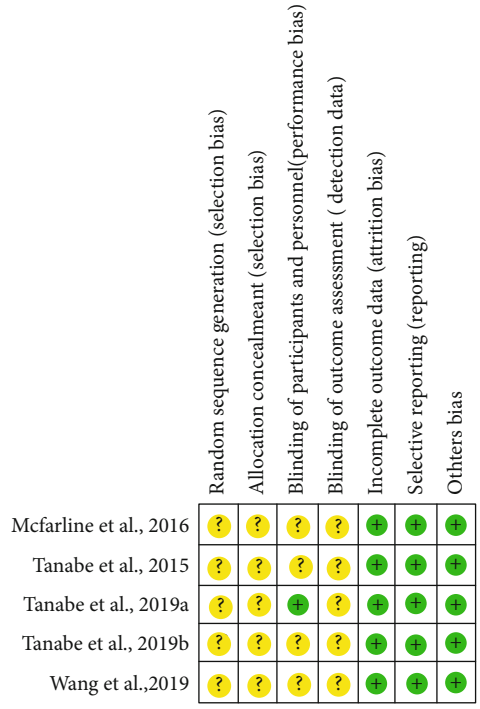

Figure 2: Risk of bias summary: review authors' judgments about the risk of bias item for each included study. The items in the Systematic Review Centre for Laboratory animal Experimentation (SYRCLE) risk of bias assessment were scored with "yes" indicating low risk of bias, "no" indicating high risk of bias, or "unclear" indicating that the item was not reported, resulting in an unknown risk of bias. Green: low risk of bias; yellow: unclear risk of bias; red: high risk of bias.

missing data were balanced among the groups. In terms of the selected outcome reporting, all studies ($n = 5$; 100%) were classified as low risk of bias since the study protocol is not available, but the published articles include all expected results (Figure 2). All studies followed the methodology and presented the proposed results and approval on the ethics committee and information regarding the statistics used.

4. Discussion

Our study performed a systematic review to investigate the available scientific evidence of the effects of curcumin supplementation on inflammatory markers, muscle damage, and sports performance during acute physical exercise in sedentary individuals. In addition, we analyzed the methodological quality of studies that address this issue. We hope that these guidelines can improve research quality, reproducibility, and viability and yield studies with a low risk of bias, especially about the food supplementation in inflammatory diseases. In this sense, our review showed that curcumin supplementation reduced inflammation and muscle pain resulting from acute physical activity. In addition, it has improved muscle recovery and sports performance and reduced fatigue (Figure 3).

Regular physical exercise promotes health benefits [25]. However, long-term acute and intense physical exercise, associated with the insufficient recovery period, results in muscle damage, increased reactive oxygen species (ROS), and inflammation [26, 27]. The production of ROS can alter cellular functions and cause inflammation, leading to increased fatigue, decreased muscle function, and performance [28–30]. When practiced with adequate intensity and volume, postexercise inflammatory responses are physiological and indispensable for regenerating damaged muscles. However, they can impair muscle regeneration when uncontrolled, leading to oxidative damage, protein catabolism, and late-onset muscle pain, resulting in decreased sports performance [31, 32]. In this sense, controlling or minimizing marked inflammatory responses and muscle damage can promote faster recovery, maximize training and performance, and prevent injuries [2].

Thus, supplementation with dietary compounds has been increasingly frequent for potential use in improving sports performance and accelerating postexercise recovery. Scientific evidence has shown curcumin's potential in reducing postexercise inflammation [17, 20, 22]. The mechanisms involved are related to its ability to modulate proinflammatory cytokines and signaling pathways, in addition to its effectiveness in blocking the increased activation of NF-κB, which in turn regulates the expression of TNF-α and inflammatory proteins [17, 33–37].

The proinflammatory cytokines TNF-α, IL-6, and IL-8 were evaluated as markers of inflammation by the studies included in this systematic review [2, 3, 22]. Tanabe et al. [2] observed no effect of curcumin supplementation for TNF-α. However, McFarlin et al. [22] reported sustained suppression of TNF-α in the curcumin-supplemented group compared to the placebo group. Curcumin's effectiveness in reducing TNF-α may be subject to a minimum dosage of 400 mg administered before and for 72 hours after exercise, which may explain the differences observed concerning the studies by Tanabe et al. [2].

McFarlin et al. [22] reported that supplementation with 400 mg of curcumin effectively reduced IL-8 levels resulting from exercise practice. In the study by Tanabe et al. [3], 7 days of 180 mg of curcumin supplementation before exercise also reduced the serum concentration of IL-8 12 hours after exercise. McFarlin et al. [22] observed that the inhibition of the transcription factor NF-κB could be related to the reduction of IL-8 levels and the tendency to decrease to IL-6. Studies have shown that the promoters of the cytokines IL-6 and IL-8 have binding sites for NF-κB, C/EBPβ, and c-Jun [38, 39]. Thus, curcumin's therapeutic potential in inflammation may be related to its direct action of inhibiting NF-κB, which influences the regulation of the expression of IL-6 and IL-8 [40].

Recent studies with protocols that used curcumin supplementation ranging from 0.18 g to 0.4 g/day also have shown benefits in reducing pain and muscle damage, which reflects in the decrease in serum CK [2, 3, 22]. Intense exercise leads to an increase in muscle injury markers, such as CK and lactate dehydrogenase (LDH), which are used as an indication of increased muscle damage induced by exercise (EIMD)

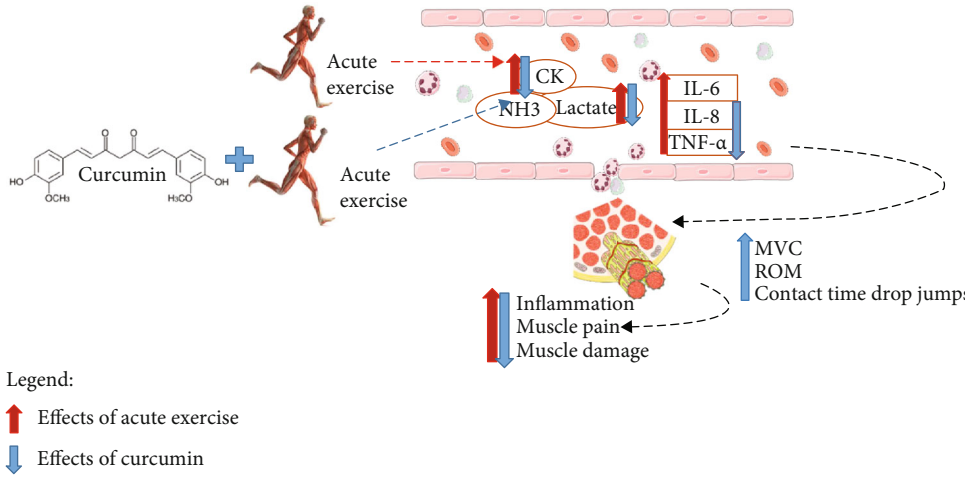

Figure 3: Potential positive effects of curcumin supplementation during acute physical exercises in sedentary individuals. CK: creatine kinase; NH3: ammonia; IL-8: interleukin-6; IL-8: interleukin-8; TNF-α: tumor necrosis factor-alpha; MVC torque: maximum voluntary contraction torque; ROM: range of motion.

[41, 42]. EIMD can affect muscle pain performance and enzyme activity, reducing the sports performance of athletes and physical activity practitioners [42–44].

In this sense, all studies included in this review evaluated the ability of curcumin to mitigate muscle pain and damage, in addition to preventing injuries [2, 3, 20–22]. In two studies, Tanabe et al. [3, 20] described that the administration of 180 mg of curcumin (Theracurmin-Theravalues®) caused a significant reduction in muscle pain when administered four [3] and seven [20] days later the eccentric contraction exercise.

However, Tanabe et al. [2] have found no significant effect on muscle pain using 150 mg of curcumin or placebo orally before and 12 hours after eccentric exercise. In addition, Mcfarlin et al. [22] have also reported no difference in subjective quadriceps muscle pain or daily life activities when investigating the effect of supplementation with curcumin (400 mg 24 hours before and 72 hours after) compared to placebo. Thus, curcumin supplementation may have affected pain and muscle damage when administered on recovery days [3] and for a more extended period [20]. Even so, differences in muscle pain results may be due to the subjective and individual perception of pain intensity among participants of the studies.

The effect of curcumin supplementation on serum CK activity levels after exercise was investigated by four studies included in this review [2, 3, 20, 22]. Three of them have shown significantly lower serum CK levels in the group supplemented with curcumin when compared to the placebo group [2, 3, 22]. Although Tanabe et al. [20] did not report significant differences, they observed that CK levels showed less tendency to increase in the group supplemented with curcumin.

Thus, it is possible that the direct action of curcumin in the inhibition of NF-κB can inhibit enzymes that generate ROS, such as COX-2 [39]. It has also been reported that another possible mechanism for reducing CK activity through curcumin is the inhibition of the production of histamine and prostaglandin due to the suppression of the positive regulation of COX-2, showing a protective effect of the membrane, influencing vascular permeability. This inhibition reduces the permeability of the membranes, reducing the intracellular flow of CK. Thus, vascular permeability may be the key factor in reducing muscle inflammation and pain caused by EIMD [45, 46]. Although the mechanisms linked to the positive effects of curcumin during physical activities, as well as the doses and exposure time, are poorly understood, the evidence on the anti-inflammatory potential of these molecules is more objective and suggests a reduction in proinflammatory markers promoting a rapid tissue recovery after stress.

The EIMD triggers an inflammatory response associated with decreased muscle strength, ROM, localized swelling, DOMS, and increased CK, lactate dehydrogenase (LDH), and myoglobin (Mb) [5]. Mechanical stress during acute exercise and subsequent inflammatory responses lead to reduced muscle performance. Thus, MVC and ROM changes reflect the EIMD dimension, and therefore, these parameters can be used as performance markers [47]. In this sense, Tanabe et al. [2] and Tanabe et al. [20] demonstrated curcumin's action on muscle performance. They have found that curcumin supplementation 180 mg/day for 4 and 7 days after performing eccentric exercises, respectively, improved the range of motion (ROM). The same group of researchers has found the improvement in MVC torque or the lesser magnitude of its decline among those who consumed curcumin after exercise [2, 3].

The MVC and ROM markers are decreased by the activation of NF-κB under high mechanical stress caused by the excessive use of some joints in sport, which generates fragments of the extracellular matrix of bone or cartilage [47]. Innate immunity recognizes these fragments by toll-like receptors. The cellular activation of NF-κB mediated by this process stimulates the secretion of products responsible for the production of tissue damage, such as inflammatory cytokines (IL-1, IL-1b, IL-2, IL-15, IL-21, and TNF-α),

chemokines (CCL-19, CCR-7), and metalloproteases (MMP-13, ADAMSTS-4) (Wainstein GE 2014). The curcumin action probably minimizes the tissue's disabling effects, blocking the NF-κB signaling pathway and thus providing less muscle damage and a consequently smaller decrease in MVC and ROM [48, 49].

In addition, the increased serum concentrations of NH_3 and lactate during exercise are related to muscle fatigue and intensify according to the exercise's intensity and length. High concentrations of lactate and ammonia indicate an increased concentration of hydrogen ions and consequent muscle acidosis, which reduces muscles' strength and working capacity [50]. Wang et al. [21] reported a reduction in lactate and ammonia (NH3) levels among participants who ingested curcumin compared to the placebo group, consequently showing a reduction in muscle fatigue.

The results by Wang et al. [21] also show that consumption of 230.9 mg/day of curcumin before acute exercise decreased exercise-induced liver injury indicators (aspartate aminotransferase (AST) and alanine aminotransferase (ALT)) and improved lipid metabolism through decreased triglycerides (TG) and increased levels of high-density lipoprotein (HDL) compared to the placebo group. In turn, ROS is related to the disruption of the cell membrane integrity caused by lipid peroxidation, with the consequent release of specific cytosol enzymes or proteins, such as AST and ALT in the blood [51].

Curcumin supplementation reduces damage and improves liver inflammation [52] by inhibiting NF-κB activation, decreasing ICAM-1, COX-2, and MCP-1, and reducing intrahepatic gene expression of monocyte chemoattracting protein-1, CD11b, procollagen type I, and tissue metalloproteinase inhibitor [53, 54]. In addition, this compound can affect adiposity and lipid metabolism through several mechanisms, including the modulation of energy metabolism and inflammation [55]. In clinical practice, there is evidence about the effectiveness of curcumin supplementation in reducing the levels of plasma triglycerides and cholesterol [36, 56, 57], which suggests its hypocholesterolemic effect [17].

Curcumin has been approved by the Food and Drug Administration (FDA) as a safe compound [13]. In addition, clinical trials have assessed its safety and concluded that dosages up to 12 g/day are safe and nontoxic for human consumption for three months [13, 58]. Only one [22] out of the five studies included in this review evaluated the side effects of curcumin supplementation, and no adverse gastrointestinal effects were reported. Despite the positive reports described in this review, we believe it is necessary to evaluate the results with caution due to heterogeneity of the individual studies, mainly concerning methodological consistency to interpret the evidence available and so to avoid reporting bias and consequently to decrease the reproduction of the error through the research process.

5. Strength and Limitations

Considering a more comprehensive analysis of the scientific evidence in clinical trials, the risk of bias was assessed as a quality criterion complementary to the information reported in the studies reviewed. The main methodological limitations were identified in all studies analyzed. Surprisingly, no study fulfilled all methodological criteria; this finding indicates that specific reporting bias has been systematically reproduced through the research process, despite advances in regulatory strategies to stimulate the development of robust clinical research. Bias analysis showed that key characteristics such as random sequence generation or random outcome assessment and blinding of participants (caregivers and outcome evaluator) were not reported with sufficient information in the studies. Due to the marked variability identified in the reviewed studies (i.e., characteristics related to population, treatment protocols, and outcome evaluation), the findings of this systematic review were qualitatively presented. Thus, it was not possible to evaluate the results based on a meta-analysis [59, 60]. In addition, the funnel plot method was not used to explore heterogeneity since the number of included studies was less than the minimum recommended (10) for this type of analysis [61]. We believe that the results presented in this study are important and valuable as they bring new knowledge about the potential use of curcumin and its benefits in the practice of strenuous exercise by sedentary individuals. However, they should also be treated with caution, as the low number of clinical trials found on the subject can be pointed out as a limitation of this review because when there are fewer studies, the power of the tests is too low to distinguish chance from real asymmetry [61–63]. In this context, further studies are needed to ensure the benefits of curcumin supplementation during acute and high-intensity physical exercise and to elucidate other possible mechanisms.

6. Conclusion

Curcumin supplementation has been shown to improve sports performance, providing less EIMD and reducing fatigue by decreasing CK activity. In addition, curcumin exerts an anti-inflammatory effect by modulating proinflammatory cytokines. Curcumin supplementation is safe and probably represents beneficial sport potential, demonstrating effectiveness before and/or after acute physical exercise in sedentary individuals.

Data Availability

The data can be made available upon request to the email kelly.dias@ufv.br.

Conflicts of Interest

The authors declare that they have no conflict of interest.

Acknowledgments

The authors are grateful for the support provided by Conselho Nacional de Desenvolvimento Científico e Tecnológico—Brazil (CNPq) (Finance Code 428701/2018-3), Fundação de Amparo à Pesquisa do Estado de Minas

Gerais—Brazil (FAPEMIG), and Coordenação de Aperfeiçoamento de Pessoal de Niıvel Superior—Brazil (CAPES).

Supplementary Materials

Table S1: full search strategy in PubMed, Scopus, Web of Science, and Embase, including search terms and filters. *(Supplementary Materials)*

References

[1] C. C. Huang, W. C. Huang, S. C. Yang, C. C. Chan, and W. T. Lin, "Ganoderma tsugae hepatoprotection against exhaustive exercise-induced liver injury in rats," *Molecules*, vol. 18, no. 2, pp. 1741–1754, 2013.

[2] Y. Tanabe, S. Maeda, N. Akazawa et al., "Attenuation of indirect markers of eccentric exercise-induced muscle damage by curcumin," *European Journal of Applied Physiology*, vol. 115, no. 9, pp. 1949–1957, 2015.

[3] Y. Tanabe, K. Chino, T. Ohnishi et al., "Effects of oral curcumin ingested before or after eccentric exercise on markers of muscle damage and inflammation," *Scandinavian Journal of Medicine & Science in Sports*, vol. 29, no. 4, pp. 524–534, 2019.

[4] J. Fridén and R. L. Lieber, "Structural and mechanical basis of exercise-induced muscle injury," *Medicine and Science in Sports and Exercise*, vol. 24, no. 5, pp. 521–529, 1992.

[5] I. G. Fatouros and A. Z. Jamurtas, "Insights into the molecular etiology of exercise-induced inflammation: opportunities for optimizing performance," *Journal of Inflammation Research*, vol. 21, pp. 175–186, 2016.

[6] F. Drobnic, J. Riera, G. Appendino et al., "Reduction of delayed onset muscle soreness by a novel curcumin delivery system (Meriva®): a randomised, placebo-controlled trial," *Journal of the International Society of Sports Nutritionss*, vol. 11, no. 1, 2014.

[7] J. N. Sciberras, S. D. R. Galloway, A. Fenech et al., "The effect of turmeric (curcumin) supplementation on cytokine and inflammatory marker responses following 2 hours of endurance cycling," *Journal of the International Society of Sports Nutrition*, vol. 12, no. 1, 2015.

[8] R. González-Bartholin, K. Mackay, D. Valladares, H. Zbinden-Foncea, K. Nosaka, and L. Peñailillo, "Changes in oxidative stress, inflammation and muscle damage markers following eccentric versus concentric cycling in older adults," *European Journal of Applied Physiology*, vol. 119, no. 10, pp. 2301–2312, 2019.

[9] G. Howatson, M. P. McHugh, J. A. Hill et al., "Influence of tart cherry juice on indices of recovery following marathon running," *Scandinavian Journal of Medicine & Science in Sports*, vol. 20, no. 6, pp. 843–852, 2010.

[10] J. R. Trombold, J. N. Barnes, L. Critchley, and E. F. Coyle, "Ellagitannin consumption improves strength recovery 2-3 d after eccentric exercise," *Medicine and Science in Sports and Exercise*, vol. 42, no. 3, pp. 493–498, 2010.

[11] F. Kiuchi, Y. Goto, N. Sugimoto, Y. Tsuda, N. Akao, and K. Kondo, "Nematocidal activity of turmeric: synergistic action of curcuminoids," *Chemical & Pharmaceutical Bulletin*, vol. 41, no. 9, pp. 1640–1643, 1993.

[12] B. Kocaadam and N. Şanlier, "Curcumin, an active component of turmeric (curcuma longa), and its effects on health," *Critical Reviews in Food Science and Nutrition*, vol. 57, no. 13, pp. 2889–2895, 2017.

[13] S. C. Gupta, S. Patchva, and B. B. Aggarwal, "Therapeutic roles of curcumin: lessons learned from clinical trials," *AAPS Journal*, vol. 15, no. 1, pp. 195–218, 2013.

[14] X.-Y. Xu, X. Meng, S. Li, R.-Y. Gan, Y. Li, and H.-B. Li, "Bioactivity, health benefits, and related molecular mechanisms of curcumin: current progress, challenges, and perspectives," *Nutrients*, vol. 10, no. 10, 2018.

[15] A. Amalraj, C. Divya, and S. Gopi, "The effects of bioavailable curcumin (Cureit) on delayed onset muscle soreness induced by eccentric continuous Exercise: a randomized, placebo-controlled, double-blind clinical study.," *Journal of Medicinal Food*, vol. 23, no. 5, pp. 545–553, 2020.

[16] S. A. Basham, H. S. Waldman, B. M. Krings, J. Lamberth, J. E. W. Smith, and M. J. McAllister, "Effect of curcumin supplementation on exercise-induced oxidative stress, inflammation, muscle damage, and muscle soreness," *Journal of Dietary Supplements*, vol. 17, no. 4, pp. 401–414, 2020.

[17] K. Sahin, R. Pala, M. Tuzcu et al., "Curcumin prevents muscle damage by regulating NF-*K*B and Nrf2 pathways and improves performance: an in vivo model," *Journal of Inflammation Research*, vol. 9, pp. 147–154, 2016.

[18] M. J. Page, J. E. McKenzie, P. M. Bossuyt et al., "The PRISMA 2020 statement: an updated guideline for reporting systematic reviews," *The BMJ*, 2021.

[19] C. R. Hooijmans, M. M. Rovers, R. B. M. De Vries, M. Leenaars, M. Ritskes-Hoitinga, and M. W. Langendam, "SYRCLE's risk of bias tool for animal studies," *BMC Medical Research Methodology*, vol. 14, no. 1, pp. 1–9, 2014.

[20] Y. Tanabe, K. Chino, H. Sagayama et al., "Effective timing of curcumin ingestion to attenuate eccentric exercise–induced muscle soreness in men," *Journal of Nutritional Science and Vitaminology*, vol. 65, no. 1, pp. 82–89, 2019.

[21] I. L. Wang, C. Y. Hsiao, Y. H. Li, F. B. Meng, C. C. Huang, and Y. M. Chen, "Nanobubbles water curcumin extract reduces injury risks on drop jumps in women: a pilot study," *Evidence-Based Complementary and Alternative Medicine*, vol. 2019, 9 pages, 2019.

[22] B. K. McFarlin, A. S. Venable, A. L. Henning et al., "Reduced inflammatory and muscle damage biomarkers following oral supplementation with bioavailable curcumin," *BBA Clinical*, vol. 5, pp. 72–78, 2016.

[23] N. Kawanishi, T. Mizokami, H. Niihara, K. Yada, and K. Suzuki, "Macrophage depletion by clodronate liposome attenuates muscle injury and inflammation following exhaustive exercise," *Biochemistry and Biophysics Reports*, vol. 5, pp. 146–151, 2016.

[24] G. A. Brooks, "Intra-and extracellular lactate shuttles," *Medicine & Science in Sports & Exercise*, vol. 32, no. 4, pp. 790–799, 2000.

[25] J. Steele, J. Fisher, M. Skivington et al., "A higher effort-based paradigm in physical activity and exercise for public health: making the case for a greater emphasis on resistance training," *BMC Public Health*, vol. 5, p. 300, 2017.

[26] F. S. Lira, J. R. Neto, G. D. Pimentel et al., "Importância dos efeitos fisiológicos do exercício na promoção da saúde," *Inova Saúde*, vol. 1, no. 1, 2012.

[27] M. S. Campbell, N. A. Carlini, and B. S. Fleenor, "Influence of curcumin on performance and post-exercise recovery," *Critical Reviews in Food Science and Nutrition*, 2021.

[28] J. Finaud, G. Lac, and E. Filaire, "Oxidative stress: relationship with exercise and training," *Sports Medicine*, vol. 36, no. 4, pp. 327–358, 2006.

[29] N. Sallam and I. Laher, "Exercise Modulates Oxidative Stress and Inflammation in Aging and Cardiovascular Diseases," *Oxidative Medicine and Cellular Longevity*, vol. 2016, 32 pages, 2016.

[30] Z. Radak and A. W. Taylor, "Exercise and hormesis," in *In The Science of Hormesis in Health and Longevity*, pp. 63–73, Elsevier, 2018.

[31] D. García-López, M. J. Cuevas, M. Almar, E. Lima, J. A. De Paz, and J. González-Gallego, "Effects of eccentric exercise on NF-*K*B activation in blood mononuclear cells," *Medicine and Science in Sports and Exercise*, vol. 39, no. 4, pp. 653–664, 2007.

[32] E. Ferraro, A. M. Giammarioli, S. Chiandotto, I. Spoletini, and G. Rosano, "Exercise-induced skeletal muscle remodeling and metabolic adaptation: redox signaling and role of autophagy," *Antioxidants Redox Signal*, vol. 21, no. 1, pp. 154–176, 2014.

[33] H. Y. Li, M. Yang, Z. Li, and Z. Meng, "Curcumin inhibits angiotensin II-induced inflammation and proliferation of rat vascular smooth muscle cells by elevating PPAR-γ activity and reducing oxidative stress," *International Journal of Molecular Medicine*, vol. 39, no. 5, pp. 1307–1316, 2017.

[34] J. Wang, H. Wang, R. Zhu, Q. Liu, J. Fei, and S. Wang, "Anti-inflammatory activity of curcumin-loaded solid lipid nanoparticles in IL-1β transgenic mice subjected to the lipopolysaccharide-induced sepsis," *Biomaterials*, vol. 53, pp. 475–483, 2015.

[35] F. Antoine and D. Girard, "Curcumin increases gelatinase activity in human neutrophils by a P38 mitogen-activated protein kinase (MAPK)-independent mechanism," *Journal of Immunotoxicology*, vol. 12, no. 2, pp. 188–193, 2015.

[36] Y. Panahi, N. Khalili, M. S. Hosseini, M. Abbasinazari, and A. Sahebkar, "Lipid-modifying effects of adjunctive therapy with curcuminoids-piperine combination in patients with metabolic syndrome: results of a randomized controlled trial," *Complementary Therapies in Medicine*, vol. 22, no. 5, pp. 851–857, 2014.

[37] Y. Zhang, Z. Liu, J. Wu et al., "New MD2 inhibitors derived from curcumin with improved anti-inflammatory activity," *European Journal of Medicinal Chemistry*, vol. 148, pp. 291–305, 2018.

[38] C. Georganas, H. Liu, H. Perlman, A. Hoffmann, B. Thimmapaya, and R. M. Pope, "Regulation of IL-6 and IL-8 expression in rheumatoid arthritis synovial fibroblasts: the dominant role for NF-*K*B but not C/EBPβ or c-Jun," *Journal of Immunology*, vol. 165, no. 12, pp. 7199–7206, 2000.

[39] H. Khalaf, J. Jass, and P. E. Olsson, "Differential cytokine regulation by NF-*K*B and AP-1 in Jurkat T-cells," *BMC Immunology*, vol. 11, 2010.

[40] A. I. Dongari-Bagtzoglou and J. L. Ebersole, "Increased presence of interleukin-6 (IL-6) and IL-8 secreting fibroblast subpopulations in adult periodontitis," *Journal of Periodontology*, vol. 69, no. 8, pp. 899–910, 1998.

[41] J. C. Tee, A. N. Bosch, and M. I. Lambert, "Metabolic consequences of exercise-induced muscle damage," *Sports Medicine*, vol. 2, pp. 827–836, 2007.

[42] A. Córdova, J. Mielgo-Ayuso, C. I. Fernandez-Lazaro, A. Caballero-García, E. Roche, and D. Fernández-Lázaro, "Effect of iron supplementation on the modulation of iron metabolism, muscle damage biomarkers and cortisol in professional cyclists," *Nutrients*, vol. 11, no. 3, 2019.

[43] U. Proske and D. L. Morgan, "Muscle damage from eccentric exercise: mechanism, mechanical signs," *The Journal of Physiology*, vol. 1, pp. 333–345, 2001.

[44] T. A. H. Järvinen, M. Järvinen, and H. Kalimo, "Regeneration of injured skeletal muscle after the injury," *Muscles, Ligaments and Tendons Journal*, pp. 337–345, 2019.

[45] K. Moriyuki, F. Sekiguchi, K. Matsubara, H. Nishikawa, and A. Kawabata, "Curcumin inhibits the proteinase-activated receptor-2-triggered prostaglandin E2 production by suppressing cyclooxygenase-2 upregulation and Akt-dependent activation of nuclear factor-*K*B in human lung epithelial cells," *Journal of Pharmacological Sciences*, vol. 114, no. 2, pp. 225–229, 2010.

[46] A. E. Nugroho, Z. Ikawati, and K. Maeyama, "Effects of benzylidenecyclopentanone analogues of curcumin on histamine release from mast cells," *Biological & Pharmaceutical Bulletin*, vol. 32, no. 5, pp. 842–849, 2009.

[47] D. Fernández-Lázaro, J. Mielgo-Ayuso, J. S. Calvo, A. C. Martínez, A. C. García, and C. I. Fernandez-Lazaro, "Modulation of exercise-induced muscle damage, inflammation, and oxidative markers by curcumin supplementation in a physically active population: a systematic review," *Nutrients*, vol. 1, 2020.

[48] N. Alamdari, P. O'Neal, and P.-O. Hasselgren, "Curcumin and muscle wasting – a new role for an old drug?," *Nutrition*, vol. 25, no. 2, pp. 125–129, 2009.

[49] J. W. Daily, M. Yang, and S. Park, "Efficacy of turmeric extracts and curcumin for alleviating the symptoms of joint arthritis: a systematic review and meta-analysis of randomized clinical trials," *Journal of Medicinal Food*, vol. 1, pp. 717–729, 2016.

[50] R. C. de Moraes Bertuzzi, A. E. Silva, C. C. Abad, and F. de Oliveira Pires, "Metabolismo Do Lactato: Uma Revisão Sobre a Bioenergética e a Fadiga Muscular," *Revista Brasileira de Cineantropometria e Desempenho Humano*, vol. 11, no. 2, pp. 226–234, 2009.

[51] W. C. Huang, W. C. Chiu, H. L. Chuang et al., "Effect of curcumin supplementation on physiological fatigue and physical performance in mice," *Nutrients*, vol. 7, no. 2, pp. 905–921, 2015.

[52] M. C. Ramirez-Tortosa, C. L. Ramirez-Tortosa, M. D. Mesa, S. Granados, Á. Gil, and J. L. Quiles, "Curcumin ameliorates rabbits's steatohepatitis via respiratory chain, oxidative stress, and TNF-α," *Free Radical Biology & Medicine*, vol. 47, no. 7, pp. 924–931, 2009.

[53] I. A. Leclercq, G. C. Farrell, C. Sempoux, A. Peña, and Y. Dela Horsmans, "Curcumin inhibits NF-*K*B activation and reduces the severity of experimental steatohepatitis in mice," *Journal of Hepatology*, vol. 41, no. 6, pp. 926–934, 2004.

[54] F. Vizzutti, A. Provenzano, S. Galastri et al., "Curcumin limits the fibrogenic evolution of experimental steatohepatitis," *Laboratory Investigation*, vol. 90, no. 1, pp. 104–115, 2010.

[55] E. Panzhinskiy, Y. Hua, P. A. Lapchak et al., "Novel curcumin derivative CNB-001 mitigates obesity-associated insulin resistances," *The Journal of Pharmacology and Experimental Therapeutics*, vol. 349, no. 2, pp. 248–257, 2014.

[56] A. Mohammadi, A. Sahebkar, M. Iranshahi et al., "Effects of supplementation with curcuminoids on dyslipidemia in obese patients: a randomized crossover trial," *Phytotherapy Research*, vol. 27, no. 3, pp. 374–379, 2013.

[57] A. Sahebkar, M. Serban, S. Ursoniu, and M. Banach, "Effect of curcuminoids on oxidative stress : a systematic review and meta-analysis of randomized controlled trials," *Journal of Functional Foods*, vol. 18, pp. 898–909, 2015.

[58] J. Epstein, I. R. Sanderson, and T. T. MacDonald, "Curcumin as a therapeutic agent: the evidence fromin vitro, animal and human studies," *British Journal of Nutrition*, vol. 103, no. 11, pp. 1545–1557, 2010.

[59] J. P. Ioannidis, N. A. Patsopoulos, and H. R. Rothstein, "Reasons or excuses for avoiding meta-analysis in forest plots," *BMJ*, vol. 336, no. 7658, pp. 1413–1415, 2008.

[60] A. B. Haidich, "Meta-analysis in medical research," *Hippokratia*, vol. 14, no. 1, pp. 29–37, 2010.

[61] J. A. C. Sterne, M. Egger, D. Moher, and I. Boutron, "Chapter 10: Addressing reporting biases," *Cochrane Handbook for Systematic Reviews of Interventions version 5.2.0 (updated June 2017), Cochrane*, J. P. T. Higgins, R. Churchill, J. Chandler, and M. S. Cumpston, Eds., 2017, https://training.cochrane.org/sites/training.cochrane.org/files/public/uploads/resources/Handbook5_1/Chapter_10_Handbook_5_2_10.pdf.

[62] J. P. T. Higgins, J. Thomas, J. Chandler, M. Cumpston, T. Li, and M. J. Page, "Cochrane Handbook for Systematic Reviews of Interventions," *The Cochrane Collaboration*2011, https://handbook-5-1.cochrane.org/chapter_10/10_4_3_1_recommendations_on_testing_for_funnel_plot_asymmetry.htm.

[63] J. A. Sterne, A. J. Sutton, J. P. Ioannidis et al., "Recommendations for examining and interpreting funnel plot asymmetry in meta-analyses of randomized controlled trials," *BMJ*, vol. 343, p. d4002, 2011.

Hindawi
Oxidative Medicine and Cellular Longevity
Volume 2021, Article ID 5662550, 7 pages
https://doi.org/10.1155/2021/5662550

Research Article

High Level of Inflammatory Cytokines in the Tears: A Bridge of Patients with Concomitant Exotropia and Dry Eye

Feng Gao,[1] **Xiaoping Hong**,[2,3] **Fadian Ding**,[4] **Shirong Huang**,[5] **Wei Lian**,[4] **Hanjun Wang**,[1] **Weidong Zheng**,[3] **Jun Ni**,[6] **Min Chen**,[5] **and Qicai Liu**[7]

[1]*Department of Pathology, 1st Affiliated Hospital, Fujian Medical University, Fuzhou 350004, China*
[2]*Department of Ophthalmology, The Second Affiliated Hospital, Fujian Medical University, Quanzhou 362000, China*
[3]*Department of Ophthalmology, 1st Affiliated Hospital, Fujian Medical University, Fuzhou 350004, China*
[4]*Department of Surgery, 1st Affiliated Hospital, Fujian Medical University, Fuzhou 350004, China*
[5]*Department of Laboratory Medicine, Fujian Medical University, Fuzhou 350004, China*
[6]*Department of Rehabilitation Medicine, 1st Affiliated Hospital, Fujian Medical University, Fuzhou 350004, China*
[7]*Center for Reproductive Medicine, 1st Affiliated Hospital, Fujian Medical University, Fuzhou 350004, China*

Correspondence should be addressed to Weidong Zheng; wdzheng1996@163.com, Min Chen; cmjy503@163.com, and Qicai Liu; lqc673673673@163.com

Received 30 May 2021; Revised 5 August 2021; Accepted 18 September 2021; Published 7 October 2021

Academic Editor: Reggiani Vilela Gonçalves

Concomitant exotropia have obvious symptoms of eye discomfort in adults, and the presence of ocular surface inflammation in patients may be important mediators between concomitant exotropia and dry eye. Oculus Keratograph eye comprehensive analyzer was performed to detect noninvasive tear break time, noninvasive tear height, and eye red index, while the ocular surface disease index and schirmer I testing were made. The levels of IL-6, IL-10, IL-17A, IL-12P70, INF-γ, and TNF-α were detected in tears in patients with concomitant exotropia and healthy controls matched by age and gender through the Simoa technology. IL-6 was significantly higher in patients with concomitant exotropia (4.683 ± 1.329) pg/mL than that in normal group (1.455 ± 0.391) pg/mL, $p = 0.0304$. TNF-α was also significantly higher in patients (0.2095 ± 0.0703) pg/mL than normal group (0.0513 ± 0.0149) pg/mL, $p = 0.0397$. The levels of inflammatory factors in strabismic patients vs. normal controls were as follows: IL-17A (0.1551 pg/mL ∶ 0.0793 pg/mL), IL-10 (0.3358 pg/mL ∶ 0.0513 pg/mL), IL-12p70 (0.0253 pg/mL ∶ 0.0099 pg/mL), and INF-γ (0.0284 pg/mL ∶ 0.009 pg/mL) were detected, and the median of them in concomitant strabismus was 1.96-6.55-fold as much as the control group. High levels of inflammatory cytokines in tears of patients with concomitant exotropia, which may be a potentially factor promoted the occurrence of dry eye in the patients with concomitant exotropia.

1. Introduction

Strabismus is a disease of eye deviation caused by the imbalance of external eye muscles in both eyes. When one eye fixates on a target, the direction of the other eye axis deviates from the direction of fixation. The normal cornea is in a central position due to prolonged oblique or alternate binoculars in one eye, which can lead to corneal overexposure and tear film instability. Previous study had found that the height of the river of tears is reduced and the tear film is unstable, and the eye red index is increased in concomitant exotropia [1].

Giannaccare et al. hypothesized that long-term deviation of the eyeball from its primary location could lead to chronic changes in the ocular surface, which could result in dry eyes through two possible mechanisms [2]. Firstly, increased exposure area of conjunctiva may lead to thinner tear film lipid layer and increased tear film instability [2]. Secondly, abnormal anatomical and functional relationships between the eyelids and the eyeball increase mechanical friction to the conjunctival epithelium, leading to microtrauma associated with blinking [2]. Mechanical damage to the conjunctival epithelium caused by tear film instability further activates a series of inflammatory events, and long-term

inflammatory cell infiltration and increased expression of inflammatory factors lead to further damage to the ocular surface system. We have therefore investigated if there are differences about inflammatory cytokines in our cohort of patients with concomitant exotropia and control group.

2. Methods and Materials

2.1. Participants and Clinical Information Collection. We included sixty-six patients with concomitant exotropia and sixty-six controls; inclusion criteria: (1) concomitant exotropia diagnosed in outpatient department as meeting surgical criteria; (2) the first oblique viewing angle is equal to the second oblique viewing angle, and there is no ability to control the anteroposterion in the far or near viewing, and the horizontal oblique viewing degree is >15PD (prism degree); (3) no combination of dissociated vertical deviation (DVD), superior oblique muscle palsy (SOP), and other diseases, vertical strabismus < 5PD; (4) no complaints of eye discomfort except strabismus; (5) no history of ophthalmic disease or operation; (6) patients with paralytic strabismus, secondary strabismus, perceptual strabismus, residual strabismus, combined keratitis, eyelid gland dysfunction, and Sjogren's syndrome were excluded. There was no significant difference in the number of cases, strabismus, and dominant eye among all subgroups, which showed comparability. There were no significant difference in the age or gender ratios of participants between the concomitant exotropia group and control group (Table 1). At the same time, we collected the ocular surface disease index (OSDI), the height of the river of tears, the tear film rupture time, the tear secretion level, and the eye red index including the adults and children.

2.2. Ocular Surface Analysis. Oculus Keratograph eye comprehensive analyzer was performed to detect noninvasive tear break time (NIBUT), noninvasive tear height (NITMH), and eye red index. Both eyes of exotropia patients were measured separately. First, the right eye was measured, then the left eye was measured for 3 consecutive times, and the average value was taken. All patients were examined by the same experienced staff [3]. The normal reference value of tear film rupture time is 10-15 mm, while <10 mm is hyposecretion, and <5 mm is dry eye. The height of river of tears was 0.2 mm as the critical value, and <0.2 mm was diagnosed as dry eye [4]. The eye red index was less than 2 points for mild hyperemia, 2.1 to 3.0 points for moderate hyperemia, and 3.1 to 4.0 points for severe hyperemia.

2.3. Schirmer I Testing and OSDI. To obtain the height of the river of tears at the lowest part of the crescent curve page for measurement, the unit is expressed in mm, and the critical value of the height of the river of tears is 0.2 mm[5]. The normal reference value of Schirmer I testing is 10-15 mm/5 min, while <10 mm/5 min is hyposecretion, and < 5 mm/5 min is dry eye. OSDI test includes 12 questions and three parts: part 1 refers to ocular pain or visual difficulties; part 2 is about visual functionality; and part 3 is analyses of environmental factors.

Table 1: The ocular surface analysis of included subjects.

	Number	Year	p	F/M	p
A. srabismus	36	28.11 ± 1.75		19 : 17	
A. control	36	31.56 ± 2.03	0.2029	19 : 17	>0.05
C. srabismus	30	9.80 ± 0.74		15 : 15	
C. control	30	8.77 ± 0.67	0.3041	15 : 15	>0.05

2.4. Tears Collect. Inclusion criteria for the experimental group: (1) clinical diagnosis was concomitant exotropia, and refractive errors (spherical ≤ ±1.00D, anastigmate or cylindrical ≤ 0.50) were corrected by wearing glasses, while there were no neurological diseases or craniofacial abnormalities. (2) Except for strabismus and refractive errors, the patients had no history of other visual defects and eye diseases and no family genetic history (including history of strabismus). Inclusion criteria for the control group: (1) refractive errors (spherical ≤ ±1.00D, anastigmate or cylindrical ≤ 0.50) were corrected by wearing glasses while no neurological disease, no craniofacial abnormalities, no history of visual impairment or eye disease, and no family history of hereditary diseases (including strabismus). (2) No related symptoms such as dry eyes. We collected relevant clinical information, including gender, age, and course of the disease, corneal light reflection test, eye movement (intermittence/constancy), strabismus degree, and the dominant eye. There were no significant differences in the age or gender ratios of participants between the concomitant exotropia group and control group (Table 2). The study was approved by the ethics committee of 1st Affiliated Hospital of Fujian Medical University. Informed consent was obtained from legal guardians or participants.

We use tears adsorption filter paper (Tianjin Jingming New Technology Development Co., LTD., Tianjin; China Strip, hereinafter referred to as China Strip) to collect tears from the subjects. Schirmer tear test strips were customised with filter paper labeled with fluorescent-sodium and are of structure of 40 mm × 5 mm filter strips with millimeter scale ranging from 0 to 30 mm. The tears samples were eluted with 200 μL PBS and shaken for 5 hours at room temperature, and the samples were stored in a refrigerator at -80°C [6].

2.5. Measurement of Inflammatory Cytokines in the Tears. For SIMOA experiments, tear samples were prepared according to the kit specific manufacturer's instruction. Inflammatory cytokine levels were measured using SIMOA HD-X Cytokine 6-Plex panel standards, and samples were run utilizing manufacturer's assay instructions.

2.6. Statistical Analyses. All of the data was analyzed with the SPSS 20.0 program (IBM Corp. SPSS Statistics for Windows, version 20.0, Armonk, NY, USA). All the experimental results were statistically analyzed to compare the differences between groups by t-test, and $p < 0.05$ was considered statistically significant.

Table 2: The basic clinical information of the included subjects for tear analysis.

	Exotropia group ($n = 11$)	Control group ($n = 11$)	p
Gender (male : female)	6 : 5	6 : 5	>0.05
Age (year)	6 ± 0.4264	6 ± 0.4045	>0.05
Time (year)	1.25 ± 0.217	—	
Corneal light reflection test	−20.42 ± 1.9604	—	
Movement (unrestricted : restricted)	6 : 14	—	
Strabismus degree	−42.5Δ ± 3.5906	—	
The dominant eye (OD : OS)	6 : 5	—	
Symptoms (foreign-body sensation, pain, irritation, ocular fatigue, and eye redness)	2	—	

3. Results

3.1. Dry Eye-Related Indicator Is Abnormal in Adults While It Is Normal in Children. In order to further clarify the ocular surface of patients with concomitant exotropia. The ocular surface disease index (OSDI), the height of the river of tears, the tear film rupture time, the Schirmer I testing, and the eye red index were measured in 66 patients with concomitant exotropia including adults and children. In our study, we found that the height of the river of tears was decreased (0.2061 ± 0.0068 mm vs. 0.2353 ± 0.0083 mm, $p < 0.01$). And the eye red index of adult patients with exotropia was increased compared to the control group (1.497 ± 0.1348 vs. 1.161 ± 0.1008, $p < 0.05$). Schirmer I testing showed that the tear secretion level of adult patients with exotropia was lower than that of control group (9.333 ± 0.5633 mm/5 min vs. 10.84 ± 0.4815 mm/5 min, $p < 0.05$). The OSDI score (18.99 ± 2.426 vs. 14.58 ± 2.101, $p = 0.1735$) and tear film rupture time (6.881 ± 0.7390 s vs. 8.846 ± 0.7674 s, $p = 0.069$) were no found the statistical difference between concomitant exotropia and control.

However, in the children group, the measurement of OSDI (4.080 ± 0.9179 vs. 3.837 ± 0.9062, $p > 0.05$), tear film rupture time (9.658 ± 0.7309 s vs. 9.728 ± 0.8429 s, $p > 0.05$), eye red index (0.6833 ± 0.06380 vs. 0.6000 ± 0.05296, $p > 0.05$), river of tears height (0.2410 ± 0.0060 mm vs. 0.2417 ± 0.0069 mm, $p > 0.05$), and tear secretion level (10.42 ± 0.4133 mm/5 min vs. 11.31 ± 0.4016 mm/5 min, $p > 0.05$) did not find statistical differences (Figure 1).

3.2. Inflammation Cytokines in Tears Promoted the Occurrence of Dry Eye in Children with Concomitant Exotropia. We found that adults had obvious dry eye-related symptoms in concomitant exotropia, while children had no significant difference compared to the control group. A variety of tear proteins are significantly associated with aging in strabismus patients, many of which were associated with inflammation, immune response, and cell death [7]. The persistence of inflammatory cytokines in tears may be associated with the occurrence of dry eyes in concomitant exotropia. To investigate the different levels in the children with exotropia and control, we used SIMOA technology to measure the levels of inflammatory cytokines in tears in strabismus and normal patients. Levels of INF-γ, IL-10, IL-12p70, IL-17A, IL-6, and TNF-α were measured. We found the expression of INF-γ, IL-10, IL-12p70, and IL-17A in tears of strabismus patients, which were no significantly higher than those of normal subjects, while IL-6 and TNF-α were statistically significant (Table 3, Figure 2).

3.3. Mechanistic Hypothesis of Ocular Surface Inflammation Cytokines and Dry Eye in Patients with Concomitant Exotropia. The role of multiple inflammatory factors in dry eye symptoms of patients with concomitant exotropia is unknown. Firstly, increased exposure and local lesions in concomitant exotropia lead to increased expression of inflammatory factors, especially IL-6 and TNF-α, in the tears. Secondly, the increased expression of inflammatory cytokines may lead to goblet cell apoptosis and the occurrence of dry eye. Thirdly, related literature supports that IL-6 and TNF-α may activate downstream NF-κB [8], p38MAPK [9], and JNK[10] pathways through TNF receptor 1 and activate downstream caspase-8[11] through TNF receptor 2 to induce apoptosis of functional cells (Figure 3).

4. Discussion

We have shown here that dry eye-related indicator is abnormal in adults while it is normal in children, which included the ocular surface disease index (OSDI), the height of the river of tears, the tear film rupture time, the tear secretion level, and the eye red index. The concentration of tear mediators increased obviously in concomitant exotropia, and the IL-6 and TNF-α could be important mediators of inflammation. Inflammatory cytokines may be involved in goblet cell apoptosis through a variety of signaling pathways. Early intervention in these patients can avoid long-term high concentration of inflammatory factors and the occurrence of dry eye.

Patients with concomitant exotropia have dry eyes and tear film instability before surgery. The height of lacrimal river in patients with exotropia and esotropia was 0.21 ± 0.06 mm and 0.17 ± 0.05 mm, and the mean BUT was <7 S. The mean conjunctival red eye index in patients with exotropia was 0.83 ± 0.37 [1]. With the increase of age, the conjunctival red eye index in patients with strabismus

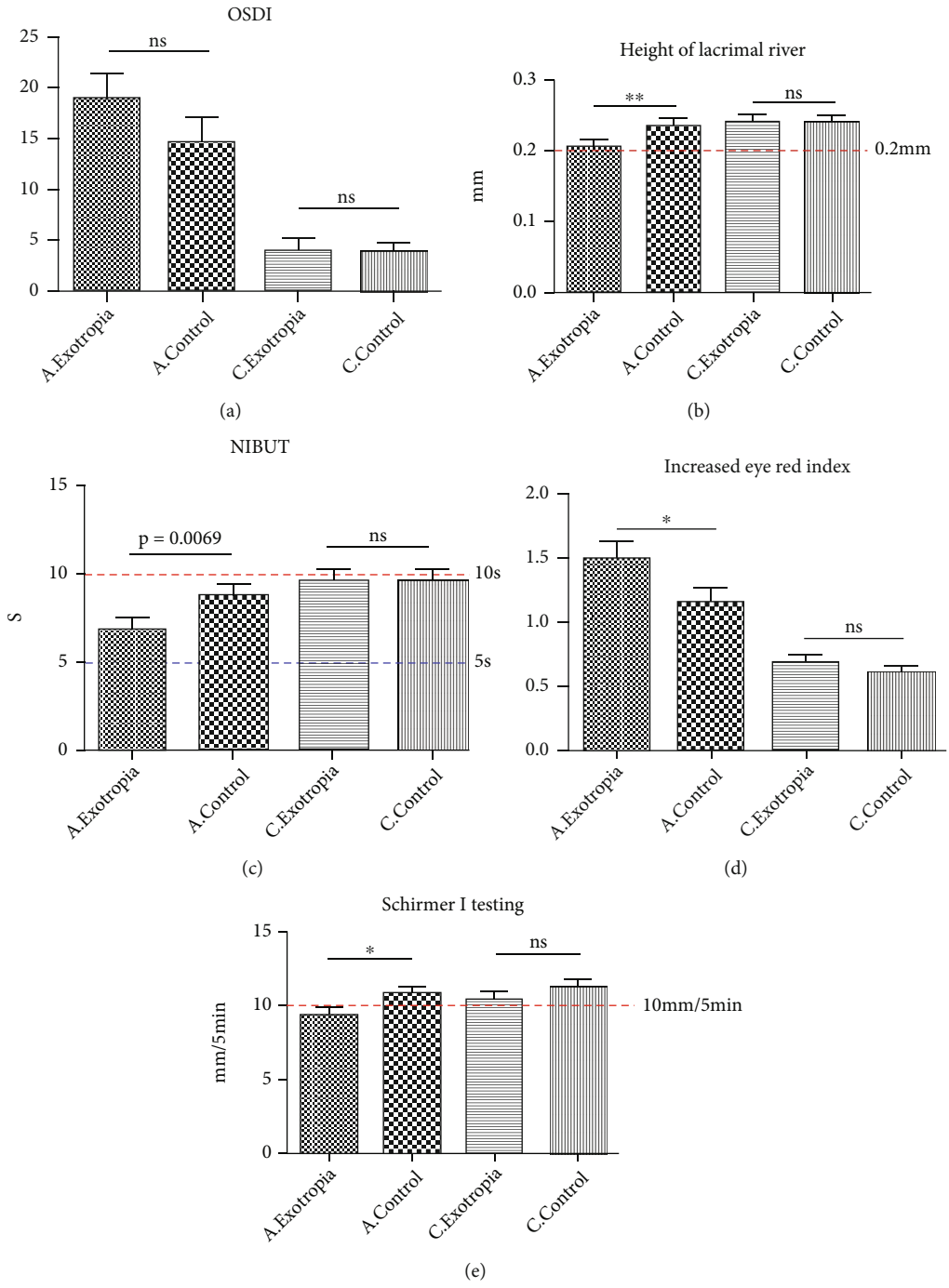

Figure 1: The ocular surface analysis in patients with concomitant exotropia. (a) The ocular surface disease index (OSDI); (b) the height of the river of tears; (c) the noninvasive tear film rupture time (NIBUT); (d) the eye red index; (e): the schirmer I testing. A. exotropia: concomitant exotropia in adult; C. exotropia: concomitant exotropia in children; A. control: control group in adult; C. control: control group children.

Table 3: The level of inflammatory cytokines in the tears.

	INF-γ (pg/mL)	IL-10 (pg/mL)	IL-12p70 (pg/mL)	IL-17A (pg/mL)	IL-6 (pg/mL)	TNF-α (pg/mL)
Exotropia	0.0284 ± 0.0125	0.3358 ± 0.1872	0.0253 ± 0.0078	0.1551 ± 0.0437	4.683 ± 1.329	0.2095 ± 0.0703
Control	0.0090 ± 0.0024	0.0513 ± 0.0149	0.0099 ± 0.0023	0.0793 ± 0.0313	1.455 ± 0.391	0.0513 ± 0.0149
p	0.1434	0.1506	0.0729	0.1739	0.0304	0.0397

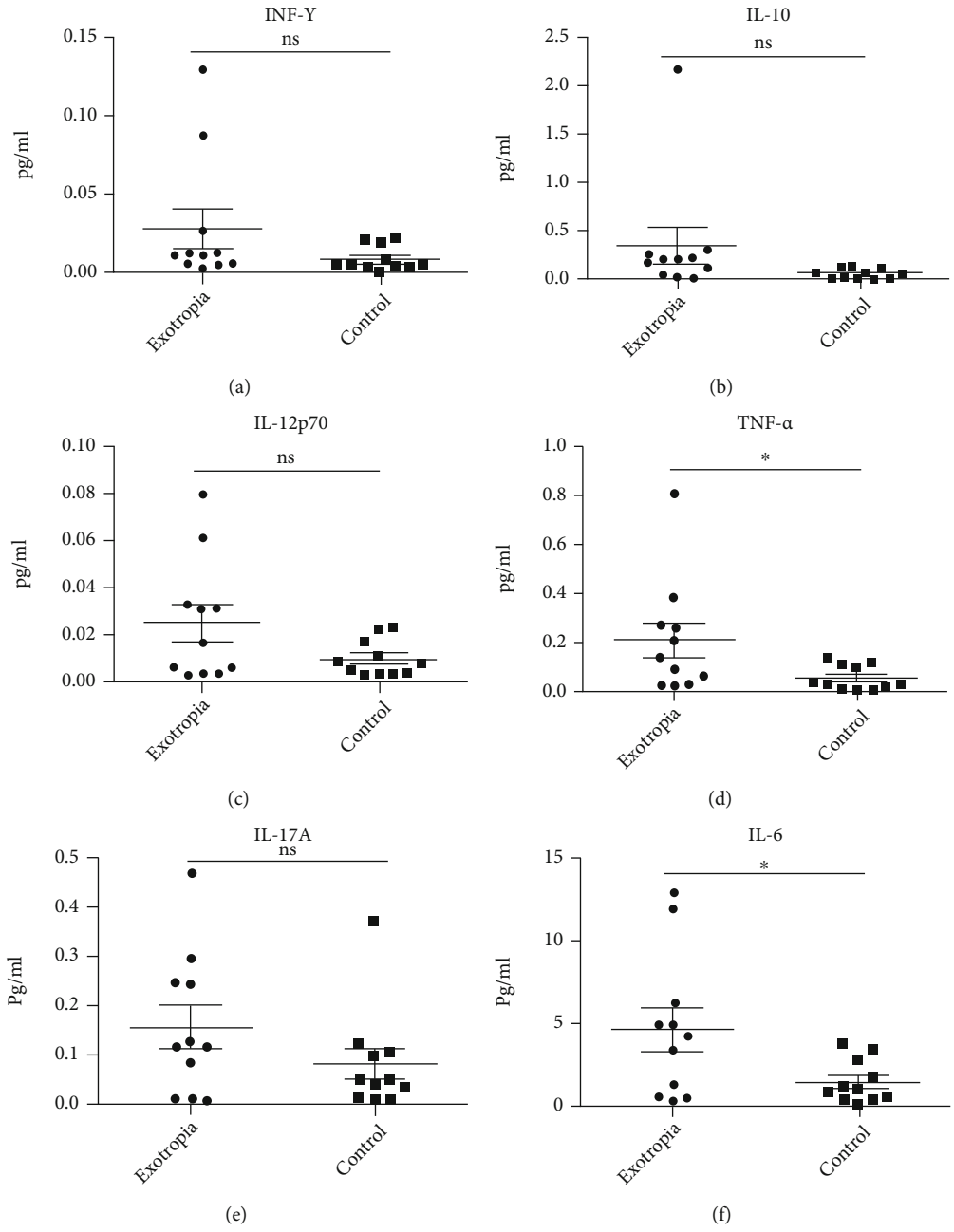

Figure 2: The level of inflammatory cytokines in tears of patients with concomitant exotropia. (a) INF-γ; (b) IL-10; (c) IL-12p70; (d) TNF-α; (e) IL-17A; (f) IL-6.

increased [1]. There were statistically significant differences in NIBUT and eye red index among multiple age groups in the concomitant exotropia [12]. A variety of tear proteins are significantly associated with aging in strabismus patients; many of which were associated with inflammation, immune response, and cell death. The persistence of inflammatory cytokines in ocular surface resulted in a series of pathophysiological changes, associated with abnormal of dry eye-related examines.

In this study, we selected several inflammatory cytokines associated with dry eye, including IL-17A, IL-10, IL-12p70, INF-γ, IL-6, and TNF-α. Dry eyes are a common ocular disease characterized by reduced tear production on both sides and unstable tear film. Goblet cell loss was directly related to surface cell apoptosis after chronic inflammatory injury, resulting in further tear film instability/imbalance [13]. IL-17A, a Th17-related cytokine, played an important role in the pathogenesis of dry eye disease, and its expression in tears may be a diagnostic biomarker for dry eye disease [14]. Significant differences in the concentration of cytokines (IL-6, IL-10, and TNF-α) were detected in tear samples collected from patients with dry eyes [15, 16]. Luminex technique indicated that the level of IL-12p70 in peripheral blood of patients with dry eye was significantly higher than

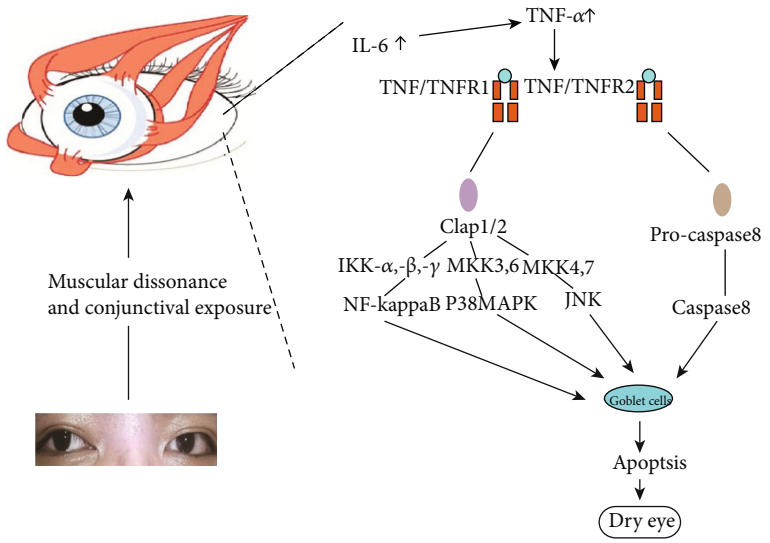

Figure 3: The role of TNF-α and IL-10 in the ocular inflammation and dry eyes.

that of normal control group [17]. Interferon-γ and IL-17A induced dry eye surface injury and the density of goblet cells in mice [18].

TNF-α and IL-6 are important factors of goblet cell apoptosis and dry eye symptoms in patients with concomitant exotropia. The production of TNF-α and IL-1 leads to the damage of dry eye surface in mice [18]. NF-κB activation was an important regulator of TNF-α mediated apoptosis of corneal fibroblasts [19]. The activation of NF-κB resulted in inflammation and apoptosis by on the ocular surface of dry eye, thereby reducing tear secretion [8]. TNF-α induces cell apoptosis by activating the p38 MAPK signaling pathway and acts as an effective TNF-α antagonist to prevent p38 MAPK-dependent apoptosis induced by TNF-α in cells [9].

The study has several limitations. Firstly, the number of samples included in this study was small, because we need to conduct rigorous screening of the subjects included in the study, and, it should be tested as soon as possible to prevent long-term storage of samples. Secondly, the experimental results of this study were not repeated for many times, and the test operation process was standardized by professional technicians without any information about sample type. Thirdly, some cytokine concentration in the research was lower than LLOQ, and we treated this part of data in accordance with the LLOQ of the corresponding panel, and this alternative result was reasonable.

5. Conclusion

In summary, we found that high expression levels of inflammatory factors (IL-6, and TNF-α) in tears of patients with concomitant exotropia were significant higher than the control, which could be a potential factor who promoted the occurrence of dry eye in the patients with concomitant exotropia. Further studies are needed to determine the ocular surface inflammation in patients with strabismus and whether the early intervention of ocular surface inflammation is beneficial to the prognosis of patients with concomitant strabismus.

Data Availability

The data used to support the findings of this study are currently under embargo while the research findings are commercialized. Requests for data, 12 months after publication of this article, will be considered by the corresponding author.

Ethical Approval

All human studies were approved by the Ethics Committee of the First Affiliated Hospital of Fujian Medical University (MTCA, ECFAH of FMU [2019] 001) and (MTCA, ECFAH of FMU [2015] 084-1).

Conflicts of Interest

All authors certify that they have no any financial interest or nonfinancial interest in the subject matter or materials discussed in this manuscript.

Authors' Contributions

Feng Gao and Xiaoping Hong contributed equally to this work.

Acknowledgments

We would like to thank the students (Yuxin Liu, Yue Luo, Xiaoxia Luo, and Junjie Lai) from the Department of Medical Laboratory of Fujian Medical University for their support in language processing. We would like to thank the Southeast Eye Hospital of Fuzhou for providing tear samples. The presentation of the manuscript in "preprint" in research square according to the following link https://www.researchsquare.com/article/rs-115845/v1. This work was

supported by the National Natural Science Foundation of China (No. 81871293) and Medical Innovation in Fujian Province (2019-CX-27). These funding sources played key supportive role for sample collection, molecular analysis of patient samples, and bioinformatics analysis.

References

[1] S. Jinxin, H. Zhaoqin, Z. Cui, X. Jintao, W. Jie, and X. Yongxin, "Study on ocular surface tear in patients with concomitant strabismus," *Chinese Journal of Practical Ophthalmology*, vol. 35, no. 1, pp. 41–44, 2017.

[2] G. Giannaccare, P. Versura, S. Sebastiani, C. Fariselli, M. Pellegrini, and E. Campos, "Dry eye disease in strabismus patients: does eye deviation harm ocular surface?," *Medical Hypotheses*, vol. 111, pp. 15–18, 2018.

[3] Z. Yiwen, T. Zhoujunyi, J. Yuebo, H. Yanling, H. Jing, and L. Zhanguo, "Clinical significance of comprehensive ocular surface analyzer in evaluating dry eye of Sjogren's syndrome," *New Advances in Ophthalmology*, vol. 36, no. 7, pp. 630–633, 2016.

[4] M. Qi and L. N. Xiao, "Measurement of the height of the river of tears," *Chinese Journal of Ophthalmology*, vol. 51, no. 3, p. 224, 2015.

[5] I. M. Balmus, R. O. Cojocariu, A. Ciobica et al., "Preliminary study on the tears oxidative stress status and sleep disturbances in irritable bowel syndrome patients," *Oxidative Medicine and Cellular Longevity*, vol. 2020, Article ID 4690713, 9 pages, 2020.

[6] E. Y. Zernii, O. S. Gancharova, V. E. Baksheeva et al., "Mitochondria-targeted antioxidant SkQ1 prevents anesthesia-induced dry eye syndrome," *Oxidative Medicine and Cellular Longevity*, vol. 2017, Article ID 9281519, 17 pages, 2017.

[7] J. Nättinen, A. Jylhä, U. Aapola et al., "Age-associated changes in human tear proteome," *Clinical Proteomics*, vol. 16, no. 1, p. 11, 2019.

[8] Y. Li, R. Jin, L. Li et al., "Expression and role of nucleotide-binding oligomerization domain 2 (NOD2) in the ocular surface of murine dry eye," *Investigative Ophthalmology & Visual Science*, vol. 60, no. 7, pp. 2641–2649, 2019.

[9] N. Chen, F. Wei, L. Wang, S. Cui, Y. Wan, and S. Liu, "Tumor necrosis factor alpha induces neural stem cell apoptosis through activating p38 MAPK pathway," *Neurochemical Research*, vol. 41, no. 11, pp. 3052–3062, 2016.

[10] R. Wang, I. Kwon, N. Singh et al., "Type 2 cGMP-dependent protein kinase regulates homeostasis by blocking c-Jun N-terminal kinase in the colon epithelium," *Cell Death and Differentiation*, vol. 21, no. 3, pp. 427–437, 2014.

[11] L. Xu, Y. Zhang, X. Qu et al., "DR5-Cbl-b/c-Cbl-TRAF2 complex inhibits TRAIL-induced apoptosis by promoting TRAF2-mediated polyubiquitination of caspase-8 in gastric cancer cells," *Molecular Oncology*, vol. 11, no. 12, pp. 1733–1751, 2017.

[12] R. Hao, S. Y. Suh, A. Le, and J. L. Demer, "Rectus extraocular muscle size and pulley location in concomitant and pattern exotropia," *Ophthalmology*, vol. 123, no. 9, pp. 2004–2012, 2016.

[13] T. Yamaguchi, "Inflammatory response in dry eye," *Investigative Ophthalmology & Visual Science*, vol. 59, no. 14, pp. DES192–DES199, 2018.

[14] R. Liu, C. Gao, H. Chen, Y. Li, Y. Jin, and H. Qi, "Analysis of Th17-associated cytokines and clinical correlations in patients with dry eye disease," *PLoS One*, vol. 12, no. 4, article e0173301, 2017.

[15] K. VanDerMeid, S. Su, K. Krenzer, K. Ward, and J. Zhang, "A method to extract cytokines and matrix metalloproteinases from Schirmer strips and analyze using Luminex," *Molecular Vision*, vol. 17, pp. 1056–1063, 2011.

[16] J. Benitez-del-Castillo, J. Cantu-Dibildox, S. M. Sanz-González, V. Zanón-Moreno, and M. D. Pinazo-Duran, "Cytokine expression in tears of patients with glaucoma or dry eye disease: a prospective, observational cohort study," *European Journal of Ophthalmology*, vol. 29, no. 4, pp. 437–443, 2019.

[17] H. Zhao, Q. Li, M. Ye, and J. Yu, "Tear luminex analysis in dry eye patients," *Medical Science Monitor: International Medical Journal of Experimental and Clinical Research*, vol. 24, pp. 7595–7602, 2018.

[18] Y. Yang, C. Huang, X. Lin et al., "0.005% preservative-free latanoprost induces dry eye-like ocular surface damage via promotion of inflammation in mice," *Investigative Ophthalmology & Visual Science*, vol. 59, no. 8, pp. 3375–3384, 2018.

[19] R. Mohan, R. Mohan, W. Kim, and S. Wilson, "Modulation of TNF-alpha-induced apoptosis in corneal fibroblasts by transcription factor NF-kappaB," *Investigative Ophthalmology & Visual Science*, vol. 41, no. 6, pp. 1327–1336, 2000.

Hindawi
Oxidative Medicine and Cellular Longevity
Volume 2021, Article ID 1438837, 10 pages
https://doi.org/10.1155/2021/1438837

Research Article

DNA Methylation Pattern of CALCA and CALCB in Extremely Premature Infants with Monochorionic Triplets after Single-Embryo Transfer

Feng Gao,[1] Yujia Guo,[2] Xingting Chen,[2] Qiuyang Gu,[3] Shirong Huang,[4] Qingquan Chen,[4] Xiaoming Xu,[5] Kai Zeng,[6] Huilin Zhou,[2] Yilu Zou,[2] and Qicai Liu[2]

[1]*Department of Pathology, 1st Affiliated Hospital, Fujian Medical University, Fuzhou 350004, China*
[2]*Center for Reproductive Medicine, 1st Affiliated Hospital, Fujian Medical University, Fuzhou 350004, China*
[3]*Department of Medical Ultrasonography, 1st Affiliated Hospital, Fujian Medical University, Fuzhou 350005, China*
[4]*Department of Laboratory Medicine, Fujian Medical University, 350004 Fuzhou, China*
[5]*Beijing Perfect Family Hospital, Beijing 100032, China*
[6]*Department of Anesthesiology, 1st Affiliated Hospital, Fujian Medical University, Fuzhou 350005, China*

Correspondence should be addressed to Qicai Liu; lqc673673673@163.com

Feng Gao, Yujia Guo, Xingting Chen, and Qiuyang Gu contributed equally to this work.

Received 29 May 2021; Revised 15 August 2021; Accepted 5 September 2021; Published 5 October 2021

Academic Editor: Mariaurea Matias Sarandy

Compared with full-term peers, premature infants are more likely to suffer from neonatal diseases and death. Variations in DNA methylation may affect these pathological processes. Calcitonin gene-related peptide (CGRP) plays a complex and diversified role in reproduction and chronic inflammation, and participates in the functional maintenance of vascular adaptation and trophoblast cells during pregnancy. Here, premature live births with single-chorionic triple embryos after single-embryo transfer were used as research objects, while full-term infants with double embryos and double-chorionic twins were used as controls. DNA was extracted from umbilical cord tissues for pyrosequencing to detect the methylation level of CpG island in CGRP promoter region. The average values of CGRP methylation in the umbilical cord tissues of very premature fetuses were higher than that of normal controls obtained from the databases. Immunofluorescence results showed that the expression of αCGRP was decreased in the blood vessel wall of the umbilical cord of monozygotic triplets, especially in death cases, while the βCGRP had a compensatory expression. In conclusion, our findings suggest that hypermethylation of CGRP might be considered as an important cause of serious neonatal morbidities.

1. Introduction

Impaired blood circulation in the umbilical cord or placenta might lead to intrauterine growth restriction and premature delivery and is considered as an important complication during pregnancy [1]. Calcitonin gene-related peptide (CGRP) is regarded as the most effective vasodilator, and it plays a complex and diversified role in chronic low-grade inflammation [2]. It is closely related to functional maintenance of vascular adaptation and trophoblast cells during pregnancy [3]. It comprises two subtypes CALCA (αCGRP) and CALCB (βCGRP), and these coordinate with molecular signaling network of decidualization, placenta formation, and fetal growth to promote successful pregnancy outcomes [3, 4]. But the role of it in finely synchronized molecular and cellular events during preterm labor still remains to be unknown.

Our previous studies have revealed that abnormal secretion of βCGRP is caused by CALCB mutation, which lose its inhibitory effect on inflammatory cells, resulting in obliterative vasculitis and perineuritis [5]. At the same time, interleukin- (IL-) 6, IL-10, and tumor necrosis factor-α (TNF-

α) were highly expressed in CGRP-KO rats, which might be involved in the occurrence of fetal inflammation [6]. CGRP can inhibit the synthesis and/or release of inflammatory factors such as TNF-α, IL-1, and IL-12 by regulating cytokine expression of macrophages through cAMP/PKA signaling pathway and inhibiting the differentiation of Th1 lymphocytes. CGRP can also regulate the balance between Th1/Th2 cells, promoting the release of IL-10 and IL-4 from macrophages and Th2 lymphocytes and inhibiting the antigen presentation of Th1 cells, thereby inhibiting Th1 cell-mediated cellular immunity [7, 8]. Therefore, we speculated that CGRP might participate in immune regulation and inhibition of inflammation during pregnancy, thereby affecting fetal development and progression of labor.

In addition to the influence of neurological factors, CGRP expression also plays an important regulatory role in its own gene structure and methylation modification. There is a large CpG island in the $5'$ flanking promoter region of the CALCA and contains a microbial infection-specific response elements that regulate the transcription of procalcitonin (PCT) during bacterial infection [9]. The structure of CALCB is similar to that of CALCA, and it consists of two different CpG-rich regions, wherein one is located around exon 1, and the other is located about 1.5 kb upstream [10]. Single-egg multiple births might occur due to different methylation patterns during embryonic development, and this might be a reason for the differences in fetal development [11]. The monochorionic triplet (MCTA) genetic background is a common, reliable, and excellent sample for studying the role of CGRP in pregnancy maintenance. Hence, in this study, the methylation levels and expression location of CALCA and CALCB in the umbilical cord tissues of monochorionic three amniotic sacs were detected, and the relationship between them and the very preterm birth were evaluated.

2. Materials and Methods

2.1. Research Subject. A case of monochorionic triplets and the very premature live births of three boys after single blastocyst transplantation were collected as research subjects from the Reproductive Medicine Center of the First Affiliated Hospital of Fujian Medical University in April 2020. In addition, those undergoing double blastocyst transplantation in the same period were selected. Chorionic twins and two full-term live births were used as controls. General information including age, basic hormone levels, fetal development process, and family history were collected. After obtaining their consent, the remaining umbilical cord and placental tissue samples from *in vitro* pathological diagnosis were collected for methylation and immunohistochemical testing.

2.2. Database Retrieval and Prediction. To study the relationship between gene methylation in umbilical cord or cord blood and preterm birth, two matching databases were found. Genome wide DNA methylation profiling of 152 umbilical cord blood samples from CCCEH birth cohort. The Illumina Infinium 450k Human DNA methylation Beadchip was used to obtain DNA methylation profiles across approximately 450,000 CpGs in cord blood samples. https://www.ncbi.nlm.nih.gov/geo/query/acc.cgi?acc=GSE69176.

An Epigenetic-Senescence-Signature, based on six CpGs, was either analyzed by pyrosequencing or by barcoded bisulfite amplicon sequencing. https://www.ncbi.nlm.nih.gov/geo/query/acc.cgi?acc=GSE82234.

2.3. Pyrosequencing. DNA was extracted from umbilical cord tissues (about 5 cm from placenta attachment) of three infants with single chorionic triplets and preterm live birth after single blastocyst transplantation and double blastocyst transplantation double chorionic twins and two full-term live births using the Tiangen DNA Extraction Kit (TIANGEN, Beijing, China) according to manufacturer's instructions. DNA was sent directly to Gene Tech (Shanghai) Co, Ltd. (Gene Tech, Shanghai, China) for pyrosequencing to detect the methylation level of CpG island in CGRP promoter region. The sequencing primers, conditions, and sequencing sequences used are shown in Figure 1.

2.4. Immunofluorescence. The immunofluorescence measurements were performed as previously described [12]. The procedure is briefly described as follows: umbilical cord tissue and placental tissue were fixed in 4% formalin overnight, embedded in paraffin, sectioned at 4 mm. Immunofluorescence confocal microscopy was also undertaken to determine the correlation of CALCA (αCGRP) and CALCB (βCGRP). CALCA was detected with rabbit antihuman polyclonal antibody (1 : 50 dilution; A11804, Abclonal, CN), and CALCB was detected with rabbit antihuman polyclonal antibody (1 : 200 dilution; A5523, Abclonal, CN). The secondary antibody was rhodamine- (TRI-TC-) conjugated goat anti-rabbit IgG or FITC-labeled goat anti-rabbit IgG. Nuclei were stained with DAPI solution.

3. Results

3.1. Clinical Data of Identical Triple Pregnancies. A 29-year-old female patient was treated with in vitro fertilization (IVF) and transplanted a fresh cycle of one blastocyst (4AB) on day 5, which is a monochorionic triple amniotic pregnancy shown in pregnancy ultrasound. This blastocyst was premature rupture of membranes at 25 W + 1 week, and three boys were born prematurely. The newborns had an Apgar score of 4 and a weight of 800 g. One of the newborns was short in height and malnourished and died after rescue (Table 1). General clinical data show that the patient has lived with the current husband for 6 years, married for 5 years, and has an average sex life of 3-4/month. The husband has ejaculated and has not been pregnant yet. The patient was diagnosed with "polycystic ovary syndrome" in 2015. In 2016, the patient underwent a series of operations, such as laparoscopic ovarian perforation, hysteroscopy, and bilateral salpingectomy. Patient's infusion during surgery is normal. The pathological results after surgery showed endometrial polyps. Basic endocrine examination: FSH 1.11 IU/L, LH 6.4 IU/L, E2 35.2 miu/L, T 57.6 nmol/L, and

CALCA

Primer Set 1	Score: 62
General Warnings	

F1	F1	TTATAGTTTYGGGATGTAGTTGTTG
R1	R1	TTTCAACCTCTCCACCATCT
S1	S1	TGTTGAGTTTATYGTATAGGTA

	PCR Product	Forward PCR Primer, F1	Reverse PCR Primer, R1	Sequencing Primer, S1
Length, bp	109	25	20	22
Position, 5'- 3'		538 - 562	646 - 627	558 - 579
Tm, °C		65.4	66.1	45.9
%GC	35.8	32.0	45.0	27.3
Sequence to Analyze	GYGTTYGGAT YGGTTGTAGT AGATYGYGYG TTGYGYGTTT TATYGGGAGA TGGTGGAGA			

CALCB

Primer Set 0	Score: 79
GeneralWarnings	

F1	F1	GGTCAGTTTTGGTTATTTTGGAT
R1	R1	CCTCACCTAACCACTAAAATTTCA
S1	S1	TTTTTAGTTATTTTTGTAATAAG

	PCR Product	Forward PCR Primer, F1	Reverse PCR Primer, R1	Sequencing Primer, S1
Length, bp	175	23	24	23
Position, 5'- 3'		184 - 206	358 - 335	236 - 258
Tm, °C		67.1	67.4	47.6
%GC	36.0	34.8	37.5	13.0
Sequence to Analyze	AGYGGGGTTT TYGYGGGGAA GGYGTTTATA GTAGGTGTGG TGTTTATTTY GGGTYGATYG GTYGTTYGYG TTGTTTTGAA ATTTTAGT			

Figure 1: Primers, conditions, and sequencing sequences of CALCA and CALCB methylation.

AMH 5.95 ng/mL. Birth history: 0-0-0-0. Not pregnant for 6 years without contraception. The semen of the man is normal, the chromosomes of both men and women are normal, and the close relatives of both men and women do not have multiple births. All human studies were approved by the Ethics Committee of the First Affiliated Hospital of Fujian Medical University (MTCA, ECFAH of FMU [2019] 001) and (MTCA, ECFAH of FMU [2015] 084-1).

2019.8.23 Ultrasound showed 5 antral follicles on the left ovary, 27 ∗ 22 mm follicles on the right ovary, and 3-4 antral follicles, Em: 13.0 cm, C Type. GnRH-a ultralong regimen was used, and leuprolide was adjusted down 3.75 mg/d after communication with the patient. 2019.9.10 Leuprolide was used to downregulate for 27 days, blood hormone: E2: 33.19 pmol/l, FSH: 2.42 IU/L, LH: 0.51 IU/L, *P*: 0.64 nmol/L. Vaginal B-ultrasound shows that 8-9 antral follicles can be seen on the left ovary, 4 antral follicles can be seen on the right ovary, Em: 2.0 mm, C Type. After communicating with the patient, she was given LH 150 IU/day and HMG225 IU/d growth hormone 4 IU/d started. 2019-9-30 Gn11day, vaginal B-ultrasound: there are 22 follicles in both ovaries, of which 6 are >1.8 cm follicles. Blood hormone: E2: 7678 pmol/L, *P* 1.11 nmol/L, LH: 1.25 IU/L. Stop Gn, Azer 200ug trigger, OPU operation for 38 hours. 12 eggs were examined, 10 of which were mature. IVF short-term fertilization, seven appeared 2PN, and D3 high-quality 3 embryos. A fresh cycle embryo is transferred and administered: dydrogesterone 20 mg bid po∗10 d; progesterone suppository 2 tabletsbid pv∗10 d.

Frozen embryos: D5 (4AB, 4BB), D6 (4CC+).

Fresh cycle embryo transfer: single blastocyst transplantation (2PN-4CII-8CII-4BA) (Figure 2(a)), the transplant process went smoothly. Day 11, blood HCG 194.7 mIu/mL, day 14, blood HCG 595.1 mIu/mL, 6 W + 4 ultrasound shows gestational sac size: 3.5 ∗ 1.4 ∗ 2.3 (cm). Gross pathology showed single placenta, three amniotic sacs, and three umbilical cords (Figures 2(b) and 2(c)). Histopathology showed acute chorioamnionitis and chorionic plate vasculitis (Figure 2(d)). No triplet transfusion syndrome was found.

3.2. Ultrasound Monitoring Results. Early ultrasound (12 W) of three independent fetuses (a, b, and c), a single placenta, and three independent amniotic sacs were shown in Figure 3(a). Color Doppler ultrasound NT examination revealed three fetuses and one placental echo in the uterine cavity, and the three fetuses were arranged in the upper right (a), upper left (b), and lower right (c) quadrants. Echoes of the diaphragm were seen among the three fetuses, and the three diaphragms and the placenta showed a T sign. The placenta was located in the posterior wall, covering the cervix by its lower edge. Maturity level was 0 (Figure 3(b)). Ultrasound examination in second trimester (20 weeks) revealed placental maturity level of I and thickness of about 3.23 cm (Figure 3(c)).

Table 1: General condition of newborns with three births with monochorionic three amniotic sac.

Fetus	Survival	Apgar score	Weight (g)	Height (cm)	Health status	Birth defects	Other
A	Yes	4	806	25	General	None	Healthy discharge
B	Yes	4	833	25	General	None	Healthy discharge
C	Yes	4	800	22	Unhealthy	None	Died after rescue

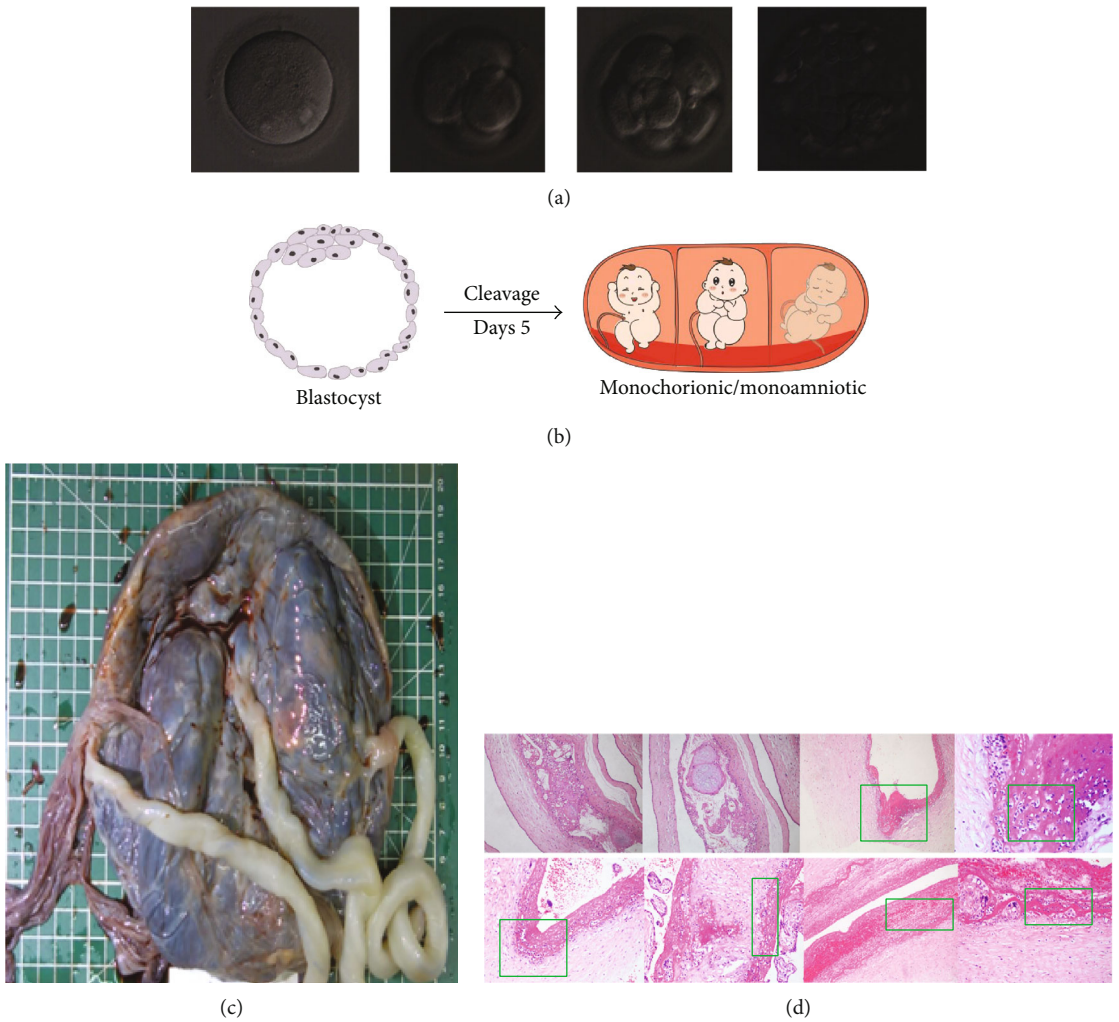

Figure 2: Clinical data of identical triple pregnancies. (a) Embryo development (2PN-4CII-8CII-4BA), scale 0.0002 mm; (b) identical triplet pattern diagram; (c) identical triple placenta umbilical cord and blood vessels on the umbilical cord (Left: general sample image of placenta and umbilical cord; upper right: pathological image of umbilical cord blood vessel of fetus A; middle right: pathological image of umbilical cord blood vessel of fetus B; lower right: pathological image of umbilical cord blood vessel of fetus); (d) chorioamnionitis and chorionic plate vasculitis, scale bar 0.003 mm; green box marketed and highlight show inflammatory cell infiltration area.

3.3. Database Search Results. The umbilical vein (6 samples) and cord blood (152 samples) were collected from the samples. The average methylation rate of CALCA was 10.08% and 9.50%, and that of CALCB were 5.31% and 7.71%, respectively.

3.4. Methylation Sequencing Results. The average values of CpG island methylation in CALCA promoter region in fetal A, B, and C umbilical cord tissues were 12.125%, 15.5%, and 18.625%, respectively, and these were higher than those in normal controls. The average methylation rate of CALCA promoter region in D and E umbilical cord tissues of full-term control fetuses was only 6.125% and 4.375%. Based on this, it was clear that the percentage of CALCA methylation in the umbilical cord tissues of premature fetuses was higher than that of full-term births, and the percentage of CALCA methylation in the C umbilical cord tissues of fetuses that died after rescue remained the highest.

Similarly, the average values of CALCB methylation in umbilical cord tissues of premature fetuses A, B, and C were 15.889%, 11.222%, and 16.667%, respectively, and were higher than those of normal controls. However, the average

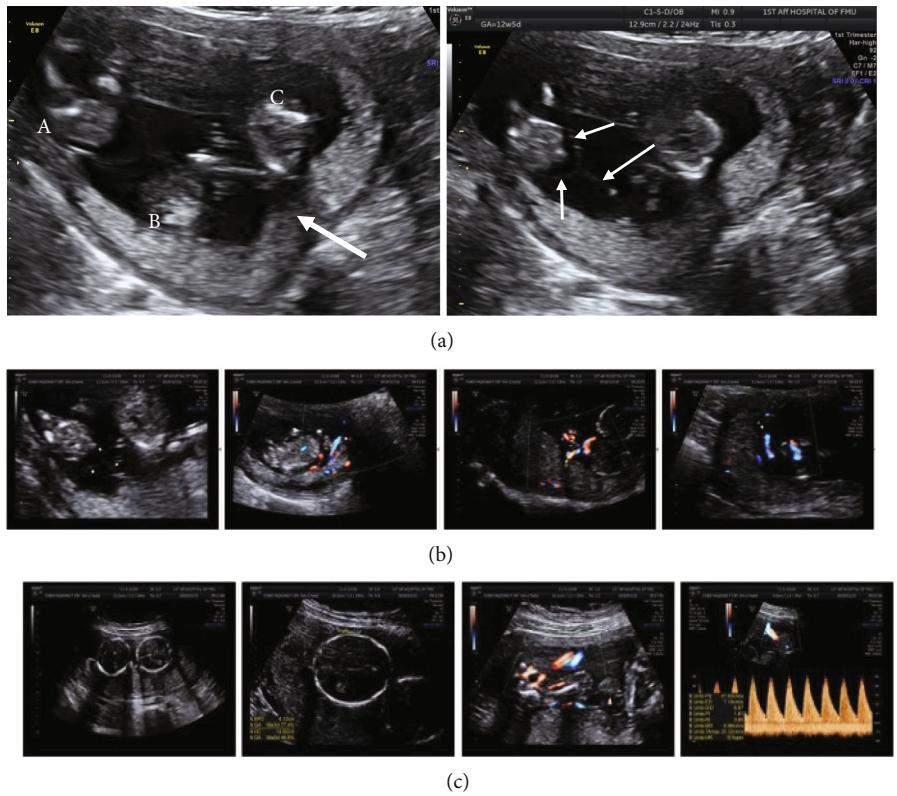

Figure 3: B-ultrasound monitoring results of identical triple pregnancies. (a) Left: three independent fetuses a, b, and c can be seen, and the arrow is a single placenta; right: three independent amniotic sacs are seen, and the arrow is the amniotic echo; (b) early color Doppler ultrasound NT examination; (c) ultrasonography in the second trimester (20 weeks).

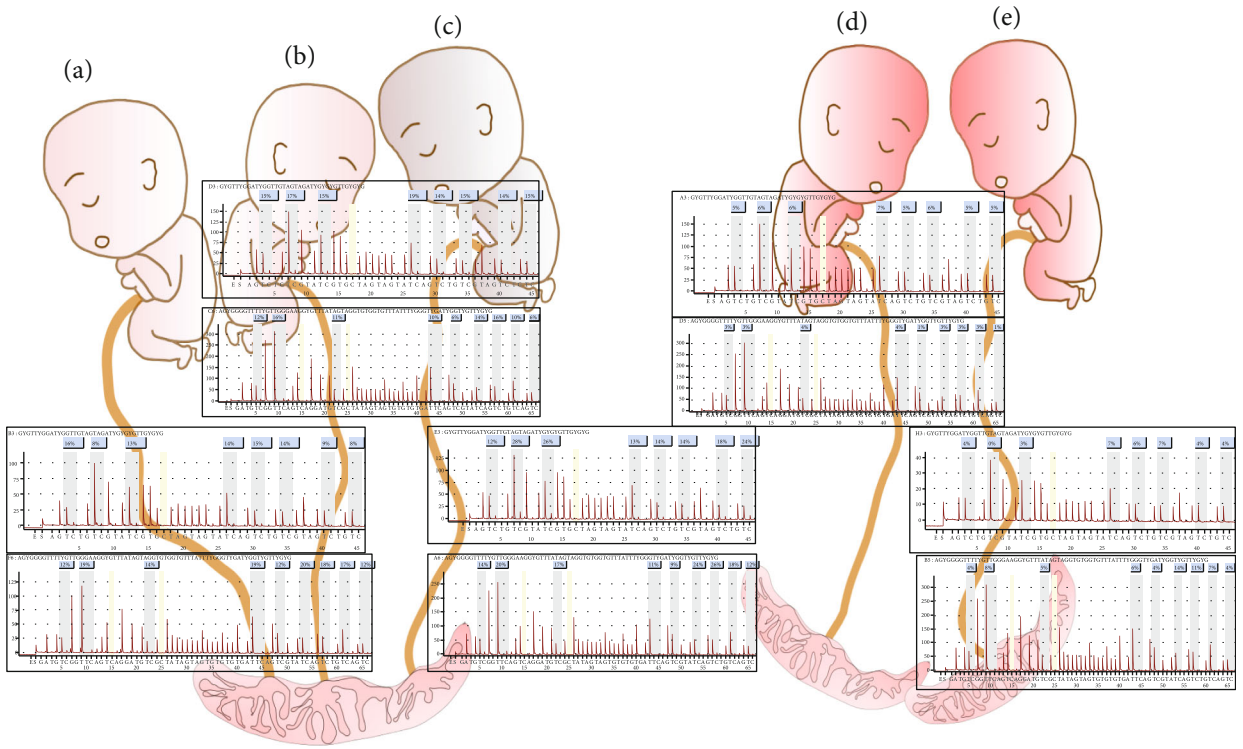

Figure 4: CALCA and CALCB methylation results of umbilical cord tissues from identical triple pregnancy and control. Among them, the identical triplets were triplet (a), triplet (b), and triplet (c) and triplet (d) and triplet (e) fraternal twins.

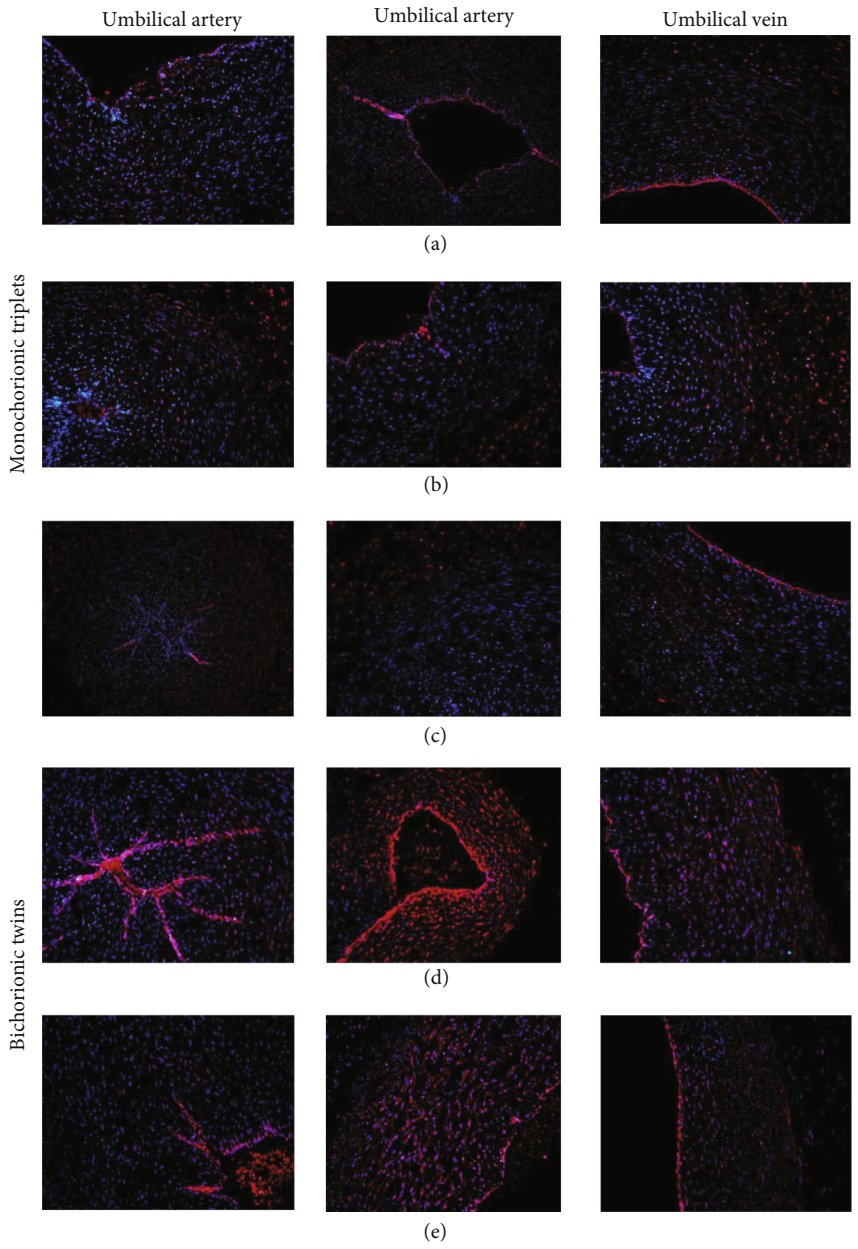

Figure 5: CALCA expression in the umbilical cord. Tissue section of umbilical cord were exposed to αCGRP IgG at 4°C for 20 minutes. The localization of αCGRP was monitored by immunofluorescence microscopy. In umbilical cord tissue, CGRP was weakly expressed, mainly in vascular endothelial cell layer. (a), (b), and (c) are identical triplets ((c) is the invalid death case); (d) and (e) are fraternal twins.

percentage of methylation of CpG island in CALCB promoter region in D and E umbilical cord tissues of full-term fetuses was only 2.778% and 7.0%. In addition, the methylation percentage of CALCB in umbilical cord tissues of premature fetuses was higher than that of term births, and the CALCB promoter region methylation percentage in the C umbilical cord tissues of fetuses that died after rescue remained the highest (Figure 4).

Among these, the identical triplets were triplet A, triplet B, and triplet C and triplet D and triplet E fraternal twins. The results of pyrophosphorylation sequencing showed that the methylation levels of CALCA and CALCB in the umbilical cord tissue of three premature births with single chorionic sac were higher than those of full-term twins with double chorionic sac, and the methylation levels of death cases after rescue were higher when compared to others.

3.5. Tissue Immunohistochemical Test Results. Immunofluorescence results revealed that the expression of αCGRP in the umbilical cord of the twin brothers (triplet A, triplet B, and triplet C) was lower than that of normal controls (triplet D and triplet E), especially in death cases (triplet C) (Figure 5). Immunofluorescence results showed that the level of βCGRP revealed no significant differences in the vascular endothelium and vascular wall of umbilical cord of

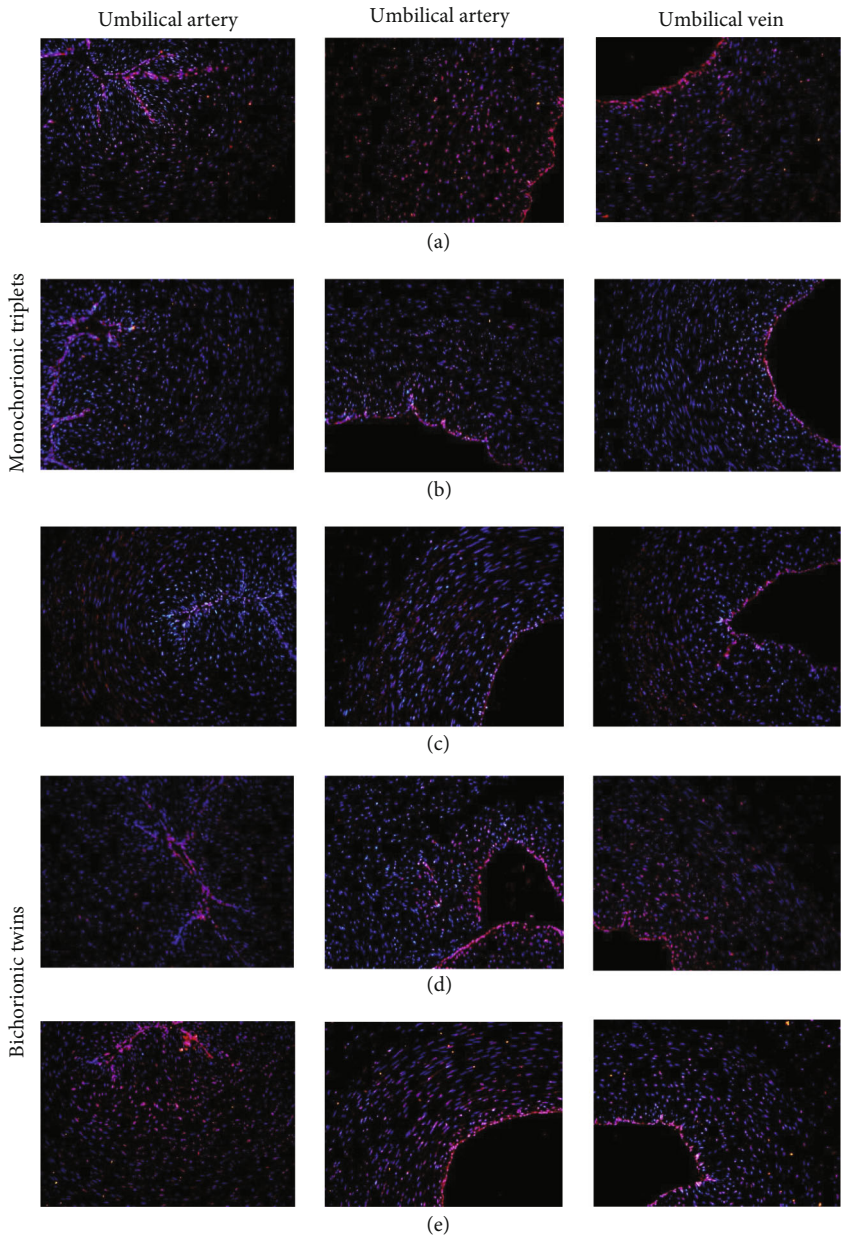

Figure 6: CALCB expression in the umbilical cord. Tissue section of umbilical cord were exposed to βCGRP IgG at 4°C for 20 minutes. The localization of βCGRP was monitored by immunofluorescence microscopy. In umbilical cord tissue, CGRP was weakly expressed, mainly in vascular endothelial cell layer. (a), (b), and (c) are identical triplets; (d) and (e) are fraternal twins.

twin brothers and normal control, including the death cases without rescue (Figure 6).

4. Discussion

Premature infants are susceptible to many complications due to impaired immunity, inflammation, and vascular regulation [13, 14]. The discovery with regard to the relationship between calcitonin/calcitonin gene-related peptide (CT/CGRP) and pregnancy highlighted new signal transmission mediators in various physiological processes including reproduction [15, 16]. In addition to vascular regulation, CGRP comprises of a variety of functions in regulating immune and inflammatory responses [17–19]. It integrates inflammatory and immune responses in the local microenvironment [5, 6, 15]. CGRP can change lymphocyte proliferation, antigen presentation, cytokine production, B lymphocyte differentiation, and adhesion molecule expression [5, 6]. Studying the effects of neuropeptides on inflammation and vascular regulation can help us to uncover the possible mechanisms in preterm infants.

Our previous study has shown that mutations or abnormal splicing of CGRP gene could lead to abnormal localization and synthesis of CGRP in cells, causing perineuritis and vasculitis [5]. Similar to vascular endothelial cells and smooth muscle cells, trophoblast cells also expressed

receptor proteins such as CRLR and RAMP1, suggesting that CGRP might be involved in the regulation of trophoblast function [20]. Long-term administration of CGRP receptor antagonist $CGRP_{8\text{-}37}$ into pregnant rats significantly reduced the weight of young rats, increased systolic blood pressure and fetal mortality in a dose-dependent manner [21, 22]. This phenomenon suggests the relationship between the expression of CGRP and premature birth.

Preterm birth is associated with DNA methylation in several different tissues, including placenta, neonatal blood, and neonate-birth saliva [23, 24]. In these previous studies, many CpG loci associated with preterm birth were located in genes associated with neuronal development and/or neurodegenerative diseases [25, 26]. This might be one of the reasons for the differences in the development of identical fetuses [27, 28]. In this study, pyrosequencing proved that CALCA and CALCB methylation levels of preterm umbilical cord tissues of single-chorionic triple-amniotic sac were higher than those of double-chorionic twins and normal controls as derived from the database. Moreover, the methylation levels of death cases after rescue were higher when compared to the other two twin brothers. Immunofluorescence results showed that the expression of αCGRP was decreased in the blood vessel wall of the umbilical cord of monozygotic triplets, especially in death cases, but no significant difference was observed in βCGRP, whether it is compensatory or not requires further in-depth study.

CGRP hypermethylation might affect vascular adaptation of umbilical cord and function of trophoblast cells during pregnancy [29]. Therefore, we hypothesized whether high methylation of CpG island in the promoter region of CGRP gene in the umbilical cord tissues led to low expression of CGRP, promoting the development of preterm birth. The two subtypes of αCGRP and βCGRP have extremely high similarities and differ only in three amino acids, where one of them is lacking, and the other changes positively or negatively [30, 31]. Compared with the wild-type control, the βCGRP mRNA levels in the dorsal root ganglia and spinal cord of αCGRP knockout mice showed no change, but the levels in the intestine were reduced by two times [32]. In the intestines of mice lacking βCGRP, the expression of αCGRP messenger RNA was increased, indicating an adaptive mechanism to compensate the lack of βCGRP.

In conclusion, this study focused on premature live births of triple-chorionic tricotyledon after single-embryo transfer. The pyrosequencing method was used to detect the methylation of CALCA and CALCB in the umbilical cord and analyzed the normal control results of database search. This revealed that CALCA and CALCB hypermethylation might affect pregnancy vascular adaptation and trophoblast cell function by regulating the expression of CGRP. It is considered as an extremely important cause of premature birth and vasculitis.

Data Availability

All data and materials generated during and/or analysed during the current study are available from the corresponding author on reasonable request.

Ethical Approval

All experimental procedures in animal work were approved by the Ethical Committee of Fujian Medical University. This study was carried out in accordance with the recommendations of Medical ethics committee of the First Affiliated Hospital of Fujian Medical University. The protocol was approved by the Medical Ethics Committee of the First Affiliated Hospital of Fujian Medical University [036] and 2018[049].

Disclosure

The funding sources played key supportive role for sample collection, molecular analysis of patient samples, and bioinformatics analysis.

Conflicts of Interest

The authors have no competing interests to declare.

Authors' Contributions

Q.-C.L., F.G., and Y.-J.G. planned the project. Q.-C. L. and F.G. conceived and designed the study. X.-T.C., K.Z., Q.-Y.G., F.G., and Q.-C.L. performed the sample collection. S.-R. H., Q.-Q.C., H.-L.Z., Y.-L.Z., and Q.-C.L. performed immunohistochemistry. Q.-C.L., F.G., and H.-L.Z. performed the expression analysis. Q.-C.L., X.-M.X., and Q.-Y.G. analyzed the data and drafted the manuscript. All authors reviewed the manuscript and approved the final version. Feng Gao, Yujia Guo, Xingting Chen, and Qiuyang Gu contributed equally to this work.

Acknowledgments

We would like to thank PhD. Li Youzhu, Center of Reproductive Medicine, the First Affiliated Hospital of Xiamen University, for his support in embryological interpretation; PhD. Xinqin He, Department of Obstetrics and Gynecology, 1st Affiliated Hospital, Fujian Medical University, for his support in tissue sample location; and the students (Yuxin Liu, Yue Luo, Xiaoxia Luo, and Junjie Lai) from the Department of Medical Laboratory of Fujian Medical University for their support in language processing. The authors sincerely thank the participants for their help and willingness to take part in this study. This work was supported by the National Natural Science Foundation of China (Nos. 82172953 and 81871293), Medical Innovation in Fujian Province (2019-CX-27 and 2020CXA030), Fujian Medical University Sailing Fund Project (2018QH1078), Key Projects of Natural Science Foundation of Fujian (2021J02036), and Youth Fund of Fujian Provincial Department of Health (2019-1-41 and 2019-1-46).

References

[1] H. Rabe, G. M. L. Gyte, J. L. Díaz-Rossello, and L. Duley, "Effect of timing of umbilical cord clamping and other strategies to influence placental transfusion at preterm birth on

maternal and infant outcomes," *Cochrane Database of Systematic Reviews*, vol. 9, article CD003248, 2019.

[2] I. Sohn, M. Sheykhzade, L. Edvinsson, and A. Sams, "The effects of CGRP in vascular tissue - classical vasodilation, shadowed effects and systemic dilemmas," *European Journal of Pharmacology*, vol. 881, p. 173205, 2020.

[3] C. Yallampalli, M. Chauhan, C. S. Thota, S. Kondapaka, and S. J. Wimalawansa, "Calcitonin gene-related peptide in pregnancy and its emerging receptor heterogeneity," *Trends in Endocrinology and Metabolism*, vol. 13, no. 6, pp. 263–269, 2002.

[4] Y. Dong, A. Betancourt, M. Chauhan et al., "Pregnancy increases relaxation in human omental arteries to the CGRP family of peptides," *Biology of Reproduction*, vol. 93, no. 6, p. 134, 2015.

[5] Q.-c. Liu, F. Chen, C.-y. Wu et al., "CALCB splice region pathogenic variants leading to plasma cell neurotropic enrichment in type 1 autoimmune pancreatitis," *Cell Death & Disease*, vol. 8, no. 2, article e2591, 2017.

[6] Q. Liu, Y. Lin, S. Zhang et al., "CGRP-mediated prolactin upregulation: a possible pathomechanism in IgG4-related disease," *Inflammation*, vol. 44, no. 2, pp. 536–548, 2021.

[7] C. C. Chen, L. C. Chang, C. H. Yao et al., "Increased calcitonin gene-related peptide and macrophages are involved in Astragalus membranaceus-mediated peripheral nerve regeneration in rats," *The American Journal of Chinese Medicine*, vol. 46, no. 1, pp. 69–86, 2018.

[8] L. H. Peng, X. Q. Qin, R. R. Tan, C. Liu, H. J. Liu, and X. Qu, "Calcitonin gene-related peptide regulates the potential antigen uptake ability of human bronchial epithelial cells," *Journal of Interferon & Cytokine Research*, vol. 38, no. 10, pp. 463–468, 2018.

[9] A. Lapillonne, E. Basson, G. Monneret, J. Bienvenu, and B. L. Salle, "Lack of specificity of procalcitonin for sepsis diagnosis in premature infants," *Lancet*, vol. 351, no. 9110, pp. 1211-1212, 1998.

[10] P. M. Broad, A. J. Symes, R. V. Thakker, and R. K. Craig, "Structure and methylation of the human calcitonin/alpha-CGRP gene," *Nucleic Acids Research*, vol. 17, no. 17, pp. 6999–7011, 1989.

[11] N. Y. Souren, L. A. Gerdes, P. Lutsik et al., "DNA methylation signatures of monozygotic twins clinically discordant for multiple sclerosis," *Nature Communications*, vol. 10, no. 1, p. 2094, 2019.

[12] K. Im, S. Mareninov, M. F. P. Diaz, and W. H. Yong, "An introduction to performing immunofluorescence staining," *Methods in Molecular Biology.*, vol. 1897, 2019.

[13] Y. Wang, L. Zhang, Y. Wu et al., "Peptidome analysis of umbilical cord mesenchymal stem cell (hUC-MSC) conditioned medium from preterm and term infants," *Stem Cell Research & Therapy.*, vol. 11, no. 1, p. 414, 2020.

[14] A. Katheria, F. Reister, J. Essers et al., "Association of umbilical cord milking vs delayed umbilical cord clamping with death or severe intraventricular hemorrhage among preterm infants," *Journal of the American Medical Association*, vol. 322, no. 19, pp. 1877–1886, 2019.

[15] S. K. Parida, D. B. Schneider, T. D. Stoss, T. H. Pauly, and J. P. McGillis, "Elevated circulating calcitonin gene-related peptide in umbilical cord and infant blood associated with maternal and neonatal sepsis and shock," *Pediatric Research*, vol. 43, no. 2, pp. 276–282, 1998.

[16] M. Chauhan, A. Betancourt, M. Balakrishnan et al., "Impaired vasodilatory responses of omental arteries to CGRP family peptides in pregnancies complicated by fetal growth restriction," *The Journal of Clinical Endocrinology and Metabolism*, vol. 101, no. 8, pp. 2984–2993, 2016.

[17] C. Schleithoff, S. Voelter-Mahlknecht, I. N. Dahmke, and U. Mahlknecht, "On the epigenetics of vascular regulation and disease," *Clinical Epigenetics*, vol. 4, no. 1, p. 7, 2012.

[18] B. Holzmann, "Antiinflammatory activities of CGRP modulating innate immune responses in health and disease," *Current Protein & Peptide Science*, vol. 14, no. 4, pp. 268–274, 2013.

[19] M. D. Harzenetter, A. R. Novotny, P. Gais, C. A. Molina, F. Altmayr, and B. Holzmann, "Negative regulation of TLR responses by the neuropeptide CGRP is mediated by the transcriptional repressor ICER," *Journal of Immunology*, vol. 179, no. 1, pp. 607–615, 2007.

[20] Y. L. Dong, S. Vegiraju, M. Chauhan, and C. Yallampalli, "Expression of calcitonin gene-related peptide receptor components, calcitonin receptor-like receptor and receptor activity modifying protein 1, in the rat placenta during pregnancy and their cellular localization," *Molecular Human Reproduction*, vol. 9, no. 8, pp. 481–490, 2003.

[21] Y. L. Dong, S. Vegiraju, M. Chauhan et al., "Involvement of calcitonin gene-related peptide in control of human fetoplacental vascular tone," *American Journal of Physiology. Heart and Circulatory Physiology*, vol. 286, no. 1, pp. H230–H239, 2004.

[22] P. R. R. Gangula, Y. L. Dong, S. J. Wimalawansa, and C. Yallampalli, "Infusion of pregnant rats with calcitonin gene-related peptide (CGRP)8-37, a CGRP receptor antagonist, increases blood pressure and fetal mortality and decreases fetal growth," *Biology of Reproduction*, vol. 67, no. 2, pp. 624–629, 2002.

[23] X. M. Wang, F. Y. Tian, L. J. Fan, C. B. Xie, Z. Z. Niu, and W. Q. Chen, "Comparison of DNA methylation profiles associated with spontaneous preterm birth in placenta and cord blood," *BMC Medical Genomics*, vol. 12, no. 1, p. 1, 2019.

[24] T. P. York, S. J. Latendresse, C. Jackson-Cook et al., "Replicated umbilical cord blood DNA methylation loci associated with gestational age at birth," *Epigenetics*, vol. 15, no. 11, pp. 1243–1258, 2020.

[25] X. G. Wang and R. K. Bhandari, "DNA methylation dynamics during epigenetic reprogramming of medaka embryo," *Epigenetics*, vol. 14, no. 6, pp. 611–622, 2019.

[26] T. M. Everson, T. M. O'Shea, A. Burt et al., "Serious neonatal morbidities are associated with differences in DNA methylation among very preterm infants," *Clinical Epigenetics*, vol. 12, no. 1, p. 151, 2020.

[27] S. Mani and M. Mainigi, "Embryo culture conditions and the epigenome," *Seminars in Reproductive Medicine*, vol. 36, no. 3/4, pp. 211–220, 2018.

[28] B. Novakovic, S. Lewis, J. Halliday et al., "Assisted reproductive technologies are associated with limited epigenetic variation at birth that largely resolves by adulthood," *Nature Communications*, vol. 10, no. 1, p. 3922, 2019.

[29] Y. L. Dong, S. Vegiraju, and C. Yallampalli, "Ca2+ signaling in human fetoplacental vasculature: effect of CGRP on umbilical vein smooth muscle cytosolic Ca2+ concentration," *American Journal of Physiology. Heart and Circulatory Physiology*, vol. 289, no. 2, pp. H960–H967, 2005.

[30] P. L. Tsiolaki, G. I. Nasi, F. A. Baltoumas et al., "αCGRP, another amyloidogenic member of the CGRP family," *Journal of Structural Biology*, vol. 203, no. 1, pp. 27–36, 2018.

[31] F. Gao, G. Liu, J. Wang et al., "Methylation of CALCA and CALCB in pancreatic ductal adenocarcinoma," *Oxidative Medicine and Cellular Longevity.*, vol. 2021, article 2088345, pp. 1–13, 2021.

[32] B. Schütz, D. Mauer, A.-M. Salmon, J.-P. Changeux, and A. Zimmer, "Analysis of the cellular expression pattern of β-CGRP in α-CGRP-deficient mice," *The Journal of Comparative Neurology*, vol. 476, no. 1, pp. 32–43, 2004.

Hindawi
Oxidative Medicine and Cellular Longevity
Volume 2021, Article ID 9690047, 13 pages
https://doi.org/10.1155/2021/9690047

Research Article

Study of the Possible Alleviated Role of Atorvastatin on Irinotecan-Induced Lingual Mucosal Damage: Histological and Molecular Study

Eetmad A. Arafat,[1] **S. M. Abo El-khair**,[2] **A. Z. Elsamanoudy**,[2,3] **and Dalia A. Shabaan**[1]

[1]*Histology and Cell Biology Department, Faculty of Medicine, Mansoura University, Egypt*
[2]*Medical Biochemistry and Molecular Biology Department, Faculty of Medicine, Mansoura University, Egypt*
[3]*Department of Clinical Biochemistry, Faculty of Medicine, King Abdulaziz University, Jeddah, Saudi Arabia*

Correspondence should be addressed to Eetmad A. Arafat; arafateetmad@gmail.com

Received 6 May 2021; Revised 5 August 2021; Accepted 3 September 2021; Published 30 September 2021

Academic Editor: Maria do Carmo Gouveia Peluzio

Background. Oral mucositis is the most debilitating and troublesome adverse effect of irinotecan (CPT-11) treatment. It adversely affects the patient quality of life. The aim of this work was to study the histological, immunohistochemical, and molecular changes in the oral mucosa by CPT-11 and the possible alleviated role of atorvastatin. *Methods*. Rats were randomly divided into control, CPT-11-treated group, and CPT-11+ atorvastatin-treated group. At the end of the experiment, the anterior two-thirds of the tongue was dissected out and divided into two parts: one part for light microscopic examination and the second for molecular study. *Results*. CPT-11-treated group revealed loss of normal mucosal organization, areas of ulceration and inflammation, and loss of architecture of lingual papillae. A significant decrease in immunohistochemical and molecular gene expression of Ki-67 and antiapoptotic Bcl-2 levels was observed. A significant increase in NF-κB immunohistochemical and mRNA gene expression level and a nonsignificant increase in Nrf2 gene expression were detected. Coadministration of atorvastatin showed remarkable improvement in the histopathological picture with a significant increase in Ki-67 and Bcl-2, a significant decrease in NF-κB protein and gene expression, and a significant increase in Nrf2 gene expression. *Conclusion*. Atorvastatin substantially attenuates CPT-11-induced oral mucositis through the initiation of the antiapoptotic gene, modulation of the inflammatory, and antioxidant gene expression.

1. Introduction

Chemotherapy drugs are a widely used cancer treatment approach that interferes with the division of cancer cells and can be administered either alone or in combination with other modalities [1].

Chemotherapy's biggest drawback is its lack of selectivity, as it works on both tumor cells and healthy cells that proliferate quickly [2]. For example, the oral mucosa is lined with a rapidly proliferating epithelium that is highly sensitive to chemotherapy damage [3]. Oral mucosal injury is clinically important because it adversely affects a patient's quality of life [4].

Irinotecan (CPT-11) is a camptothecin derivative and a recently developed chemotherapy drug effective against multiple malignant tumours, including colorectal, stomach, ovary, and lung cancers, as well as central nervous system tumours, including recurrent glioblastomas, rhabdomyosarcomas, and other sarcomas [5]. It inhibits topoisomerase-1, an enzyme involved in DNA replication, and causes several single-strand DNA breakdowns and cell division inhibition [6].

Mucosal damage and inflammation are the most debilitating and troublesome adverse effects of CPT-11 treatment. For example, gastrointestinal mucositis is most noticeable in the oral cavity and the small intestine, and its extent depends

on treatment regimen, treatment duration, patient age, and patient-related genetic factors [7]. Patients with severe mucositis that are undergoing multicycle chemotherapy or combined regimens may require delayed treatment cycles or reduced dosages [8]. Until recently, the management of oral mucositis was mainly palliative and included oral hygiene, analgesics or local anaesthetics, and protective coating agents [9].

The statin family of drugs is one of the chief drugs used in the treatment of hypercholesterolemia and coronary artery diseases. Statins also speed up epithelization and accelerate wound healing by preventing the adhesion of leukocytes onto inflammation sites to consequently decrease inflammatory cytokines. Statins have also been proven to improve macrophage accumulation at the site of injury, thus, enhancing keratinocytes and endothelial cell proliferation [10]. To date, no evidence-based approaches for the avoidance and treatment of oral mucositis exist [11]. Statin drugs may be useful against oral mucositis, but its principal mechanism of action is incompletely understood. This study investigated structural changes in oral mucosa under CPT-11 treatment and the possible role of atorvastatin in mucositis alleviation via histological, immunohistochemical, and molecular investigations.

2. Materials and Methods

2.1. Chemicals. CPT-11 was obtained from Sigma Aldrich Chemical Co (Cat # 1347609 USP Sigma Aldrich). Atorvastatin (20 mg) was purchased from Pfizer Company for Pharmaceutical and Chemical industries (New York, USA).

2.2. Experimental Animals. The experiment was carried out on 50 adult Sprague–Dawley male albino rats that weighed 180–200 g and were 6 weeks old. The rats were obtained from the animal house at the Faculty of Pharmacy, Mansoura University. The animals were sheltered in plastic cages (2 rats/cage) with stainless steel wire-bar lids. They were held in a controlled temperature (22°C ± 2°C) and humidity under a constant 12 h light-dark cycle. The rats were allowed free access to water and a standard rat diet during this period. The rats were acclimatized for one week before the experiment began. The experimental protocols and procedures were reviewed and permitted by the institutional review board, Faculty of Medicine, University of Mansoura (Ref R.21.04.1293).

2.3. Experimental Protocol. The rats were randomly allocated into three groups:

Group I (control group): 30 rats were equally divided into three subgroups of 10 rats each: subgroup Ia: negative control distilled water (-ve control DW) rats were given DW (1 mL) by gastric tube once daily for 5 days; subgroup Ib: negative control buffer (-ve control buffer) rats were given single IP injections of (sorbitol/lactic acid buffer; 45 mg/mL of sorbitol, 0.9 mg/mL of lactic acid, pH 3.4); and subgroup 1c: positive control atorvastatin (+ve control Atorvastatin) rats were given atorvastatin dissolved in DW (5 mg/kg) by gastric tube once daily for 5 days.

Group II: (CPT-11-treated group): 10 rats received 200 mg/kg of irinotecan in a sorbitol/lactic acid buffer as a single IP injection [12].

Group III: (CPT-11 + atorvastatin-treated group): 10 rats received a single IP injection of irinotecan as in group II + atorvastatin dissolved in DW and administered via a gastric tube in a dose of 5 mg/kg. The treatment occurred daily for 5 days [13].

At the end of the experiment, (24 hours from the last dose of atorvastatin) the rats ($N = 50$) were sacrificed by IP administration of pentobarbital (40 mg/kg), then the tongue of each rat was dissected out, and its anterior two-thirds was divided into two parts. The first part was fixed in 10% buffered formalin and prepared for light microscope examination. The second part was snap-frozen in liquid nitrogen and stored at −80°C for molecular study.

2.3.1. Histological Study. The specimens were fixed in 10% buffered formalin, dehydrated, and processed for paraffin block preparations. The 5 μm thick paraffin sections were obtained and used for light microscopic study using hematoxylin and eosin (H&E) [14].

2.3.2. Immunohistochemical Staining. Multiple immunohistochemical markers were used, including Ki67, Bcl2, and nuclear factor kappa-beta (NF-κB). Ki67 is a nuclear protein closely related to the cell cycle and is a marker of cell proliferation [15]. Bcl2 is an antiapoptotic marker [16]. NF-κB acts as a major mediator of inflammation in a variety of inflammatory diseases [17]. Primary antibodies used in this study are Ki-67 using rabbit monoclonal [SP6] antirat Ki67 (1 : 500; Abcam); Bcl-2 Mouse monoclonal Cat. # sc-7382, dilution 1|50 Santa Cruz Biotechnology; and NF-κB rabbit polyclonal antibody; Cat. #RB-9034-R7; dilution 1/100; Thermo Scientific, CA, USA.

The 5 μm thick paraffin sections on positively charged glass slides were deparaffinized and hydrated by boiling the sections for 15 m in 10 mM citrate buffer for antigen retrieval. Nonspecific reactions were inhibited by putting the slides in 3% bovine serum albumin for 30 m. Next, the sections were incubated overnight with the primary antibody at 4°C. Endogenous peroxidase activity was blocked with 10% H2O2 in PBS. Detection was achieved via incubation in biotinylated secondary antibodies for 1 h, then labeled horseradish peroxidase for 1 h, followed by 3, 3′-diaminobenzidine (DAB) as a chromogen. Mayer's hematoxylin was used for counterstaining. Negative control sections were obtained by replacing the 1ry antibodies with phosphate-buffered saline. Positive immunohistochemical staining for Ki-67 was detected by brown nuclei, while Bcl2 and NF-κB were identified as brown cytoplasmic staining [18].

2.3.3. Morphometric Study. An optical microscope (Olympus, Tokyo, Japan) joined to a Leica digital camera (ICC50) was used for image capturing. The images were analyzed on an Intel Core I3-based computer using Video Test morphology software (Saint Petersburg, Russia). All measurements were taken at a magnification (400×). Five

randomly selected, nonoverlapping fields were examined from each rat (5 rats/group) to measure:

(1) The two main diameters of lingual papillae (mean length and width of the filiform and fungiform) using H&E-stained sections

(2) The number of Ki-67 positive cells

(3) The number of BcL2 positive cells

(4) The area % of positive anti-NFκB immune reactions

2.3.4. Molecular Study. The liquid nitrogen frozen tongue tissue samples (30–50 mg) were utilized for total RNA extraction and the real-time qRT-PCR assessment of Ki-67, Bcl-2, NF-κB, and transcription factor NF-E2-related factor (Nrf2) expression.

Total RNA was extracted from the rats' tongue via the Tri-Fast TM reagent (PeqLab. Biotechnologie GmbH, Carl-Thiersch St. 2B 91052 Erlongen, Germany, Cat. No. 30-2010), and the purity was estimated via a NanoDrop™ 2000 Spectrophotometer (Thermo Scientific, USA). The cDNA synthesis by reverse transcription reactions was performed with the Maxima First Strand cDNA Synthesis Kit (Thermo Scientific, Waltham, MA, USA, cat No. #K1641). Ki-67, Bcl-2, NF-κB, and Nrf2 expressions were quantified via real-time PCR (Applied Biosystem 7500, real-time PCR detection system-Life Technology, Carlsbad, CA, USA-Applied Biosystem SYBR® Green PCR Master Mix (2X)-Life Technology, USA, Cat. no. 4344463). The thermal cycling reaction was performed as follows: the mixtures were incubated for 10 min at 95°C, then 40 cycles of 15 s at 95°C, 1 min at 60°C and, and finally, 15 s at 95°C, 1 min at 60°C, and 15 s at 95°C. The primer sequences used [19–21] were described in supplement material 1.

2.3.5. Statistical Analysis. The collected data were coded, processed, and analyzed using the SPSS (Statistical Package for Social Sciences) version 26 for Windows® (IBM SPSS Inc., Chicago, IL, USA).

Quantitative data were expressed as mean ± SD (standard deviation). One-way analysis of the variance was used to test the significance between three and more independent groups. Post hoc Tukey was used to assess the significance between every two adjacent groups.

In all applied tests, the P values associated with test statistics indicated the significance level at which the null hypothesis (the hypothesis of no difference) was rejected, and it was set at 0.05 so that P values ≥ 0.05 are statistically nonsignificant, P values < 0.05 are significant, and P values < 0.01 are highly significant.

3. Results

3.1. H&E Stain. The H&E-stained tongue sections the control group (Figure 1(a) revealed that the dorsal surface was studded with conical-shaped filiform papillae). The papillae had a connective tissue (CT) core covered with stratified squamous keratinized epithelium with pointed tips. The papillae were regularly arranged and had a uniform shape and height (a1-2). The fungiform papillae had a distinctive mushroom shape with a broad top and a narrow base and were located between the filiform papillae, and taste buds were observed on their top surfaces. They were lined with stratified squamous keratinized epithelium (a3). The lamina propria contained CT with small-sized blood vessels. The main bulk of the tongue contained skeletal muscle fibers running in various directions. The muscle fibers were surrounded by the perimysium and endomysium that continued with the lamina propria CT (a4). The ventral surface of the tongue was covered with well-developed stratified squamous keratinized epithelium without lingual papillae (a5).

The CPT-11-treated group (Figure 1(b)) lost the normal organization of the dorsal surface papillae. Some of the filiform papillae were completely lost with multiple ulcerative areas (b1). Other papillae were short with blunted ends (b1). Areas of hyperkeratosis and keratin separation from the underlying epithelium were obvious (b2-3). Some of the epithelial cells showed vacuolar degeneration, while other cells revealed nuclear changes, including pyknosis, chromatin condensation, and chromatin margination with a crescent appearance (b2). The fungiform papillae were atrophied with ill-distinguished taste bud cells (b3). The skeletal muscle fibers were disorganized and widely separated (b4). The ventral surface showed a noticeable decrease in the thickness of the stratified squamous keratinized epithelium. The lamina propria revealed inflammatory cell infiltration and dilated, congested blood vessels (b5).

The CPT − 11 + atorvastatin − treated group (Figure 1(c)) showed restoration of normal lingual papillae organization (c1). The filiform papillae were covered with keratinized, stratified squamous epithelium with pointed ends. Most of the papillae had a uniform shape and height (c2). Most of the epithelium showed normal cytoplasm and nuclear appearances, apart from a few with nuclear chromatin margination and pyknotic nuclei (c3). The fungiform papillae were similar to that of the control group (c3). The CT had a normal arrangement of muscle fibers (c4). The ventral surface had average-sized, noninterrupted keratinized stratified squamous epithelium. The lamina propria displayed a disappearance of inflammatory cell infiltration and had normal-sized, noncongested blood vessels (c5).

3.2. Immunohistochemical Results

3.2.1. Anti-Ki67. Ki-67 immunohistochemical staining in the control groups revealed a positive reaction in the nuclei of the basal and suprabasal layers of the stratified epithelium on the dorsal surface of the tongue (Figure 2(a)). The CPT-11-treated group had few cells with positive reactions in their nuclei. The cells were mainly in the basal layer of epithelium (Figure 2(b)). The CPT − 11 + atorvastatin group revealed positive reactions in the nuclei of most of the basal and suprabasal epithelial cells (Figure 2(c)).

3.2.2. Anti-Bcl2. The control group had positive immunohistochemical reactions to Bcl2 in the cytoplasm of the stratified squamous epithelium (Figure 3(a)). The CPT-11-

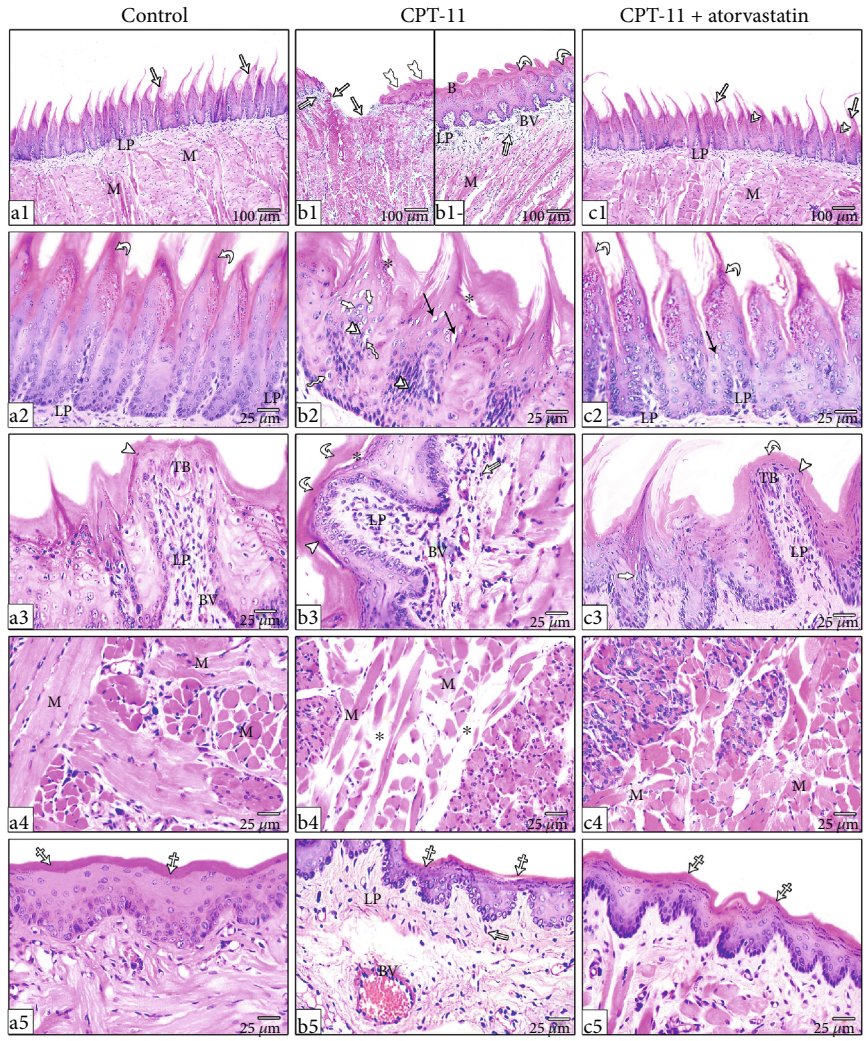

Figure 1: H&E-stained sections from the tongue of the control group (a), the dorsal surface showing regularly arranged conical shape filiform papillae (arrow) covered by stratified squamous keratinized epithelium with pointed tips (curved arrow) and underlying connective tissue cores continue with the lamina propria (LP). A characteristic fungiform papilla has broad top and narrow base with vascular connective tissue core (BV) and is covered by stratified squamous keratinized epithelium (arrowhead) contains barrel-shaped pale stained taste buds (TB). Bundles of lingual muscle fibers (M) run in various directions and surround by endomysium and perimysium that are continued with the connective tissue corium of both surfaces. The ventral surface is covered by smooth stratified squamous keratinized epithelium (crossed arrow) without papillae. CPT-11-treated group (b), the dorsal surface reveals the area of mucosal ulceration (arrow), other areas with short or absent filiform papillae (thick-tailed arrow), and blunt-ended tops (B) with inflammatory cell infiltration (double arrow) and congested blood vessels (BV) in the lamina propria (LP). The cells of stratified epithelium reveal vacuolation (zigzag arrow) and nuclear changes; chromatin margination with crescent formation (black arrow), pyknosis (thick white arrow), and chromatin condensation (double arrowheads). The fungiform papillae (arrowhead) show loss of taste buds and congested vascular core (LP) with inflammatory cell infiltration (double arrow). The papillae are covered by a thick layer of keratin (curved arrow) with areas of keratin separation (white asterisks). Disturbed organization of muscle fibers (M) with wide separation (black asterisks). The ventral surface shows thinning of the stratified epithelium with thin keratin layer (crossed arrow), and the lamina propria (LP) showed congested blood vessels (BV) with inflammatory cell infiltration (double arrow). CPT − 11 + atorvastatin treated group (c), the dorsal surface reveals normal orientation of the lingual papillae (arrow). Most of the filiform papillae are long with pointed tips and covered by stratified squamous keratinized epithelium (curved arrow), few papillae with loss of their tips (double arrowheads). Most of the cells are normal with few ones with marginated chromatin (black arrow) and few pyknotic nuclei (thick white arrow). Normal fungiform papillae (arrowhead) with taste bud (TB), normal thickness of keratin layer (curved arrow), and connective tissue core (LP) are observed. The organization of muscle layer (M) and the ventral surface (crossed arrow) closely resemble those of the control. (H&E a1, b1, c1 X100, a2 − 5, b2 − 5, c2 − 5 X400).

treated group had relatively negative Bcl2 immune expression in the cytoplasm of the stratified squamous cells (Figure 3(b)). The CPT − 11 + atorvastatin − treated group showed moderate positive immunohistochemical expression in the cytoplasm of the stratified squamous epithelium cells (Figure 3(c)).

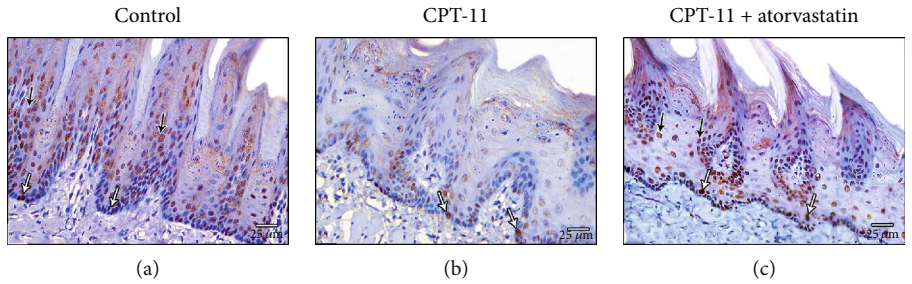

Figure 2: Ki-67 immunohistochemical staining. (a) (The control group) the dorsal surface shows frequent cells with positive immunoexpression in their nuclei in the basal (white arrow) and suprabasal layers (black arrow). (b) CPT-11-treated group reveals few positive cells mainly in the basal epithelial layer (white arrow). (c) CPT − 11 + atorvastatin treated group shows numerous immunostaining cells in the basal (white arrow) and suprabasal layers (black arrow) epithelial layer. (Ki-67 a-c X400).

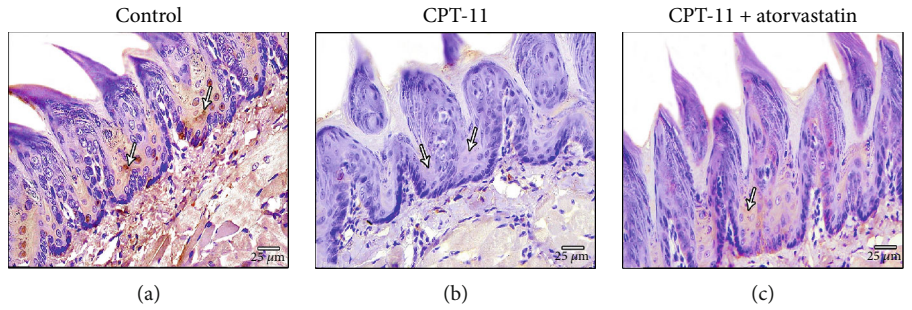

Figure 3: Bcl2 immunohistochemical staining. (a) The control group shows strong positive cytoplasmic immunoexpression to Bcl2 in most of the dorsal epithelial cells (arrow). (b) CPT-11-treated group reveals negative cytoplasmic reaction in most epithelial cells (arrow). (c) CPT − 11 + atorvastatin − treated group shows positive cytoplasmic immunoexpression with moderate density (arrow) in most of the epithelial cells. (Bcl2 a-c X400).

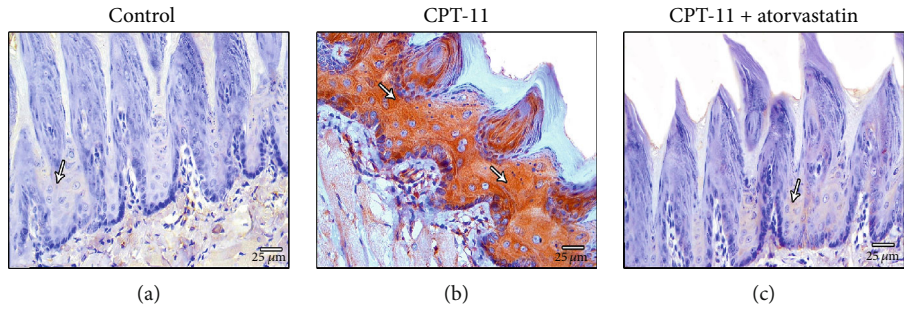

Figure 4: NF-κB immunohistochemical staining. (a) The control group shows negative immunoexpression to NF-κB in the cytoplasm of dorsal epithelial cells (arrow). (b) CPT-11-treated group reveals a strong positive cytoplasmic reaction in most epithelial cells (arrow). (c) CPT − 11 + atorvastatin treated group shows weak positive to negative cytoplasmic immunoexpression (arrow) in most of the epithelial cells. (NF-*K*b a-c X400).

3.2.3. NF-κB. NF-κB immunohistochemical staining in the control groups revealed negative immune reactions in the cytoplasm of almost all epithelial cells (Figure 4(a)). The CPT-11-treated group had positive immune reactions in the cytoplasm of most cells of the different epithelial layers (Figure 4(b)). The CPT − 11 + atorvastatin − treated group had a few dispersed positive cells (Figure 4(c)).

3.3. Morphometric and Statistical Results. A nonsignificant change in the two main diameters of the filiform and the fungiform papillae was observed in the three-control subgroups. A statistically significant decrease was observed in the length and width of both filiform and fungiform papillae in the CPT-11-treated group compared to the control group. A nonsignificant change in the CPT − 11 + atorvastatin group in comparison to the control group was observed, but a significant increase was observed compared to the CPT-11-treated group (Tables 1 and 2).

A statistically significant decrease in the number of Ki-67 and Bcl2 positive cells in the CPT-11-treated group was observed, and a nonsignificant change in the CPT − 11 + atorvastatin group in comparison to the control group was

Table 1: Morphometric study of the length and width of filiform papillae within the control and the experimental groups.

	Study groups					
	Group Ia (-ve control DW)	Group Ib (-ve control buffer)	Group Ic (+ve control atorvastatin)	Group 11 (CPT-11-treated)	Group III (CPT-11 + atorvastatin)	Test of significance
Mean length (μm)	310.26 ± 44.52	307.22 ± 45.35	312.03 ± 39.52	166.72 ± 20.18	302.22 ± 32.44	
P_1		0.782	0.848	<0.001**	0.425	
P_2			0.593	<0.001**	0.580	$F = 85.471$ $P < 0.001^{**}$
P_3				<0.001**	0.276	
P_4					<0.001**	
Mean width (μm)	107.75 ± 32.65	110.75 ± 30.45	105.75 ± 30.44	94.88 ± 15.65	102.43 ± 29.5	
P_1		0.430	0.557	0.005*	0.218	
P_2			0.229	<0.001**	0.078	$F = 57.719$ $P < 0.001^{**}$
P_3				0.021*	0.444	
P_4					0.046*	

SD: standard deviation, F for ANOVA test. *Statistically significant if $P \leq 0.05$. **Highly statistically significant result if $P \leq 0.001$. P_1: comparison in relation to (-ve control DW) group. P_2: comparison in relation to (-ve control buffer) group. P_3: comparison in relation to (+ve control Atorvastatin) group. P_4: comparison in relation to (CPT-11) group.

Table 2: Morphometric study of the length and width of fungiform papillae within the control and the experimental groups.

	Study groups					
	Group Ia (-ve control DW)	Group Ib (-ve control buffer)	Group Ic (+ve control atorvastatin)	Group 11 (CPT-11-treated)	Group III (CPT-11 + atorvastatin)	Test of significance
Mean length (μm)	224.15 ± 21.79	218.15 ± 23.59	220.15 ± 19.55	188.51 ± 36.4	219.22 ± 20.33	
P_1		0.404	0.675	<0.001∗∗	0.529	
P_2			0.850	<0.001∗∗	0.918	$F = 32.209$ $P < 0.001^{**}$
P_3				<0.001∗∗	0.984	
P_4					<0.001∗∗	
Mean width (μm)	175.61 ± 24.35	177.55 ± 20.35	174.5 ± 22.25	110.93 ± 31.11	169.24 ± 18.41	
P_1		0.715	0.889	<0.001∗∗	0.320	
P_2			0.654	<0.001∗∗	0.274	$F = 81.456$ $P < 0.001^{**}$
P_3				<0.001∗∗	0.395	
P_4					< 0.001∗∗	

Table 3: Number of anti-Ki 67 and anti-Bcl2 immune-stained cells within the control and the experimental groups.

	Study groups					Test of significance
	Group Ia (-ve control DW)	Group Ib (-ve control buffer)	Group Ic (+ve control atorvastatin)	Group 11 (CPT-11-treated)	Group III (CPT-11 + atorvastatin)	
Anti-Ki 67	54.12 ± 2.3	50.22 ± 1.8	52.15 ± 2.4	22.3 ± 1.9	49.33 ± 2.1	
P_1		0.667	0.882	<0.001∗∗	0.395	$F = 27.410$ $P < 0.001^{**}$
P_2			0.836	<0.001∗∗	0.964	
P_3				<0.001∗∗	0.703	
P_4					<0.001∗∗	
Anti-Bcl2	15.2 ± 2.5	16.2 ± 1.4	15.5 ± 2.2	2.6 ± 2.1	13.8 ± 1.9	
P_1		0.626	0.918	<0.001∗∗	0.472	$F = 23.257$ $P < 0.001^{**}$
P_2			0.782	<0.001∗∗	0.260	
P_3				<0.001∗∗	0.508	
P_4					<0.001∗∗	

Table 4: The area percentage of positive anti-NFκB immune reactions within the control and the experimental groups.

	Study groups					Test of significance
	Group Ia (-ve control DW)	Group Ib (-ve control buffer)	Group Ic (+ve control atorvastatin)	Group 11 (CPT-11-treated)	Group III (CPT-11 + atorvastatin)	
	2.5 ± 1.9	2.2 ± 1.5	3.3 ± 1.5	18.4 ± 2.8	4.2 ± 2.1	
P_1		0.527	0.460	<0.001∗∗	0.184	KW = 17.549 $P < 0.001^{**}$
P_2			0.255	<0.001∗∗	0.122	
P_3				<0.001∗∗	0.288	
P_4					<0.001∗∗	

SD: standard deviation, KW for Kruskal Wallis test. ∗Statistically significant if $P \leq 0.05$. ∗∗Highly statistically significant result if $P \leq 0.001$. P_1: comparison in relation to (-ve control DW) group. P_2: comparison in relation to (-ve control buffer) group. P_3: comparison in relation to (+ve control atorvastatin) group. P_4: comparison in relation to (CPT-11) group.

observed (Table 3). A significant increase in the area percentage of the NF-κB immunohistochemical results in the CPT-11-treated group was observed, but a nonsignificant change in the CPT − 11 + atorvastatin group was observed in comparison to the control group (Table 4).

3.4. Molecular Study Results. The immune-histochemical results were supported by the molecular gene expression results, since both Ki-67 and antiapoptotic Bcl-2 mRNA gene expression were significantly decreased ($P < 0.001$) in the tongue tissue of the CPT-11-treated groups. The gene expression levels increased in the CPT − 11 + atorvastatin to reach about the normal level of Ki-67 (0.95 ± 0.23) and even above normal levels of Bcl-2 (1.33 ± 0.32; Figures 5 and 6).

The gene expression changes in NF-κB were consistent with the results of the histological examination of the tongue tissue samples. CPT-11 affects lingual cells by inducing marked inflammatory responses and increasing NF-κB (2.36 ± 0.27, $P < 0.001$). In addition, atorvastatin increases NF-κB mRNA levels, but not as much as CPT-11 (1.84 ± 0.28, $P < 0.001$); however, the coadministration of both drugs neutralized their individual effects on gene expression, which was still decreased, but above its normal levels (1.58 ± 0.23, $P < 0.001$; Figure 7).

Nrf2 enhances antioxidant formation in response to oxidative stress through the Nrf2/ARE pathway. Atorvastatin caused highly significant increases in Nrf2 gene expression (2.14 ± 0.33, $P < 0.001$), while CPT-11 led to insignificant increases in its mRNA levels (1.35 ± 0.33, $P = 0.061$). CPT − 11 + atorvastatin resulted in highly significant increases in its gene expression (2.06 ± 0.41, $P < 0.001$; Figure 8).

4. Discussion

Oral mucositis is one of the most debilitating complications of chemotherapy and has proven clinical and financial implications. Despite the availability of multiple treatment services, there remains a need for the successful alleviation and prevention of chemotherapy-induced mucositis. In this study, the tongue was chosen to study the effects of CPT-11 on oral tissue since the tongue acts as a mirror of general personal health [22], especially the filiform papillae that can be damaged faster than other types of papillae [23].

The oral mucositis mechanism occurred as follows. Initially, chemotherapy causes cell damage and free radical production that activates a great number of transcription factors, such as NF-κB. These transcription factors subsequently upregulate several genes that affect mucosal cell

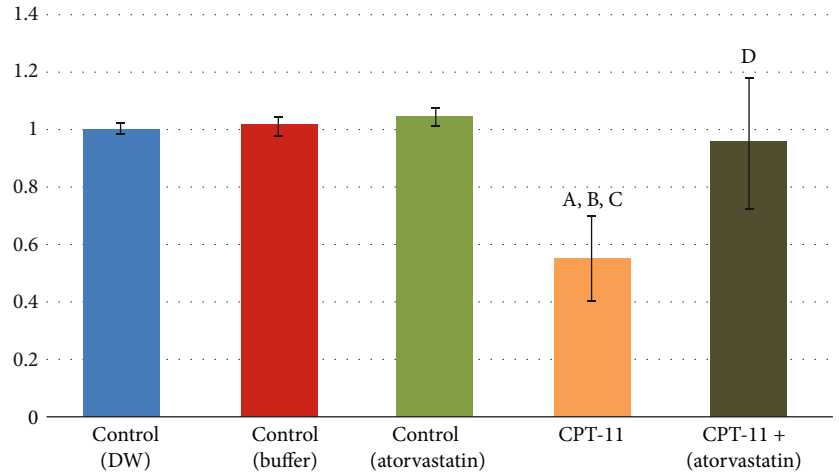

Figure 5: PCR level of KI-67 within the control and the experimental groups. (a) Comparison in relation to (-ve control DW) group. (b) Comparison in relation to (-ve control buffer) group. (c) comparison in relation to (+ve control atorvastatin) group. (d) Comparison in relation to (CPT-11) group.

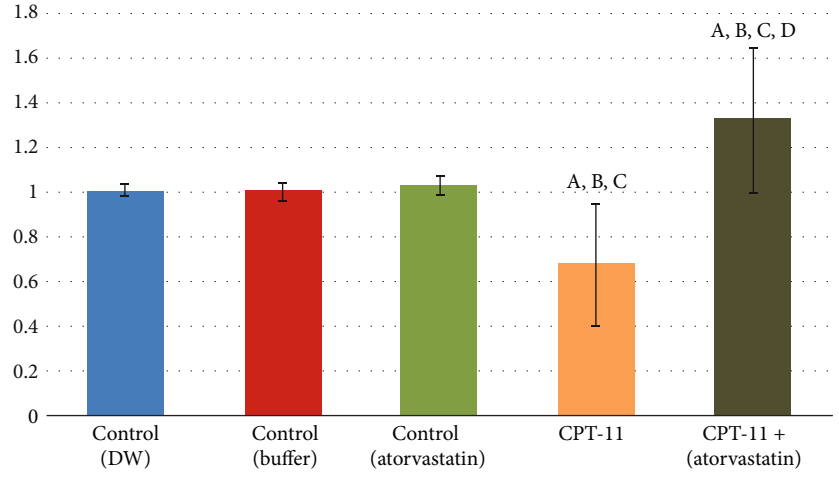

Figure 6: PCR level of BCL2 within the control and the experimental groups. (a) Comparison in relation to (-ve control DW) group. (b) Comparison in relation to (-ve control buffer) group. (c) Comparison in relation to (+ve control atorvastatin) group. (d) Comparison in relation to (CPT-11) group.

integrity, which results in basal epithelial cell death, apoptosis, tissue harm, and increased inflammatory factors, which increase cell death. Finally, the upregulation of proinflammatory cytokines occurs, including tumor necrosis factor-(TNF-) α, interleukin-1β (IL-1β), and interleukin-6 (IL-6), and the inflammatory processes are intensified, which causes ulcerations in the mucosa and speeds secondary infections [24, 25].

The CPT-11 treatment greatly disturbed the normal histological structure of the tongue. The dorsal surface revealed severely disrupted lingual papillae with some filiform papillae having blunted ends and others being atrophied. The results were confirmed by morphometric measurements of the two main diameters of the filiform papillae. A statistically significant reduction in the width and height of the papillae in comparison to the control group was observed. These results agree with Ibrahim and Elwan [12]. CPT-11 triggers its antitumor action by inflicting direct DNA damage and activating the innate immune response by initiating oxidative stress and releasing reactive oxygen species. CPT-11 also damages healthy cells, thus, causing gastrointestinal mucositis [26].

Our results showed an obvious thinning of the stratified squamous epithelium on both the dorsal and ventral surfaces of the tongue. These results were in line with Ibrahim and Elwan [12] and could be due to the reduction in cell proliferation, which was confirmed by a significant reduction in Ki-67 expression (a proliferation marker). Ki-67 expression was low in the immunohistochemical and gene expression results as well. This coincides with the results reported by de M Rêgo et al. [27] showing the antiproliferative role of CPT-11 that could explain the tongue's mucosal damage detected in this study. In the same context, a remarkable thickening of the keratin layer was observed,

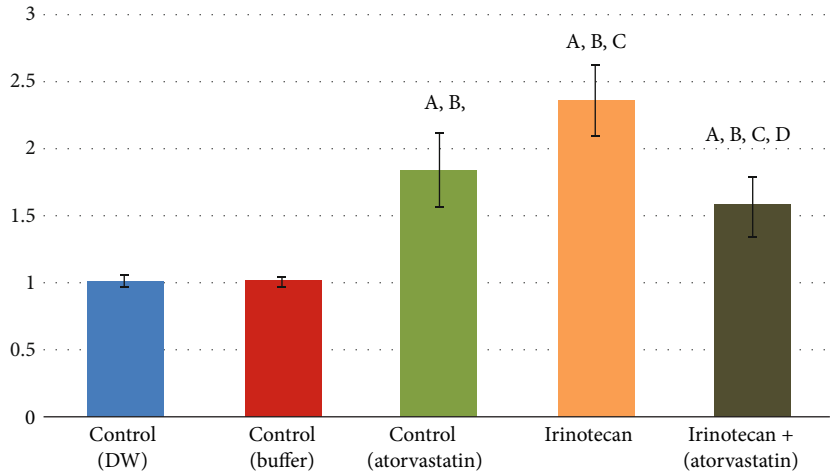

Figure 7: PCR level of NF-Kb level within the control and the experimental groups. (a) Comparison in relation to (-ve control DW) group. (b) Comparison in relation to (-ve control buffer) group. (c) Comparison in relation to (+ve control atorvastatin) group. (d) Comparison in relation to (CPT-11) group.

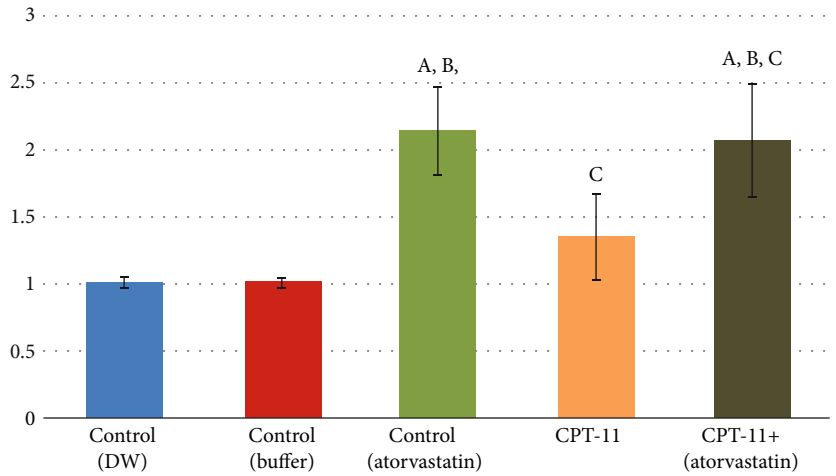

Figure 8: Nr-F2 level within the control and the experimental groups. (a) Comparison in relation to (-ve control DW) group. (b) Comparison in relation to (-ve control buffer) group. (c) Comparison in relation to (+ve control atorvastatin) group. (d) Comparison in relation to (CPT-11) group.

which was previously explained by the high sensitivity of taste buds to chemotherapy, taste bud damage, and the loss of sensory innervation which has been documented to have a role in disturbed keratinization and a loss of taste sensation [28]. In contrast, Kattaia et al. [29] attributed the hyperkeratinization of lingual papillae to the deficiency of the epidermal growth factor, which is involved in normal keratinization programming.

Vacuolar degeneration was observed in some stratified epithelium cells. The affected cells revealed vacuolated cytoplasm with condensed pyknotic nuclei. Our results were in harmony with Al Refai [30]. These degenerative changes could be due to the inhibition of topoisomerase I, which results in DNA damage and fragmentation. In contrast, the release of reactive oxygen species causes metabolism impairment in progenitor cells, DNA damage in the epithelial cells, mitosis inhibition, and increased apoptosis [31]. These results were confirmed by the immunohistochemical examination of Bcl2 immunostained sections and the quantitative real-time PCR of the Bcl2 mRNA, an antiapoptotic marker, which was significantly reduced in the CPT-11-treated group. Indeed, DNA injury triggered by the inhibition of topoisomerase I results in the stimulation of several pathways that are implicated in apoptotic death and inflammatory responses [32]. The decreased Bcl2 expression detected in the current study shows the action of CPT-11's antineoplastic effects by stimulating tumor cell apoptosis [33]. This could also affect nontumor cells, leading to the mucosal damage and mucositis observed in this study. These results were confirmed recently by Dai et al. [34], who showed that SN-38 (active metabolite of CPT-11) inhibits cell proliferation by arresting the cell cycle and stimulating apoptosis by blocking the antiapoptotic gene transcription of Bcl2.

In the present study, excess inflammatory cell infiltrations and dilated, congested blood vessels were obvious in the tongue CT of the CPT-11-treated group. Reactive oxygen species cause a series of biological events, resulting in the synthesis of different proinflammatory cytokines. These cytokines invade the epithelium, endothelium, and CT, causing tissue injury [35]. The damaging action of inflammatory mediators directly or indirectly increased vascular permeability and the absorption of cytotoxic drugs into the oral mucosa [36].

The histological results were confirmed by the significant increases in the expression of NF-κB in the CPT-11-treated group at the mRNA level by qRT-PCR and the protein levels by immunohistochemical examination. NF-κB is a main facilitator of proinflammatory gene initiation and functions [37], and it is also considered the main regulator in cellular proliferation, differentiation, angiogenesis, and apoptosis [38]. The NF-κB signalling pathway includes a family of transcription factors that plays a role in immunity and inflammation [39]. NF-κB is expressed in cells in response to various stressors, such as chemotherapy, to enhance cell survival. Many anticancer drugs, including CPT-11, enhance the gene expression of NF-κB. This drug-induced activation is clinically undesirable as it may cause cells to develop a resistance to chemotherapeutic treatment [40]. Moreover, it is reported that the induction of the NF-κB gene may trigger the induction of other inflammation genes [41], thus, causing inflammation as observed in the current study.

Surprisingly, the Nrf2 gene expression was increased in the CPT-11-treated animals. This result could be explained by the fact that Nrf2 is a transcription factor that enhances antioxidant production in response to oxidative stress through the Nrf2/ARE pathway, since CPT-11 induces oxidative stress [42]. Thus, increased Nrf2 gene expression could be a defense mechanism against CPT-11-induced oxidative stress. The Nrf2 antioxidant mechanism in response to oxidative stress could be explained as follows: Nrf2 is a member of the Cap'n'Collar transcription factor family. Its main function is to reestablish cellular redox homeostasis. The Nrf2 redox defense system mediates its effect through enzymes that are involved in sulfhydryl metabolism and iron homeostasis. NADPH is an essential coenzyme for the redox cycling mechanisms of the KEAP1/NRF2 pathway since NADPH coordinates a perfect reorganization of the cellular metabolism. This is helpful to resist many redox stressors and, consequently, to maintain normal cellular homeostasis [43]. The oxidative stress in this study had possible inducing factors, including the chemotherapeutic effect of CPT-11 [44] and the associated inflammatory reaction [45].

In this work, the CPT 11 + atorvastatin group had almost normal tongue architecture with preserved papillae and taste buds. These results are in line with the results of previous researchers who attributed the ability of statins to interfere with topoisomerase II function by inhibiting the action of the Ras-homologous GTPase Rac1, which is essential for the multiple cleavage process in DNA. A similar effect was shown in liver cells and cardiomyocytes after exposure to doxorubicin [46, 47]. In addition, Ziegler et al. [25] reported that the pretreatment of human keratinocytes in vitro with lovastatin reduced the DNA damage by doxorubicin by 75%. Statins decreased ATR/Chk1-regulated replicative stress, thus, preventing DNA damage, and mm preserving keratinocytes. Our histological results were in line with the expression of Bcl2 at the molecular and the immunohistochemical levels. Our results revealed the upregulation of the Bcl2 gene and protein levels in the atorvastatin-treated group, which could be due to the cytoprotective effect of statins caused by the inhibition of apoptotic cell death. This study confirms the upregulating effect of the statin drug family on Bcl2 gene expression as reported by Franke et al. [48].

Our results revealed a significant decrease in the expression of NF-κB mRNA and proteins in the atorvastatin-treated group. The anti-inflammatory property of statins was shown to be due to their inhibitory effects on inducible nitric oxide synthetases (iNOS), which are commonly utilized by cells as proinflammatory cytokines [49]. In addition, atorvastatin was reported to decrease TNF/IFN-stimulated iNOS expression in the endothelium cells of the aorta [50] and at the molecular level, as reported recently by Wang et al. [51].

Our results also revealed increased Nrf2 gene expression in the CPT − 11 + atorvastatin group. This result confirmed the stimulant effect of atorvastatin on the gene expression of Nrf2 as a marker of antioxidant defense and provided evidence of its potential protective effects against oxidative stress damage by oxidative stress induction caused by various inducers, including chemotherapy. The induction of Nrf2 gene expression by statins was also reported previously by Ihoriya et al. [52] and recently by Bao et al. [53], who reported that statins had an antioxidant effect by suppressing the formation of oxygen free radicals by inhibiting the activation of the NADPH oxidase complex, which is responsible for superoxide generation [54]. In addition to its cholesterol-lowering action, it has several cholesterol-independent effects that are valuable for human health. These pleiotropic effects include antioxidant properties [55], anti-inflammatory effects, immunomodulatory effects [56], and endothelial cell-defending actions through the upregulation of endothelial nitric oxide synthase (eNOS) [57].

5. Conclusions

In conclusion, the current study revealed prominent rat mucosal damage in the form of lingual mucositis that is induced by CPT-11 chemotherapy, an important alternative for patients with mucositis. The mechanism of CPT-11-induced mucosal damage could be related to chronic inflammation, oxidative stress, and an imbalance of the apoptotic and antiapoptotic pathways. These results were confirmed at the histological and molecular levels. Atorvastatin could play a protective role against CPT-11 mucosal damage by inducing an antiapoptotic gene and modulating inflammatory and antioxidant gene expressions.

Data Availability

The data that support the findings of this study are available from the corresponding author upon reasonable request.

Conflicts of Interest

The authors declare that they have no conflicts of interest.

Supplementary Materials

Supplementary material 1: description of the primer sequences used in this study. *(Supplementary Materials)*

References

[1] M. K. Anderson and L. Matey, "Irinotecan: 25 years of cancer treatment. Overview of cancer and cancer treatment," in *Chemotherapy and Immunotherapy Guidelines and Recommendations for Practice*, M. M. Olsen, L. F. KB, and K. J. Brassil, Eds., Oncology Nursing Society, Pittsburgh, PA., 2019.

[2] G. Ruiz-Esquide, B. Nervi, A. Vargas, and A. Maíz, "Tratamiento y prevención de la mucositis oral asociada al tratamiento del cáncer," *Revista Médica de Chile*, vol. 139, no. 3, pp. 373–381, 2011.

[3] K. Miyano, M. Eto, S. Hitomi et al., "Author correction: the Japanese herbal medicine Hangeshashinto enhances oral keratinocyte migration to facilitate healing of chemotherapy-induced oral ulcerative mucositis," *Scientific Reports*, vol. 10, no. 1, article 19806, 2020.

[4] A. H. M. Al-Rudayni, D. Gopinath, M. K. Maharajan, and R. K. Menon, "Impact of oral mucositis on quality of life in patients undergoing oncological treatment: a systematic review," *Translational Cancer Research*, vol. 9, no. 4, pp. 3126–3134, 2020.

[5] C. Bailly, "Irinotecan: 25 years of cancer treatment," *Pharmacological Research*, vol. 148, article 104398, 2019.

[6] K. Gokduman, "Strategies targeting DNA topoisomerase I in cancer chemotherapy: camptothecins, nanocarriers for camptothecins, organic non-camptothecin compounds and metal complexes," *Current Drug Targets*, vol. 17, no. 16, pp. 1928–1939, 2016.

[7] M. Cinausero, G. Aprile, P. Ermacora et al., "New frontiers in the pathobiology and treatment of cancer regimen-related mucosal injury," *Frontiers in Pharmacology*, vol. 8, p. 354, 2017.

[8] M. Thomsen and L. Vitetta, "Adjunctive treatments for the prevention of chemotherapy- and radiotherapy-induced mucositis," *Integrative Cancer Therapies*, vol. 17, no. 4, pp. 1027–1047, 2018.

[9] E. B. Rubenstein, D. E. Peterson, and M. Schubert, "Clinical practice guidelines for the prevention and treatment of cancer therapy-induced oral and gastrointestinal mucositis (vol 100, Supplement 9, pg 2026, 2004)," *Cancer*, vol. 101, no. 8, pp. 1921–2046, 2004.

[10] C. Liu, J. Zhu, B. Hai et al., "Single intraosseous injection of simvastatin promotes endothelial progenitor cell mobilization, neovascularization, and wound healing in diabetic rats," *Plastic and Reconstructive Surgery*, vol. 145, no. 2, pp. 433–443, 2020.

[11] G. Daugėlaitė, K. Užkuraitytė, E. Jagelavičienė, and A. Filipauskas, "Prevention and treatment of chemotherapy and radiotherapy induced oral mucositis," *Medicina*, vol. 55, no. 2, p. 25, 2019.

[12] M. A. A. H. Ibrahim and W. M. Elwan, "Effect of irinotecan on the tongue mucosa of juvenile male albino rat at adulthood," *International Journal of Experimental Pathology*, vol. 100, no. 4, pp. 244–252, 2019.

[13] C. A. Medeiros, R. F. Leitão, R. N. Macedo et al., "Effect of atorvastatin on 5-fluorouracil-induced experimental oral mucositis," *Cancer Chemotherapy and Pharmacology*, vol. 67, no. 5, pp. 1085–1100, 2011.

[14] M. Gamble, "The hematoxylins and eosin," in *Theory and Practice of Histological Techniques*, Elsevier, 2008.

[15] P. H. Tan, B. H. Bay, G. Yip et al., "Immunohistochemical detection of Ki67 in breast cancer correlates with transcriptional regulation of genes related to apoptosis and cell death," *Modern Pathology*, vol. 18, no. 3, pp. 374–381, 2005.

[16] H. Ozer, G. Yenicesu, S. Arici, M. Cetin, E. Tuncer, and A. Cetin, "Immunohistochemistry with apoptotic-antiapoptotic proteins (p53, p21, bax, bcl-2), c-kit, telomerase, and metallothionein as a diagnostic aid in benign, borderline, and malignant serous and mucinous ovarian tumors," *Diagnostic Pathology*, vol. 7, no. 1, p. 124, 2012.

[17] Y. M. Han, J. Koh, J. W. Kim et al., "NF-kappa B activation correlates with disease phenotype in Crohn's disease," *PloS One*, vol. 12, no. 7, article e0182071, 2017.

[18] I. B. Buchwalow and W. Böcker, "Working with antibodies," in *Immunohistochemistry: Basics and Methods*, Springer, Berlin, Heidelberg, 2009.

[19] R. Li, K. Zhao, Q. Ruan, C. Meng, and F. Yin, "The transcription factor Foxd3 induces spinal cord ischemia-reperfusion injury by potentiating microRNA-214-dependent inhibition of Kcnk2," *Experimental and Molecular Medicine*, vol. 52, no. 1, pp. 118–129, 2020.

[20] F. M. Ghoneim, H. Alrefai, A. Z. Elsamanoudy, S. M. Abo El-Khair, and H. A. Khalaf, "The protective role of prenatal alpha lipoic acid supplementation against pancreatic oxidative damage in offspring of valproic acid-treated rats: histological and molecular study," *Biology*, vol. 9, no. 9, p. 239, 2020.

[21] J. Qian, M. Lv, and W. Zhang, "The function of DREAM gene mediated by NF-kB signal pathway in the pathogenesis of osteosarcoma," *Journal of B.U.ON.*, vol. 22, no. 4, pp. 1068–1072, 2017.

[22] Z. Altayeb and M. Salem, "The effect of ethanol on rat tongue and the possible protective role of royal jelly: light and scanning electron microscopic study," *Egyptian Journal of Histology*, vol. 40, no. 3, pp. 265–276, 2017.

[23] H. I. Osman, N. Abdel-Razek, and S. A. Koura, "Histological changes of rat lingual papillae due to chromium toxicity and the protective role of vitamin E," *Egyptian Dental Journal*, vol. 52, pp. 193–200, 2006.

[24] H. Kashiwazaki, T. Matsushita, J. Sugita et al., "Professional oral health care reduces oral mucositis and febrile neutropenia in patients treated with allogeneic bone marrow transplantation," *Supportive Care in Cancer*, vol. 20, no. 2, pp. 367–373, 2012.

[25] V. Ziegler, A. Albers, and G. Fritz, "Lovastatin protects keratinocytes from DNA damage-related pro-apoptotic stress responses stimulated by anticancer therapeutics," *Biochimica et Biophysica Acta*, vol. 1863, no. 6 Part A, pp. 1082–1092, 2016.

[26] R. J. Gibson, J. M. Bowen, E. Alvarez, J. Finnie, and D. M. K. Keefe, "Establishment of a single-dose irinotecan model of gastrointestinal mucositis," *Chemotherapy*, vol. 53, no. 5, pp. 360–369, 2007.

[27] J. F. de M Rêgo, R. Salles Scortegagna de Medeiros, M. I. Braghiroli et al., "Expression of ERCC1, Bcl-2, Lin28a, and

Ki-67 as biomarkers of response to first-line platinum-based chemotherapy in patients with high-grade extrapulmonary neuroendocrine carcinomas or small cell lung cancer," *Ecancermedicalscience*, vol. 11, p. 767, 2017.

[28] R. O. M. Mohsen, A. M. Halawa, and R. Hassan, "Role of bone marrow-derived stem cells versus insulin on filiform and fungiform papillae of diabetic albino rats (light, fluorescent and scanning electron microscopic study)," *Acta Histochemica*, vol. 121, no. 7, pp. 812–822, 2019.

[29] A. A. A. Kattaia, A. O. Selim, S. A. Selim, and S. A. Abd El-Baset, "Epidermal growth factor attenuates lingual papillae lesions in a rat model of sialoadenectomy," *Tissue and Cell*, vol. 63, p. 101319, 2020.

[30] A. S. Al Refai, "Effects of Kurdistan honey on the tongue of chemotherapy treated albino rats (immunohistochemical study)," *Journal of Cytology and Histology*, vol. 5, no. 6, 2014.

[31] S. T. Sonis, "Pathobiology of mucositis," *Seminars in Oncology Nursing*, vol. 20, no. 1, pp. 11–15, 2004.

[32] J. M. Bowen, R. J. Gibson, A. G. Cummins, and D. M. K. Keefe, "Intestinal mucositis: the role of the Bcl-2 family, p53 and caspases in chemotherapy-induced damage," *Supportive Care in Cancer*, vol. 14, no. 7, pp. 713–731, 2006.

[33] D. Korbakis and A. Scorilas, "Treatment of gastric cancer cells with 5-fluorouracil/leucovorin and irinotecan induces distinct alterations in the mRNA expression of the apoptosis-related genes, including the novel gene BCL2L12," *Tumour Biology*, vol. 30, no. 2, pp. 100–107, 2009.

[34] X. Dai, G. Wu, Y. Zhang et al., "Design, synthesis, and in vitro/in vivo anti-cancer activities of novel (20S)-10,11-methylenedioxy-camptothecin heterocyclic derivatives," *International Journal of Molecular Sciences*, vol. 21, no. 22, p. 8495, 2020.

[35] L. Chen, H. Deng, H. Cui et al., "Inflammatory responses and inflammation-associated diseases in organs," *Oncotarget*, vol. 9, no. 6, pp. 7204–7218, 2018.

[36] L. Saso, S. Suzen, F. Borges, and T. Csont, "Chemistry and pharmacology of modulators of oxidative stress," *Current Medicinal Chemistry*, vol. 27, no. 13, pp. 2038-2039, 2020.

[37] T. Liu, L. Zhang, D. Joo, and S. C. Sun, "NF-κB signaling in inflammation," *Signal Transduction and Targeted Therapy*, vol. 2, no. 1, 2017.

[38] M. Karin, Y. Cao, F. R. Greten, and Z. W. Li, "NF-κB in cancer: from innocent bystander to major culprit," *Nature Reviews Cancer*, vol. 2, no. 4, pp. 301–310, 2002.

[39] C. M. Simplicio-Revoredo, R. de Oliveira Pereira, M. de Almeida Melo et al., "Expression of Nrf2 and NF-κB transcription factors in breast cancer and breast fibroadenoma: insights for a new therapeutic approach," *Oncotarget*, vol. 11, no. 18, pp. 1629–1636, 2020.

[40] T. Samuel, K. Fadlalla, D. N. Gales, B. D. Putcha, and U. Manne, "Variable NF-κB pathway responses in colon cancer cells treated with chemotherapeutic drugs," *BMC Cancer*, vol. 14, no. 1, p. 599, 2014.

[41] D. K. Sarkar, D. Jana, P. S. Patil et al., "Role of NF-κB as a prognostic marker in breast cancer: a pilot study in Indian patients," *Indian Journal of Surgical Oncology*, vol. 4, no. 3, pp. 242–247, 2013.

[42] X. Bao, J. Wu, S. Kim, P. LoRusso, and J. Li, "Pharmacometabolomics reveals irinotecan mechanism of action in cancer patients," *Journal of Clinical Pharmacology*, vol. 59, no. 1, pp. 20–34, 2019.

[43] W. L. Wu and T. Papagiannakopoulos, "The pleiotropic role of the KEAP1/NRF2 pathway in cancer," *Annual Review of Cancer Biology*, vol. 4, no. 1, pp. 413–435, 2020.

[44] L. Milkovic, N. Zarkovic, and L. Saso, "Controversy about pharmacological modulation of Nrf2 for cancer therapy," *Redox Biology*, vol. 12, pp. 727–732, 2017.

[45] B. D. Cameron, K. R. Sekhar, M. Ofori, and M. L. Freeman, "The role of Nrf2 in the response to normal tissue radiation injury," *Radiation Research*, vol. 190, no. 2, pp. 99–106, 2018.

[46] F. Wartlick, A. Bopp, C. Henninger, and G. Fritz, "DNA damage response (DDR) induced by topoisomerase II poisons requires nuclear function of the small GTPase Rac," *Biochimica et Biophysica Acta*, vol. 1833, no. 12, pp. 3093–3103, 2013.

[47] M. I. D. A. C. Campos, C. N. Campos, F. M. Aarestrup, and B. J. V. Aarestrup, "Oral mucositis in cancer treatment: natural history, prevention and treatment," *Molecular and Clinical Oncology*, vol. 2, no. 3, pp. 337–340, 2014.

[48] C. Franke, M. Nöldner, R. Abdel-Kader et al., "Bcl-2 upregulation and neuroprotection in guinea pig brain following chronic simvastatin treatment," *Neurobiology of Disease*, vol. 25, no. 2, pp. 438–445, 2007.

[49] A. M. Abeles and M. H. Pillinger, "Statins as antiinflammatory and immunomodulatory agents: a future in rheumatologic therapy?," *Arthritis and Rheumatism*, vol. 54, no. 2, pp. 393–407, 2006.

[50] A. H. Wagner, O. Schwabe, and M. Hecker, "Atorvastatin inhibition of cytokine-inducible nitric oxide synthase expression in native endothelial cells in situ," *British Journal of Pharmacology*, vol. 136, no. 1, pp. 143–149, 2002.

[51] H. Y. Wang, Y. Hou, J. Sun, Q. L. Xu, D. Q. Zhang, and Y. C. Han, "Effect of atorvastatin on expression of TLR4 and NF-κB in stroke rats and its protective effect on brain," *European Review for Medical and Pharmacological Sciences*, vol. 24, no. 20, pp. 10799–10805, 2020.

[52] C. Ihoriya, M. Satoh, N. Komai, T. Sasaki, and N. Kashihara, "Nuclear factor erythroid 2-related factor 2 is activated by rosuvastatin via p21cip1 upregulation in endothelial cells," *Biochemical Pharmacology*, vol. 4, p. 157, 2014.

[53] S. Bao, J. Lin, M. Xie, C. Wang, and X. Nie, "Simvastatin affects Nrf2/MAPK signaling pathway and hepatic histological structure change in Gambusia affinis," *Chemosphere*, vol. 269, p. 128725, 2021.

[54] A. Sarmanova, M. Doherty, C. Kuo et al., "Statin use and risk of joint replacement due to osteoarthritis and rheumatoid arthritis: a propensity-score matched longitudinal cohort study," *Rheumatology*, vol. 59, no. 10, pp. 2898–2907, 2020.

[55] M. Ashrafizadeh, Z. Ahmadi, T. Farkhondeh, and S. Samarghandian, "Modulatory effects of statins on the autophagy: a therapeutic perspective," *Journal of Cellular Physiology*, vol. 235, no. 4, pp. 3157–3168, 2019.

[56] S. K. Shin, J. H. Cho, E. J. Kim et al., "Anti-inflammatory and anti-apoptotic effects of rosuvastatin by regulation of oxidative stress in a dextran sulfate sodium-induced colitis model," *World Journal of Gastroenterology*, vol. 23, no. 25, p. 4559, 2017.

[57] A. C. Medeiros, Í. M. Azevedo, M. L. Lima, I. Araújo Filho, and M. D. Moreira, "Efeitos da sinvastatina na mucosite gastrointestinal induzida por 5-fluorouracil em ratos," *Revista do Colégio Brasileiro de Cirurgiões*, vol. 45, no. 5, 2018.

Hindawi
Oxidative Medicine and Cellular Longevity
Volume 2021, Article ID 7308897, 17 pages
https://doi.org/10.1155/2021/7308897

Research Article

Olaparib: A Clinically Applied PARP Inhibitor Protects from Experimental Crohn's Disease and Maintains Barrier Integrity by Improving Bioenergetics through Rescuing Glycolysis in Colonic Epithelial Cells

Dominika Kovács,[1] **Viola Bagóné Vántus**,[1] **Eszter Vámos**,[1] **Nikoletta Kálmán**,[1] **Rudolf Schicho**,[2,3] **Ferenc Gallyas**,[1,4,5] **and Balázs Radnai**[1]

[1]*Department of Biochemistry and Medical Chemistry, Medical School, University of Pécs, 7624 Pécs, Hungary*
[2]*Division of Pharmacology, Otto Loewi Research Center, Medical University of Graz, Universitätsplatz 4, 8010 Graz, Austria*
[3]*BioTechMed, 8010 Graz, Austria*
[4]*Szentagothai Research Centre, University of Pecs, 7624 Pecs, Hungary*
[5]*HAS-UP Nuclear-Mitochondrial Interactions Research Group, 1245 Budapest, Hungary*

Correspondence should be addressed to Balázs Radnai; balazs.radnai@aok.pte.hu

Received 18 April 2021; Accepted 24 August 2021; Published 15 September 2021

Academic Editor: Mariaurea Matias Sarandy

Crohn's disease (CD) is an inflammatory disorder of the intestines characterized by epithelial barrier dysfunction and mucosal damage. The activity of poly(ADP-ribose) polymerase-1 (PARP-1) is deeply involved in the pathomechanism of inflammation since it leads to energy depletion and mitochondrial failure in cells. Focusing on the epithelial barrier integrity and bioenergetics of epithelial cells, we investigated whether the clinically applied PARP inhibitor olaparib might improve experimental CD. We used the oral PARP inhibitor olaparib in the 2,4,6-trinitrobenzene sulfonic acid- (TNBS-) induced mouse colitis model. Inflammatory scoring, cytokine levels, colon histology, hematological analysis, and intestinal permeability were studied. Caco-2 monolayer culture was utilized as an epithelial barrier model, on which we used qPCR and light microscopy imaging, and measured impedance-based barrier integrity, FITC-dextran permeability, apoptosis, mitochondrial oxygen consumption rate, and extracellular acidification rate. Olaparib reduced the inflammation score, the concentration of IL-1β and IL-6, enhanced the level of IL-10, and decreased the intestinal permeability in TNBS-colitis. Blood cell ratios, such as lymphocyte to monocyte ratio, platelet to lymphocyte ratio, and neutrophil to lymphocyte ratio were improved. In H_2O_2-treated Caco-2 monolayer, olaparib decreased morphological changes, barrier permeability, and preserved barrier integrity. In oxidative stress, olaparib enhanced glycolysis (extracellular acidification rate), and it improved mitochondrial function (mitochondrial coupling efficiency, maximal respiration, and spare respiratory capacity) in epithelial cells. Olaparib, a PARP inhibitor used in human cancer therapy, improved experimental CD and protected intestinal barrier integrity by preventing its energetic collapse; therefore, it could be repurposed for the therapy of Crohn's disease.

1. Introduction

Inflammatory bowel disease (IBD) is a chronic and remitting inflammatory disease of the gut. More than 1 million inhabitants in the USA and approximately 2.5 million in Europe suffer from IBD, and its incidence is permanently rising [1]. IBD exhibits two main forms, namely, ulcerative colitis (UC) and Crohn's disease (CD), and it appears in flare-up and remission phases [2]. Although UC and CD are two distinct forms of IBD, they share the phenomenon of epithelial barrier dysfunction. Barrier failure often results in increased intestinal permeability, a condition called "leaky gut" [3]. In

this disorder, the gut microbiota can directly enter the colonic tissue and induce the activation of immune cells causing chronic inflammation [4, 5]. The initiators of increased gut permeability are not clearly elucidated, but it is often suggested that increased permeability is a consequence of altered energy metabolism and mitochondrial dysfunction of intestinal epithelial cells (IEC) [6]. For example, investigations with conplastic mouse strains, which share the same nuclear genome but have different mitochondrial genomes, demonstrated that those mice with high mucosal respiratory chain activity and elevated concentration of ATP develop less intense colitis than those that produce a smaller amount of mucosal ATP [7]. In CD patients, increased mucosal permeability in the ileum was accompanied by mitochondrial swelling and decreased ATP concentration [8]. In addition, the activity of complex II (CII), a part of the mitochondrial electron transport chain (ETC), was found to be abolished in the colon of UC patients [9]. Another group found lower levels of CI and CIV in IBD patients compared to control subjects and also measured lower ATP concentrations [10]. Furthermore, enhanced lactate levels were found in CD patients in comparison with healthy individuals, which correlated with the disease activity [11]. All these results suggest mitochondrial dysfunction, disturbed oxidative phosphorylation, and enhanced glycolytic activity in the mucosa of IBD patients.

Under physiological conditions, IECs use butyrate as a primary energy source [12]. Butyrate is produced by several species of the microbiota, and it is catabolized in IECs via β-oxidation and citric acid cycle (CAC) [13–15]. In addition, dehydrogenases of these catabolic pathways reduce NAD^+ and FAD to $NADH+H^+$ and $FADH_2$ which promote the reduction of the mitochondrial respiratory chain CI and CII [16]. Thereafter, CI, CIII, and CIV pump protons across the inner membrane from the matrix to the intermembrane space raising a proton gradient [16]. At the end of ETC, CIV consumes O_2 and reduces it to H_2O. Finally, the proton gradient drives F_OF_1-ATPase, which produces ATP from ADP and P_i [16].

However, in inflammation, mitochondrial dysfunction and mitochondria-derived ROS increase. Under these circumstances, IECs switch their metabolism from oxidative phosphorylation (OXPHOS) to aerobic glycolysis [13, 17]. In aerobic glycolysis, glucose transforms to lactate without oxygen consumption, although sufficient amount of oxygen is present in the cells [18]. In this situation, glycolysis produces ATP and, as a by-product, lactate is synthesized from pyruvate by lactate dehydrogenase [17]. Since the mitochondria are a major source of ROS [19], the catabolic pathway via glycolysis and lactate dehydrogenase bypasses the mitochondria and do not feed mitochondrial ROS generation [20]. Thus, the cell shuts down the mitochondria to protect itself from mitochondrial ROS [21]. This concept is strengthened by the findings that proinflammatory cytokines (TNF-α, IL-1β, and IFN-γ) increased the rate of glycolysis in rat enterocytes and also triggered ATP turnover [22]. Also *C. rodentium* infection in mice induced aerobic glycolysis and enhanced the level of sodium-glucose transporter 4 and lactate dehydrogenase A. At the same time, enzymes of CAC and OXPHOS were downregulated [23]. Most importantly, a strong expression of glycolytic enzymes was found in the colon of IBD patients [24]. In active CD, lactate levels were significantly higher compared to the control subjects [11]. Therefore, in colitis, aerobic glycolysis becomes the main source of ATP. Nevertheless, in severe inflammation, activation of the enzyme poly(ADP-ribose)-polymerase-1 (PARP-1) blocks glycolysis [25], i.e., it terminates the "last safe way" of energy production and forces the cells along the death pathway causing strong mucosal damage with severe ulceration and compromised barrier function.

PARP-1 has been long involved in cancer development and inflammation. Accordingly, PARP-$1^{-/-}$ mice were protected in 2,4,6-trinitrobenzene sulphonic acid- (TNBS-) induced colitis [26] and pharmacological inhibitors of PARP-1 improved dextran sodium sulfate-induced [27] and TNBS-induced colitis [28] in rodents. PARP-1 is activated by DNA damage and catalyzes polyADP-ribosylation (PARylation) of numerous nuclear proteins using NAD^+ as a substrate [29]. This process is a part of the DNA damage response leading to activation of the DNA repair enzymes [30]. However, excessive PARP activation can totally deplete NAD^+ pools, which makes cellular energy metabolism impossible [31]. Several lines of evidence demonstrate that PARP activation not only depletes NAD^+ pools but also inhibits the enzyme hexokinase, which catalyzes the first step of glycolysis [25]. As a result, repressed glycolysis cannot feed CAC with Acetyl-CoA (produced by pyruvate dehydrogenase from the glycolytic end-product pyruvate), and CAC is not able to reduce NAD^+ and FAD to feed mitochondrial ETC and OXPHOS [32], so PARP-induced mitochondrial dysfunction originates, at least partially, from the decreased substrate flow from glycolysis to CAC and ETC [25]. Since, in severe colitis, glycolysis is the main source of ATP (because of mitochondrial shutdown) [21] and also glycolysis is inhibited by PARP [25], IECs have to face with energetic collapse and they lose the ability to form a strong and continuous barrier [7].

In the present study, we investigated whether olaparib, a PARP inhibitor used in human cancer therapy, has a beneficial effect in a CD mouse model and, accordingly, whether it could be repurposed for CD treatment. To answer this question, we applied olaparib during a TNBS-induced experimental colitis model. Additionally, since IECs are the first line of defence in the colon and barrier interruption is a hallmark of IBD, we used Caco-2 colonic epithelial cells and investigated barrier function and energy production *in vitro*.

2. Materials and Methods

2.1. Animals and Experimental Colitis. Male CD1 mice (Jackson Laboratory, Bar Harbor, ME, USA) were bred and maintained at the SPF animal facility of the Department of Immunology and Biotechnology, Medical School, University of Pécs. At the age of 6-8 weeks, they were transported to our animal house facility and acclimatized for 2 weeks under standardized circumstances. Standard laboratory chow and water were available ad libitum. Experimental procedures

were approved by the Animal Research Review Committee of the University of Pécs, Medical School (Permit number: BA02/2000-4/2017). For the colitis experiments, we used the vehicle (VEH), TNBS, and TNBS+olaparib (TNBS+olap) treatment groups. In total, 72 animals were used; 1 mouse died during the experiments before evaluation. In our experimental setting, every group contained 3-9 animals. We performed 3 independent experiments including in total 9 VEH, 26 TNBS, 9 TNBS+20 mg olaparib, and 27 TNBS +50 mg olaparib). The age-matched (8-10 weeks), sex-matched (male), and bodyweight-matched (30-40 g) animals were randomly divided into groups by a technician. During the experiments, mice were individually housed to avoid aggressive behavior. Individual housing was approved by the Animal Research Review Committee of the University of Pécs. The experimental period lasted in total for 4 days (Figure 1(a)). On day 1, olaparib treatment started (pretreatment), and thereafter, we administered it daily once for 3 times (thus, in total, we performed 4 olaparib treatments). On day 0, animals were treated with TNBS (1 bolus), and on day 3, mice were anesthetized and euthanized. Olaparib (AZD2281, MedChemExpress, New Jersey, USA) was administered intraperitoneally (single injection) on the day before TNBS challenge, followed by daily administration for 3 days at the dose of 20 or 50 mg/kg bodyweight. The applied dose of olaparib was selected based on literature data [33]. The vehicle group received sterile distilled water containing 4% DMSO and 30% PEG300. After 12 hrs fasting, mice were anesthetized with 5% isoflurane (Baxter Hungary Ltd., Budapest, Hungary) in 100% oxygen in an anaesthetic chamber. Colitis was induced by a single intracolonic injection of TNBS (4 mg in 100 μl of 30% ethanol; Sigma-Aldrich, Missouri, USA) through a catheter inserted 3 cm into the colon. The VEH group received an equal volume of 30% ethanol. Animals were weighed daily during the experiment and sacrificed 72 hrs after TNBS administration. Mice were anesthetized with 5% isoflurane and decapitated gently by a dedicated surgical scissor to collect the highest possible amounts of trunk blood. This technique was approved by the Animal Research Review Committee of the University of Pécs. Trunk blood was collected; the colons were removed, measured, weighted, and opened longitudinally to detect the macroscopic colon damage. Tissue samples were processed for further analyses. Treatments and macroscopical scoring were carried out blind.

2.2. Intestinal Permeability Measurement. Intestinal permeability was determined by measuring the concentration of fluorescein isothiocyanate (FITC)-dextran (40 kDa; Sigma-Aldrich Missouri, USA) in serum. 3 days after TNBS treatment, FITC-dextran solution (100 μl of a 60 mg/ml solution) was administered intrarectally. Serum was collected 1 hour after the administration, and fluorescence intensities were detected by a Promega GloMax plate reader (excitation, 490 nm; emission, 510–570 nm). A standard curve was generated from a serial dilution of FITC-dextran in PBS.

2.3. Hematological Analysis. At the endpoint of the TNBS model, mice were anesthetized with 5% isoflurane and decapitated gently by a dedicated surgical scissor, and trunk blood was collected directly into microtainer tubes (Becton Dickinson, Hungary) containing EDTA as an anticoagulant. Hematological parameters were determined by a Sysmex XN-1000-V Multispecies Hematology Analyzer (Sysmex America Inc., USA) within 2 hours of sampling. Lymphocyte to monocyte ratio (LMR), platelet to lymphocyte ratio (PLR), neutrophil to lymphocyte ratio (NLR), and neutrophil to monocyte ratio (NMR) were calculated from the absolute cell counts for each animal separately.

2.4. Macroscopic Scoring. Colonic tissue damage score was assessed by a macroscopic scoring system described previously [34]. Briefly, individual points were added for ulcers (0.5 points for each 0.5 cm), adhesions (0 points = absent, 1 point = 1 adhesion, and 2 points = 2 or more adhesions or adhesions to organs), colon shortening, based on a mean length of a healthy colon (1 point = >15%, 2 points = >25%), wall thickness (measured in mm), consistency of the stool, and the presence of blood in the stool (hemorrhage, fecal blood, or diarrhea increase the total points by 1).

2.5. Histology of Colon Tissue. Segments of the distal colon were stapled flat onto a cardboard with the mucosal side up and fixed for at least 24 hrs in 10% neutral-buffered formalin. Tissue was then dehydrated and embedded in paraffin, and standard hematoxylin staining was performed on 5 μm thick sections. To this end, slides were deparaffinized, cleared in xylol, rehydrated in a descending ethanol series, stained with hematoxylin solution according to Gill II, and cleared in tap water. Images were taken with an Olympus DP50 camera and processed with cellSens imaging software (Olympus, Vienna, Austria).

2.6. Cytokine Levels of Colon Tissue. Levels of inflammatory cytokines IL-1β, IL-6, TNF-α, and IL-10 were measured in colon tissues. Tissue was homogenized mechanically in an extraction buffer supplemented with protease inhibitor cocktail (Sigma-Aldrich, Missouri, USA). Bradford assay (Bio-Rad Laboratories, California, USA) was used to measure the concentration of total protein. Subsequently, normalization of protein concentrations was performed and cytokine levels were determined by Ready-Set-Go ELISA kits (eBioscience, California, USA) according to the manufacturer's instructions.

2.7. Epithelial Cell Culture. The Caco-2 human colon carcinoma epithelial cell line was purchased from the American Type Culture Collection (ATCC, Virginia, USA) and cultured in Eagle's minimum essential medium (Biosera, France) supplemented with 20% fetal bovine serum (Corning, New York, USA) and 1% nonessential amino acid solution (Sigma-Aldrich, Missouri, USA). Cells were maintained in a humidified incubator containing 5% CO_2 at 37° C.

2.8. RNA Isolation and qPCR. Total RNA was extracted from the Caco-2 monolayer using NucleoSpin RNA Plus kit (Macherey-Nagel, Germany) according to the manufacturer's protocol. It was quantified using a Nanodrop spectrophotometer and Qubit 2.0 fluorometer (Thermo Fisher

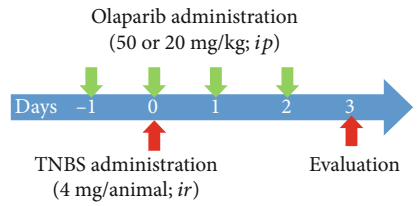

(a)

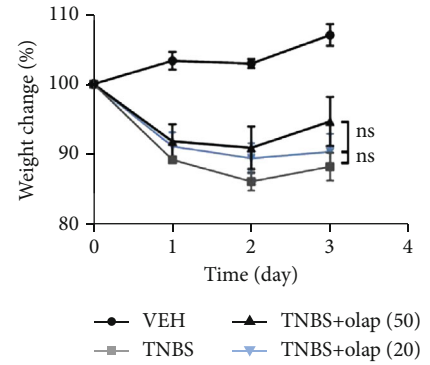

(b)

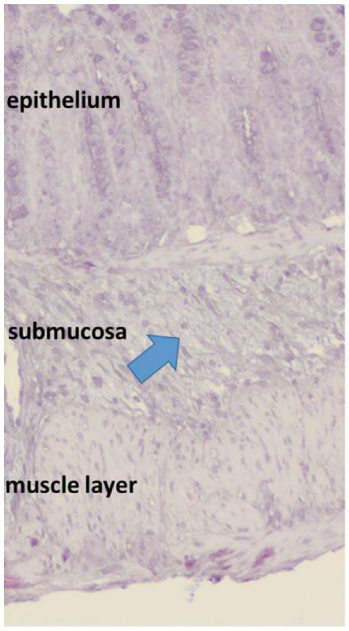

TNBS+VEH

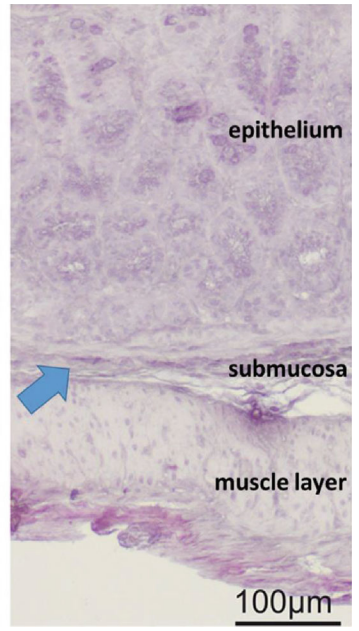

TNBS+olap (50)

(c)

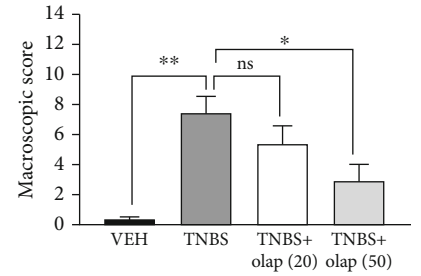

(d)

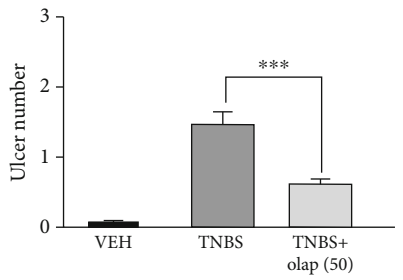

(e)

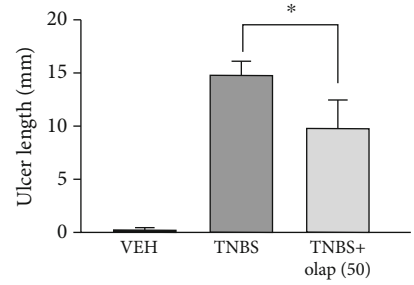

(f)

Figure 1: Continued.

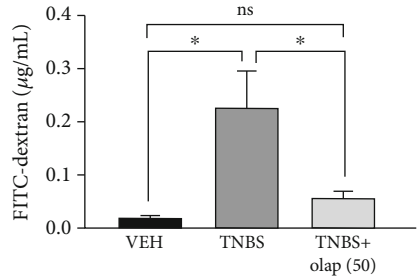

(g)

Figure 1: Olaparib treatment attenuated TNBS-induced colitis in mice. (a) Experimental protocol of TNBS-induced colitis and olaparib treatment. (b) Bodyweight changes (percentage of the initial bodyweight of each animal) in every experimental group. Data from one of three independent experiments are expressed as mean ± SEM ($n = 4$-7). (c) Representative images of hematoxylin staining of colon cross-sections from the TNBS- and TNBS+olap (50)-treated mice. Arrows indicate the most affected part of the colon tissue, the submucosa. (d) Macroscopic score in every experimental group. Data combined from 2 separate experiments ($n = 9$-21). (e) Ulcer number and (f) ulcer length in the VEH, TNBS, and TNBS+olap (50) groups. Data combined from 3 separate experiments ($n = 9$-27). (g) Intestinal permeability based on the measurement of FITC-dextran in blood samples 3 days after TNBS treatment. Data from one of three independent experiments are expressed as mean ± SEM ($n = 5$-8); ns: not significant; $^{*}P < 0.05$, $^{**}P < 0.01$, and $^{***}P < 0.001$. VEH: vehicle; TNBS: 2,4,6-trinitrobenzene sulphonic acid; olap (50): 50 mg/kg olaparib; olap (20): 20 mg/kg olaparib.

Scientific, USA). 1 μg of total RNA was reverse-transcribed with M-MuLV RT (Maxima First-Strand cDNA Synthesis Kit, Thermo Fisher Scientific, USA). 100 ng cDNA was used in 20 μl reactions for real-time PCR using the Xceed qPCR SG 2× Mix (Institute of Applied Biotechnologies, Praha-Strašnice, Czech Republic) and a CFX96 Touch Real-Time PCR Detection System (Bio-Rad, USA). After 40 cycles of PCR reaction, products were run on a 1.5% agarose gel using 20 bp DNA Ladder (Lonza, Basel, Switzerland). Data were analyzed by ΔCt method. As a reference for gene expression, we used β-actin expression. Primers for the investigated gene expression were as follows: (i) β-actin (121 bp): forward 5′-GCATGGGTCAGAAGGATTCC-3′, reverse 5′-CAGA TTTTCTCCATGTCGTCCC-3′; (ii) PARP-1 (109 bp): forward 5′-CGAGTCGAGTACGCCAAGAG-3′, reverse 5′-CATCAAACATGGGCGACTGC-3′; (iii) PARP-2 (97 bp): forward 5′-GCCAGCAAAAGGGTCTCTGA-3′, reverse 5′-CATGAGCCTTCCCCACCTTG-3′; and (iv) PARP-3 (115 bp): forward 5′-CCTGAGGCTCATGGAGAGTTG-3′, reverse 5′-TGGAGCCATGGCCAAGAAAA-3′. The efficiency of the reactions was in all cases near 100%.

2.9. Impedance-Based Barrier Integrity Measurements. First, the epithelial barrier integrity was determined by measuring electrical impedance using xCELLigence RTCA DP Real-Time Cell Analyzer (ACEA Biosciences, California, USA). Caco-2 cells were seeded on RTCA E-plates (E-plate 16) at a density of 10^5 cells/well. We applied the control (CTRL) and H_2O_2 or H_2O_2+olaparib treatment groups. After attaining confluency, the monolayers were treated with different concentrations of H_2O_2 (100, 200, 500, and 1000 μM) or with olaparib (10 μM) as a pretreatment, 30 min before H_2O_2. The CTRL and H_2O_2 treatment groups received the same amount of DMSO as the olaparib-treated cells. The cell index (CI) was continuously monitored by the equipment for 24 hours.

2.10. FITC-Dextran Epithelial Permeability Assay. Permeability was assessed by measuring the flux of FITC-dextran from the upper compartment to the lower compartment in Transwell plates (pore size 0.4 μm; polyester membrane, Corning, New York, USA). Caco-2 cells were grown until full confluency in 12 well Transwell plates. Here, we applied the same treatment groups as described in the impedance-based technique. Cells were treated with 1000 μM H_2O_2 or pretreated with 10 μM olaparib for 30 minutes. After 24 hours, FITC-dextran solution (1 mg/ml) was added to the upper chamber. 1 hour later, a medium from the lower chamber was collected and the fluorescence intensities were detected by a Promega GloMax plate reader (Promega, USA) at 490-nm excitation and 510–570 nm emission wavelengths.

2.11. Determination of Apoptosis. Mouse Annexin V & Dead Cell Kit (Merck Millipore, Massachusetts, USA) was used for the quantitative analysis of live, early, and late apoptotic and necrotic cells. Caco-2 cells were seeded onto 6-well plates at a density of 10^6 cells/well. Treatments and treatment groups were exactly the same as described above at the FITC-dextran assay. 24 hrs after treatment, cells were trypsinized and collected; sample preparation was performed as suggested by the manufacturer. Briefly, 100 μL of cell suspension was incubated with 100 μl of Muse Annexin V & Dead Cell reagent for 20 minutes, in the dark at room temperature. After staining, the assay was performed with a Muse Cell Analyzer (flow cytometer).

2.12. Seahorse XFp Cell Mito Stress Test. Measurement of the oxygen consumption rate (OCR) and extracellular acidification rate (ECAR) in Caco-2 monolayers was performed by a Seahorse XFp Extracellular Flux Analyzer (Agilent Technologies, California, USA). The day before the assay, the Seahorse XFp Sensor Cartridge was hydrated with XF Calibrant Solution and was kept at 37°C in a CO_2-free incubator overnight. Caco-2 cells were seeded on XFp Miniplates

at a density of 1.5×10^4 cells/well. After reaching 100% confluence, cells were treated exactly as described at the FITC-dextran assay. After the treatment, a complete growth medium was replaced with an unbuffered, serum-free Agilent XF Base assay medium, pH 7.4. XFp Mito Stress Test Kit was used to test mitochondrial function. Injection of oligomycin, carbonyl cyanide-4 (trifluoromethoxy) phenylhydrazone (FCCP), and the mix of rotenone and antimycin A allows determining the key bioenergetic parameters: basal respiration, ATP production-linked respiration (ATP production), maximal respiration, spare respiratory capacity, nonmitochondrial respiration, proton leak, and coupling efficiency. Oligomycin inhibits the F_O subunit of the F_OF_1-ATP synthase, thereby indicating ATP-linked OCR, i.e., level of ATP synthesis. ATP-linked respiration is calculated by the difference between baseline OCR and OCR after oligomycin injection. Distracting nonmitochondrial respiration from the OCR after FCCP injection represents maximal respiration. FCCP is a mitochondrial uncoupler, which separates the activity of phosphorylation and oxidation. Under these circumstances, ETC might work with its maximum rate and consumes higher amounts of O_2 without developing membrane potential between the two sides of the mitochondrial inner membrane. Spare respiratory capacity is defined by the difference between maximal and basal respiration. The mixture of rotenone and antimycin A inhibits CI and CIII, respectively; thus, mitochondrial ETC and O_2 consumption are blocked. The final concentrations of the modulators were 1 μM. OCR after rotenone/antimycin A injection represents nonmitochondrial respiration. ATP-linked respiration divided by basal respiration reveals coupling efficiency.

2.13. Light Microscopy Imaging. Caco-2 cells were seeded at a density of 10^6 cells/well on 6-well plates. After reaching confluency, the monolayers were treated exactly as described at the FITC-dextran assay. 24 hours later, monolayers were visualized by EVOS XL Core Cell Imaging System (Thermo Fisher Scientific, USA) using a 20× objective.

2.14. Statistical Analysis. Experimental data were analyzed by using GraphPad Prism Software (GraphPad Software Inc., California, USA). Statistical difference between groups was established by Student's *t*-test, with Bonferroni correction; *P* values less than 0.05 were considered statistically significant.

3. Results

3.1. Olaparib Improved TNBS-Colitis in Mice. To evaluate the effect of olaparib in experimental colitis, we used the TNBS-colitis model (Figure 1(a)), a mouse model of CD [35]. Olaparib was used as a pretreatment in 20 and 50 mg/kg bodyweight dose. On the one hand, olaparib failed to significantly ameliorate weight loss in TNBS-challenged animals (Figure 1(b)). But on the other hand, it decreased inflammation scores by more than ~50% in 50 mg/kg ($n = 21$), but not in 20 mg/kg dosage ($n = 9$) (Figure 1(d)). Hence, we used 50 mg/kg dose in the further experiments. Olaparib impeded histological injury in the colon (Figure 1(c)), reduced the number of ulcers ($n = 27$) (Figure 1(e)) and their lengths ($n = 27$) (Figure 1(f)), and most importantly, diminished FITC-dextran permeability ($n = 8$) (Figure 1(g)) compared to the CTRL group ($n = 5$). Levels of inflammatory cytokines were also modulated. Olaparib diminished IL-1β (Figure 2(a)) and IL-6 (Figure 2(b)) proinflammatory cytokine levels, but enhanced anti-inflammatory IL-10 production (Figure 2(c)) in the colon ($n = 13$). Interestingly, we could not find statistically significant alteration in the TNF-α level (Figure 2(a)). We also evaluated numerous hematological parameters in colitic mice (Figure 3(a)). We found only 2 parameters, namely, the amounts of lymphocytes and monocytes, which were significantly modulated by the treatments. In agreement with others' findings on colitis models, TNBS substantially reduced lymphocyte number in mice ($n = 9$), while olaparib counteracted this effect ($n = 20$). In contrast, monocyte number was higher in the TNBS group ($n = 9$), whereas it was significantly less elevated in the TNBS+olaparib group (Figure 3(a)) ($n = 20$). We calculated specific blood cell ratios, which were previously shown to be changed in CD [36] based upon the individual blood cell counts. Similarly to CD, neutrophil to lymphocyte ratio (NLR) (Figure 3(e)) and platelet to lymphocyte ratio (PLR) (Figure 3(c)) were both increased in TNBS-colitis and they were markedly reduced by olaparib treatment. Again, as in CD, lymphocyte to monocyte ratio (LMR) (Figure 3(b)) was reduced in experimental colitis, and it was amended by the PARP inhibitor. Unfortunately, TNBS-induced changes in the neutrophil to monocyte ratio (NMR) (Figure 3(d)) did not reach statistical significance compared to the vehicle. However, olaparib improved NMR related to the TNBS-treated group.

3.2. Caco-2 Colonic Epithelial Cells Expressed PARP-1, PARP-2 and PARP-3. Olaparib has been shown to inhibit three members of the PARP enzyme family, namely, PARP-1 ($IC_{50} = 5$ nM), PARP-2 ($IC_{50} = 1$ nM), and PARP-3 ($IC_{50} = 4$ nM) [37]. Thus, we investigated the basal expression profile of the three target isoforms in untreated Caco-2 cells forming a confluent monolayer. We detected continuous PARP-1, PARP-2, and PARP-3 mRNA expressions (Figures 4(a)–4(c)), but with different expression rates (PARP-1 > PARP-2 > PARP-3) (Figure 4(c)). In Caco-2 cells, PARP-1 was the most highly expressed isoform. PARP-2 and PARP-3 mRNA expressions were at about ~9-fold and~335-fold weaker compared to PARP-1 (Figure 4(c)).

3.3. Olaparib Improved Barrier Function of Epithelial Monolayer in Oxidative Stress. Caco-2 monolayers are widely used as a model for intestinal epithelial barrier [38]. Since the activity of PARP-1, PARP-2, and PARP-3 isoforms can be induced by DNA-damage [39], and as oxidative stress induces mucosal injury in IBD [40, 41], we tested different H_2O_2 concentrations (100-1000 μM) on Caco-2 monolayers. We assessed barrier integrity by an impedance-based technique (Figure 4(d)). Lower concentrations of H_2O_2 (100-500 μM) did not considerably modify cell index (CI; calculated from TEER impedance values) meaning they did not

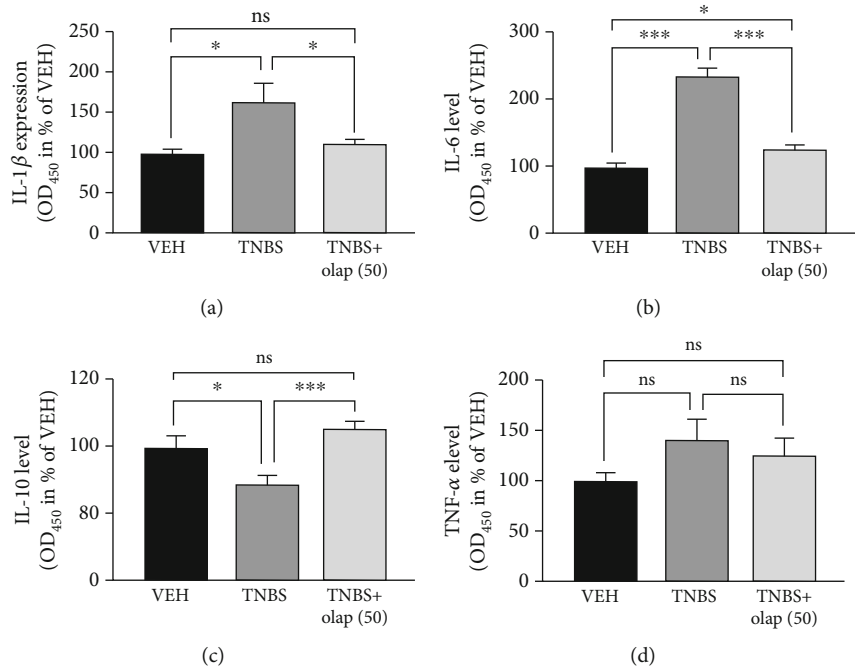

Figure 2: Olaparib decreased colonic proinflammatory cytokine (IL-1β and IL-6) and increased anti-inflammatory IL-10 cytokine levels. Cytokine levels of (a) IL-1β, (b) IL-6, (c) IL-10, and (d) TNF-α. Data combined from 2 separate experiments ($n = 9$-13) and expressed as mean ± SEM; ns: not significant; $^{*}P < 0.05$, $^{**}P < 0.01$, and $^{***}P < 0.001$. VEH: vehicle; TNBS: 2,4,6-trinitrobenzene sulphonic acid; olap (50): 50 mg/kg olaparib.

impair barrier integrity. However, 1 mM H_2O_2 rapidly and permanently decreased CI. After 24 hrs, 1 mM H_2O_2 strongly eroded the epithelial monolayer (Figure 4(d)). Consequently, in the further experiments, we applied 1 mM concentration of H_2O_2 to challenge the barrier. Olaparib pretreatment, 30 min before H_2O_2 exposure, improved CI compared to H_2O_2-treated cells and protected monolayer integrity (Figure 5(b)). To confirm these findings, we also performed FITC-dextran *trans*-epithelial permeability assay in the same model at the endpoint of the impedance-based measurement, after 24 hrs incubation (Figure 5(a)). We detected about ~20-fold increase in FITC-dextran fluorescent intensity after H_2O_2 treatment (i.e., FITC-dextran could pass the monolayer) in relation to CTRL. In contrast, olaparib reduced H_2O_2-induced FITC-dextran permeability near to the level of control (Figure 5(a)). To even further refine our results, we performed microscopic imaging and observed morphological changes in the structure of epithelial monolayer after H_2O_2 treatment. We realized compromised, in some places broken monolayer, with presumably dying cells, which lost their connection to neighbors in the monolayer. Olaparib prevented these morphological changes and kept the cells as an integral part of the barrier in their normal, epithelial phenotype (Figure 5(c)).

3.4. Olaparib Protected against Oxidative Stress-Induced Cell Death in Epithelial Barrier. To assess whether oxidative stress-induced barrier dysfunction involves epithelial cell death we performed flow cytometry analysis using Annexin V/7-AAD labeling (Figure 5(d)). H_2O_2 (1 mM) induced a marked increase in the amount of 7-AAD positive dead, basically necrotic cells (5.87% of total cells; 4.89-fold increase) compared to CTRL. In addition, it enhanced the annexin V/7-AAD double-positive, late apoptotic cell number (31.9% of total cells; 6.86-fold increase). In our hands, H_2O_2 had no significant effect on early apoptosis. Olaparib protected against H_2O_2-induced cell death, i.e., it reduced necrotic cell death (1.25% of total cells; 4.70-fold decrease) and late apoptosis (5.73%; 5.17-fold decrease) almost to the level of CTRL (Figure 5(d)).

3.5. PARP Inhibition Recovered Glycolytic Activity Compromised by H_2O_2 Treatment. In inflammation, colonocytes switch their oxidative metabolism (butyrate consumption) to aerobic glycolysis and produce lactate [13, 17] (Figure 6(a)). Thus, we investigated the glycolytic activity by measuring extracellular acidification rate (ECAR), i.e., lactate production (Figure 6(b)), two hours after H_2O_2 treatment in the early phase of oxidative stress. H_2O_2 caused a dramatic collapse in basal ECAR (w/o oligomycin) compared to CTRL, which was markedly enhanced by olaparib (Figure 6(b) (1-3 points of the measurement) and Figure 6(c)). Oligomycin treatment increased ECAR both in the CTRL and H_2O_2+olaparib-treated cells compared to the untreated (w/o oligomycin) group but failed to stimulate acidification in the H_2O_2-damaged monolayer (Figure 6(b) (4-6 points of measurement) and Figure 6(d)). FCCP, rotenone, and antimycin A did not influence ECAR significantly in either treatment groups (Figure 6(b) (7-12 points of measurement)).

Hematological parameters	Unit	CTRL		TNBS		TNBS + olaparib	
		mean	*SEM*	*mean*	*SEM*	*mean*	*SEM*
WBC	(10^9/L)	4,50	± 0,684	4,28	±0,518	4,71	±0,280
RBC	(10^9/L)	8,71	± 0,491	10,62	±0,470	10,03	±0,286
HGB	(g/L)	147,45	± 3,223	169,38	±6,793	162,40	±3,821
HCT	(%)	44,84	± 2,718	50,86	±2,044	49,67	±1,258
MCV	(fL)	51,43	± 0,810	47,97	±0,511	49,71	±0,747
MCH	(pg)	16,54	± 0,452	16,02	±0,167	16,26	±0,204
MCHC	(g/L)	322,33	± 9,521	333,75	±4,753	328,05	±5,309
PLT	(10^9/L)	1242,50	± 112,356	1310,87	±95,849	1347,42	±82,603
RDW-SD	(f/L)	25,93	± 1,040	22,88	±0,340	23,54	±0,752
RDW-CV	(%)	17,28	± 0,539	18,04	±0,422	17,56	±0,228
PDW	(fL)	7,07	± 0,318	7,74	±0,490	7,20	±0,219
MPV	(fL)	6,88	± 0,156	6,89	±0,174	6,73	±0,111
P-LCR	(%)	6,63	± 0,975	6,99	±1,258	6,05	±0,692
PCT	(%)	0,75	± 0,080	0,88	± 0,055	0,79	± 0,056
NRBC	(10^9/L)	0,25	± 0,217	0,02	± 0,003	0,02	± 0,007
NEUT	(10^9/L)	1,11	± 0,156	2,08	± 0,366	2,13	± 0,259
LYMPH	(10^9/L)	$2{,}09^A$	± 0,309	$1{,}15^B$	± 0,149	$1{,}82^A$	± 0,212
MONO	(10^9/L)	$0{,}14^A$	± 0,040	$0{,}32^B$	± 0,073	$0{,}22^A$	± 0,036
EO	(10^9/L)	0,11	± 0,026	0,04	± 0,028	0,14	± 0,030
BASO	(10^9/L)	0,01	± 0,002	0,01	± 0,002	0,01	± 0,004

(a)

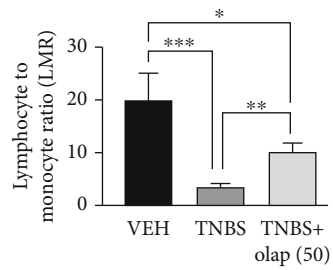

(b)

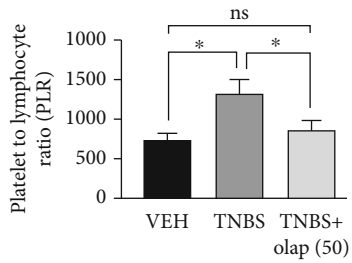

(c)

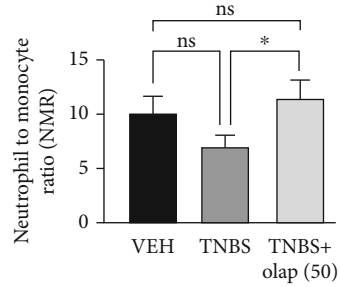

(d)

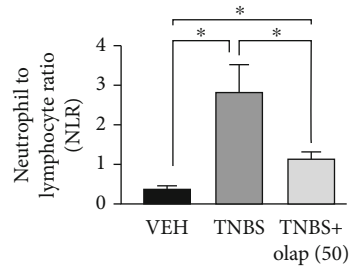

(e)

Figure 3: Olaparib modified hematological parameters and improved blood cell ratios in TNBS-treated mice. (a) Hematological parameters in the VEH, TNBS, and TNBS+olap (50) groups. Mean values ± SEM are shown in the table. A, B = different letters in each row indicate significant differences between groups ($P < 0.05$). Data combined from 3 separate experiments ($n = 9$-20). (b) Lymphocyte to monocyte ratio (LMR), (c) platelet to lymphocyte ratio (PLR), (d) neutrophil to monocyte ratio (NMR) (e), and neutrophil to lymphocyte ratio (NLR) values were calculated for each mouse individually before the averages were determined. Mean ± SEM is shown; ns: not significant; $^*P < 0.05$, $^{**}P < 0.01$, and $^{***}P < 0.001$. Data are combined from 3 separate experiments ($n = 9$-20). Abbreviations: WBC: white blood cell number; RBC: red blood cell number; HGB: hemoglobin; HCT: hematocrit; MCV: mean corpuscular volume; MCH: mean corpuscular hemoglobin; MCHC: mean corpuscular hemoglobin concentration; PLT: platelet count; RDW-SD: red cell distribution width-standard deviation; RDW-CV: red cell distribution width-coefficient of variation; PDW: platelet distribution width; MPV: mean platelet volume; P-LCR: platelet large cell ratio; PCT: procalcitonin; NRBC: nucleated red blood cells; NEUT: neutrophil count; LYMPH: lymphocyte count; MONO: monocyte count; EO: eosinophil count; BASO: basophil count.

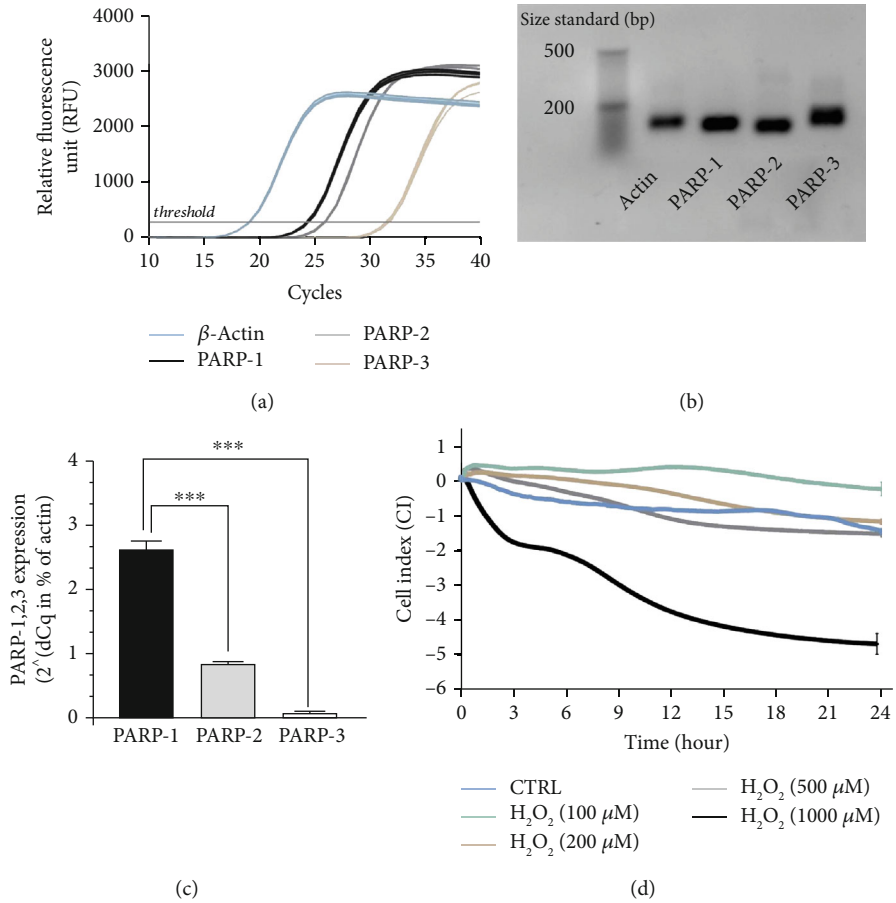

Figure 4: PARP-1, PARP-2, and PARP-3 are expressed in Caco-2 monolayers and high concentration of H_2O_2 disrupted barrier integrity. (a) Representative amplification curves of PARP-1, PARP-2, PARP-3, and β-actin quantitative real-time PCR (each containing three biological replicates and three technical replicates (data for biological replicates is not shown)). β-Actin is used as reference gene. (b) Agarose gel electrophoresis of the PCR products of the amplification (after 40th cycles) introduced in (a). Nonquantitative gene amplicons visualized in a 1.5% agarose gel. (product size: β-actin: 121 bp, PARP-1: 109 bp, PARP-2: 97 bp, and PARP-3: 115 bp; size standard from LONZA DNA ladder, 20 bp). (c) Relative gene expression results (2^(-dCq mean)), where β-actin expression is considered 100% (data is not shown). The relative differences (dCq) between the average Cq for the β-actin and the mean Cq per individual samples (PARP-1, PARP-2, and PARP-3). (d) Effect of H_2O_2 at different concentrations (100-1000 μM) on the disruption of epithelial barrier integrity of Caco-2 monolayers. Electrical impedance was monitored every 3 minutes for 24 hours with an xCELLigence RTCA instrument. Impedance-related cell index (CI) values from one of three independent experiments are expressed as mean ± SD (n = 4-6).

3.6. PARP Inhibitor Olaparib Preserved Mitochondrial Respiration in H_2O_2-Induced Stress. Under physiologic conditions, butyrate is the main source of ATP in colonocytes [12], and butyrate metabolism involves dynamic mitochondrial ETC activity and continuous OXPHOS [42]. Therefore, we investigated the activity of ETC and OXPHOS by measuring the oxygen consumption rate in our epithelial barrier model (Figure 7(a)). First, the basal respiration (OCR w/o oligomycin, green field on Figure 7(a)) was determined. H_2O_2 reduced basal respiration in epithelial cells compared to CTRL, and olaparib did not modulate this effect (Figure 7(b) (1-3 points of measurement and Figure 7(c)) indicating that olaparib had no effect on basal respiration. After oligomycin treatment, the ATP production-linked OCR (OCR with oligomycin, yellow field on Figure 7(a)) can be measured that reflects the activity of OXPHOS and ATP generation. Oligomycin reduced OCR and OXPHOS xoverall in all three experimental groups (Figure 7(b) (4-6 points of measurement]) and Figure 7(d)), but H_2O_2-treated cells consumed O_2 even to a lesser extent than CTRL, which suggested a reduced ATP production. Olaparib had no significant effect on the ATP-linked OCR in H_2O_2-treated cells (Figure 7(d)). Furthermore, olaparib ameliorated the H_2O_2-induced decline in coupling efficiency (Figure 7(e)). In contrast, FCCP, an uncoupling agent that induces maximal respiration in the mitochondria (OCR with FCCP, beige field on Figure 7(a)), enhanced OCR in all three groups in different extents (Figure 7(b) (7-10 points of measurement)). We detected the highest OCR in CTRL, the lowest in the H_2O_2-induced cells while olaparib counteracted the effect of H_2O_2 (Figure 7(b) (7-10 points of measurement) and Figure 7(f)). FCCP application also determined spare respiratory capacity (blue field on Figure 7(a)). Spare respiratory capacity was intensely reduced by H_2O_2 compared to CTRL, but olaparib

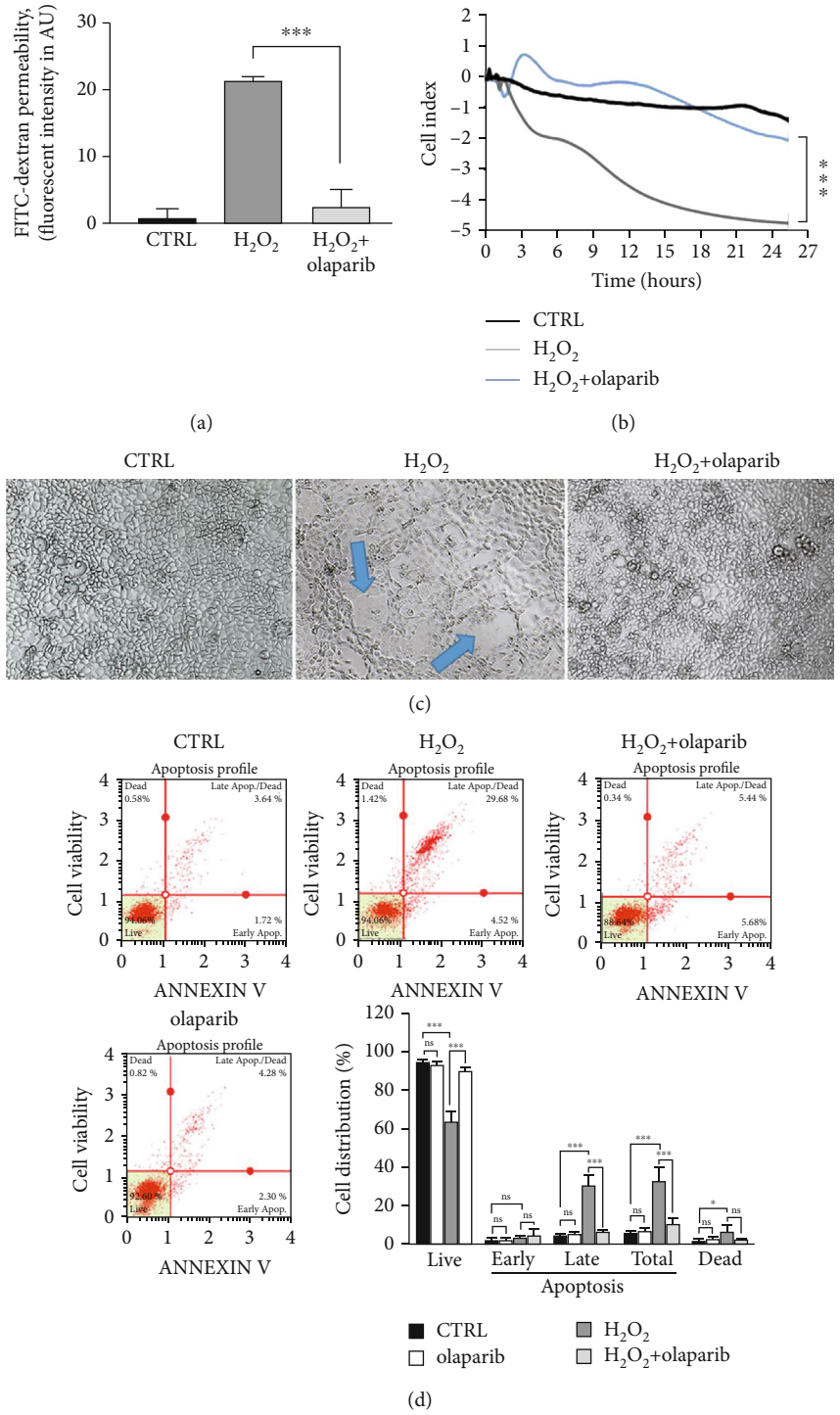

FIGURE 5: Olaparib improved epithelial barrier integrity in H_2O_2-treated Caco-2 monolayers. Caco-2 monolayers were pretreated with 10 μM olaparib for 30 minutes before 1 mM H_2O_2 treatment for 24 hours in all experimental settings. The CTRL and H_2O_2 groups received the same amount of DMSO as the olaparib-treated cells. (a) FITC-dextran epithelial permeability assay. 40 kDa FITC-dextran (1 mg/ml) was added to the upper chamber of the Transwell plate. After 1 hour of incubation, the medium from the lower chamber was collected and the fluorescence intensities were measured. Data combined from 2 separate experiments ($n = 4$). (b) Electrical impedance monitoring of Caco-2 monolayers using E-Plates and xCELLigence RTCA instrument. Data from one of three experiments are expressed as mean ± SD ($n = 4$-6). (c) Representative light microscopy images of confluent Caco-2 monolayers after 24 hours treatment. (d) Determination of apoptosis and necrosis in Caco-2 monolayers analyzed by Muse Annexin V & Dead Cell Kit. Representative apoptosis profiles and the percentage of live, early apoptotic, late apoptotic, total apoptotic, and necrotic cells are presented. Data are combined from 2 separate experiments ($n = 4$) and expressed as mean ± SD; ns: not significant; $^*P < 0.05$, $^{**}P < 0.01$, and $^{***}P < 0.001$.

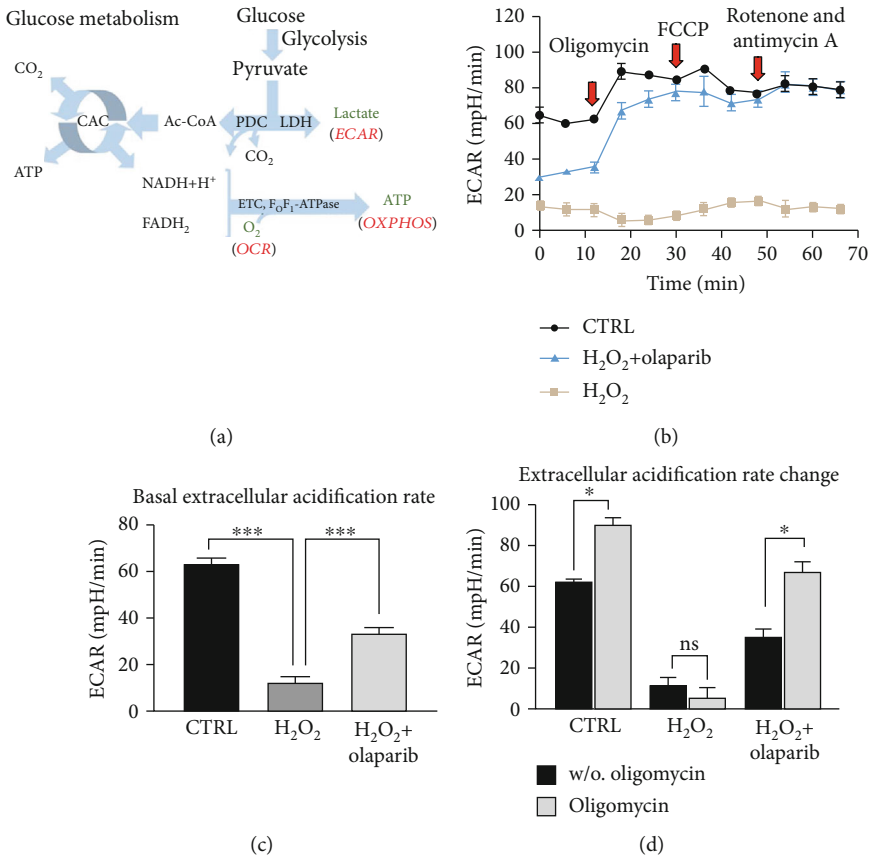

Figure 6: Olaparib improved aerobic glycolysis in Caco-2 monolayers exposed to H_2O_2-induced oxidative stress. Seahorse XFp Mito Stress test was performed after Caco-2 monolayers were pretreated with 10 μM olaparib for 30 minutes and then treated with 1000 μM H_2O_2 for 2 hours. The CTRL and H_2O_2 groups received the same amount of DMSO as the olaparib-treated cells. Oligomycin (1 μM), FCCP (1 μM), and the mixture of rotenone and antimycin A (1 μM) were added sequentially during the measurement. (a) Schematic illustration of glucose metabolism. (b) Extracellular acidification rate (ECAR), (c) basal ECAR, and (d) ECAR changes are shown. ECAR changes were calculated by the difference between ECAR before and after oligomycin injection. Data combined from 2 separate experiments ($n = 4$); ns: not significant; $^*P < 0.05$, $^{**}P < 0.01$, and $^{***}P < 0.001$. Abbreviations: PDC: pyruvate dehydrogenase complex; LDH: lactate dehydrogenase; CAC: citric acid cycle; ETC: mitochondrial electron transport chain; ECAR: extracellular acidification rate; OCR: oxygen consumption rate; OXPHOS: oxidative phosphorylation.

attenuated this reduction (Figure 7(g)). H_2O_2 reduced proton leak (orange field on Figure 7(a)) compared to CTRL, and it was further reduced by olaparib in Caco-2 cells (Figure 7(h)).

4. Discussion

The anti-inflammatory role of PARP inhibition is thoroughly established; however, introduction of PARP inhibitors into clinical therapy of anti-inflammatory diseases has not been initiated yet because of the potential risk in long-term use of the drugs [33]. In this study, we intended to provide experimental support for repositioning the PARP inhibitors (which are successfully applied in human cancer therapy) for the clinical management of the acute flare-up periods of CD. For that purpose, we used a TNBS-induced experimental colitis model in mice, which is widely accepted for studying CD, since they share many pathological (clinical, histological, and biochemical) characteristics [35]. Furthermore, enhanced PARP-1 expression was found in the colon of rodents [43, 44] in experimental colitis models, as well as in IBD patients [45], which makes the model more valuable for studying PARP inhibitors. In this report, we explicitly focused on the epithelial barrier function, cell survival, and bioenergetics; hence, we used a Caco-2 monolayer as an *in vitro* model of intestinal epithelial barrier [46]. We demonstrate that olaparib improves inflammation in TNBS-colitic mice and that it protects Caco-2 epithelial barrier in oxidative stress by rescuing glycolytic activity and by protecting some aspects of mitochondrial function.

In a recent review about repurposing PARP inhibitors for the therapy of nononcological diseases [33], Berger et al. did not consider IBD among those chronic diseases, in which the assumed benefits vs. the risks justify first priority of repurposing. However, the available preclinical data on IBD models successfully utilized outdated PARP inhibitors such as 3-aminobenzamide [47]. Our findings of *in vivo* anti-inflammatory effects of olaparib, a PARP inhibitor approved for human cancer therapy, may justify initiation of clinical trials for repurposing this drug for IBD therapy. We hypothesize that PARP inhibition might be beneficial in the acute flare-ups of severe CD, where detrimental

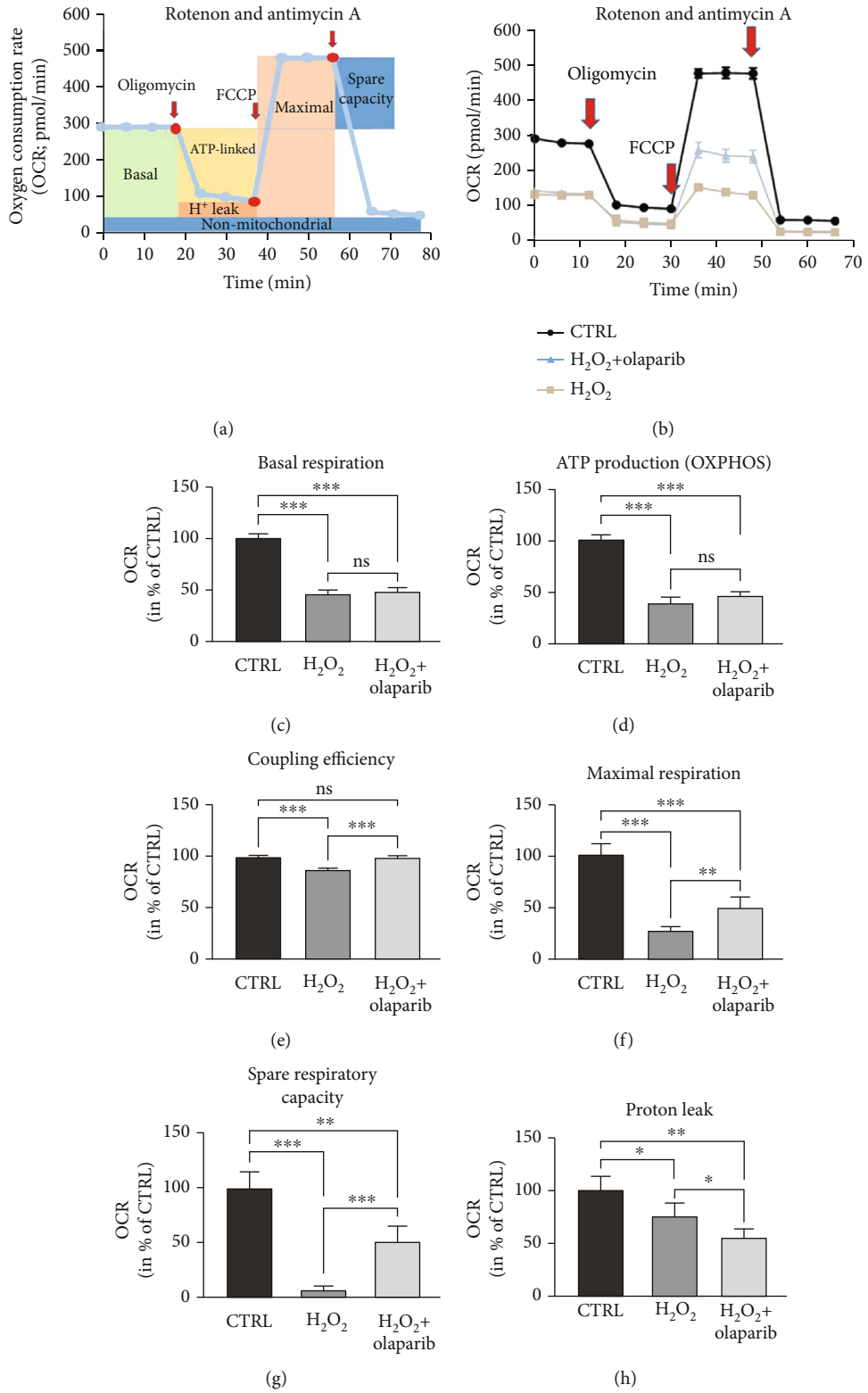

Figure 7: Olaparib protected mitochondrial function in Caco-2 monolayers subjected to H_2O_2-induced oxidative stress. Caco-2 monolayers were pretreated with 10 μM olaparib for 30 minutes and then treated with 1000 μM H_2O_2 for 2 hours. The CTRL and H_2O_2 groups received the same amount of DMSO as the olaparib-treated cells. Seahorse XFp Mito Stress test was performed, when oligomycin (1 μM), FCCP (1 μM), and the mixture of rotenone and antimycin A (1 μM) were injected sequentially. (a) Key parameters of mitochondrial respiration measured by Seahorse XFp Extracellular Flux Analyzer. (b) Measurement of oxygen consumption rate (OCR). Data combined from 2 separate experiments are expressed as mean ± SD ($n = 4$). Bioenergetic parameters: (c) basal respiration, (d) ATP production, (e) coupling efficiency, (f) maximal respiration, (g) spare respiratory capacity, and (h) proton leak were calculated. Results are expressed in percentage of control (mean ± SD of two independent experiments, $n = 4$); ns: not significant; $^{**}P < 0.01$, $^{***}P < 0.001$.

ulceration and tissue damage are caused by the energetic collapse of mucosal cells. It could be especially true in the severe cases of drug nonresponders, e.g., those one-third of IBD patients who primarily do not respond to infliximab (anti-TNF-α mAb; commonly prescribed drug in IBD) [48] or to other pharmacological therapies.

We demonstrated that olaparib improved TNBS-induced colitis in mice, reduced histological damage of the colon, diminished the number and length of the ulcers, inhibited proinflammatory cytokine production (IL-1β, IL-6), but it enhanced the level of anti-inflammatory cytokine IL-10. Inflammatory cytokines participating in the generation of colon damage are predominantly produced by activated leukocytes [49]. The fact that PARP inhibition reduces leukocyte infiltration into the colon in experimental colitis is well characterized [50–52]. Accordingly, we investigated hematological parameters from peripheral blood in our TNBS-colitis model. Several types of blood cell ratios were recently highlighted as possible diagnostic parameters in IBD [36, 53]. Specifically in CD, NLR and PLR were suggested to be valuable diagnostic factors [36]. Moreover, NLR might predict disease severity [54]; however, this notion is debated [55]. In detail, elevated NLR, PLR, and reduced LMR were found in CD patients compared to control subjects, while NMR was not modified [36]. In our experiments, alterations in NLR, PLR, LMR ,and NMR in TNBS-treated mice followed the observed changes in CD patients. In addition, olaparib effectively reversed CD-specific alterations in PLR and LMR, and most importantly, it reduced NLR. NLR was found to be a significant predictor of infliximab drug response in CD patients [56]. That is, the anti-inflammatory efficacy of infliximab correlated with decreased NLR in CD. Olaparib's identical anti-inflammatory effect in our TNBS-colitis model underlines the drug's potential in CD therapy.

Elevated NLR can also refer to oxidative stress in CD patients [57], which is an important inducer of PARP activation [58]. In active CD, excessive amounts of ROS are produced by the immune cells. The main source of ROS in immune cells is the H_2O_2 production [59], and H_2O_2 causes DNA damage in colonocytes [60] that triggers PARP activation. High concentrations of ROS result in apoptosis of IECs leading to disruption of epithelial barrier integrity in the colon, which is a definite hallmark of IBD. Accordingly, we treated Caco-2 monolayer with high concentration of H_2O_2 (1 mM) to imitate a strong oxidative stress-injured barrier, *in vitro*. We demonstrated that Caco-2 monolayer cells expressed PARP-1 mRNA in a high extent similarly to colonic mucosa [45]. In addition, we detected PARP-2 and PARP-3 expressions, however, in a decreasingly lower extent. That is, Caco-2 cells express the mRNA of olaparib's target enzymes (PARP-1, PARP-2, and PARP-3); furthermore, in the monolayer, these cells mimic the intestinal barrier [46]. Therefore, the Caco-2 monolayer seemed to be an appropriate model to investigate the effect of PARP-inhibition on barrier integrity, *in vitro*. Our results showed that olaparib preserved the Caco-2 monolayer integrity in oxidative stress and protected the epithelial cells from apoptosis. These findings indicated that colonic epithelial cells might be direct targets of olaparib in TNBS-colitis, and barrier protection might be one of the key components of its anti-inflammatory action.

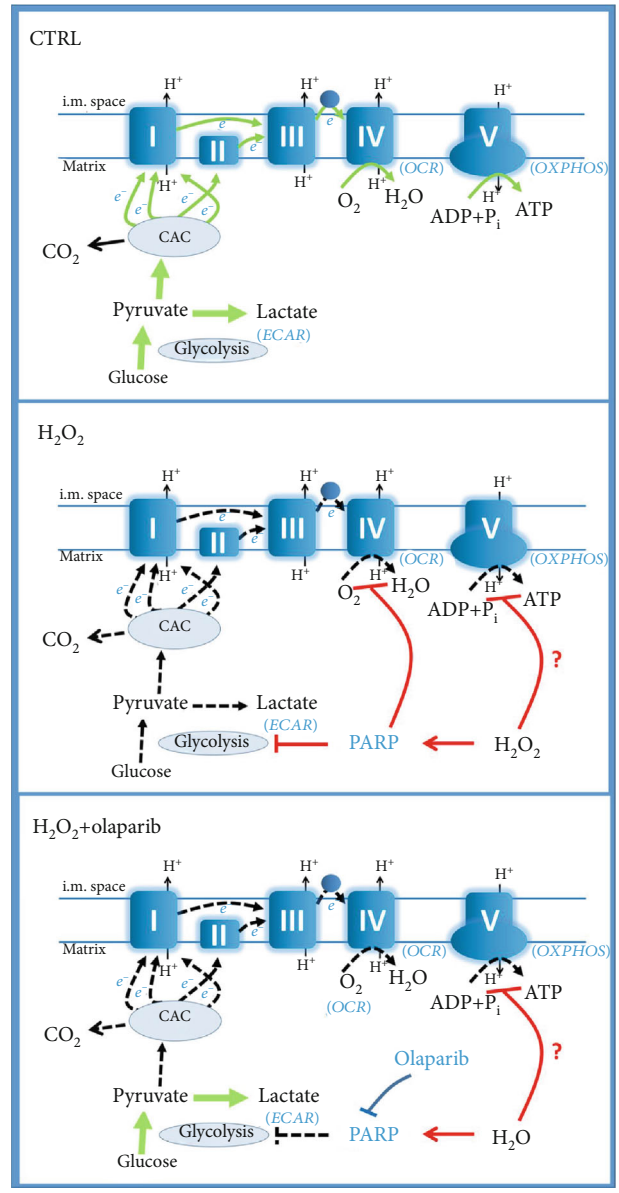

Figure 8: Schematic illustration of the assumed mechanistic effect of olaparib. CAC: citric acid cycle; OCR: oxygen consumption rate; OXPHOS: oxidative phosphorylation; ECAR: extracellular acidification rate; PARP: poly(ADP-ribose) polymerase.

Reduced barrier integrity and increased gut permeability are typical signs of IBD. They have been recently associated with epithelial cell death, mitochondrial dysfunction, and depleted energy metabolism in IECs. IECs produce ATP predominantly by aerobic glycolysis in colitis. However, overactivation of PARP might fully block glycolysis [25]. To study the metabolic effect of olaparib in epithelial cell death, we induced powerful oxidative stress (1 mM H_2O_2, 2 hrs) in Caco-2 monolayer and determined various parameters of the energy metabolism (Figure 8). The H_2O_2 stress dramatically decreased basal ECAR (basal glycolysis) and induced

energetic collapse in Caco-2 cells. Lower proton leak rate in H_2O_2-treated cells compared to control also reflected this metabolic failure, because ATP demand reduces proton motive force and diminish proton leakage [61, 62]. In contrast, olaparib significantly enhanced ECAR in H_2O_2-treated cells. Our results are strongly supported by the finding that poly(ADP-ribose) (PAR) binds to the PAR-binding motif in hexokinase and inhibits it thereby reducing glycolysis [25]. These data indicate that olaparib exerted its effect by inhibiting PAR production, thereby preventing PAR-mediated inhibition of hexokinase and the blockade of aerobic glycolysis (Figure 8).

Oligomycin is a F_OF_1-ATPase inhibitor, which blocks OXPHOS. As expected, oligomycin had no effect on ECAR in the H_2O_2 treatment group; however, it intensely increased ECAR in H_2O_2+olaparib-treated cells. An explanation for this finding might be that oligomycin blocked ATP synthesis and cells could not compensate for the lack of ATP by boosting glycolysis in H_2O_2 treatment group because of the strong PARP-mediated repression of hexokinase. Olaparib, however, prevented PARP activation and glycolytic collapse in H_2O_2+olaparib-treated cells (Figure 8) even in the presence of oligomycin. One may say that oxidative stress per se might affect glycolytic enzymes and not only PARP activation regulates glycolytic activity. By using FCCP (mitochondrial uncoupler), rotenone, and antimycin A (inhibitors of ETC) mitochondrial energy production is totally abrogated. Under these circumstances, glycolysis remains the ultimate source of ATP (Figure 8). The fact that ECAR could reach the level of CTRL cells in the H_2O_2+olaparib group after FCCP, rotenone and antimycin A treatment clearly indicated that glycolytic enzymes were not significantly affected by the oxidative stress in our system, and glycolytic energy production was controlled by PARP activation. Thus, olaparib protected from PARP-induced energetic collapse by improving aerobic glycolysis in oxidative stress (Figure 8).

Previous studies indicated that the mitochondria are the primary source of ROS in IECs during inflammation [63] and PARP-1 activation in oxidative stress causes mitochondrial dysfunction [25]. Accordingly, we wanted to know whether olaparib can prevent mitochondrial failure in our model. We found that basal respiration, mitochondrial ATP production, and nonmitochondrial oxygen consumption were strongly impeded in oxidative stress, and olaparib could not reverse these changes. However, it increased maximal respiration, spare respiratory capacity, and coupling efficiency and reduced proton leak. For understanding these results, we should consider the direct and indirect effects of H_2O_2 on CAC enzymes, ETC complexes, and F_OF_1-ATPase and the effects of PARP activation on glycolysis and ETC complexes.

Previous studies using the DNA-alkylating agent N-methyl-N-nitroso-N-nitroguanidine (MNNG) for PARP activation reported mitochondrial dysfunction [25]. MNNG treatment resulted in decreased basal OCR, maximal OCR, ATP synthesis, and ECAR, while PARP inhibition significantly reversed these changes. Most importantly, they found that administration of pyruvate completely prevented MNNG-induced mitochondrial failure [25]. That is, the mitochondrial dysfunction was a direct consequence of downregulated glycolysis, i.e., it compromised fuel supply for the CAC and ETC. Our results led to the same conclusion, namely, PARP activation reduced glycolysis and caused mitochondrial dysfunction (Figure 8).

In contrast to MNNG-induced PARP activation, we found that inhibition of the enzyme did not prevent the H_2O_2-induced reduction of basal respiration and mitochondrial ATP production. On the other hand, olaparib enhanced ECAR, i.e., it effectively prevented glycolytic collapse (Figure 8). Additionally, it increased maximal respiration, spare respiratory capacity, coupling efficiency, and reduced proton leak, i.e., it increased efficacy of OXPHOS. The discrepancy between our results and the previous ones [25] can be resolved by considering that MNNG alkylates the DNA leading to DNA breaks and PARP activation. H_2O_2, however, induces oxidative DNA damage-mediated PARP activation but can cause direct structural impairment to CAC, ETC, and F_OF_1-ATPase components as collateral damage. It is well established that H_2O_2 deteriorates CAC activity and reduces proton motive force, which is a prerequisite for mitochondrial pyruvate transport [64]. Also, F_OF_1-ATPase was reported to be susceptible to oxidative stress [65, 66]. In addition, ROS and especially H_2O_2 can directly block many components of the respiratory chain, such as NADH dehydrogenase or cytochrome c oxidase [65]. Our findings that maximal OCR of the H_2O_2+olaparib treatment group could not reach the maximum OCR level of control cells are in line with the notion that ETC is sensitive toward oxidative stress (Figure 8). The observed difference between maximal OCRs of the two groups could be the result of oxidative damage to CAC, ETC, and F_OF_1-ATPase components in the H_2O_2+olaparib group. Because the glycolytic fuel supply pathway was unimpeded in both groups, thanks to olaparib's inhibitory effect on PARP in the H_2O_2+olaparib group. Furthermore, the observed increase of maximal OCR in the H_2O_2+olaparib group vs. the H_2O_2 group could result from direct control of the ETC by PARylation. Studies found excessively PARylated mitochondrial proteins, including components of ETC. In addition, PARP-inhibitors such as 3-aminobenzamide and nicotinamide prevented the H_2O_2-induced electron transport blockade on CIV in isolated mitochondria [67]. These results suggest that PARP could regulate ETC activity on CIV, and it also proposed a mitochondrial target for PARP inhibitors. Another study suggested a pivotal role for PARP-1 in mitochondrial energy homeostasis and demonstrated CI as a mitochondrial target of PARP-1 activation [68]. However, it should be noted that the existence of PARP-1 or other PARP isoforms in the mitochondria is debated. But whether present or not in the mitochondria, PARP has a clear effect on mitochondrial function [69].

5. Conclusion

In conclusion, olaparib, a PARP inhibitor used in human oncotherapy, restored bioenergetics by glycolytic reactivation of colonic epithelial cells, and it decreased cell death. Epithelial cell protection might be a cause of improved barrier function that eventually resulted in reduced incidence

and severity of CD-like symptoms in an experimental rodent IBD model. However these findings provide experimental evidence for repurposing olaparib for IBD treatment and highlight its potential in the therapy of CD; clinical application of the drug in IBD needs further investigations.

Data Availability

The data underlying this article are available in the article.

Conflicts of Interest

The authors declare that there is no conflict of interest regarding the publication of this paper.

Acknowledgments

This work was supported by the European Union, cofinanced by the European Social Fund (EFOP-3.6.1-16-2016-00004) and by the Ministry of Finance, Hungary (GINOP-2.3.3-15-2016-00025 and GINOP-2.3.2-15-2016-00049G). This work was also supported by the János Bolyai Research Scholarship of the Hungarian Academy of Sciences (BO/00855/18/5 to BR) and the New National Excellence Program of the Ministry for Innovation and Technology from the source of the National Research, Development and Innovation Fund (UNKP-19-4-PTE-405 and UNKP-20-5-PTE-762 to BR). Work in the lab of RS is funded by the Austrian Science Fund (FWF grant P33325).

References

[1] G. G. Kaplan, "The global burden of IBD: from 2015 to 2025," *Nature Reviews Gastroenterology & Hepatology*, vol. 12, no. 12, pp. 720–727, 2015.

[2] A. Kaser, S. Zeissig, and R. S. Blumberg, "Inflammatory bowel disease," *Annual Review of Immunology*, vol. 28, no. 1, pp. 573–621, 2010.

[3] S. Citi, "Intestinal barriers protect against disease," *Science*, vol. 359, no. 6380, pp. 1097-1098, 2018.

[4] L. C.-H. Yu, "Microbiota dysbiosis and barrier dysfunction in inflammatory bowel disease and colorectal cancers: exploring a common ground hypothesis," *Journal of Biomedical Science*, vol. 25, no. 1, p. 79, 2018.

[5] M. Camilleri, K. Madsen, R. Spiller, B. G. van Meerveld, and G. N. Verne, "Intestinal barrier function in health and gastrointestinal disease," *Neurogastroenterology & Motility*, vol. 24, no. 6, pp. 503–512, 2012.

[6] E. Rath, A. Moschetta, and D. Haller, "Mitochondrial function – gatekeeper of intestinal epithelial cell homeostasis," *Nature Reviews Gastroenterology & Hepatology*, vol. 15, no. 8, pp. 497–516, 2018.

[7] F. Bär, W. Bochmann, A. Widok et al., "Mitochondrial gene polymorphisms that protect mice from colitis," *Gastroenterology*, vol. 145, no. 5, pp. 1055–1063.e3, 2013.

[8] J. D. Söderholm, G. Olaison, K. H. Peterson et al., "Augmented increase in tight junction permeability by luminal stimuli in the non-inflamed ileum of Crohn's disease," *Gut*, vol. 50, no. 3, pp. 307–313, 2002.

[9] S. Santhanam, S. Rajamanickam, A. Motamarry et al., "Mitochondrial electron transport chain complex dysfunction in the colonic mucosa in ulcerative colitis," *Inflammatory Bowel Diseases*, vol. 18, no. 11, pp. 2158–2168, 2012.

[10] S. Heller, H. M. Penrose, C. Cable et al., "Reduced mitochondrial activity in colonocytes facilitates AMPKα2-dependent inflammation," *The FASEB Journal*, vol. 3, pp. 2013–2025, 2017.

[11] J. Cai, H. Chen, M. Weng, S. Jiang, and J. Gao, "Diagnostic and clinical significance of serum levels of D-lactate and diamine oxidase in patients with Crohn's disease," *Gastroenterology Research and Practice*, vol. 2019, Article ID 8536952, 7 pages, 2019.

[12] W. E. Roediger, "Role of anaerobic bacteria in the metabolic welfare of the colonic mucosa in man," *Gut*, vol. 21, no. 9, pp. 793–798, 1980.

[13] L. E. Glover, J. S. Lee, and S. P. Colgan, "Oxygen metabolism and barrier regulation in the intestinal mucosa," *The Journal of Clinical Investigation*, vol. 2126, pp. 3680–3688, 2016.

[14] N. D. Mathewson, R. Jenq, A. V. Mathew et al., "Gut microbiome-derived metabolites modulate intestinal epithelial cell damage and mitigate graft-versus-host disease," *Nature Immunology*, vol. 17, no. 5, pp. 505–513, 2016.

[15] H. M. Hamer, D. Jonkers, K. Venema, S. Vanhoutvin, F. J. Troost, and R. J. Brummer, "Review article: the role of butyrate on colonic function," *Alimentary Pharmacology & Therapeutics*, vol. 27, no. 2, pp. 104–119, 2008.

[16] E. Fernandez-Vizarra and M. Zeviani, "Mitochondrial disorders of the OXPHOS system," *FEBS Letters*, vol. 8, pp. 1062–1106, 2021.

[17] C. C. Gillis, E. R. Hughes, L. Spiga et al., "Dysbiosis-associated change in host metabolism generates lactate to support _Salmonella_ growth," *Cell Host & Microbe*, vol. 23, no. 1, pp. 54–64.e6, 2018.

[18] B. Kelly and L. A. J. O'Neill, "Metabolic reprogramming in macrophages and dendritic cells in innate immunity," *Cell Research*, vol. 25, no. 7, pp. 771–784, 2015.

[19] K. Hadrava Vanova, M. Kraus, J. Neuzil, and J. Rohlena, "Mitochondrial complex II and reactive oxygen species in disease and therapy," *Redox Report*, vol. 25, no. 1, pp. 26–32, 2020.

[20] K. A. Brand and U. Hermfisse, "Aerobic glycolysis by proliferating cells: a protective strategy against reactive oxygen species," *The FASEB Journal*, vol. 11, no. 5, pp. 388–395, 1997.

[21] H. R. Molavian, M. Kohandel, and S. Sivaloganathan, "High concentrations of H_2O_2 make aerobic glycolysis energetically more favorable for cellular respiration," *Frontiers in Physiology*, vol. 7, p. 362, 2016.

[22] S. Berg, P. L. Sappingto, L. J. Guzik, R. L. Delude, and M. P. Fink, "Proinflammatory cytokines increase the rate of glycolysis and adenosine-5'-triphosphate turnover in cultured rat enterocytes," *Critical Care Medicine*, vol. 3, pp. 1203–1212, 2003.

[23] D. Carson, R. Barry, E. G. D. Hopkins et al., "Citrobacter rodentium induces rapid and unique metabolic and inflammatory responses in mice suffering from severe disease," *Cellular Microbiology*, vol. 22, no. 1, article e13126, 2020.

[24] N. Vermeulen, S. Vermeire, I. Arijs et al., "Seroreactivity against glycolytic enzymes in inflammatory bowel disease," *Inflammatory Bowel Diseases*, vol. 17, no. 2, pp. 557–564, 2011.

[25] S. A. Andrabi, G. K. E. Umanah, C. Chang et al., "Poly(ADP-ribose) polymerase-dependent energy depletion occurs through inhibition of glycolysis," *Proceedings of the National Academy of Sciences of the United States of America*, vol. 111, no. 28, pp. 10209–10214, 2014.

[26] B. Zingarelli, P. W. Hake, T. J. Burroughs, G. Piraino, M. O'Connor, and A. Denenberg, "Activator protein-1

signalling pathway and apoptosis are modulated by poly(ADP-ribose) polymerase-1 in experimental colitis," *Immunology*, vol. 113, no. 4, pp. 509–517, 2004.

[27] S. Peng, L. Shen, M.-X. Tian, H.-M. Li, and S.-S. Wang, "Poly(-ADP-ribose) polymerase-1 inhibitor ameliorates dextran sulfate sodium-induced colitis in mice by regulating the balance of Th17/Treg cells and inhibiting the NF-κB signaling pathway," *Experimental and Therapeutic Medicine*, vol. 21, p. 134, 2020.

[28] S. Sánchez-Fidalgo, I. Villegas, A. Martín, M. Sánchez-Hidalgo, and C. Alarcón de la Lastra, "PARP inhibition reduces acute colonic inflammation in rats," *European Journal of Pharmacology*, vol. 563, no. 1-3, pp. 216–223, 2007.

[29] D. S. Kim, S. Challa, A. Jones, and W. L. Kraus, "PARPs and ADP-ribosylation in RNA biology: from RNA expression and processing to protein translation and proteostasis," *Genes & Development*, vol. 34, no. 5-6, pp. 302–320, 2020.

[30] T. Jubin, A. Kadam, M. Jariwala et al., "The PARP family: insights into functional aspects of poly (ADP-ribose) polymerase-1 in cell growth and survival," *Cell Proliferation*, vol. 49, no. 4, pp. 421–437, 2016.

[31] S. Pazzaglia and C. Pioli, "Multifaceted role of PARP-1 in DNA repair and inflammation: pathological and therapeutic implications in cancer and non-cancer diseases," *Cell*, vol. 9, p. 41, 2019.

[32] Z. Chen, J. Dudek, C. Maack, and U. Hofmann, "Pharmacological inhibition of GLUT1 as a new immunotherapeutic approach after myocardial infarction," *Biochem Pharmacol*, vol. 190, article 114597, 2021.

[33] N. A. Berger, V. C. Besson, A. H. Boulares et al., "Opportunities for the repurposing of PARP inhibitors for the therapy of non-oncological diseases," *British Journal of Pharmacology*, vol. 175, no. 2, pp. 192–222, 2018.

[34] R. Schicho, M. Bashashati, M. Bawa et al., "The atypical cannabinoid O-1602 protects against experimental colitis and inhibits neutrophil recruitment," *Inflammatory Bowel Diseases*, vol. 17, no. 8, pp. 1651–1664, 2011.

[35] E. Antoniou, G. A. Margonis, A. Angelou et al., "The TNBS-induced colitis animal model: an overview," *Annals of Medicine and Surgery*, vol. 11, pp. 9–15, 2016.

[36] J.-R. Feng, X. Qiu, F. Wang et al., "Diagnostic value of neutrophil-to-lymphocyte ratio and platelet-to-lymphocyte ratio in Crohn's disease," *Gastroenterology Research and Practice*, vol. 2017, Article ID 3526460, 5 pages, 2017.

[37] L. Oplustil O'Connor, S. L. Rulten, A. N. Cranston et al., "The PARP inhibitor AZD2461 provides insights into the role of PARP3 inhibition for both synthetic lethality and tolerability with chemotherapy in preclinical models," *Cancer Research*, vol. 76, no. 20, pp. 6084–6094, 2016.

[38] T. Lea, "Caco-2 Cell Line," in *The Impact of Food Bioactives on Health: In Vitro and Ex Vivo Models*, K. Verhoeckx, P. Cotter, I. López-Expósito, C. Kleiveland, T. Lea, A. Mackie, T. Requena, D. Swiatecka, and H. Wichers, Eds., Springer International Publishing, Cham, Switzerland, 2015.

[39] N. C. Hoch and L. M. Polo, "ADP-ribosylation: from molecular mechanisms to human disease," *Genet Mol Biol*, vol. 43, no. 1, article e20190075, 2020Supplement 1, 2020.

[40] A. D'Odorico, S. Bortolan, and R. Cardin, "Reduced plasma antioxidant concentrations and increased oxidative DNA damage in inflammatory bowel disease," *Scandinavian Journal of Gastroenterology*, vol. 36, no. 12, pp. 1289–1294, 2001.

[41] L. Lih-Brody, S. R. Powell, K. P. Collier et al., "Increased oxidative stress and decreased antioxidant defenses in mucosa of inflammatory bowel disease," *Digestive Diseases and Sciences*, vol. 41, no. 10, pp. 2078–2086, 1996.

[42] D. R. Donohoe, N. Garge, X. Zhang et al., "The microbiome and butyrate regulate energy metabolism and autophagy in the mammalian colon," *Cell Metabolism*, vol. 13, no. 5, pp. 517–526, 2011.

[43] I. Crespo, B. San-Miguel, C. Prause et al., "Glutamine treatment attenuates endoplasmic reticulum stress and apoptosis in TNBS-induced colitis," *PLoS One*, vol. 7, no. 11, article e50407, 2012.

[44] R. R. Gerner, V. Klepsch, S. Macheiner et al., "NAD metabolism fuels human and mouse intestinal inflammation," *Gut*, vol. 67, no. 10, pp. 1813–1823, 2018.

[45] H. M. El-Emshaty, A. A. Abdelfatah, H. Ismail, F. M. El-Taweel, and M. M. El-Hemaly, "Potential association of poly(-ADP-ribose) polymerase-1 (PARP-1) with CD133 and G2/M as independent predictors in colorectal cancer development," *Biochemistry Letters*, vol. 14, no. 1, pp. 156–166, 2019.

[46] L. Peng, Z. He, W. Chen, I. R. Holzman, and J. Lin, "Effects of butyrate on intestinal barrier function in a Caco-2 cell monolayer model of intestinal barrier," *Pediatric Research*, vol. 61, no. 1, pp. 37–41, 2007.

[47] H. B. Jijon, T. Churchill, D. Malfair et al., "Inhibition of poly(-ADP-ribose) polymerase attenuates inflammation in a model of chronic colitis," *American Journal of Physiology. Gastrointestinal and Liver Physiology*, vol. 279, no. 3, pp. G641–G651, 2000.

[48] J. T. Bjerrum, C. Steenholdt, M. Ainsworth et al., "Metabonomics uncovers a reversible proatherogenic lipid profile during infliximab therapy of inflammatory bowel disease," *BMC Medicine*, vol. 15, no. 1, p. 184, 2017.

[49] W. Strober and I. J. Fuss, "Proinflammatory cytokines in the pathogenesis of inflammatory bowel diseases," *Gastroenterology*, vol. 140, no. 6, pp. 1756–1767.e1, 2011.

[50] B. Zingarelli, M. O'Connor, and P. W. Hake, "Inhibitors of poly (ADP-ribose) polymerase modulate signal transduction pathways in colitis," *European Journal of Pharmacology*, vol. 469, no. 1-3, pp. 183–194, 2003.

[51] B. Zingarelli, C. Szabó, and A. L. Salzman, "Blockade of poly(-ADP-ribose) synthetase inhibits neutrophil recruitment, oxidant generation, and mucosal injury in murine colitis," *Gastroenterology*, vol. 116, no. 2, pp. 335–345, 1999.

[52] R. di Paola, E. Mazzon, W. Xu et al., "Treatment with PARP-1 inhibitors, GPI 15427 or GPI 16539, ameliorates intestinal damage in rat models of colitis and shock," *European Journal of Pharmacology*, vol. 527, no. 1-3, pp. 163–171, 2005.

[53] M. Celikbilek, S. Dogan, O. Ozbakır et al., "Neutrophil-lymphocyte ratio as a predictor of disease severity in ulcerative colitis," *Journal of Clinical Laboratory Analysis*, vol. 27, no. 1, pp. 72–76, 2013.

[54] W.-M. Kang, C.-Z. Zhu, X.-X. Yang et al., "Application of the Onodera prognostic nutrition index and neutrophil-to- lymphocyte ratio in risk evaluation of postoperative complications in Crohn's disease," *Scientific Reports*, vol. 7, no. 1, p. 8481, 2017.

[55] S.-Q. Gao, L.-D. Huang, R.-J. Dai, D. D. Chen, W. J. Hu, and Y. F. Shan, "Neutrophil-lymphocyte ratio: a controversial marker in predicting Crohn's disease severity," *International Journal of Clinical and Experimental Pathology*, vol. 8, no. 11, pp. 14779–14785, 2015.

[56] M. K. Wlodarczyk, A. E. Sobolewska, K. Stec-Michalska, J. J. Fichna, and M. E. Wisniewska-Jarosinska, "Neutrophil-lymphocyte ratio in Crohn's disease patients predicts sustained response to infliximab 52-week therapy," *Journal of Gastrointestinal and Liver Diseases*, vol. 24, pp. 127-128, 2015.

[57] F. Eraldemir, M. Musul, A. Duman, B. Oztas, C. Baydemir, and S. Hulagu, "The relationship between neutrophil/lymphocyte and platelet/lymphocyte ratios with oxidative stress in active Crohn's disease patients," *Hippokratia*, vol. 20, no. 4, pp. 368–373, 2016.

[58] A. A. Pieper, A. Verma, J. Zhang, and S. H. Snyder, "Poly (ADP-ribose) polymerase, nitric oxide and cell death," *Trends in Pharmacological Sciences*, vol. 20, no. 4, pp. 171–181, 1999.

[59] B. Beltrán, P. Nos, F. Dasí et al., "Mitochondrial dysfunction, persistent oxidative damage, and catalase inhibition in immune cells of naïve and treated Crohn's disease," *Inflammatory Bowel Diseases*, vol. 16, no. 1, pp. 76–86, 2010.

[60] P. Rosignoli, R. Fabiani, A. de Bartolomeo et al., "Protective activity of butyrate on hydrogen peroxide-induced DNA damage in isolated human colonocytes and HT29 tumour cells," *Carcinogenesis*, vol. 22, no. 10, pp. 1675–1680, 2001.

[61] M. D. Brand, L.-F. Chien, E. K. Ainscow, D. F. S. Rolfe, and R. K. Porter, "The causes and functions of mitochondrial proton leak," *Biochimica et Biophysica Acta (BBA) - Bioenergetics*, vol. 1187, no. 2, pp. 132–139, 1994.

[62] M. Wikström and R. Springett, "Thermodynamic efficiency, reversibility, and degree of coupling in energy conservation by the mitochondrial respiratory chain," *Communications Biology*, vol. 3, no. 1, p. 451, 2020.

[63] M. G. Basilicata, G. Pepe, S. F. Rapa et al., "Anti-inflammatory and antioxidant properties of dehydrated potato-derived bioactive compounds in intestinal cells," *Int J Mol Sci*, vol. 20, no. 23, p. 6087, 2019.

[64] L. Tretter and V. Adam-Vizi, "Inhibition of Krebs cycle enzymes by hydrogen peroxide: a key role of α-ketoglutarate dehydrogenase in limiting NADH production under oxidative stress," *The Journal of Neuroscience*, vol. 20, no. 24, pp. 8972–8979, 2000.

[65] Y. Zhang, O. Marcillat, C. Giulivi, L. Ernster, and K. J. A. Davies, "The oxidative inactivation of mitochondrial electron transport chain components and ATPase.," *The Journal of Biological Chemistry*, vol. 265, no. 27, pp. 16330–16336, 1990.

[66] G. Lippe, M. Comelli, D. Mazzilis, F. D. Sala, and I. Mavelli, "The inactivation of mitochondrial F_1 ATPase by H_2O_2 is mediated by iron ions not tightly bound in the protein," *Biochemical and Biophysical Research Communications*, vol. 181, no. 2, pp. 764–770, 1991.

[67] R. Halmosi, Z. Berente, E. Osz, K. Toth, P. Literati-Nagy, and B. Sumegi, "Effect of poly(ADP-ribose) polymerase inhibitors on the ischemia-reperfusion-induced oxidative cell damage and mitochondrial metabolism in Langendorff heart perfusion system," *Molecular Pharmacology*, vol. 59, no. 6, pp. 1497–1505, 2001.

[68] A. Kadam, T. Jubin, R. Roychowdhury et al., "Insights into the functional aspects of poly(ADP-ribose) polymerase-1 (PARP-1) in mitochondrial homeostasis in Dictyostelium discoideum," *Biology of the Cell*, vol. 112, no. 8, pp. 222–237, 2020.

[69] A. Tapodi, Z. Bognar, C. Szabo, F. Gallyas, B. Sumegi, and E. Hocsak, "PARP inhibition induces Akt-mediated cytoprotective effects through the formation of a mitochondria-targeted phospho-ATM-NEMO-Akt-mTOR signalosome," *Biochemical Pharmacology*, vol. 162, pp. 98–108, 2018.

Hindawi
Oxidative Medicine and Cellular Longevity
Volume 2021, Article ID 9981480, 24 pages
https://doi.org/10.1155/2021/9981480

Research Article

Melatonin Ameliorates Corticosterone-Mediated Oxidative Stress-Induced Colitis in Sleep-Deprived Mice Involving Gut Microbiota

Ting Gao, Zixu Wang, Jing Cao, Yulan Dong, and Yaoxing Chen

College of Veterinary Medicine, China Agricultural University, Haidian, Beijing 100193, China

Correspondence should be addressed to Yaoxing Chen; yxchen@cau.edu.cn

Received 12 March 2021; Accepted 20 May 2021; Published 23 June 2021

Academic Editor: Mariaurea Matias Sarandy

Background. Inflammatory bowel disease (IBD) is a result of a complex interplay, making development of a specific treatment a challenging task. Corticosterone was considered a risk factor of stress relative enteritis. Our previous studies found that melatonin exerts an improvement effect in sleep deprivation (SD)- induced corticosterone overproduction and colitis. A present study further explored the mechanism whereby melatonin prevented corticosterone-mediated SD-induced colitis. *Methods*. A 72-hour SD mouse model with or without melatonin supplementation and fecal microbiota transplantation (FMT) to investigate the core role of corticosterone in melatonin-mediated gut microbiota improving SD-induced colitis. Further, corticosterone-treated mice were assessed to the effect of melatonin on corticosterone-mediated gut microbiota dysbiosis-induced colitis. Meanwhile, an in vitro test studied modulatory mechanism of metabolite melatonin. *Results*. SD caused an excessive corticosterone, gut microbiota disorder and colitis phenotype. Similarly, corticosterone-supplemented mice also exhibited gut microbiota dysbiosis and colitis, and the FMT from SD-mice to normal mice could restore the SD-like colitis, but no change in the corticosterone level, which suggested that corticosterone-mediated intestinal microbiota imbalance plays a central role in SD-induced colitis. Further, we demonstrated melatonin-mediated MT2 weakened GR feedback, suppressed oxidative stress, restored the intestinal microbiota and its metabolites homeostasis, and inactivated the STAT3/AP-1/NF-κB pathway-induced inflammatory response in vivo and in vitro. *Conclusions*. We revealed that excessive corticosterone is a core risk factor for SD-induced colitis and provided a better understanding of the effects of melatonin, expected to be a personalized targeted therapy drug, on corticosterone-mediated gut microbiota inducing colitis.

1. Introduction

Modern lifestyle, which includes long working hours and commuting times, psychological stress, personal choices, and social and family demands, has led to an increase in short sleep durations [1]. Acute periods of sleep deprivation (SD) can result in intestinal barrier dysfunction, including intestinal mucosal damage, and intestinal microbiota disturbance in rodents [2], which can be a risk factor for frequent inflammatory bowel disease (IBD) [3, 4]. IBD pathogenesis has been linked to the presence of symbiotic microorganisms living in the intestinal tract [5, 6]. Research has also suggested that IBD-associated genetic defects can lead to pathobiont accumulation and penetration into the intestinal tissue, which further promotes dysbiosis and inflammation [6]. Sleep plays an integral role in intestinal health and also has been shown to significantly impact intestinal microbiome and metabolism [2, 7]. However, whether SD-mediated intestinal microbiota disorders induced intestinal mucosal damage and eventually lead to the occurrence of IBD has yet to be investigated.

Previous researches demonstrated that SD, which may be a stressor, could activate the hypothalamic-pituitary-adrenal (HPA) axis in rats [8], which triggered the synthesis and production of corticosterone (CORT) in a dynamic manner [9]. Recent studies have shown that CORT may cause an imbalance in the gut microbes [10, 11], including the downregulation of intestinal microbiota richness and relative abundance of Bacteroidetes and an increase in Firmicutes and Proteobacterium. Considering that the gut microbiota constitutes the intestinal barrier, promotes the continuous existence of the gut microbiota, stimulates intestinal epithelial cell

regeneration, produces mucus, and nourishes mucosa [12], we assessed the impact of SD-induced IBD related to the increase of CORT production-mediated intestinal microbiota dysbiosis.

Melatonin (MT) is a circulating hormone primarily produced from tryptophan by the pineal gland. This hormone has received widespread interest because it acts as a homeostatic regulator of the HPA axis [13], which is associated with diminished overall CORT secretion and increased sensitivity to CORT feedback. Moreover, as a molecule with many functions that serves as the primary signal mediating microbial metabolism, circadian rhythms, and intestinal mucosal immune cells, MT has potential for use in treating intestinal diseases [14]. However, whether MT shapes intestinal biological functions through the CORT-mediated intestinal microbiota has yet to be investigated.

Therefore, in the current study, we (1) use mouse faeces microbiota transplant (FMT) experiment to investigate SD-mediated intestinal microbiota disorder-induced colitis and to investigate whether MT administration could improve SD-induced colitis via restoring gut microbiota homeostasis; (2) further verify the core role of excessive CORT-mediated intestinal microbiota imbalance in SD-induced colitis and verify whether MT administration could suppress this process; and (3) explore the signaling pathway in MT improving CORT-mediated intestinal microbiota disorder and intestinal mucosal injury using in vivo and in vitro.

2. Materials and Methods

All experiments were conducted according to the Guide for the Care and Use of Laboratory Animals published by the Animal Welfare Committee of the Agricultural Research Organization, China Agricultural University (Approval No. CAU20170911-2).

2.1. Animals and Treatments. A total of SPF 132 male ICR mice (8 weeks old; Vital River Laboratory Animal Technology Co. Ltd., Beijing, China) were housed in 22 cages (6 mice/cage) under conventional conditions. After acclimatisation for one week, the mice were randomly divided into eleven groups: sleep deprivation (SD), SD+MT supplementation (SD+MT), only MT supplementation (MT), non-sleep-deprived control (CON) groups, fecal microbiota transplantation (FMT) from mice of the CON group (F-CON), FMT from mice of the SD group (F-SD), FMT from mice of SD+MT group (F-SM), FMT from mice of vehicle (F-R), only corticosterone supplementation (CORT), CORT+MT supplementation (CORT+MT), and non-CORT-treated vehicle group (CON). Specific operation is provided in the Supplementary Material.

2.2. Faecal Material Preparation and FMT Regime. Faecal material was collected from mice of the CON, SD and SD +MT groups in SD experiment and placed into Eppendorf tubes containing freezing solution (sterile saline solution with 12.5% glycerol) and homogenized [15]. For more details, see the Supplementary Material.

2.3. Cell Culture and Treatment. Mouse primary colonic intestinal epithelial cells (IECs, BALB-5047, USA) were cultured in 96-well plates (5×10^6 cells/mL) and 12-well plates (5×10^5 cells/mL). Some CORT-treated IECs (10 μM, Solarbio Ltd., Beijing, China; CORT-cells) were treated with 100 μM NAC (a free radical scavenger; MCE, New Jersey, USA; CORT+NAC-cells), 2 μM MT (Sigma-Aldrich, St. Louis, USA; CORT+MT-cells) or 20 μM RU-486 (a selective GR antagonist; MCE, New Jersey, USA; CORT+RU-486-cells). After MT supplementation for 30 min, some CORT+MT-cells were sequentially treated with 10 mM 4P-PDOT (a nonselective MT2 antagonist; MCE, New Jersey, USA; CORT+MT+4P-PDOT-cells). Each plate of treated cells was incubated for 24 h.

The cells from the 96-well plates were assessed for proliferation activity using 3-(4,5-dimethylthiazol-2-yl)-2,5-diphenyltetrazolium bromide (MTT, Sigma-Aldrich, St. Louis, MO, USA) (optical density was determined using a microplate reader (Model 680, Bio-Rad, St. Louis, MO, USA) equipped with a 570 nm wavelength filter) and reactive oxygen species (ROS) (Nanjingjianchen, Beijing, China) assays. A ROS assay kit was purchased from Sigma-Aldrich and used according to the manufacturer's instructions ($n = 9$). The intracellular ROS generation was measured using a flow cytometer with an oxidation-sensitive DCFH-DA fluorescent probe. The suspension was loaded using DCFH-DA solution at a final concentration of 50 M and was incubated for 30 min at 37°C. Then, the samples were centrifuged at 1,000 rpm for 5 min (4°C), and the cells were resuspended in phosphate-buffered saline (PBS, pH 7.2-7.4). For each treatment, 19105 cells were counted, and the experiment was performed in triplicate. Fluorescence was detected using a fluorescence microplate reader (excitation 488 nm and emission 525 nm) [16]. The cells from the 12-well plates were collected for western blotting. Each assay used a repeat of 8 wells.

2.4. Enzyme-Linked Immunosorbent Assay (ELISA). Plasma samples were collected for the detection of CORT; colon samples were collected for the detection of inflammatory factor (TNF-α, IL-10 and IL-17) concentrations using a competitive ELISA assay (USCN Life Science, Inc., Wuhan, China). All tests were performed according to the manufacturer's instructions. Eight samples were used in each group. Each sample was tested in triplicate. The data are expressed as ng/mL for plasma CORT levels and pg/mg protein for TNF-α, IL-10, and IL-17 levels in the colon tissue.

2.5. Intestinal Permeability to Fluorescein Isothiocyanate (FITC)- Dextran. Before the experiment ended at 6:00 am, all mice were deprived of food for 2 h and orally gavaged with 0.6 mg/g body weight of 4 kDa FITC-dextran at a concentration of 80 mg/mL 1 h before euthanasia. The FITC fluorescence in the serum was measured using a fluorescence spectrophotometer with wavelengths of 485 nm (excitation) and 535 nm (emission) [17]. A standard curve was created by diluting FITC-dextran in PBS. The concentration of FITC-dextran in the serum was calculated using the standard curve.

2.6. Immunohistochemical Staining. We used immunohistochemistry to stain for MUC2, ZO-1, and Claudin-1 in

paraffin intestinal sections. Sections were incubated overnight at 4°C with the monoclonal rabbit anti-mouse primary antibody (MUC2, 1 : 500; ZO-1, 1 : 200; Claudin-1, 1 : 200; Abcam, Cambridge, MA, USA). Specific operation is provided in the Supplementary Material.

2.7. Western Blotting. Portions of the colonic segments and IEC samples ($n = 9$) were rapidly homogenized in liquid nitrogen and stored at -80°C for western blotting analysis. For more details, see the Supplementary Material.

2.8. Colonic RNA and Fecal DNA Isolation and Quantitative RT-PCR Analysis. Colonic RNA was isolated using the RNeasy Mini Kit (Qiagen, Germantown, MD, USA) following the manufacturer's instructions. The quantity and integrity of the RNA were assessed spectrophotometrically with a Nanodrop apparatus (Thermo Fisher Scientific). Fecal DNA was isolated using the microflora DNA extraction kit (MoBio, 12988-10, USA) following the manufacturer's instructions. Specific DNA sequences were amplified with a Bio-Rad CFX Connect real-time PCR device (Hercules, CA, USA). The primers used are shown in Table 1.

2.9. Microbial Sequencing. The 16S rRNA gene was amplified using PCR and composite specific bacterial primers as described previously [2]. For more details, see the Supplementary Material.

2.10. Metabolomics Profiling. We performed LC-MS analyses on a quadrupole-time-of-flight (Q-TOF) 6510 mass spectrometer (Agilent Technologies, Santa Clara, CA, USA) with an electrospray ionization source [18]. For more details, see the Supplementary Material.

2.11. Statistical Analysis of Data. Data are expressed as the mean ± standard error and were analyzed using SPSS 10.0 statistical software (SPSS, Inc., Chicago, IL, USA). Differences between groups were statistically analyzed using ANOVA followed by two-way ANOVA, which was used to determine the significance of differences among groups ($p < 0.05$ and $p < 0.01$).

3. Results

3.1. Effect of MT Supplementation on SD Enhances CORT Secretion and Intestinal Microbiota Disorder in the Colon. To clarify whether MT improved SD-induced CORT overproduction and intestinal dysbiosis, we established an acute continuous 72 h SD mouse model. The results showed a significant increase in the ROS content (47.6%, $p = 0.004$; Figure S1A), expression level of GR protein (52.6%, $p = 0.001$; Figure S1B), and HSP90 mRNA (50.9%, $p \leq 0.001$; Figure S1C), as well as a decrease in the HSP70 (38.1%, $p = 0.004$; Figure S1D) and P23 mRNA (25.6%, $p = 0.014$; Figure S1E) in the SD group compared with that in the CON group. However, MT pretreatment effectively reversed these SD-induced changes. Next, analysis of intestinal microbiota composition was performed (Figure S1F-I), and results showed an upregulation of relative abundance in Firmicutes (51.9%, $p \leq 0.001$, Figure S1G) and Proteobacterium (67.3%, $p = 0.009$, Figure S1H) and a downregulation of Bacteroidetes (15.7%, $p = 0.042$, Figure S1F) and Prevotellaceae (30.1%, $p = 0.016$, Figure S1I) in the SD group compared with that in the control group. By contrast, MT pretreatment attenuated these effects of SD on the intestinal microbiota disorder. Consequently, MT pretreatment attenuated the excessive CORT and intestinal microbiota imbalance in SD mice.

3.2. FMT Promotes Reestablishment of the Colitis Phenotype and Microbiota Disorder in Mice. We explore whether FMT from the SD mice induced a colitis phenotype in receiving mice. The present results demonstrated that there was a remarkable reduction in the expression level of MUC2, TJ (ZO-1 and Claudin-1) and Card9 proteins by 43.2% ($p = 0.001$, Figures S2A and D), 63.9% ($p \leq 0.001$, Figures S2B and E), 35.6% ($p = 0.021$, Figures S2C and F), and 29.8% ($p = 0.034$, Figure S2I), as well as a significant increase in the DAI score, intestinal permeability, and colonic IL-17 level by 36.1% ($p = 0.003$, Figure S2G), 42.6% ($p \leq 0.001$, Figure S2H), and 78.3% ($p \leq 0.001$, Figure S2J) in the F-SD group compared with that in the F-CON group. However, the stimulatory effects of F-SD on changes in colitis were reversed in the colon by F-SM supplementation.

Further, we examined whether F-SD caused an intestinal microbiota disorder. The relative abundance of Firmicutes and Proteobacterium was significantly elevated by 36.3% ($p = 0.010$, Figure S2L) and 57.7% ($p \leq 0.001$, Figure S2N) in the F-SD group, respectively, versus the F-CON group. By contrast, Bacteroidetes and Prevotellaceae contents were significantly reduced by 32.5% ($p = 0.032$, Figure S2K) and 46.3% ($p = 0.010$, Figure S2M) in the colon of the F-SD group versus that of the control group. However, in the F-SM and F-R groups, all index was restored to the level of the F-CON group, resulting in no statistically significant differences among the F-SM, F-R and F-CON groups ($p > 0.783$).

In conclusion, SD-mediated intestinal microbiota imbalance induced colitis, while MT supplementation improved colitis via restoring intestinal microbiota dysbiosis.

3.3. Effect of MT Supplementation on CORT Treatment Impairs the Intestinal Mucosa Barrier, Mitochondrial Function, and Antioxidant Capacity of the Colon. Further, we observed the plasma CORT level significantly increased by 74.3% ($p = 0.002$, Figure 1(a)) in the CORT group compared with the CON group. Consistent with the increase in CORT, there was an increase in clinical score (202.9%, $p = 0.003$, Figures 1(a) and 1(e)), DAI score (69.9%, $p \leq 0.001$, Figure 1(f)), intestinal permeability (67.8%, $p = 0.003$, Figure 1(g)), and a reduction in the colonic length (21.2%, $p = 0.023$, Figures 1(b) and 1(c)) and the levels of the MUC2 (27.8%, $p = 0.010$, Figure 1(h)), ZO-1 (39.4%, $p = 0.007$, Figure 1(i)), and Claudin-1 (47.7%, $p = 0.030$, Figure 1(j)) proteins in CORT-treated mice. Additionally, CORT caused increases in the expression levels of the Cytochrome C (160.3%, $p = 0.029$, Figure 1(k)) and Caspase-9 (51.9%, $p \leq 0.001$, Figure 1(l)) proteins and reductions in the Mfn2, VDAC1, and Calpain-1 proteins by 30.1%

Table 1: Primers of target genes and reference gene.

Gene	Sense	Antisense
HSP90	ACGAGGAAGAGAAGAAGAAAATGG	GCAGGGTGAAGACACAAGCC
HSP70	CGGTGCCCGCCTACTTC	TCCTTCTTGTGCTTCCTCTTGA
P23	ATGCGTTTGGAGAAGGACAGA	CAGGGATGAAGTGATGGTGAGA
GAPDH	CCGAGAATGGGAAGCTTGTC	TTCTCGTGGTTCACACCCATC
Firmicutes	GGAGCATGTGGTTTAATTCGAAGCA	AGCTGACGACAACCATGCAC
Bacteroidetes	GAGAGGAAGGTCCCCCAC	CGCTACTTGGCTGGTTCAG
Proteobacteria	GGTTCTGAGAGGAGGTCCC	GCTGGCTCCCGTAGGAGT
Prevotellaceae	CACCAAGGCGACGATCA	GGATAACGCCCGGACCT
Escherichia coli	GGAGCAAACAGGATTAGATACCC	AACCCAACATTTCACAACACG

($p = 0.006$, Figure 1(m)), 15.7% ($p = 0.002$, Figure 1(n)) and (213%, $p = 0.029$, Figure 1(o)), respectively, compared with the CON group. Meanwhile, there was a decrease in the CAT (46.7%, $p \leq 0.001$, Figure 1(p)), GSH-Px (15.7%, $p = 0.003$, Figure 1(q)), SOD (33.9%, $p \leq 0.001$, Figure 1(r)) and T-AOC levels (44.5%, $p = 0.001$, Figure 1(s)) and an increase in the MDA level (29.7%, $p = 0.010$, Figure 1(t)) in CORT mice relative to the CON group. In contrast, MT supplementation attenuated the effects of CORT on the colonic dysfunction. The plasma CORT level, clinical score, DAI score, intestinal permeability, and expression levels of Cytochrome C, Caspase-9, and Calpain-1 proteins and MDA were decreased by 23.1-63.6% ($p = 0.004$-0.042), while the length of colon, expression levels of the TJ (ZO-1 and Claudin-1), Mfn2, VDAC1, MUC2 proteins and antioxidant enzymes were increased by 37.2-195.8% ($p = 0.001$-0.012) in the CORT+MT group compared to the CORT group. Collectively, our data indicated that MT supplementation rescued the damage to the intestinal mucosa barrier, mitochondrial function, and the antioxidant capacity caused by CORT treatment.

3.4. Effect of MT Supplementation on CORT Treatment Enhances GR Synthesis and Transport and Triggers an Inflammation Response in the Colon. We then examined whether CORT enhanced GR synthesis and transport and induced an inflammatory response in the colon (Figure 2). The western blotting results showed that expression of the GR protein and HSP90 mRNA was dramatically increased by 32.2% ($p = 0.020$, Figure 2(a)) and 87.8% ($p \leq 0.001$, Figure 2(b)), while the HSP70 and P23 mRNA levels were decreased by 34.1% ($p = 0.003$, Figure 2(c)) and 38.4% ($p \leq 0.001$, Figure 2(d)) in the CORT group relative to the CON group. However, MT supplementation obviously restored there changes, resulting in no statistically significant differences between the CON group and the MT-pretreated CORT group ($p > 0.089$).

Next, we assessed whether CORT treatment resulted in an inflammatory response. The results indicated that CORT caused an increase in the levels of colonic inflammatory molecules, such as iNOS, COX-2, and TNF-α, of 45.0% ($p = 0.008$, Figure 2(e)), 52.3% ($p = 0.009$, Figure 2(f)), and 123.2% ($p \leq 0.001$, Figure 2(g)) and a reduction in IL-10 of 60.4% ($p = 0.008$, Figure 2(h)) compared with the CON group. However, the stimulatory effects of CORT on the inflammatory response were reversed in the colon by MT supplementation ($p > 0.056$).

Similar to its effect on the inflammatory response, CORT activated the STAT3/AP-1/NF-κB pathway in the colon. The expression levels of the p-STAT3, AP-1, p-P65, and p-IκB proteins in CORT-treated mice were increased by 39.2% ($p = 0.014$, Figure 2(i)), 52.7% ($p = 0.001$, Figure 2(j)), 66.8% ($p = 0.003$, Figure 2(k)), and 101.3% ($p \leq 0.001$, Figure 2(l)), respectively, relative to the CON group. After MT supplementation, however, there was no statistically significant difference between the CON group and the MT-pretreated CORT group ($p > 0.207$).

Collectively, these results indicated that MT supplementation reversed CORT-induced colonic GR synthesis and transport and suppressed the STAT3/SP-1/NF-κB pathway activation-mediated inflammatory response.

3.5. Effect of MT Supplementation on CORT Treatment Alters the Gut Microbiota Composition of the Colon. We further investigated whether CORT and MT supplementation could affect the composition of the gut microbiota. Quantitative perspective analysis suggested that the ACE, Chao, and Shannon indexes were significantly increased by 51.5% ($p = 0.001$, Figure 3(a)), 69.9% ($p = 0.008$, Figure 3(b)), and 17.5% ($p = 0.043$, Figure 3(c)), respectively, while the Simpson index was markedly decreased by 37.5% ($p = 0.032$, Figure 3(d)). The β-diversity analysis indicated that the intestinal microbiota dispersion of CORT mice increased significantly relative to that of the CON group (Figures 3(e) and 3(f)). Moreover, there was an increase in the OTU numbers (26.9%, $p = 0.012$, Figure 3(g)) and the ratio of *Firmicutes*: *Bacteroidetes* (F : B, 31.2%, $p = 0.003$, Figure 3(h)) in the CORT group compared with the CON group. There was also a statistically significant increase in the relative abundance of Firmicutes (35.2%) and Proteobacteria (41.2%) and a decrease in the abundance of Bacteroidetes (43.9%) in CORT mice relative to control mice (Figures 3(i) and 3(j)). However, after supplementation of CORT mice with MT, the trends of all the indexes were restored to the levels of the CON group (Figures 3(k)), and there was no statistically significant difference between the CON group and the MT-supplemented group ($p > 0.613$). These results demonstrated that CORT upregulated the diversity, richness, and OTU numbers of colonic microbiota as well as the F : B ratio and that this

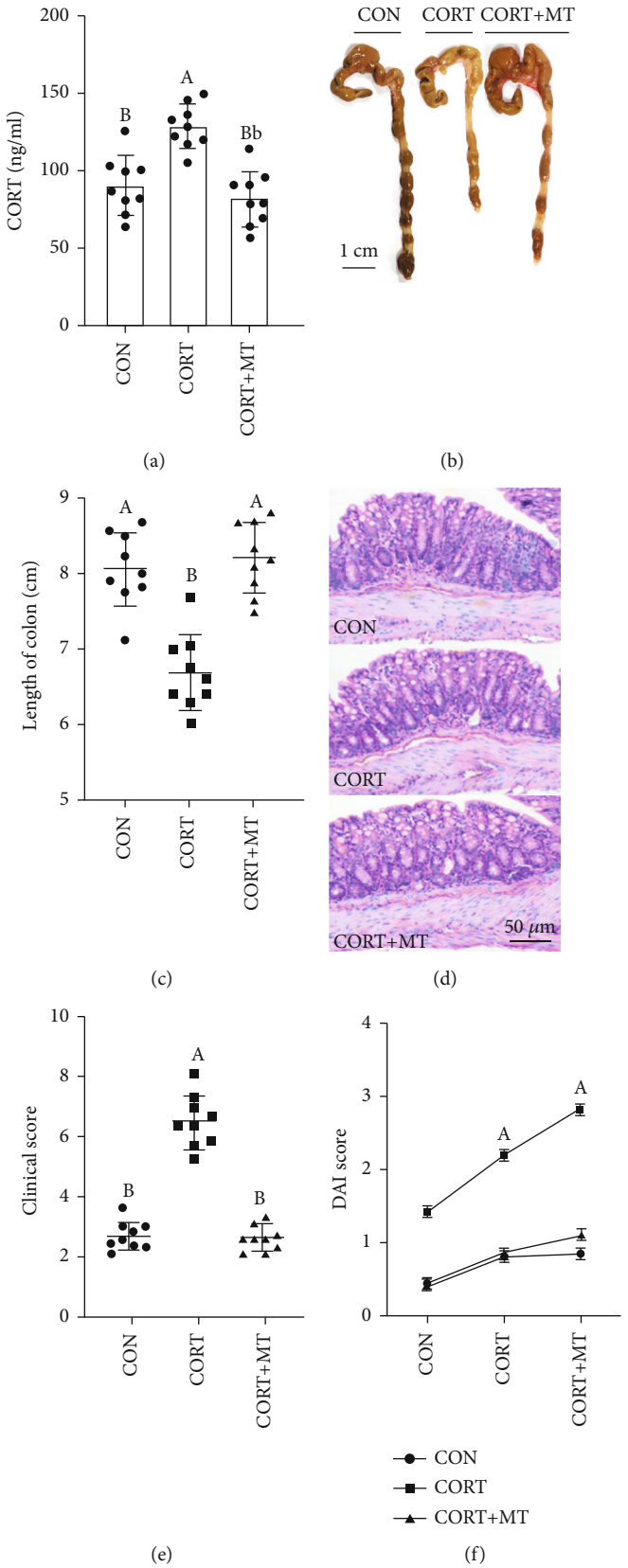

Figure 1: Continued.

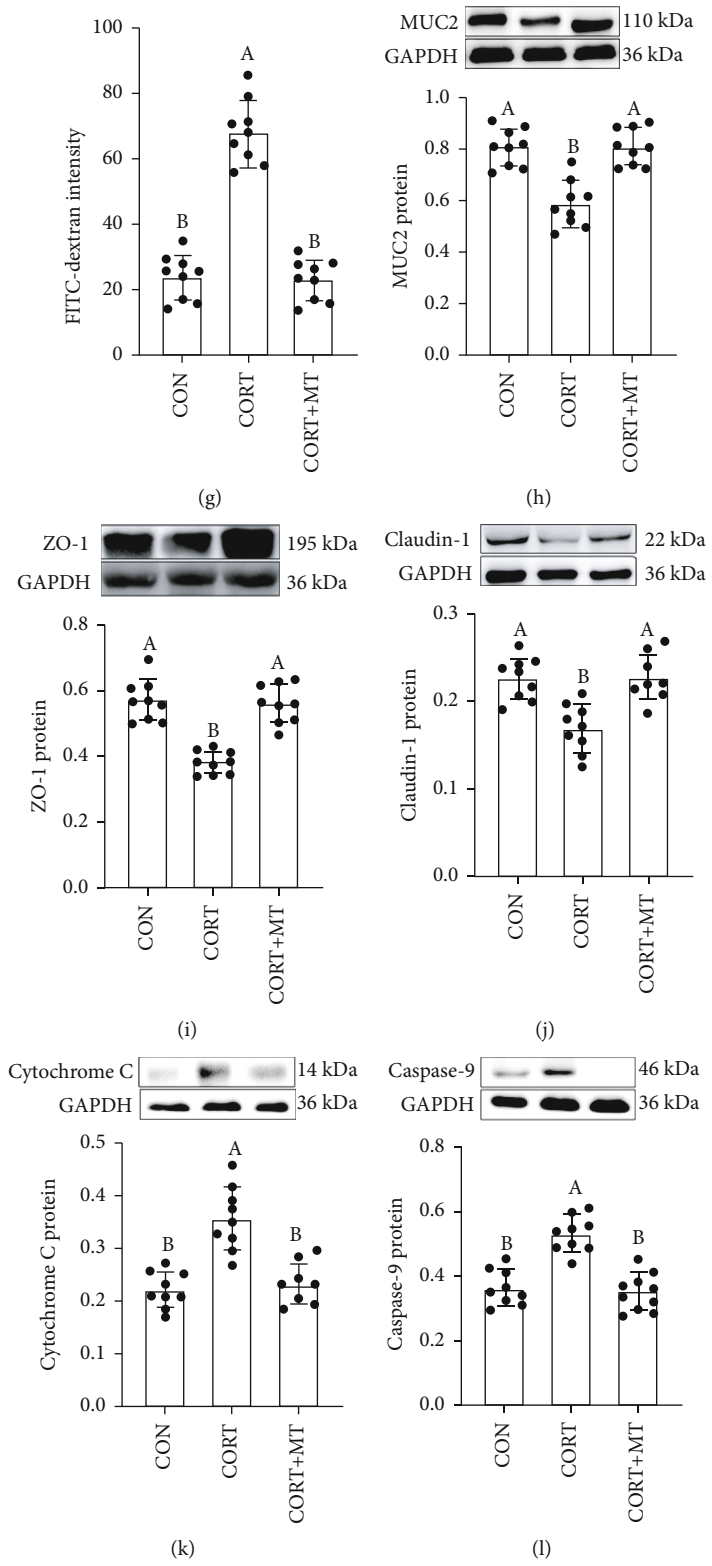

Figure 1: Continued.

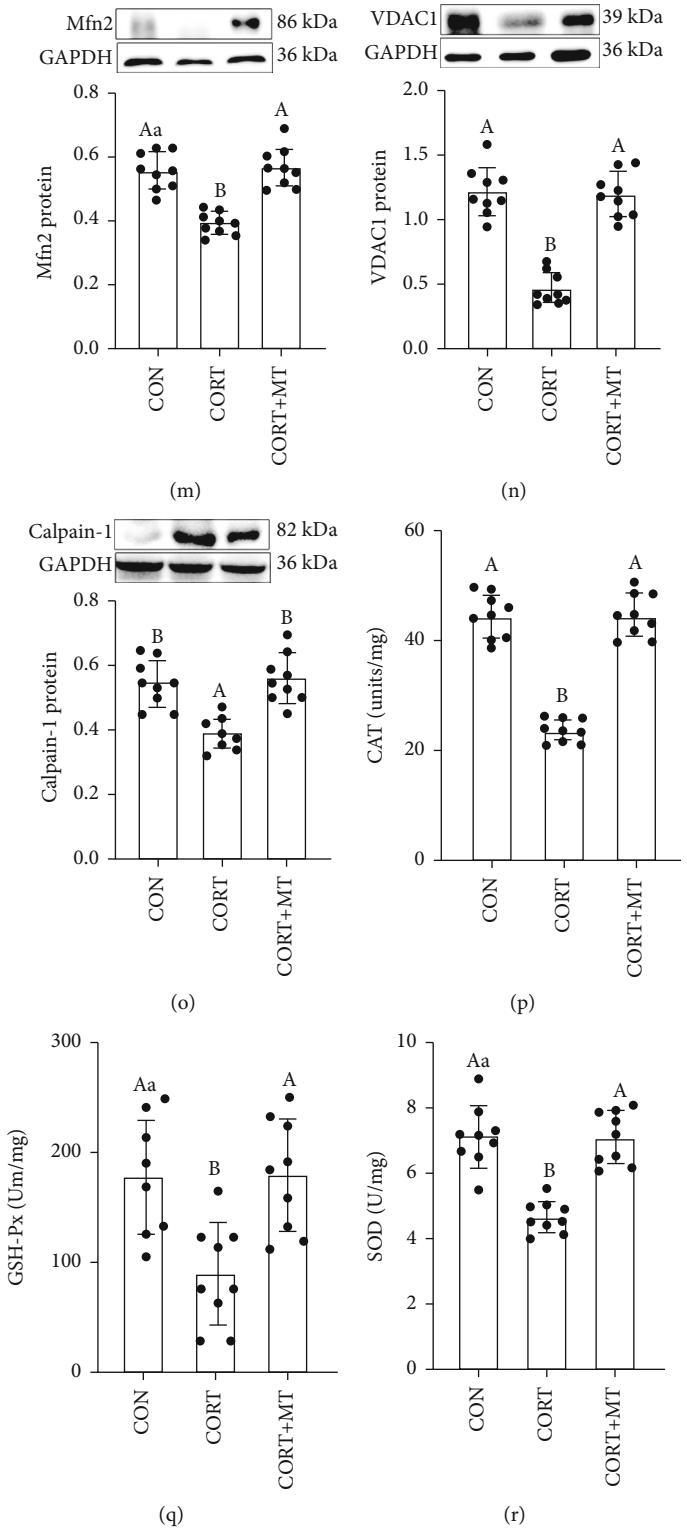

Figure 1: Continued.

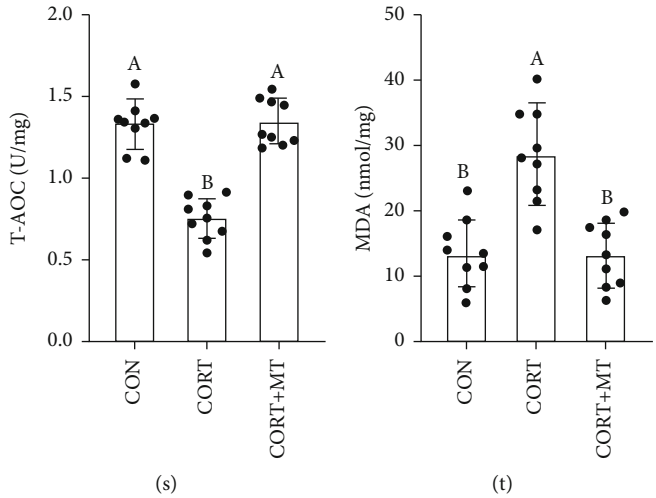

Figure 1: Effect of melatonin supplementation on improving CORT-induced intestinal barrier, mitochondrial function and antioxidant capacity impaired in mice. Serum CORT (a) concentrations; colonic length (b, c); H&E staining photographs (scale: 50 μm) (d); histological score (e); DAI score (f); relative luciferase activity (g); colonic MUC2 (h), ZO-1 (i), Claudin-1 (j), Cytochrome C (k), Caspase-9 (l), Mfn2 (m), VDAC1 (n), and Calpain-1 (o) proteins; CAT (p), GSH-Px (q), SOD (r), T-AOC (s), and MDA (t) in the CON, CORT and CORT+MT groups. Values are presented as the mean ± SE. Differences were assessed using ANOVA and are denoted as follows: different lowercase letters: $p < 0.05$; different uppercase letters: $p < 0.01$; the same letter: $p > 0.05$.

microbial composition was significantly altered by MT supplementation.

A cladogram representative of the colonic microbiota structure in mice further displayed the predominant bacteria and the greatest differences in taxa among the 3 treatment groups (Figure 4(a)). The results indicated that the predominant bacteria in the colons of CORT mice were *Bacillus*, *Prevotella*, *Alloprevotella*, *Pseudomonadaceae*, *Escherichia-Shigella*, and *Muribaculaceae*, while the predominant bacteria in the colons of CORT+MT mice were *Akkermansia*, *Bacteroidales*, and *Lactobacillus*, which are beneficial bacteria. Moreover, a genus level analysis demonstrated that CORT significantly decreased the relative abundances of *Lactobacillus*, *Bacteroides* and *Akkermansiaceae* and increased the relative abundances of *Prevotellaceae-UCG-001*, *Alistipes*, *Escherichia-Shigella*, *Rikenellaceae* and *Proteobacteriaceae*, while supplementation with MT restored the abundances of these bacteria to those of the CON group (Figure 4(b)). Figure 4(c) shows that the relative abundances of *Pseudomonadaceae*, *Moraxellaceae*, *Bacillaceae*, *Aeromonadaceae*, *Aerococcaceae*, *Peptococcaceae*, and *Muribaculaceae* in the colons of the CORT group were significantly increased by 23.7% ($p \leq 0.001$), 42.8% ($p \leq 0.001$), 29.4% ($p = 0.012$), 63.1% ($p = 0.010$), 54.3% ($p = 0.001$), 54.1% ($p = 0.001$), and 48.1% ($p = 0.002$), respectively, relative to the CON group, while the levels of *Bacteroides* and *Lactobacillus* were significantly decreased by 53.1% ($p \leq 0.001$) and 45.8% ($p = 0.003$), respectively, relative to the CON group. However, these changes were reversed by MT supplementation, and there was no significant difference among the CON, CORT, and CORT+MT groups ($p > 0.052$). These results demonstrated that MT supplementation suppressed the CORT-induced changes in the composition of the intestinal microbiota.

Furthermore, Pearson's correlation analysis showed a negative correlation between the relative abundances of *Akkermansia*, *Lactobacillus*, and *Bacteroides* and the plasma CORT level ($r^2 = 0.8780$ and $p < 0.0001$, Figure 4(d); $r^2 = 0.8622$ and $p < 0.0001$, Figure 4(e); and $r^2 = 0.9642$ and $p < 0.0001$, Figure 4 r^2), as well as a positive correlation between the relative abundances of *Prevotella*, *Allobaculum*, *Muribaculaceae*, *Proteobacteriaceae* and *Rikenellaceae* and the plasma CORT level ($r^2 = 0.9542$ and $p < 0.0001$, Figure 3(g); $r^2 = 0.8963$ and $p < 0.0001$, Figure 4(h); $r^2 = 0.9111$ and $p < 0.0001$, Figure 4(i); $r^2 = 0.8493$ and $p < 0.0001$, Figure 4(j); and $r^2 = 0.8089$ and $p < 0.0001$, Figure 4(k)). In general, MT supplementation significantly increased probiotics, which were negatively correlated with the CORT level, and suppressed pathogenic bacteria, which were positively correlated with the CORT level.

3.6. Effect of MT Supplementation on CORT Treatment Alters the Composition of Gut Microbiota Metabolites in the Colon. We further analyzed how the composition of gut microbiota metabolites responded to CORT treatment and MT supplementation. Our results suggested that CORT treatment led to a significant increase in colonic microbiota metabolite dispersion, which suggested a decrease in microbiota metabolite homogeneity (Figures 5(a) and 5(b)). The Venn diagram indicated that compared with the CON group, the levels of 412 metabolites were changed in the CORT group, while MT supplementation restored the levels of 298 of these metabolites (Figure 5(c)). Furthermore, we screened the 60 most changed metabolites in the three treatment groups (Figure 5(d)). Of these, the levels of 22 metabolites were significantly reduced and those of 38 metabolites were increased in the CORT group relative to the CON group. Specifically, there was a significant decrease in the contents of butyrate (68.9%, $p \leq 0.001$, Figure 5(e)), L-tryptophan (58.4%, $p = 0.001$, Figure 5(f)) and D-fructose (48.3%, $p \leq 0.001$,

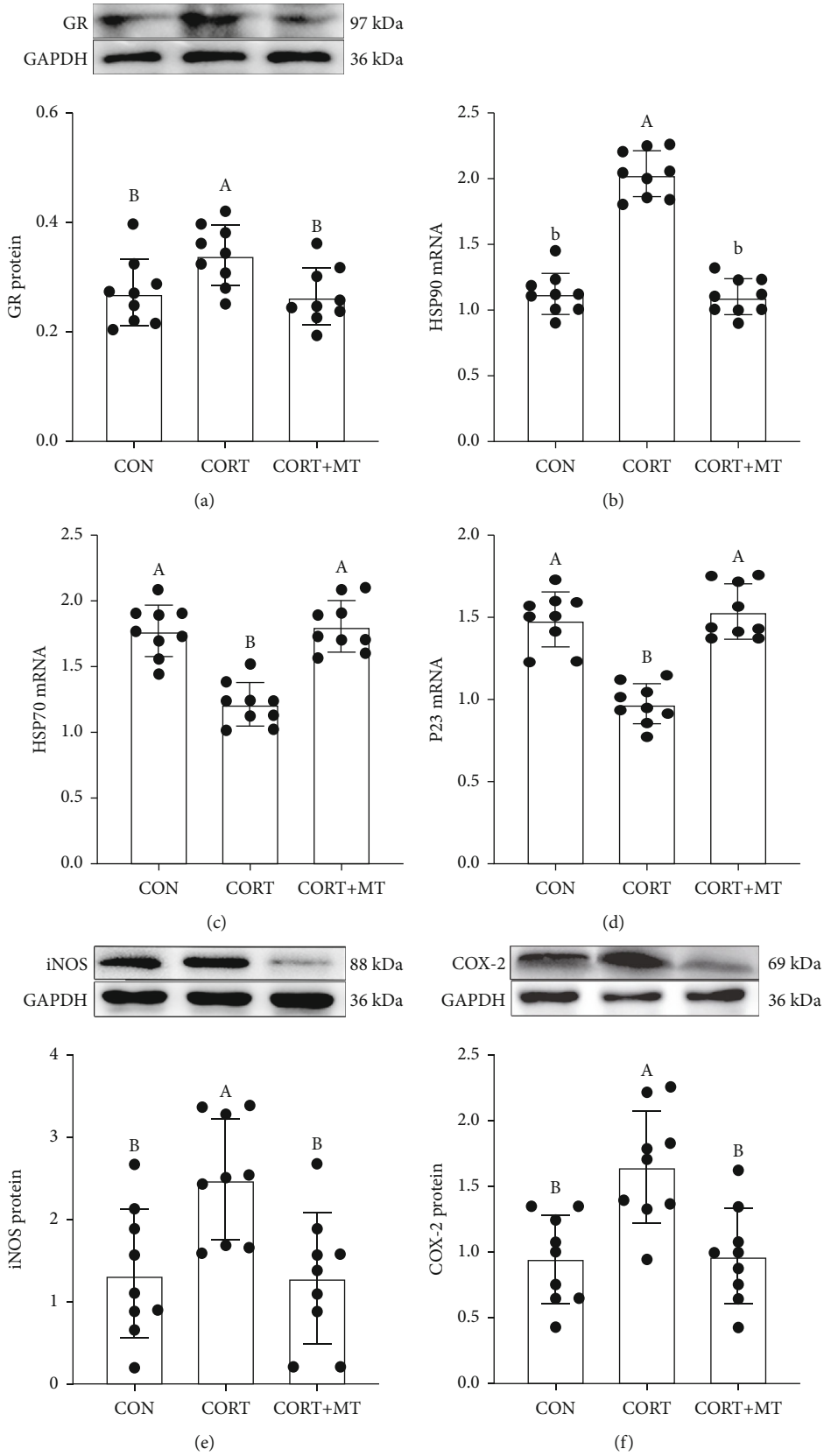

Figure 2: Continued.

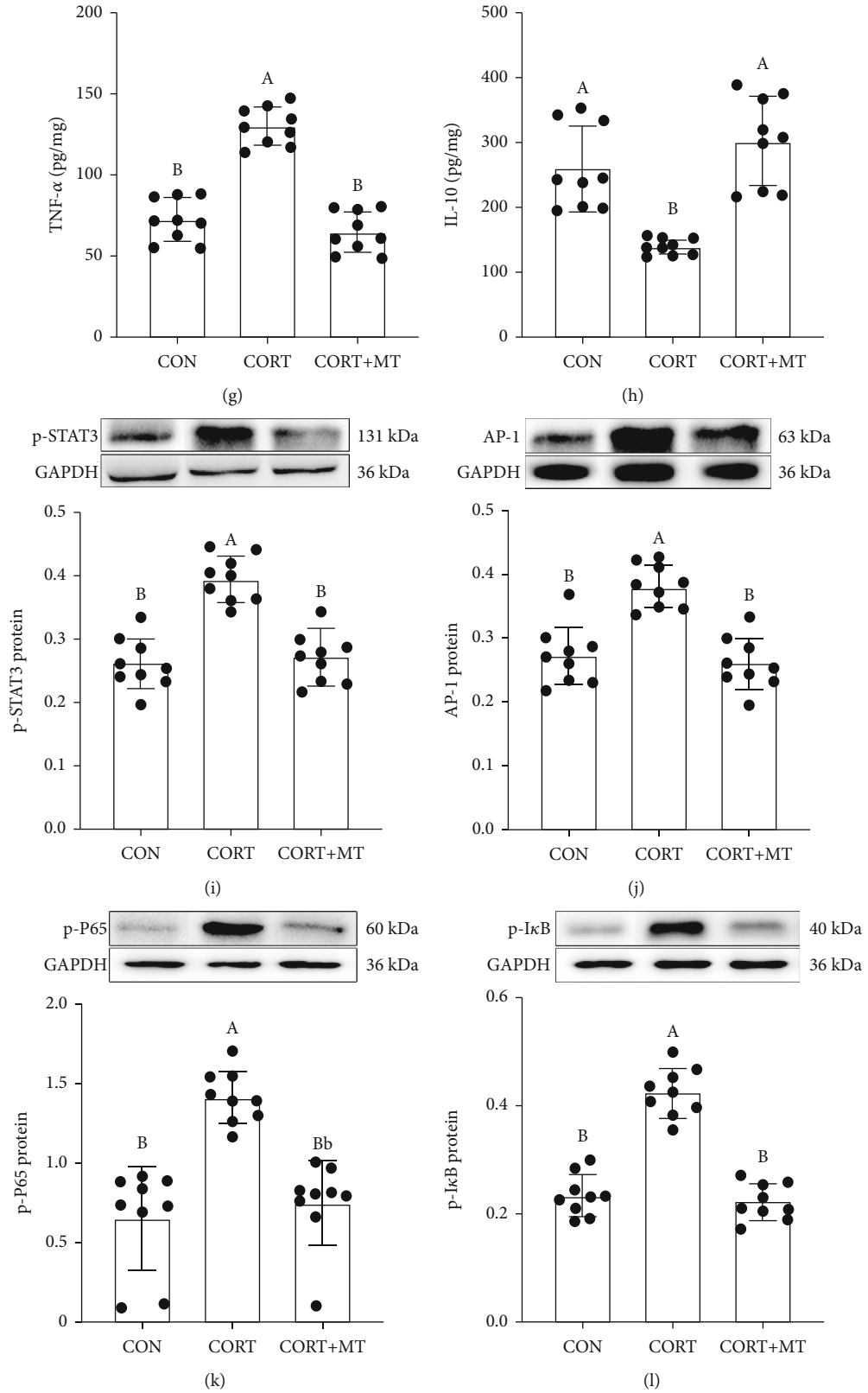

Figure 2: Effect of melatonin supplementation on improving CORT-induced GR synthesis and enhanced transport and inflammation response in mice. Colonic GR (a), HSP90 (b), HSP70 (c), P23 (d), iNOS (e), COX-2 (f), TNF-α (g), IL-10 (h), p-STAT3 (i), AP-1 (j), p-P65 (k), and p-IκB (l) levels in the CON, CORT, and CORT+MT groups were measured by qRT-PCR, ELISA, and western blotting. Values are presented as the mean ± SE. Differences were assessed using ANOVA and are denoted as follows: different lowercase letters: $p < 0.05$; different uppercase letters: $p < 0.01$; and the same letter: $p > 0.05$.

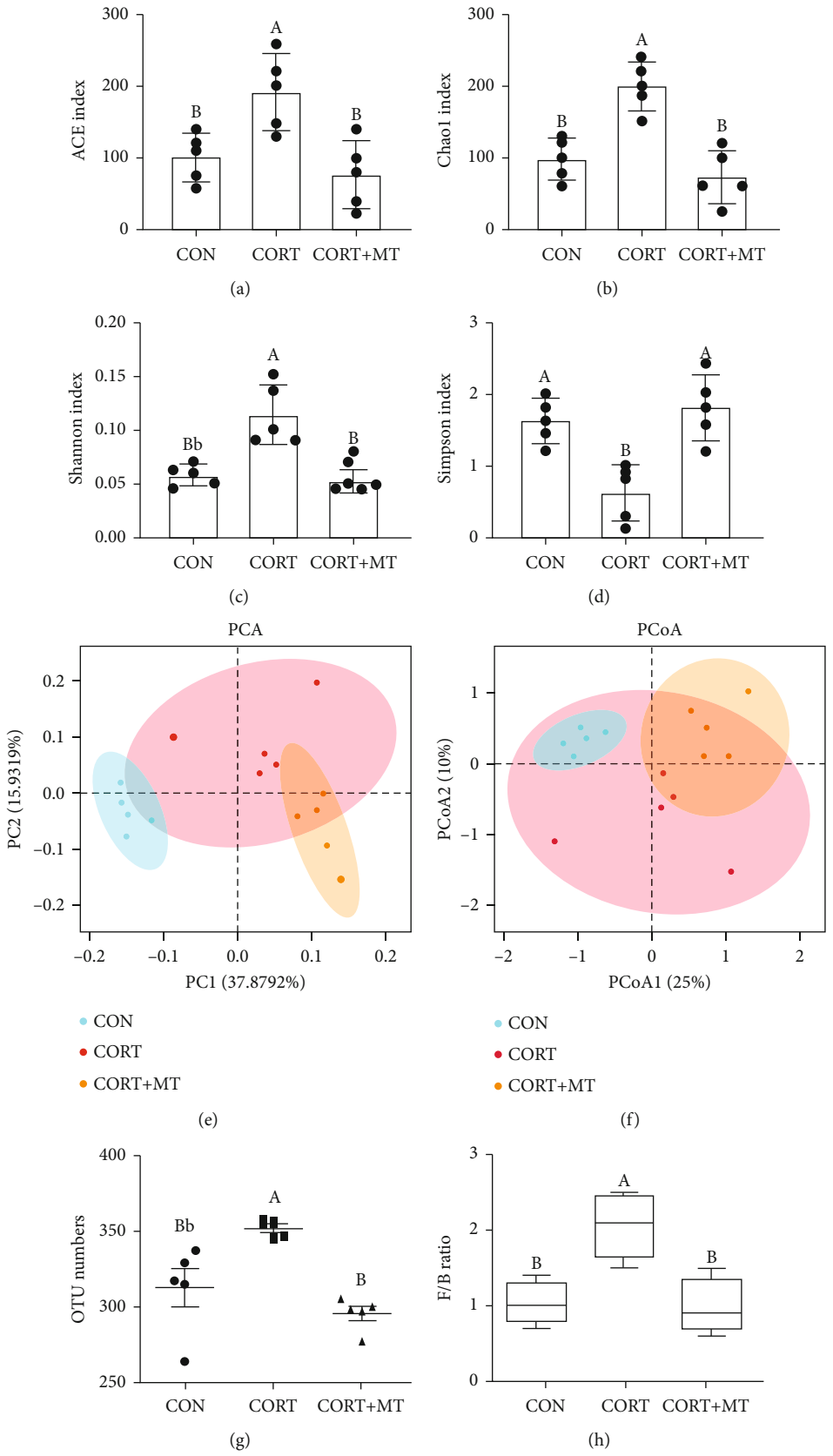

Figure 3: Continued.

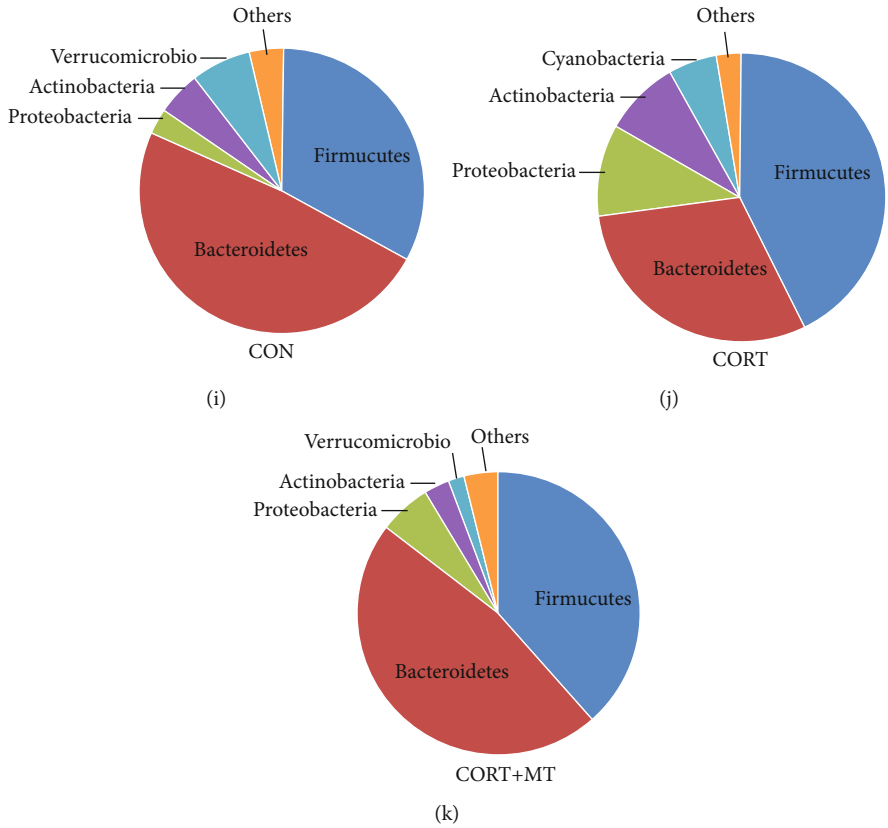

Figure 3: Effect of melatonin supplementation on improving CORT-induced colonic gut microbiota composition dysbiosis. The α-diversity includes diversity and richness. ACE index (a), Chao1 index (b), Shannon index (c), and Simpson index (d). The β-diversity shows the dispersion of each sample. Principal component analysis (PCA) (e) and PCoA score plot (f) score plot based on the Bray-Curtis score plot based on the OTU in the colon; OTU number (g); F : B ratio (h) and relative contribution of the top 4 phyla (I-K) in the CON (i), CORT (j), and CORT+MT (k) groups. Values are presented as the mean ± SE. Differences were assessed using ANOVA and are denoted as follows: different lowercase letters: $p < 0.05$; different uppercase letters: $p < 0.01$; and the same letter: $p > 0.05$.

Figure 5(g)) as well as a significant increase in the contents of 1-naphthol (94.5%, $p = 0.002$, Figure 5(h)), hypoxanthine (89.3%, $p = 0.002$, Figure 5(i)) and adenine (100.2%, $p = 0.008$, Figure 5(j)) in the CORT group compared to the CON group. However, MT supplementation restored these levels to those in the CON group ($p > 0.438$). Collectively, these results indicated that MT supplementation reversed the CORT-induced alterations of colonic microbiota metabolites.

3.7. Effect of MT Supplementation on CORT Treatment Alters the Correlation between the Gut Microbiota and Microbiota Metabolites in the Colon. We further analyzed the correlation between the gut microbiota and its metabolites in the CON, CORT, and CORT+MT groups. As shown in Figure 6(a), the most prominent alteration associated with the intestinal microbiota and its metabolites involved 12 metabolites and 83 intestinal microbiota. The levels of butyrate, L-tryptophan, and D-fructose were found to be directly proportional to the levels of *Butyricicoccus*, *Akkermansia*, and *Lactobacillus* but inversely proportional to the levels of *Alistipes*, *Peptostreptococcus*, and *Rikenellaceae*. The levels of adenine, hypoxanthine, and 1-naphthol were directly proportional to the levels of *Alistipes*, *Peptostreptococcus*, and *Rikenellaceae* and inversely proportional to the levels of *Butyricicoccus*, *Akkermansia*, and *Lactobacillus*. Further, KEGG analysis indicated CORT treatment mainly enhanced the steroid hormone biosynthesis, sphingolipid metabolism, and two-component system signaling pathways and inhibited the gap junction, bacterial invasion of epithelial cells, protein digestion and absorption, carbohydrate digestion, and absorption and gastric acid secretion pathways (Figure 6(b)). However, these changes were reversed by MT supplementation. It can be speculated that CORT treatment leads to changes in metabolite composition, especially decreases in the levels of butyrate and L-tryptophan, which in turn affect these pathways and functions, ultimately resulting in impaired intestinal barrier function.

3.8. FMT Promotes Reestablishment of the Intestinal Inflammation Response in Mice. As illustrated in Figures S3A and 3B, there was no significant difference of the plasma CORT and colonic ROS level among the F-CON, F-SD, F-SM, and F-R groups. Moreover, the expression level of p-STAT3, p-AP-1, p-IκB, and p-P65 proteins increased by 64.3% ($p = 0.006$, Figure S3C), 63.9% ($p \leq 0.001$, Figure S3D), 61.9% ($p \leq 0.001$, Figure S3E), and 72.0% ($p \leq 0.001$, Figure S3F) in the F-SD group, compared with the F-CON group. However, the stimulatory effects of F-SD on changes in colitis were reversed in the colon by F-SM supplementation.

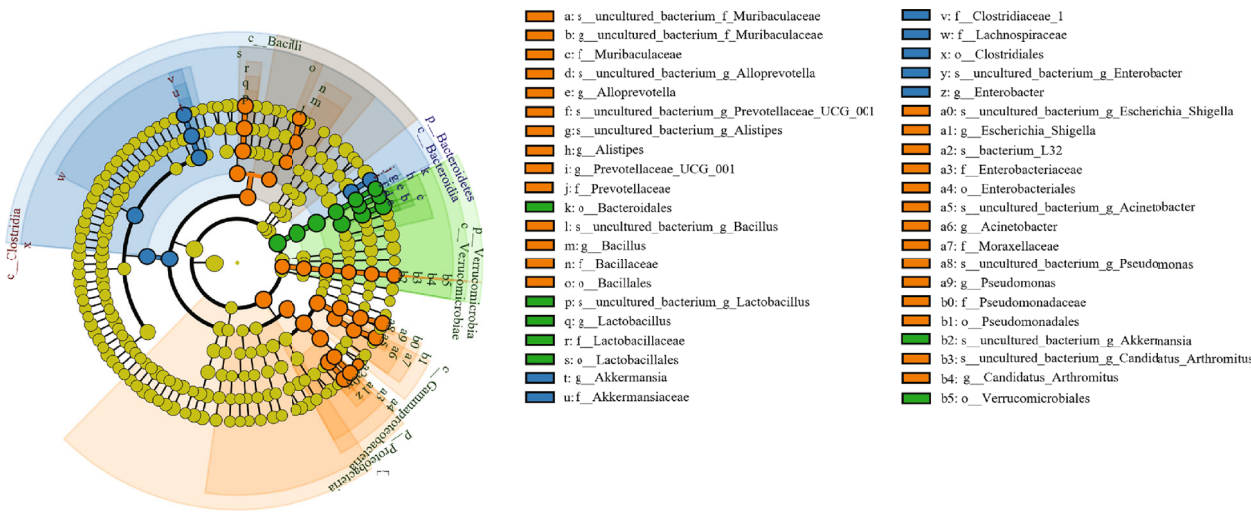

(a)

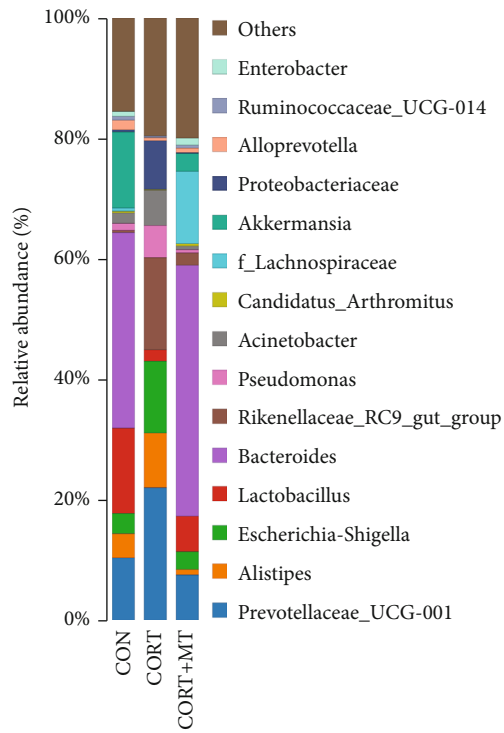

(b)

Figure 4: Continued.

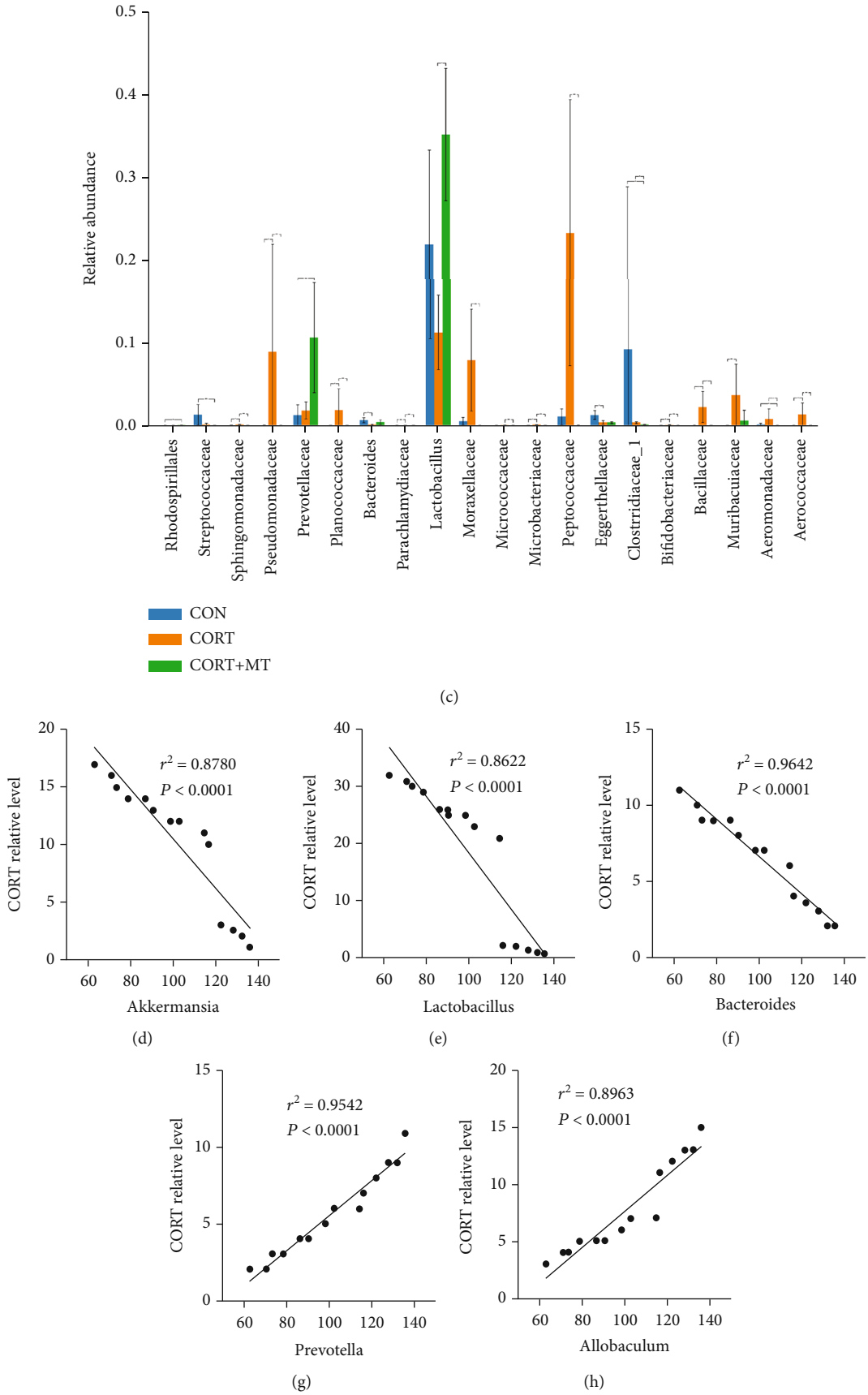

Figure 4: Continued.

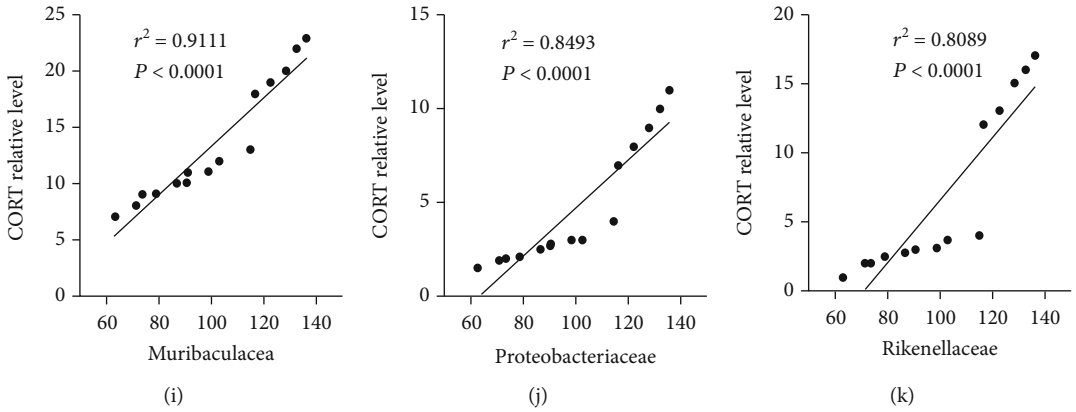

Figure 4: Effect of melatonin supplementation on improving CORT-induced colonic gut microbiota composition altered. Taxonomic cladogram obtained from LEfSe sequence analysis (a) in the colon. Biomarker taxa are highlighted by coloured circles and shaded areas. The diameter of each circle reflects the abundance of that taxa in the community; relative abundance of the top 15 genera (b) and the statistics of most change intestinal microbiota (c); correlation between the CORT level and the relative abundance of Akkermansia (d), Lactobacillus (e), Bacteroides (f), Prevotella (g), Allobaculum (h), Muribaculaceae (i), Proteobacteriaceae (j), and Rikenellaceae (k) in the CON, CORT, and CORT+MT groups in the colon. Values are presented as the mean ± SE. Differences were assessed using ANOVA and are denoted as follows: different lowercase letters: $p < 0.05$; different uppercase letters: $p < 0.01$; and the same letter: $p > 0.05$.

Collectively, these results indicated that FMT from SD mice promoted reestablishment of the intestinal microecology to activate inflammation response, while MT supplementation suppressed this process.

3.9. Effect of MT Supplementation on CORT Treatment Triggers Oxidative Stress by Enhancing GR Synthesis and Transport in IECs. We established a CORT-treated IECs model with or without MT administration (Figures 7 and 8) to investigate the mechanisms whereby MT supplementation reversed the CORT-induced intestinal homeostasis imbalance. CORT treatment induced an increase in the levels of ROS (52.7%, $p = 0.010$; Figure 7(b)), GR protein (168.1%, $p = 0.002$; Figure 7(c)) and HSP90 mRNA (178.8%, $p = 0.005$; Figure 7(e)) and a decrease in proliferative capacity (50.3%, $p \leq 0.001$; Figure 7(a)) and the levels of HSP70 (53.4%, $p = 0.029$; Figure 7(d)) and P23 mRNA (43.2%, $p = 0.003$; Figure 7(f)) compared with the control IECs. However, these changes were dramatically suppressed by MT supplementation. The improvement effects of MT were replicated by pretreatment with RU-486, a GR antagonist. Pretreatment with NAC, a free radical scavenger, similarly imitated the effects of MT, increasing proliferative capacity (100.6%, $p = 0.003$) and decreasing the levels of ROS (34.5%, $p = 0.010$) in CORT+NAC-treated IECs relative to the CORT group; however, no changes were observed in the expression levels of GR proteins and HSP70, HSP90 and P23 mRNA ($p > 0.050$) after NAC treatment. Conversely, 4P-PDOT administration significantly suppressed the beneficial effects of MT and resulted in an increase in ROS (54.0%, $p = 0.001$), GR protein (67.8%, $p \leq 0.001$), and HSP90 mRNA (61.2%, $p = 0.004$) levels and a decrease in proliferative capacity (74.5%, $p = 0.003$) and HSP70 (38.4%, $p = 0.036$) and P23 (79.0%, $p \leq 0.001$) mRNA levels compared with vehicle IECs. Our results revealed that MT-mediated MT2 receptor ameliorated CORT-induced oxidative stress by suppressing GR synthesis and transport in the gut.

3.10. Effect of MT Supplementation on CORT Treatment Induces the Activation of STAT3/AP-1/NF-κB Pathway via Inhibiting Oxidative Stress. Moreover, we observed an increase in the expression levels of p-STAT3 (97.7%, $p = 0.031$; Figure 8(a)), AP-1 (93.0%, $p = 0.016$; Figure 8(b)), p-P65 (96.1%, $p = 0.010$; Figure 8(c)), p-IκB (109.1%, $p = 0.022$; Figure 8(d)), iNOS (113.9%, $p = 0.018$; Figure 8(g)) and COX-2 (69.2%, $p = 0.016$; Figure 8(h)) and a decrease in the expression level of MT2 (61.4%, $p = 0.008$; Figure 8(f)) in CORT-treated IECs compared with the vehicle group, while CORT treatment had no effect on the expression of MT1 protein (Figure 8(e)). However, MT pretreatment could suppress this process. After treatment with RU-486 (GR antagonist), which had similar effects to MT, we observed a decrease in expression of p-STAT3 (62.7%, $p = 0.014$), AP-1 (43.7%, $p = 0.010$), p-P65 (38.4%, $p = 0.018$), p-IκB (51.1%, $p = 0.017$), iNOS (55.0%, $p = 0.014$), and COX-2 (42.8%, $p = 0.001$) in CORT+RU-486-treated IECs compared with the CORT-treated group, while RU-486 had no effect on MT1 and MT2 expression. Moreover, treatment with NAC, which inhibits oxidative stress, also restored the changes induced by CORT. Pretreatment with 4P-PDOT reversed the therapeutic effects of MT and failed to improve the changes induced by CORT. The expression of p-STAT3 (47.0%, $p = 0.047$), AP-1 (50.9%, $p = 0.006$), p-P65 (43.3%, $p = 0.016$), p-IκB (56.3%, $p = 0.015$), iNOS (55.3%, $p = 0.014$) and COX-2 (41.7%, $p = 0.015$) was increased in CORT+MT+4P-PDOT-treated IECs relative to CORT+MT-treated IECs, indicating that MT-mediated MT2 ameliorated the CORT-induced inflammatory response, resulting from STAT3/AP-1/NF-κB pathway activation.

4. Discussion

Our previous studies have demonstrated that SD, as a physiological stressor, induced an excessive CORT, gut microbiota disturbances, and colitis phenotype [2]. Moreover, the

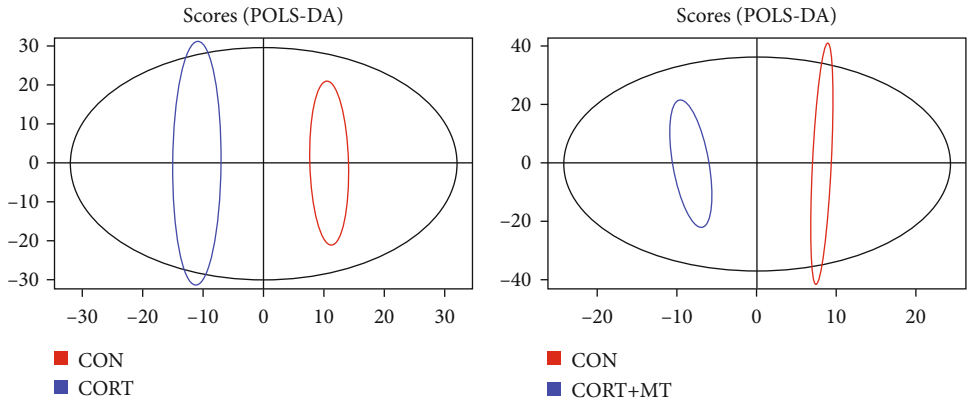

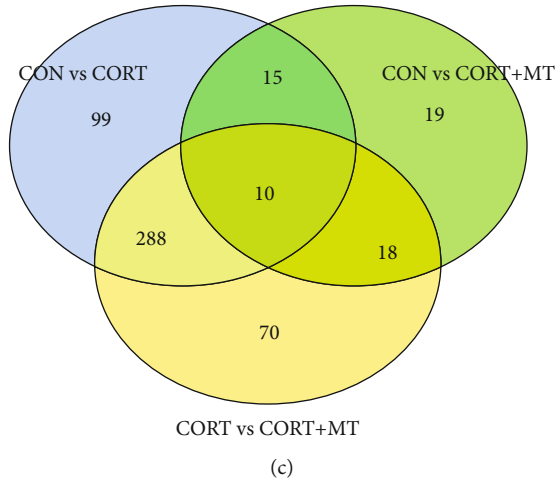

Figure 5: Continued.

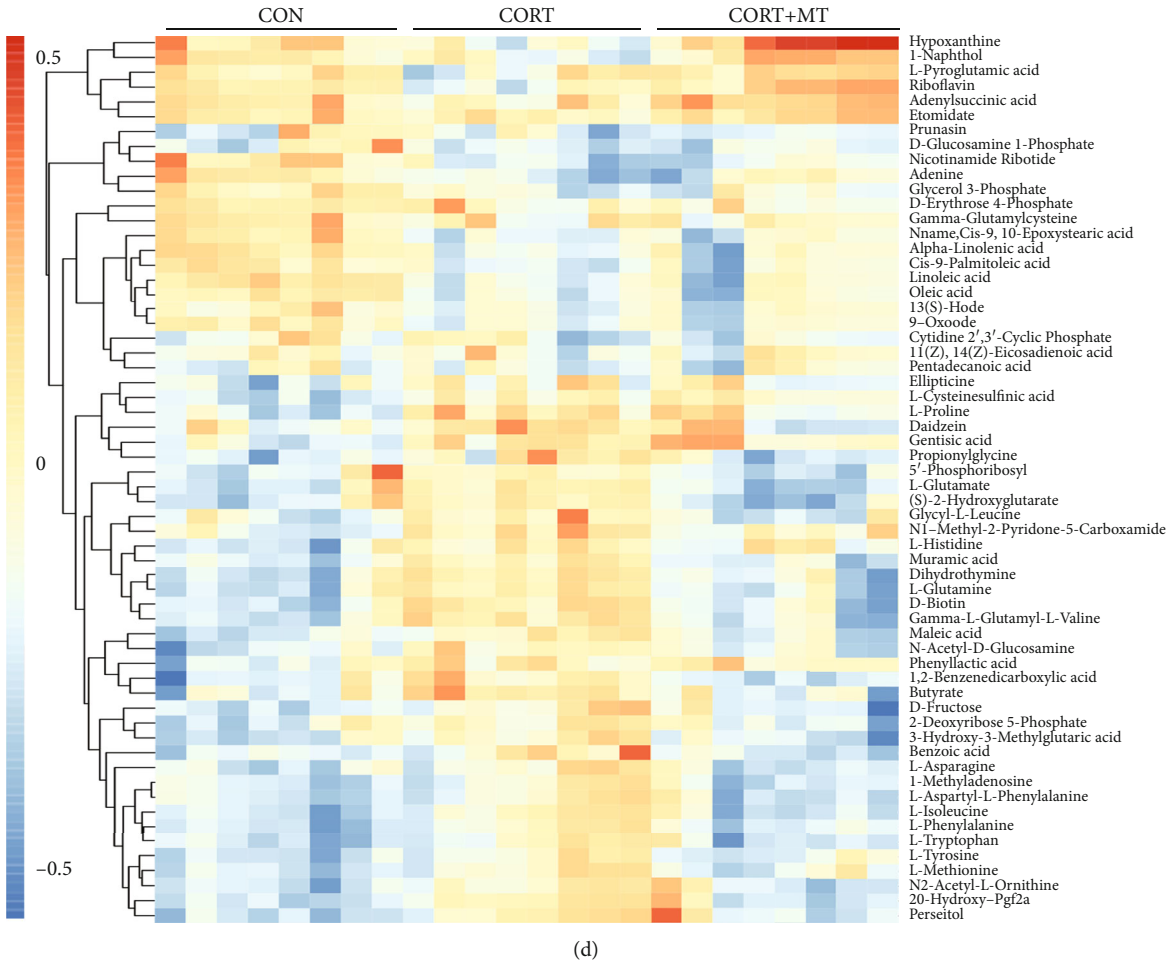

(d)

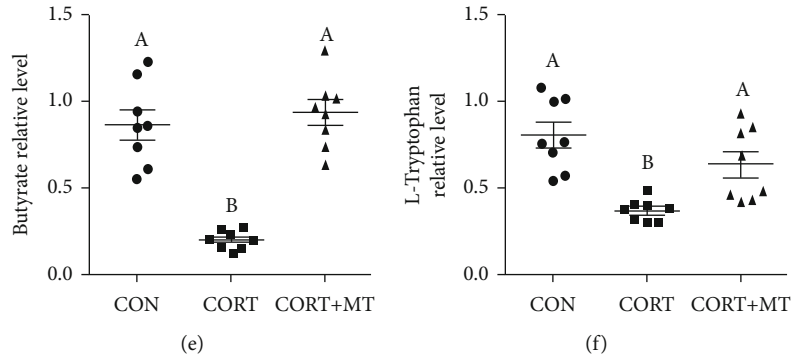

(e)

(f)

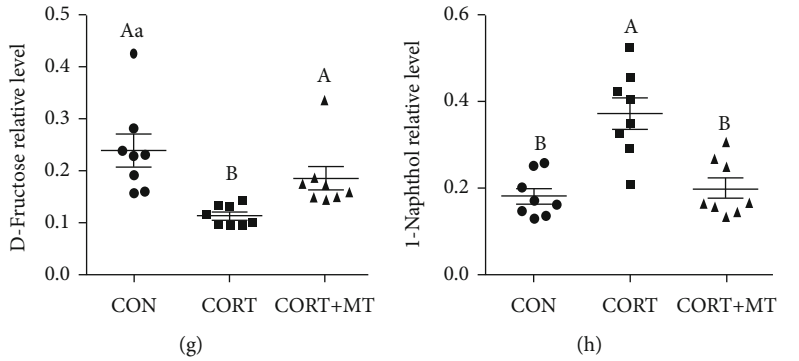

(g)

(h)

Figure 5: Continued.

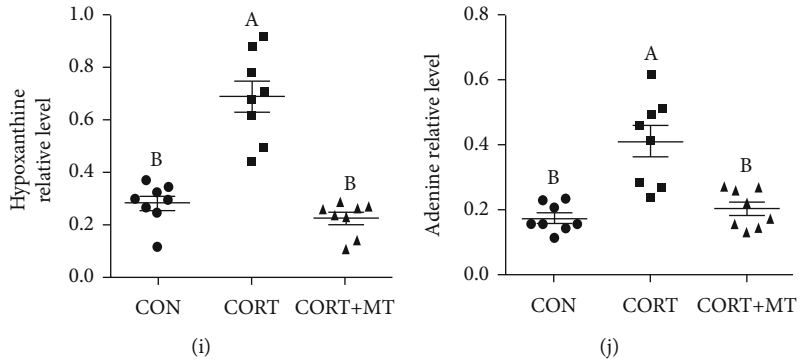

Figure 5: Effect of melatonin supplementation on improving CORT-induced colonic gut microbiota metabolite composition altered. The β-diversity of principal component analysis (PCA) (a), PCoA (b) and Venn (c) based on the microbiota metabolites in the CON, CORT, and CORT+MT groups; heat map (d) showing the relative abundance of the key identified 60 metabolites that were significantly altered by MT in CORT mice. The relative abundance of butyrate (e), L-tryptophan (f), D-fructose (g), 1-naphthol (h), hypoxanthine (i), and adenine (j) in the CON, CORT, and CORT+MT groups in the colon microbiota based on the heat map results. Values are presented as the mean ± SE. Differences were assessed using ANOVA and are denoted as follows: different lowercase letters: $p < 0.05$; different uppercase letters: $p < 0.01$; and the same letter: $p > 0.05$.

present study indicated the mice, receiving faeces microbiota from SD mice also suffered colitis phenotype and intestinal microbiota disorder, but no changes in plasma CORT were observed. However, melatonin supplementation reversed all inductions in SD-mice and transplanting faeces microbiota from SD+MT mice significantly restored SD-induced colitis and intestinal microbiota imbalance. These results emphasized the core role of overproduction CORT in SD-induced gut microbiota dysbiosis and revealed that MT-mediated gut microbiota homeostasis exerted a improvement effect in SD-induced colitis mice.

To verify the key role of excessive CORT in SD caused gut microbiota disorder, we established a CORT-treated mice. Results showed that CORT treatment induced a colitis phenotype. Meanwhile, microbial composition analysis in the present study revealed there was an increase in the diversity and richness, dispersion, OTU numbers, and the F : B ratio in CORT-treated mice. Recent studies have also shown that GCs may cause a disorder in gut microbes [11] and an increase in the F : B ratio, which is regarded as a key indicator of major changes in the gut microbiota. It has generally been assumed that GCs increase the risk of proliferation of pathogenic bacteria [19]. Our study also revealed a higher abundance of harmful bacteria (*Prevotella* and *Allobaculum)* and a lower abundance of beneficial bacteria (*Akkermansia*, *Bacteroides*, *Peptostreptococcus* and *Lactobacillus*) in the colons of mice exposed to CORT. *Bacteroides* and *Lactobacillus* are responsible for catabolizing butyrate and L-tryptophan, respectively [20]. Consistent with the microbial results, our metabolomics analysis further indicated that the relative abundance of butyrate and tryptophan in CORT mice was significantly reduced. The intestinal microbiota and its metabolites are integral mediators of intestinal barrier function and intestinal permeability and are capable of both perturbing and enhancing intestinal barrier integrity by modulating immune responses, oxidative stress, inflammation, vagal signaling, and nutrient availability [21]. Further, there was an increase in the expression levels of p-STAT3, AP-1, p-P65 and p-IκB proteins and proinflammatory factors (COX-2, iNOS and TNF-α) in CORT mice. Research has revealed that butyrate promotes proinflammatory cytokine production (e.g., IL-6, IL-8, IL-1β and TNF-α) by enhancing NF-κB activation in epithelial cells [22]. Moreover, in mice and piglets, the tryptophan supplementation reduced the symptoms of DSS-induced colitis, improved histology and intestinal permeability, and decreased the levels of local inflammatory mediators, such as IFN-γ and TNF-α [23]. Thus, our results revealed that SD-mediated CORT overproduction induced intestinal microbiota disorder and further triggered inflammation response, ultimately resulting in the occurrence of colitis.

We further investigated the cellular and molecular mechanisms underlying the cross-talk between the CORT overproduction and the gut microbiota. There was a reduction in the expression levels of HSP70 and P23 mRNA and an increase in GR protein and HSP90 mRNA in CORT-treated mice. The HSP90-GR-CORT complex, stabilized by cochaperones P23 and HSP70, ameliorated in CORT mice [24]; it moves to the nucleus and interacts with the glucocorticoid response element to regulate downstream signaling pathways [25]. This implies that GR synthesis and transport are enhanced and that the negative feedback regulation of the HPA axis is weakened in CORT mice. Consistent with HPA axis dysregulation, CORT treatment also destroyed intestinal mitochondrial function and antioxidant capacity in the colon. A high dose of GCs can indirectly induce oxidative stress through the depletion of antioxidant molecules or inhibition of antioxidant enzymes [26]. One possibility determined by our study is that dysregulation of mitochondrial functions induced the overproduction of ROS, creating a hypoxic niche due to oxygen consumption, and can affect the gut microbiota through perturbation of the normal intestinal environment, allowing bacterial antigens to penetrate the epithelium and stimulate an immune response [27]. Therefore, we concluded that the depletion of antioxidants, production of ROS, and lipid peroxidation after CORT

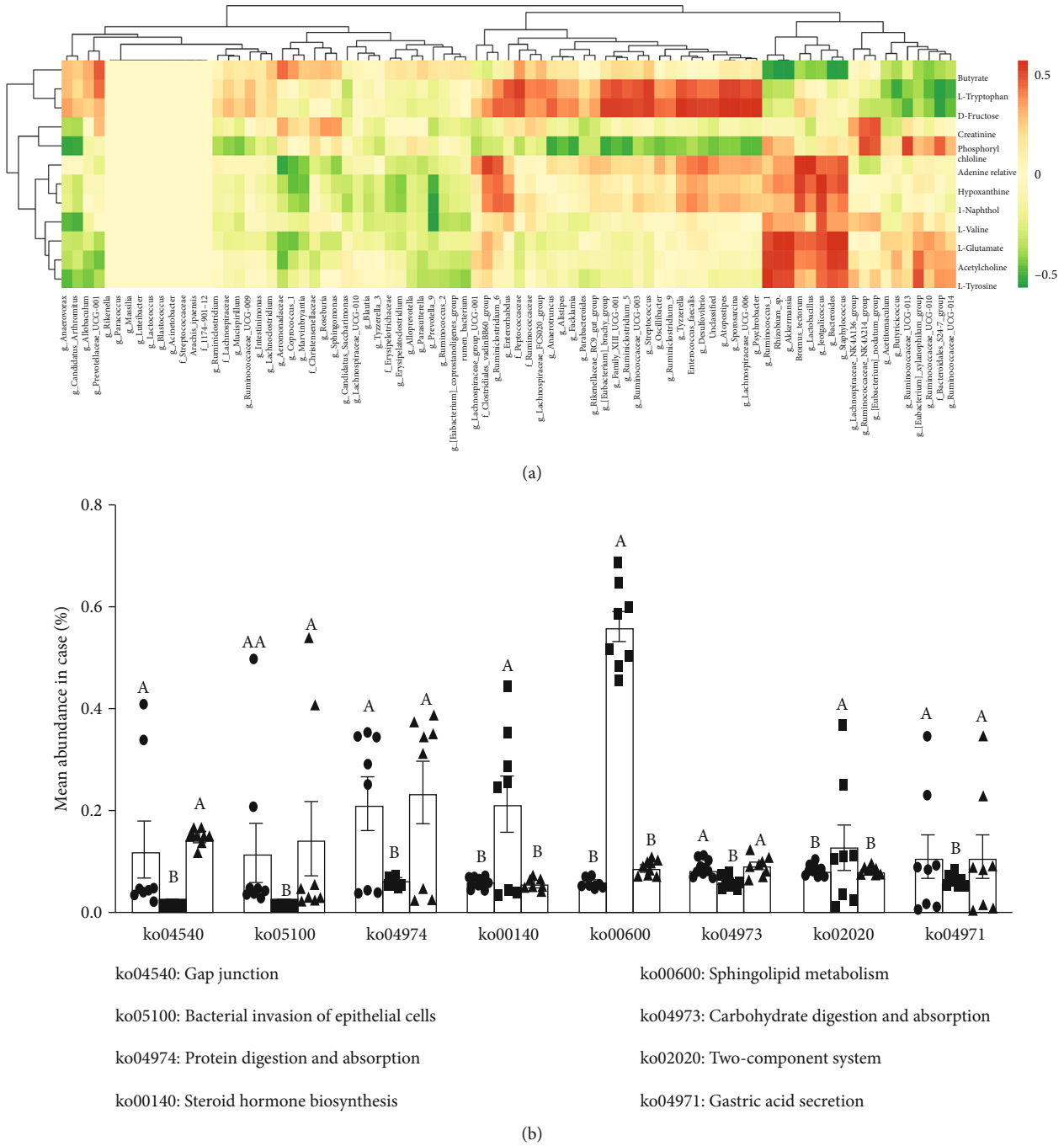

Figure 6: Correlation analysis between intestinal microbiota and metabolites in the colon of CORT mice with or without MT supplementation. Correlation of the most significant changes in intestinal microbiota and metabolites (a) and KEGG analysis (b) among the CON, CORT, and CORT+MT groups. Values are presented as the mean ± SE. Differences were assessed using ANOVA and are denoted as follows: different lowercase letters: $p < 0.05$; different uppercase letters: $p < 0.01$; and the same letter: $p > 0.05$.

exposure play an important role in intestinal microbiota imbalance-mediated inflammation response induced colitis.

Interestingly, our results showed that MT supplementation normalized the plasma CORT level in CORT-treated mice. Consistent with the reduction in CORT levels, MT enhanced the colonic mitochondrial function and antioxidant capacity and reversed intestinal microbiota metabolite dysbiosis and intestinal mucosa barrier damage. We further explored the specific mechanisms by which MT alleviated intestinal mucosa damage via in vitro experiments. Significant increases in the ROS content and expression level of the GR protein and HSP90 mRNA and a decrease in HSP70 and P23 mRNA expression were observed in colonic CORT-treated IECs. However, MT supplementation reversed the changes induced by CORT. Similarly, RU-486, a corticoid receptor antagonist replicated the effects of MT,

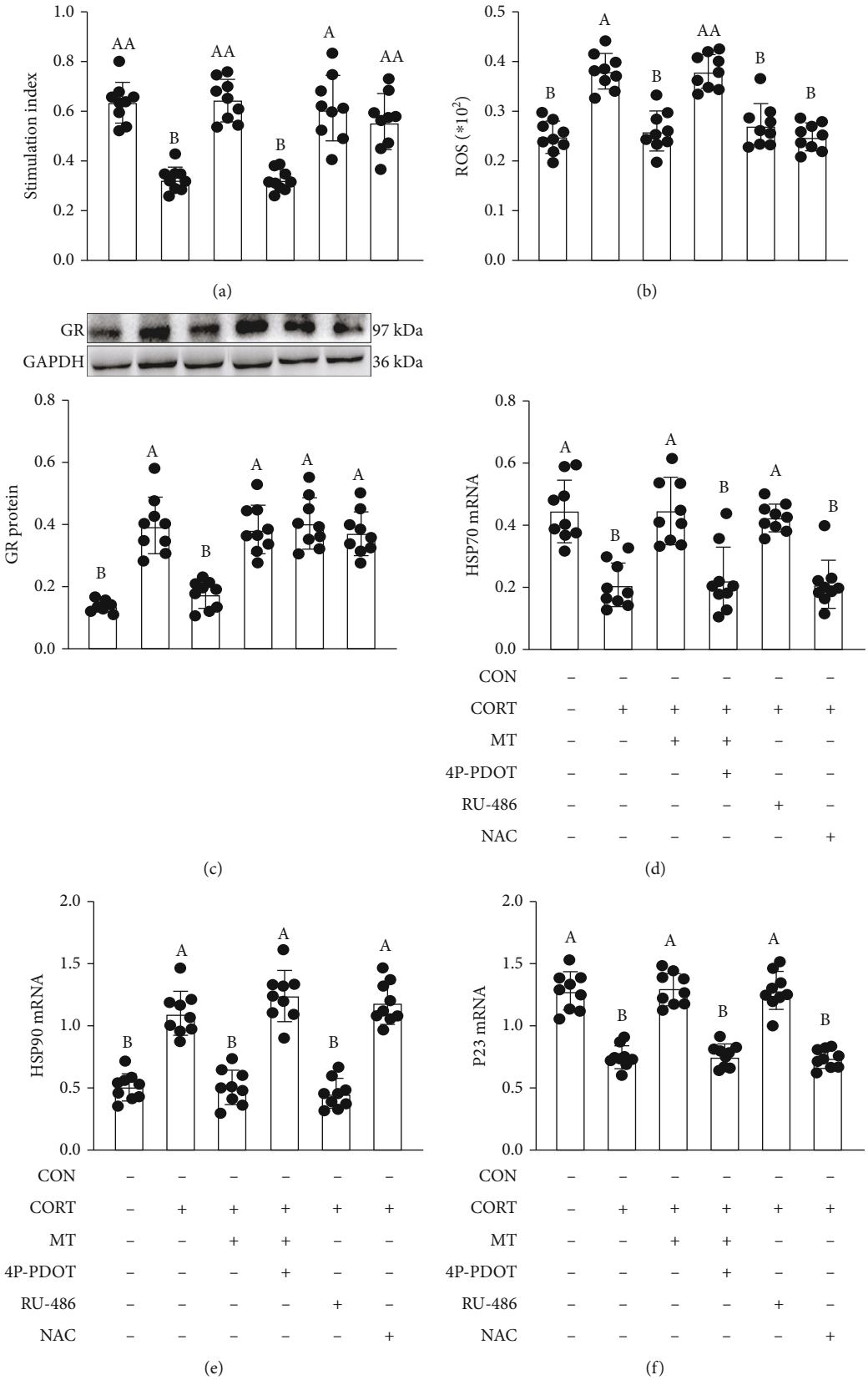

Figure 7: Improvement effect of melatonin on the relative levels of proliferation capacity (a), ROS content (b), GR (c), HSP70 (d), HSP90 (e), and P23 (f) in CORT-treated IECs. 4P-PDOT: an antagonist of MT2; RU-486: an antagonist of GR; NAC: a free radical scavenger. Values are presented as the mean ± SE. Differences were assessed using ANOVA and are denoted as follows: different lowercase letters: $p < 0.05$; different uppercase letters: $p < 0.01$; and the same letter: $p > 0.05$.

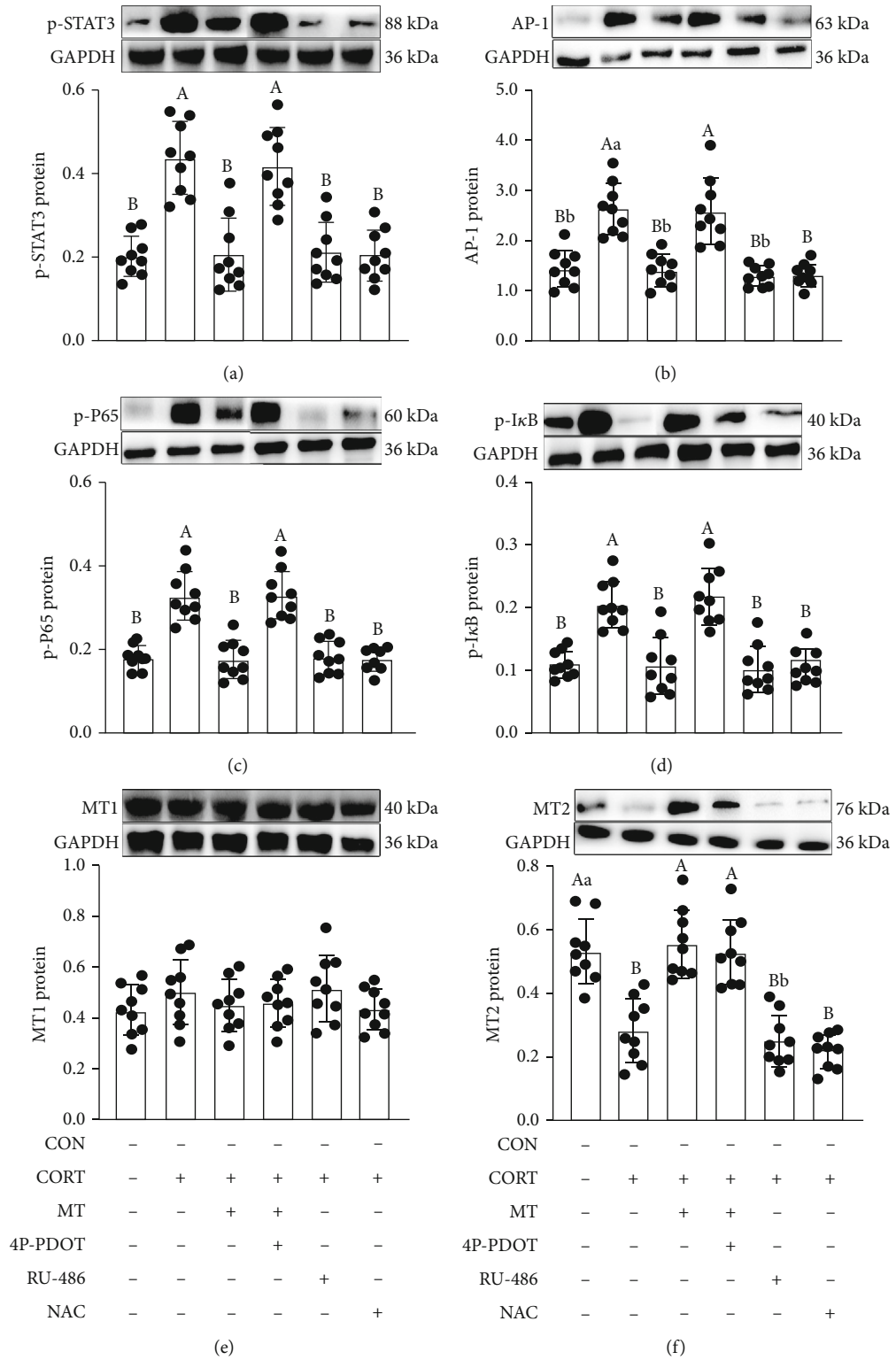

Figure 8: Continued.

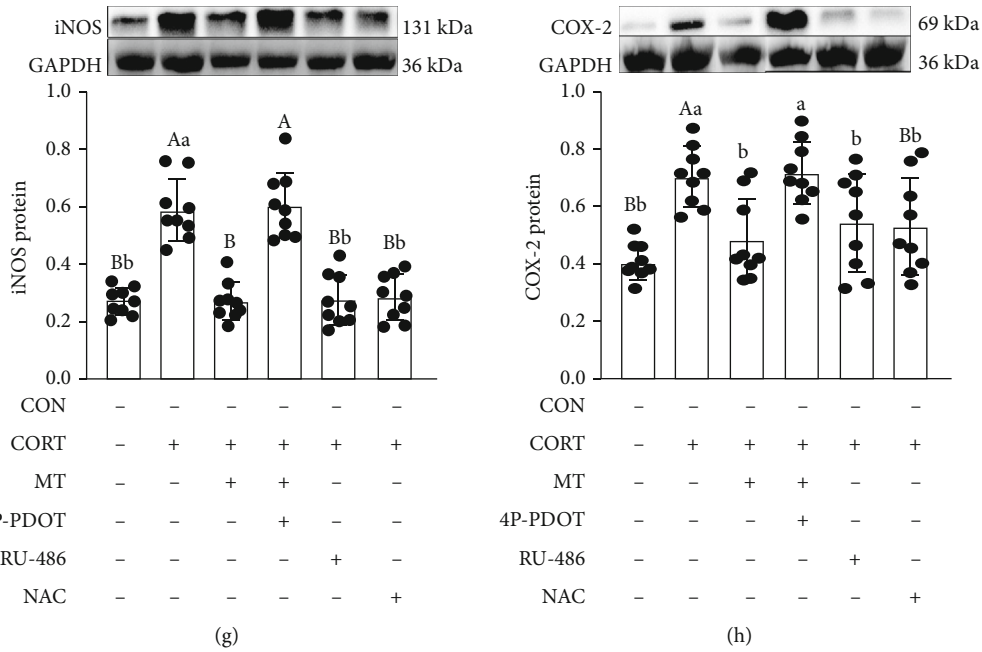

Figure 8: Improvement effect of melatonin on the relative levels of p-STAT3 (a), AP-1 (b), p-P65 (c), p-IκB (d), MT1 (e), MT2 (f), iNOS (g), and COX-2 (h) in CORT-treated IECs. 4P-PDOT: an antagonist of MT; RU-486: an antagonist of GR; NAC: a free radical scavenger. Values are presented as the mean ± SE. Differences were assessed using ANOVA and are denoted as follows: different lowercase letters: $p < 0.05$; different uppercase letters: $p < 0.01$; and the same letter: $p > 0.05$.

inducing a downregulation of ROS and HSP90 mRNA expression and an upregulation of HSP70 and P23 mRNA expression, indicating that GCs have direct effects on GR transcription regulation-mediated oxidative stress. A previous study also demonstrated that an increase in GR levels related to HPA axis disorder has close interactions with oxidative stress [28]. To further explore the mechanisms involved in the inflammatory response induced by oxidative stress in CORT-treated IECs, we focused on the NF-κB pathway, which is a critical mediator of oxidative stress. We also found NAC had a negative effect on the expression levels of p-STAT3, AP-1 p-P65, and p-IκB proteins, but no changes in the GR synthesis and transport were observed, which suggested that oxidative stress alters the activities of intracellular effectors of STAT3/AP-1/NF-κB [29]. Importantly, we observed that 4P-PDOT, an antagonist of MT2, counteracted the ameliorative effects of MT and promoted the expression level of GR protein and ROS and activated the STAT3/AP-1/NF-κB pathway. Previous studies have also demonstrated that overexpression of MT2, but not MT1, had a significant amelioration effect on oxidative stress, endoplasmic reticulum stress, and mitochondrial dysfunction [30]. These results indicated that MT, mediated by the MT2 receptor, could inhibit CORT-induced GR synthesis and transport and activation of the STAT3/AP-1/NF-κB pathway, further suppressing oxidative stress, which mediates the imbalance in the intestinal microbiota and its metabolites and, ultimately, leads to intestinal mucosa barrier dysfunction caused by SD.

This study suggested that the CORT, as a hazardous substance, plays a key role in SD-mediated gut microbiota dysbiosis-induced colitis. However, intraperitoneal injection of MT is an effective way to mitigate CORT-induced metabolic side effects via the MT2 receptor in SD mice. Importantly, our data provide novel evidence for the beneficial effects of MT as a physiological regulator of excessive CORT-mediated intestinal diseases and also support the recent broadening of the definition of probiotics to include MT-based strategies.

5. Conclusion

In conclusion, melatonin-mediated MT2 weakened GR feedback, suppressed oxidative stress, restored the intestinal microbiota and its metabolites homeostasis, and inactivated the STAT3/AP-1/NF-κB pathway-induced inflammatory response, further improving SD-induced colitis.

Data Availability

All data generated or analyzed during this study are included in this published article.

Conflicts of Interest

The authors declare that they have no potential conflicts of interest, including any financial, personal, or other relationships, with other people or organizations.

Authors' Contributions

Y.C. and T.G. contributed to the study design. Y.C. obtained funding. T.G. performed the experiments. T.G., Z.W., J.C., and Y.D. analyzed the data. T.G. and Y.C. wrote the manuscript. All authors reviewed the final manuscript.

Acknowledgments

This work was supported by the Chinese National Natural Science Foundation (31873000, 31672501) and the Beijing Natural Science Foundation (6182018).

Supplementary Materials

Supplementary 1. Figure S1: Effects of melatonin on HPA axis activity and intestinal microbiota composition in sleep-deprived mice. ROS (A) level, GR (B) protein, HSP90 (C) mRNA, HSP70 (D) mRNA, and P23 (E) mRNA expression. Relative abundance of Bacteroidetes (F), Firmicutes (G), Proteobacterium (H) and Prevotellaceae (I) in the colon of the F-CON, F-SD, F-SM, and F-R groups. Values are presented as the mean ± SE. Differences were assessed using ANOVA and are denoted as follows: different lowercase letters: $p < 0.05$; different uppercase letters: $p < 0.01$; and the same letter: $p > 0.05$.

Supplementary 2. Figure S2: FMT reestablished the intestinal microecology similar to CON, SD and SD+MT mice. Immunohistochemical staining of MUC2 (A), ZO-1 (B), and Claudin-1 (C) in colon sections (scale: 50 μm). IOD of MUC2 (D), ZO-1 (E), and Claudin-1 (F) proteins. DAI score (G); relative luciferase activity for colonic permeability (H); relative protein level of Card9 (I); IL-17 concentrations (J); relative abundance of Bacteroidetes (K), Firmicutes (L), Prevotellaceae (M), and Proteobacterium (N) in the colon of the F-CON, F-SD, F-SM, and F-R groups ($n = 12$). Values are presented as the mean ± SE. Differences were assessed using ANOVA and are denoted as follows: different lowercase letters: $p < 0.05$; different uppercase letters: $p < 0.01$; and the same letter: $p > 0.05$.

Supplementary 3. Figure S3: FMT reestablished the oxidative stress and inflammation response similar to CON, SD, and SD+MT mice. Serum CORT (A) concentrations were measured by ELISA ($n = 8$). ROS (B) level and expression level of p-STAT3 (C), p-AP-1 (D), p-IκB (E), and p-P65 (F) proteins in the F-CON, F-SD, F-SM, and F-R groups were examined by western blotting, and relative protein levels were normalized to GAPDH. Values are presented as the mean ± SE. Differences were assessed using ANOVA and are denoted as follows: different lowercase letters: $p < 0.05$; different uppercase letters: $p < 0.01$; and the same letter: $p > 0.05$.

References

[1] M. Basner, K. M. Fomberstein, F. M. Razavi et al., "American time use survey: sleep time and its relationship to waking activities," *Sleep*, vol. 30, no. 9, pp. 1085–1095, 2007.

[2] T. Gao, Z. Wang, Y. Dong et al., "Role of melatonin in sleep deprivation-induced intestinal barrier dysfunction in mice," *Journal of Pineal Research*, vol. 67, article e12574, 2019.

[3] T. D. Bradley and J. S. Floras, "Sleep apnea and heart failure. Part II. Central sleep apnea," *Circulation*, vol. 107, no. 13, pp. 1822–1826, 2003.

[4] P. Gander, M. van den Berg, and L. Signal, "Sleep and sleepiness of fishermen on rotating schedules," *Chronobiology International*, vol. 25, no. 2-3, pp. 389–398, 2008.

[5] C. O. Elson and Y. Cong, "Host-microbiota interactions in inflammatory bowel disease," *Gut Microbes*, vol. 3, no. 4, pp. 332–344, 2012.

[6] R. Caruso, B. C. Lo, and G. Núñez, "Host-microbiota interactions in inflammatory bowel disease," *Nature Reviews Immunology*, vol. 20, no. 7, pp. 411–426, 2020.

[7] Y. Li, Y. Hao, F. Fan, and B. Zhang, "The role of microbiome in Insomnia, circadian disturbance and depression," *Frontiers in Psychiatry*, vol. 9, article 669, 2018.

[8] M. O. L. Galvão, R. Sinigaglia-Coimbra, S. E. Kawakami, S. Tufik, and D. Suchecki, "Paradoxical sleep deprivation activates hypothalamic nuclei that regulate food intake and stress response," *Psychoneuroendocrinology*, vol. 34, no. 8, pp. 1176–1183, 2009.

[9] B. S. McEwen, "Sleep deprivation as a neurobiologic and physiologic stressor: allostasis and allostatic load," *Metabolism, Clinical and Experimental*, vol. 55, 10 Supplement 2, pp. S20–S23, 2006.

[10] S. Pan, A. Chen, Z. Han, Y. Wang, X. Lu, and Y. Yang, "^{1}H NMR-based metabonomic study on the effects of Epimedium on glucocorticoid-induced osteoporosis," *Journal of Chromatography B*, vol. 1038, pp. 118–126, 2016.

[11] H. Amini-Khoei, E. Haghani-Samani, M. Beigi et al., "On the role of corticosterone in behavioral disorders, microbiota composition alteration and neuroimmune response in adult male mice subjected to maternal separation stress," *International Immunopharmacology*, vol. 66, pp. 242–250, 2019.

[12] N. Burger-van Paassen, A. Vincent, P. J. Puiman et al., "The regulation of intestinal mucin MUC2 expression by short-chain fatty acids: implications for epithelial protection," *The Biochemical Journal*, vol. 420, no. 2, pp. 211–219, 2009.

[13] L. A. Brotto, A. M. Barr, and B. B. Gorzalka, "Sex differences in forced-swim and open-field test behaviours after chronic administration of melatonin," *European Journal of Pharmacology*, vol. 402, no. 1-2, pp. 87–93, 2000.

[14] N. Ma, J. Zhang, R. J. Reiter, and X. Ma, "Melatonin mediates mucosal immune cells, microbial metabolism, and rhythm crosstalk: a therapeutic target to reduce intestinal inflammation," *Medicinal Research Reviews*, vol. 40, no. 2, pp. 606–632, 2020.

[15] A. D'Amato, L. di Cesare Mannelli, E. Lucarini et al., "Faecal microbiota transplant from aged donor mice affects spatial learning and memory via modulating hippocampal synaptic plasticity- and neurotransmission related proteins in young recipients," *Microbiome*, vol. 8, no. 1, article 140, 2020.

[16] S. A. Shah, M. Khan, M. H. Jo, M. G. Jo, F. U. Amin, and M. O. Kim, "Melatonin stimulates the SIRT1/Nrf2 signaling pathway counteracting lipopolysaccharide (LPS)-induced oxidative stress to rescue postnatal rat brain," *CNS Neuroscience & Therapeutics*, vol. 23, no. 1, pp. 33–44, 2017.

[17] D. Dodd, M. H. Spitzer, W. van Treuren et al., "A gut bacterial pathway metabolizes aromatic amino acids into nine circulating metabolites," *Nature*, vol. 551, no. 7682, pp. 648–652, 2017.

[18] H. Xu, Z. Wang, L. Zhu et al., "Targeted neurotransmitters profiling identifies metabolic signatures in rat brain by LC-MS/MS: application in insomnia, depression and Alzheimer's disease," *Molecules*, vol. 23, no. 9, article 2375, 2018.

[19] R. Glaser and J. K. Kiecolt-Glaser, "Stress-induced immune dysfunction: implications for health," *Nature Reviews Immunology*, vol. 5, no. 3, pp. 243–251, 2005.

[20] M. Wlodarska, C. Luo, R. Kolde et al., "Indoleacrylic Acid Produced by Commensal *Peptostreptococcus* Species Suppresses Inflammation," *Cell Host & Microbe*, vol. 22, no. 1, pp. 25–37.e6, 2017.

[21] J. K. Nicholson, E. Holmes, J. Kinross et al., "Host-gut microbiota metabolic interactions," *Science*, vol. 336, no. 6086, pp. 1262–1267, 2012.

[22] M. Y. Lin, M. R. de Zoete, J. P. M. van Putten, and K. Strijbis, "Redirection of epithelial immune responses by short-chain fatty acids through inhibition of histone deacetylases," *Frontiers in Immunology*, vol. 6, article 554, 2015.

[23] C. J. Kim, J. A. Kovacs-Nolan, C. Yang, T. Archbold, M. Z. Fan, and Y. Mine, "L-tryptophan exhibits therapeutic function in a porcine model of dextran sodium sulfate (DSS)-induced colitis," *The Journal of Nutritional Biochemistry*, vol. 21, no. 6, pp. 468–475, 2010.

[24] E. Kirschke, D. Goswami, D. Southworth, P. R. Griffin, and D. A. Agard, "Glucocorticoid receptor function regulated by coordinated action of the Hsp90 and Hsp70 chaperone cycles," *Cell*, vol. 157, no. 7, pp. 1685–1697, 2014.

[25] B. Lee, S. G. Kim, J. Kim et al., "Brain-specific homeobox factor as a target selector for glucocorticoid receptor in energy balance," *Molecular and Cellular Biology*, vol. 33, no. 14, pp. 2650–2658, 2013.

[26] W. Zhou, J. H. Quan, Y. H. Lee, D. W. Shin, and G. H. Cha, "Toxoplasma gondii proliferation require down-regulation of host Nox4 expression via activation of PI3 kinase/Akt signaling pathway," *PLoS One*, vol. 8, no. 6, article e66306, 2013.

[27] G. Clarke, S. Grenham, P. Scully et al., "The microbiome-gut-brain axis during early life regulates the hippocampal serotonergic system in a sex-dependent manner," *Molecular Psychiatry*, vol. 18, no. 6, pp. 666–673, 2013.

[28] Y. K. Kim, K. S. Na, A. M. Myint, and B. E. Leonard, "The role of pro-inflammatory cytokines in neuroinflammation, neurogenesis and the neuroendocrine system in major depression," *Progress in Neuro-Psychopharmacology & Biological Psychiatry*, vol. 64, pp. 277–284, 2016.

[29] N. T. Moldogazieva, S. V. Lutsenko, and A. A. Terentiev, "Reactive oxygen and nitrogen species-induced protein modifications: implication in carcinogenesis and anticancer therapy," *Cancer Research*, vol. 78, no. 21, pp. 6040–6047, 2018.

[30] D. Han, Y. Wang, J. Chen et al., "Activation of melatonin receptor 2 but not melatonin receptor 1 mediates melatonin-conferred cardioprotection against myocardial ischemia/reperfusion injury," *Journal of Pineal Research*, vol. 67, article e12571, 2019.